



# NEURAL INTERFACE FOR COGNITIVE HUMAN-ROBOT INTERACTION AND COLLABORATION

EDITED BY: Hong Cheng, Zeng-Guang Hou, Xiaodong Guo,  
Mitsuhiro Hayashibe and Zhan Li

PUBLISHED IN: Frontiers in Neuroscience and Frontiers in Neurorobotics



# frontiers

## Frontiers eBook Copyright Statement

The copyright in the text of individual articles in this eBook is the property of their respective authors or their respective institutions or funders. The copyright in graphics and images within each article may be subject to copyright of other parties. In both cases this is subject to a license granted to Frontiers.

The compilation of articles constituting this eBook is the property of Frontiers.

Each article within this eBook, and the eBook itself, are published under the most recent version of the Creative Commons CC-BY licence.

The version current at the date of publication of this eBook is CC-BY 4.0. If the CC-BY licence is updated, the licence granted by Frontiers is automatically updated to the new version.

When exercising any right under the CC-BY licence, Frontiers must be attributed as the original publisher of the article or eBook, as applicable.

Authors have the responsibility of ensuring that any graphics or other materials which are the property of others may be included in the CC-BY licence, but this should be checked before relying on the CC-BY licence to reproduce those materials. Any copyright notices relating to those materials must be complied with.

Copyright and source acknowledgement notices may not be removed and must be displayed in any copy, derivative work or partial copy which includes the elements in question.

All copyright, and all rights therein, are protected by national and international copyright laws. The above represents a summary only. For further information please read Frontiers' Conditions for Website Use and Copyright Statement, and the applicable CC-BY licence.

ISSN 1664-8714

ISBN 978-2-88974-759-7

DOI 10.3389/978-2-88974-759-7

## About Frontiers

Frontiers is more than just an open-access publisher of scholarly articles: it is a pioneering approach to the world of academia, radically improving the way scholarly research is managed. The grand vision of Frontiers is a world where all people have an equal opportunity to seek, share and generate knowledge. Frontiers provides immediate and permanent online open access to all its publications, but this alone is not enough to realize our grand goals.

## Frontiers Journal Series

The Frontiers Journal Series is a multi-tier and interdisciplinary set of open-access, online journals, promising a paradigm shift from the current review, selection and dissemination processes in academic publishing. All Frontiers journals are driven by researchers for researchers; therefore, they constitute a service to the scholarly community. At the same time, the Frontiers Journal Series operates on a revolutionary invention, the tiered publishing system, initially addressing specific communities of scholars, and gradually climbing up to broader public understanding, thus serving the interests of the lay society, too.

## Dedication to Quality

Each Frontiers article is a landmark of the highest quality, thanks to genuinely collaborative interactions between authors and review editors, who include some of the world's best academicians. Research must be certified by peers before entering a stream of knowledge that may eventually reach the public - and shape society; therefore, Frontiers only applies the most rigorous and unbiased reviews.

Frontiers revolutionizes research publishing by freely delivering the most outstanding research, evaluated with no bias from both the academic and social point of view. By applying the most advanced information technologies, Frontiers is catapulting scholarly publishing into a new generation.

## What are Frontiers Research Topics?

Frontiers Research Topics are very popular trademarks of the Frontiers Journals Series: they are collections of at least ten articles, all centered on a particular subject. With their unique mix of varied contributions from Original Research to Review Articles, Frontiers Research Topics unify the most influential researchers, the latest key findings and historical advances in a hot research area! Find out more on how to host your own Frontiers Research Topic or contribute to one as an author by contacting the Frontiers Editorial Office: [frontiersin.org/about/contact](http://frontiersin.org/about/contact)

# NEURAL INTERFACE FOR COGNITIVE HUMAN-ROBOT INTERACTION AND COLLABORATION

Topic Editors:

**Hong Cheng**, University of Electronic Science and Technology of China, China  
**Zeng-Guang Hou**, Institute of Automation, Chinese Academy of Sciences (CAS), China

**Xiaodong Guo**, Huazhong University of Science and Technology, China

**Mitsuhiro Hayashibe**, Tohoku University, Japan

**Zhan Li**, University of Electronic Science and Technology of China, China

**Citation:** Cheng, H., Hou, Z.-G., Guo, X., Hayashibe, M., Li, Z., eds. (2022). Neural Interface for Cognitive Human-Robot Interaction and Collaboration. Lausanne: Frontiers Media SA. doi: 10.3389/978-2-88974-759-7

# Table of Contents

04	<b><i>Editorial: Neural Interface for Cognitive Human-Robot Interaction and Collaboration</i></b>
	Rui Huang, Lian Zeng, Hong Cheng and Xiaodong Guo
06	<b><i>Beyond Technologies of Electroencephalography-Based Brain-Computer Interfaces: A Systematic Review From Commercial and Ethical Aspects</i></b>
	Cesar Augusto Fontanillo Lopez, Guangye Li and Dingguo Zhang
29	<b><i>Effects of Long-Term Meditation Practices on Sensorimotor Rhythm-Based Brain-Computer Interface Learning</i></b>
	Xiyuan Jiang, Emily Lopez, James R. Stieger, Carol M. Greco and Bin He
43	<b><i>A Semi-active Exoskeleton Based on EMGs Reduces Muscle Fatigue When Squatting</i></b>
	Zhuo Wang, Xinyu Wu, Yu Zhang, Chunjie Chen, Shoubin Liu, Yida Liu, Ansi Peng and Yue Ma
55	<b><i>A Real-Time Stability Control Method Through sEMG Interface for Lower Extremity Rehabilitation Exoskeletons</i></b>
	Can Wang, Ziming Guo, Shengcai Duan, Bailin He, Ye Yuan and Xinyu Wu
70	<b><i>Dual-Threshold-Based Microstate Analysis on Characterizing Temporal Dynamics of Affective Process and Emotion Recognition From EEG Signals</i></b>
	Jing Chen, Haifeng Li, Lin Ma, Hongjian Bo, Frank Soong and Yaohui Shi
84	<b><i>Evaluation of Multilevel Surgeries in Children With Spastic Cerebral Palsy Based on Surface Electromyography</i></b>
	Sujiao Li, Xueqin Luo, Song Zhang, Yuanmin Tang, Jiming Sun, Qingyun Meng, Hongliu Yu and Chengyan Sun
94	<b><i>A Novel Two-Stage Refine Filtering Method for EEG-Based Motor Imagery Classification</i></b>
	Yuxin Yan, Haifeng Zhou, Lixin Huang, Xiao Cheng and Shaolong Kuang
103	<b><i>An Improvement of Robot Stiffness-Adaptive Skill Primitive Generalization Using the Surface Electromyography in Human–Robot Collaboration</i></b>
	Yuan Guan, Ning Wang and Chenguang Yang
122	<b><i>Bayesian Estimation of Potential Performance Improvement Elicited by Robot-Guided Training</i></b>
	Asuka Takai, Giuseppe Lisi, Tomoyuki Noda, Tatsuya Teramae, Hiroshi Imamizu and Jun Morimoto
135	<b><i>MCSNet: Channel Synergy-Based Human-Exoskeleton Interface With Surface Electromyogram</i></b>
	Kecheng Shi, Rui Huang, Zhinan Peng, Fengjun Mu and Xiao Yang





# Editorial: Neural Interface for Cognitive Human-Robot Interaction and Collaboration

Rui Huang<sup>1†</sup>, Lian Zeng<sup>2†</sup>, Hong Cheng<sup>1\*</sup> and Xiaodong Guo<sup>2\*</sup>

<sup>1</sup> School of Automation Engineering, University of Electronic Science and Technology of China, Chengdu, China, <sup>2</sup> Department of Orthopedics, Union Hospital, Tongji Medical College, Huazhong University of Science and Technology, Wuhan, China

**Keywords:** BCI, brain-computer interface, human-robot collaboration, EEG, exoskeleton, action recognition, rehabilitation, human-robot interaction

## Editorial on the Research Topic

### Neural Interface for Cognitive Human-Robot Interaction and Collaboration

Human-robot interaction (HRI) and collaboration is a major topic in human-coupled robotic systems. With the development of neural technologies, the neural interface called cognitive human-robot interaction has been implemented for achieving natural human-robot interaction and collaboration. This special issue will be dedicated to cognitive human-robot interactions, including brain-computer interface (BCI) with electroencephalographic (EEG), muscle signals with electromyography (EMG), and so on. The special issue is focused on the fundamentals and technologies of cognitive human-robot interaction with neural interfaces for human-coupled robotic systems. Ten articles were accepted by this special issue, the contents of these articles are briefly described as follows.

As the development of electroencephalographic techniques for commercial applications continues, their transformative potential necessitates equally significant ethical inquiries. Lopez et al. consult different databases, which presents conceptual and empirical discussions and findings about various commercial and ethical aspects of electroencephalography. Subsequently, the content is extracted from the articles and the main conclusions are presented. Finally, an external assessment of the outcomes is conducted in consultation with an expert panel in some of the topic areas such as biomedical engineering, biomechanics, and neuroscience.

Sensorimotor rhythm (SMR)-based BCIs can help users perform motor control using motor imagery. But the control paradigm of SMR BCI may not work well on a subpopulation of users. Jiang et al. investigate the behavioral and electrophysiological differences between experienced meditators and meditation naïve subjects in one-dimensional and two-dimensional cursor control tasks. The evidence shows that meditators outperformed control subjects in both tasks. Further, the meditators had a higher resting SMR predictor, more stable resting mu rhythm, and a larger control signal contrast than controls during the task.

In dynamic manufacturing and warehousing environments, workers suffer from muscle fatigue of the lower limbs caused by standing or squatting for a long period of time. Wang Z et al. design and evaluate a semi-active lower-limb exoskeleton to reduce muscle fatigue. The exoskeleton can switch three different modes depending on the EMGs of the gluteus maximus, and quadriceps. Three sets of experiments are conducted to evaluate the effect of the exoskeleton, results show that the exoskeleton not only effectively reduced muscle fatigue but also avoided interfering with the free movement of the wearer.

## OPEN ACCESS

### Edited and reviewed by:

Dingguo Zhang,  
University of Bath, United Kingdom

### \*Correspondence:

Hong Cheng  
hcheng@uestc.edu.cn  
Xiaodong Guo  
xiaodongguo@hust.edu.cn

<sup>†</sup>These authors have contributed  
equally to this work

### Specialty section:

This article was submitted to  
Neural Technology,  
a section of the journal  
Frontiers in Neuroscience

**Received:** 07 December 2021

**Accepted:** 27 January 2022

**Published:** 03 March 2022

### Citation:

Huang R, Zeng L, Cheng H and Guo X  
(2022) Editorial: Neural Interface for  
Cognitive Human-Robot Interaction  
and Collaboration.  
Front. Neurosci. 16:830877.  
doi: 10.3389/fnins.2022.830877

Exoskeleton rehabilitation robots can help paraplegics motor functions. However, achieving stable states of the human-exoskeleton system while conserving wearer strength remains challenging. Wang C et al. propose a real-time stable control gait switching method for the exoskeleton rehabilitation robot. The method uses surface electromyography (sEMG)-based HRI to realize the intention recognition, and realizes gaits planning and stability analysis based on a human kinematics model and zero moment point method. Results verified the feasibility and efficiency of the proposed gait switching method for enhancing stability and ergonomic effects of a lower limb rehabilitation exoskeleton.

The features extracted from EEG usually change dramatically, but emotion states change gradually. Most existing feature extraction approaches do not consider these differences between EEG and emotion. Chen et al. propose a novel feature extraction method based on EEG microstates for emotion recognition. This method extracts microstate characteristics as novel temporospatial features, and the dual-threshold-based atomize and agglomerate hierarchical clustering method is used to determine the optimal number of microstate classes automatically. Results indicated that microstate characteristics can effectively improve the performance of emotion recognition from EEG signals.

The root mean square (RMS) of the sEMG signal displays a positive correlation with muscle force and muscle tension under positive and passive conditions, respectively. Li et al. investigate the changes in muscle force and tension after multilevel surgical treatments, functional selective posterior rhizotomy, and tibial anterior muscle transfer surgery, and evaluate their clinical effect in children with spastic cerebral palsy (SCP) during walking. Results indicate that the neuromuscular function of cerebral palsy during walking can be evaluated by the muscle activation state and the RMS of the sEMG signal, which shows that multilevel surgical treatments are feasible and effective to treat SCP.

In the field of motor imagery (MI) classification, appropriate filtering is vital for feature extracting of EEG signals and consequently influences the accuracy of MI classification. Yan et al. propose a novel two-stage refine filtering method, it uses the gradients of any target concept flowing into the final convolutional layer to highlight the important part of training data for predicting the concept. Experiment results reveal that the proposed method reaches state-of-the-art classification kappa value levels and acquires at least 3% higher kappa values than other methods.

The generalization goals of most skill expression models in real scenarios are specified by humans or associated with other perceptual data. Guan et al. propose a framework using the Probabilistic Movement Primitives modeling to improve the robot stiffness-adaptive skill primitive generalization. It uses sEMG signal to estimate human arm endpoint stiffness, which

can then be transferred to the robot. The proposed framework can be used to trigger robot action generalization *via* observing human action, ideal for a human-robot collaboration scenario.

Improving human motor performance *via* physical guidance by an assist robot device is a major field of interest for society in many different contexts, such as rehabilitation and sports training. Takai et al. propose a Bayesian estimation method to predict whether the motor performance of a user can be improved from the initial skill level of a user or not *via* robot guidance. Results show that the proposed approach can potentially help users to decide if they should try a robot-guided training or not without conducting the time-consuming robot-guided movement training.

The HRIs have been widely used in exoskeleton robots to help predict the movement of the wearer, especially sEMG-based HRIs. But the sEMG signals from paraplegic patients' lower limbs are weak, which means an HRI based on lower limb sEMG signals cannot be applied to exoskeletons. Shi et al. propose an HRI based on upper limb sEMG signals to predict the lower limb movements of paraplegic patients. The interface constructs a channel synergy-based network to extract the contribution and synergy of different feature channels. Results show that the method has a good movement prediction performance in both within-subject and cross-subject situations.

## AUTHOR CONTRIBUTIONS

RH and LZ drafted the manuscript. XG and HC critically revised the manuscript. All authors approved the submitted version.

## FUNDING

This work was supported by the National Natural Science Foundation of China (grant nos. 82072446 and 81873999) and the Key R&D Program of Hubei Province (2020BCB050).

**Conflict of Interest:** The authors declare that the research was conducted in the absence of any commercial or financial relationships that could be construed as a potential conflict of interest.

**Publisher's Note:** All claims expressed in this article are solely those of the authors and do not necessarily represent those of their affiliated organizations, or those of the publisher, the editors and the reviewers. Any product that may be evaluated in this article, or claim that may be made by its manufacturer, is not guaranteed or endorsed by the publisher.

Copyright © 2022 Huang, Zeng, Cheng and Guo. This is an open-access article distributed under the terms of the Creative Commons Attribution License (CC BY). The use, distribution or reproduction in other forums is permitted, provided the original author(s) and the copyright owner(s) are credited and that the original publication in this journal is cited, in accordance with accepted academic practice. No use, distribution or reproduction is permitted which does not comply with these terms.



# Beyond Technologies of Electroencephalography-Based Brain-Computer Interfaces: A Systematic Review From Commercial and Ethical Aspects

Cesar Augusto Fontanillo Lopez<sup>1</sup>, Guangye Li<sup>2</sup> and Dingguo Zhang<sup>3\*</sup>

<sup>1</sup> KU-Leuven Center for IT & IP Law, KU-Leuven, Leuven, Belgium, <sup>2</sup> The Robotics Institute, School of Mechanical Engineering, Shanghai Jiao Tong University, Shanghai, China, <sup>3</sup> The Department of Electronic and Electrical Engineering, University of Bath, Bath, United Kingdom

## OPEN ACCESS

### Edited by:

Zhan Li,

University of Electronic Science and  
Technology of China, China

### Reviewed by:

Ren Xu,

Guger Technologies, Austria

Kalyana C. Veluvolu,

Kyungpook National University,  
South Korea

### \*Correspondence:

Dingguo Zhang

d.zhang@bath.ac.uk

### Specialty section:

This article was submitted to

Neural Technology,

a section of the journal

Frontiers in Neuroscience

**Received:** 28 September 2020

**Accepted:** 13 November 2020

**Published:** 17 December 2020

### Citation:

Fontanillo Lopez CA, Li G and  
Zhang D (2020) Beyond Technologies  
of Electroencephalography-Based  
Brain-Computer Interfaces: A  
Systematic Review From Commercial  
and Ethical Aspects.

Front. Neurosci. 14:611130.

doi: 10.3389/fnins.2020.611130

The deployment of electroencephalographic techniques for commercial applications has undergone a rapid growth in recent decades. As they continue to expand in the consumer markets as suitable techniques for monitoring the brain activity, their transformative potential necessitates equally significant ethical inquiries. One of the main questions, which arises then when evaluating these kinds of applications, is whether they should be aligned or not with the main ethical concerns reported by scholars and experts. Thus, the present work attempts to unify these disciplines of knowledge by performing a comprehensive scan of the major electroencephalographic market applications as well as their most relevant ethical concerns arising from the existing literature. In this literature review, different databases were consulted, which presented conceptual and empirical discussions and findings about commercial and ethical aspects of electroencephalography. Subsequently, the content was extracted from the articles and the main conclusions were presented. Finally, an external assessment of the outcomes was conducted in consultation with an expert panel in some of the topic areas such as biomedical engineering, biomechanics, and neuroscience. The ultimate purpose of this review is to provide a genuine insight into the cutting-edge practical attempts at electroencephalography. By the same token, it seeks to highlight the overlap between the market needs and the ethical standards that should govern the deployment of electroencephalographic consumer-grade solutions, providing a practical approach that overcomes the engineering myopia of certain ethical discussions.

**Keywords:** electroencephalography, brain-computer interface, commercial aspects, ethical aspects, EEG

## INTRODUCTION

Electroencephalography (EEG) is one of the most widespread neuroimaging techniques. It is not only a rapidly developing area of neuroscience research but also a technology which attracts a considerable amount of attention and investment.

Some of the keys to the success of EEG are their towering advantages among other brain-imaging techniques. Thus, EEG offers superior safety, portability, temporal resolution and cost-effectiveness

than other non-invasive methods, such as functional magnetic resonance imaging (fMRI), magnetoencephalography (MEG), or positron emission tomography (PET) (Akçakaya et al., 2014). These advantages have made EEG a widely accepted tool by the scientific community and the private sector for neuroscience research and applications.

EEG uses are extremely wide-ranging and have undergone profound changes in recent years. Initially, EEG was adopted to translate users' intentions by classifying their voluntary brain activity to actively monitor or control external devices. These applications have been called active Brain-Computer Interfaces (aBCI) and are ordinarily confined in the biomedical field for replacing, restoring, enhancing, supplementing, or improving natural central nervous system (CNS) output (Zander et al., 2010; Burwell et al., 2017; Wolpaw et al., 2020). However, at a later stage, EEG applications have evolved from their original scientific purpose to passively decode cognitive and emotional states of users' spontaneous brain activity. These new systems have extended the traditional notions of aBCI applications to passive Brain-Computer Interfaces (pBCI) (Zander and Kothe, 2011; Blankertz et al., 2016; Arico et al., 2017; Arico et al., 2018). In turn, pBCI applications have enhanced the business prospects of EEG because of their commercial value as tracking tool solutions that can be exploited in consumer markets.

During this transition, the technological improvements and implications of EEG have been profoundly considered by a wide range of literature reviews (Jackson and Bolger, 2014; Marzbani et al., 2016; Enriquez-Geppert et al., 2017). Yet the vast majority of these studies have been conducted from an engineering standpoint. Since the main proposed EEG use is as an assistive technology, most of the studies have mainly concentrated on neurofeedback improvements as it primarily relates to biomedical applications of aBCIs. In contrast, little research has been done into the intersection of the current state-of-the-art in commercial applications of EEG and their ethical concerns.

By taking into account the major market applications of EEG, the current scoping review outlines the efforts which have been made in heterogeneous business sectors, and provides illustrative examples of existing EEG projects and business initiatives. On this basis, the review also identifies the most commonly cited ethical issues that have been acknowledged in the existing literature, and elaborates upon the various postures which could be adopted with regards to the present development of EEG. Most importantly, the final goal of this review is to provide better insights about the existing opportunities and challenges for the transition into a BCI society, where the deployment of EEG technologies is carried out with respect for social ethical frameworks.

## METHODS

A comprehensive literature review was performed by applying the methodology proposed by Levac et al. (2010), Burwell et al. (2017), as an update of Arksey and O'Malley's original method of literature review (Arksey and O'Malley, 2005). The

review framework includes the original stages enumerated by the authors: (a) identifying the research question, (b) identifying relevant studies, (c) study selection, (d) charting the data and collating, summarizing, and reporting the results, and (e) consultation.

## Identifying the Research Question

The research goal is to analyze the current market applications of EEG in order to confront them with the dominant literature on ethics. The clarification of this gap could provide a pragmatic approach of the present ethical debate and inform recommendations for future research.

## Identifying Relevant Studies

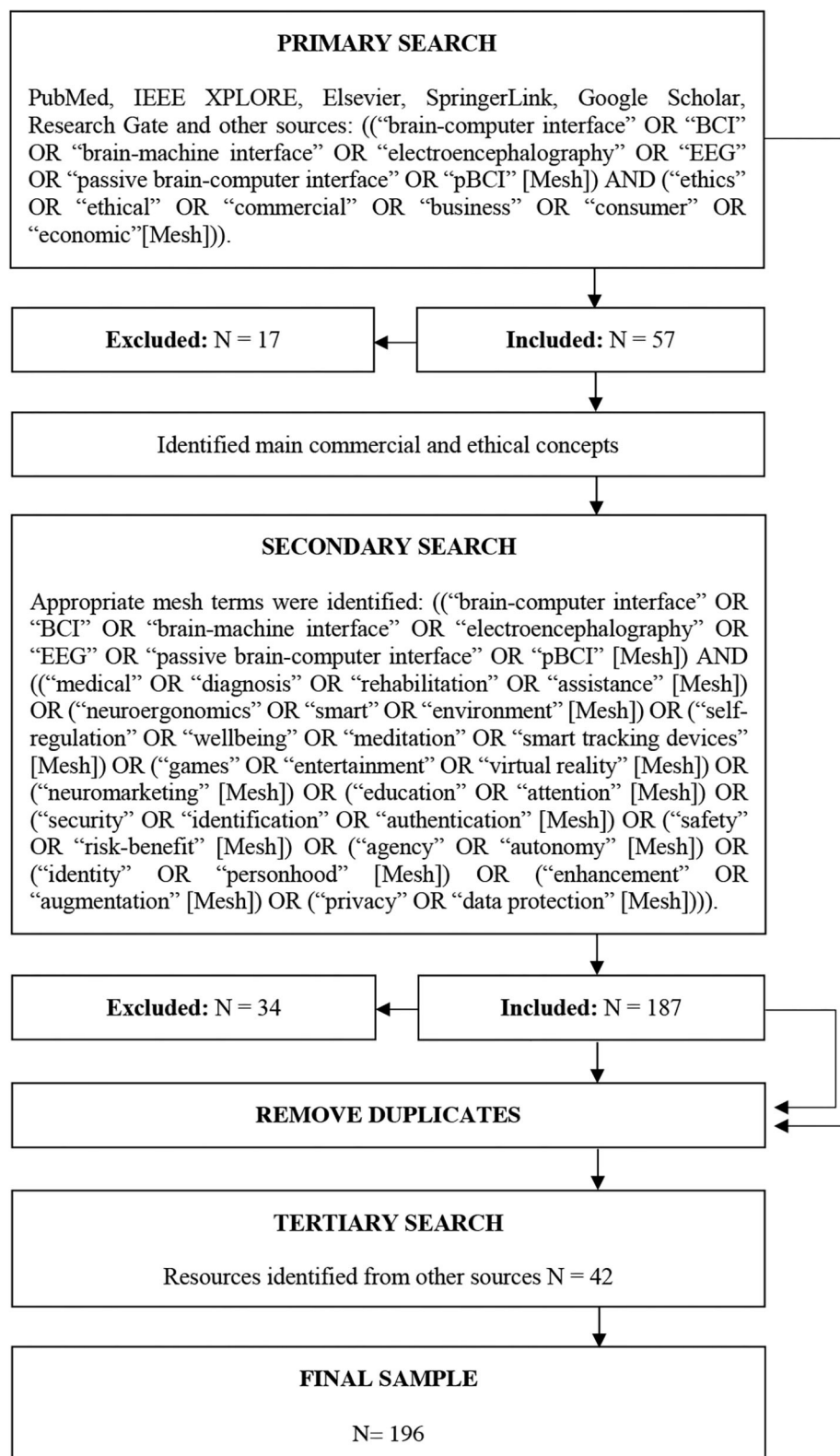
The primary searches focused on different bibliographic databases such as (a) PubMed (b) IEEE Xplore, (c) Elsevier, (d) SpringerLink, (e) Google Scholar, (f) ResearchGate, and (g) other sources (Figure 1). These databases were chosen due to their range spectrum, specifically regarding the commercial and ethical considerations of EEG. Several searches were conducted by using the keywords related to the domains of commercial applications and ethical issues of EEG in general.

The primary searches occurred during August 2018. The keywords used for the primary searches were ((“brain-computer interface” OR “BCI” OR “brain-machine interface” OR “electroencephalography” OR “EEG” OR “passive brain-computer interface” OR “pBCI” [Mesh]) AND (“ethics” OR “ethical” OR “commercial” OR “business” OR “consumer” OR “economic” [Mesh])).

Articles were included if they (1) were written in English, German, Spanish or French (2) presented conceptual discussions or empirical findings on ethics or commercial aspects of BCI, and (3) were especially related to EEG technologies. After applying these criteria, 57 articles remained from the primary search ( $N = 57$ ).

## Selecting Studies for Inclusion

A list of different EEG applications as well as a list of topics frequently discussed in the ethics literature were identified from the primary search. Following the primary search, varying keywords were generated. Then, secondary targeted searches were performed to include articles that were framed in terms of a specific topic within the domains of consumer-grade devices and ethics. The secondary searches occurred between September and December 2018. The keywords used for the secondary targeted searches were ((“brain-computer interface” OR “BCI” OR “brain-machine interface” OR “electroencephalography” OR “EEG” OR “passive brain-computer interface” OR “pBCI” [Mesh]) AND ((“medical” OR “diagnosis” OR “rehabilitation” OR “assistance” [Mesh]) OR (“neuroergonomics” OR “smart” OR “environment” [Mesh]) OR (“self-regulation” OR “well-being” OR “meditation” OR “smart tracking devices” [Mesh]) OR (“games” OR “entertainment” OR “virtual reality” [Mesh]) OR (“neuromarketing” [Mesh]) OR (“education” OR “attention” [Mesh]) OR (“security” OR “identification” OR “authentication” [Mesh]) OR (“safety” OR “risk-benefit” [Mesh]) OR (“agency” OR “autonomy” [Mesh]) OR (“identity” OR “personhood”



**FIGURE 1 |** Search strategy.



[Mesh]) OR (“enhancement” OR “augmentation” [Mesh]) OR (“privacy” OR “data protection” [Mesh])). After applying the same inclusion and exclusion criteria as the primary searches, the secondary searches yielded 187 articles. Once duplicate articles from the primary and secondary searches were excluded, there remained a total of 154 articles.

Following the primary and secondary searches, further relevant sources ( $N = 42$ ) were consulted in tertiary searches, which included, among others, several articles highlighted in the consultation phase. No duplicates were found with the previous searches. The final sample remained  $N = 196$  articles.

## Charting the Data and Collating, Summarizing, and Reporting the Results

From the primary and secondary searches ( $N = 154$ ), the specific commercial and ethical issues were identified and the content was extracted. DZ reviewed the extracted content and provided feedback on its organization. Thus, the main conclusions within the commercial and ethical realms were presented in a narrative fashion.

## Consultation

An external assessment of the outcomes of this review was conducted in consultation with three experts in some of the topic areas such as biomedical engineering, biorobotics and biomechatronics, and neuroscience. Feedback was considered to revise the manuscript as well as to ponder valuable insights that the scoping review alone would not have identified (Daudt et al., 2013).

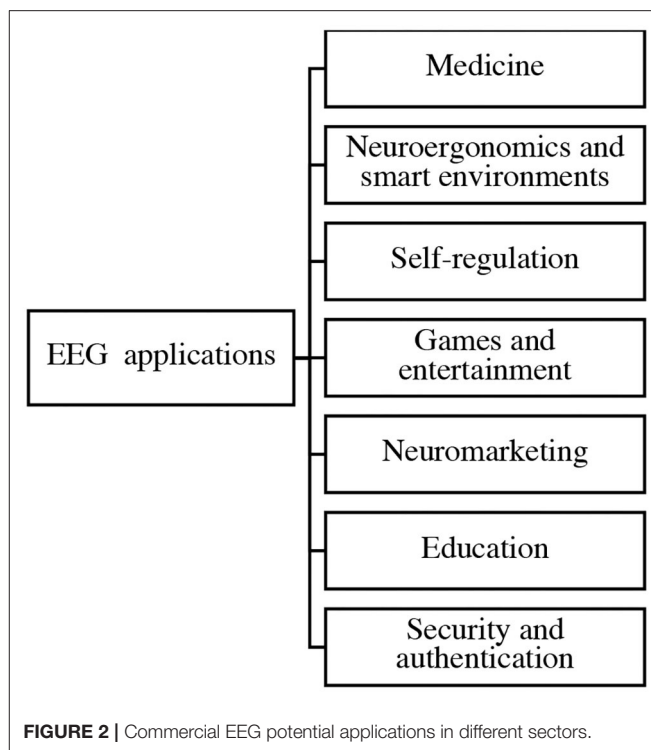
Finally, the organization of the paper remains as follows: in the first section, the results of the review will be presented and discussed from a commercial and ethical standpoint. In the second section, the conclusions of the review will be elaborated upon.

## COMMERCIAL ASPECTS

Following the cross-sectional review, the collected sources suggest that commercial applications of EEG are widely discussed across the literature. The most frequently cited applications include medical applications ( $N = 74$ ), neuroergonomics and smart environment ( $N = 41$ ), self-regulation ( $N = 26$ ), games and entertainment ( $N = 25$ ), neuromarketing ( $N = 21$ ), education ( $N = 20$ ), and security and authentication ( $N = 20$ ). Thus, the most recent practical attempts at EEG applications are presented in **Figure 2**. The same depicted order will be observed in this section.

### Medicine

The most prevalent applications of EEG technologies can be found in the medical sector ( $N = 74$ ). As identified in the literature, they are predominantly used for prediction and diagnosis of diverse clinical conditions as well as for treatment, rehabilitation and assistance of patients with certain disabilities.



**FIGURE 2 |** Commercial EEG potential applications in different sectors.

## Prediction and Diagnosis

One of the main uses of EEG is for risk prediction models, which are becoming progressively more widespread for clinical aid decision-making. These models are developed to estimate the probability of having certain diseases, events or complications given the individual's demographics, test results, or disease characteristics. In this sense, EEG data can be processed for the prediction of several health problems such as sleep disorders (Kupfer et al., 1978), seizure disorders (Mormann et al., 2000; García Bellón and Soria Bretones, 2013; Sharmila and Mahalakshmi, 2017), attention deficit hyperactivity disorders (Clarke et al., 2011; Gola et al., 2013), peripheral neuropathies, and musculoskeletal diseases (Wei et al., 2010). In recent years, different commercial initiatives have been developed in the prediction of clinical conditions. One of the most groundbreaking projects for seizure prediction has been advanced by the Spanish company MJN Neuroserveis. They have developed a discreet, portable earphone device (**Figure 3**) capable of alerting the person and the caregiver when there is a greater risk of seizure, thus preventing falls or injury (Rincón, 2017). The start-up closed a 750,000 Euro investment round for its epilepsy prediction device in 2017, financed by investors from IESE Business School and ENISA network (Hinchliffe, 2018).

Moreover, EEG is also used as an initial diagnosis assessment tool alternative to MRI and CT-SCAN due to its cost-effectiveness. Here, EEG systems have proven valuable in the diagnosis of disorders of consciousness (DOC) (Guger et al., 2018; Stefan et al., 2018) as well as in the detection of tumors and concussions (Selvam and Shenbagadevi, 2011; Sharanreddy and Kulkarni, 2013; Abdulkader et al., 2015). For DOC diagnosis

purposes, the Austrian company Guger Technologies (g.tec) has developed the EEG-based system mindBEAGLE (**Figure 4**), which provides quick and easy assessments of DOC and basic communication with certain patients (Spataro et al., 2018).

Also, companies such as BrainScope take advantage of EEG capabilities in order to pioneer the future of traumatic brain injury (TBI) assessment (**Figure 5**) (Hanley et al., 2017). At the time this review is being conducted, the company cannot actually diagnose if a tumor is present or not, so it is temporarily offering inexpensive solutions that provide preliminary insights to determine the need or not to perform a PET/MRI scan. Notwithstanding, it has been awarded more than \$27 million

from U.S. Department of Defense to develop its TBI and concussion assessment technology (Pai, 2015).

In another area, EEG technologies can also be employed to diagnose neurodegenerative disorders. A growing body of evidence supports its application for early detection of Alzheimer's disease (Jaeseung, 2004; Lazar, 2018), Parkinson's disease (Solís-Vivanco et al., 2018) and for diagnosis of different dementia subtypes (Houmani et al., 2018; Stylianou et al., 2018). These studies propel the growing interest of EEG, whose market is expected to grow worldwide as geriatric population continues to increase (Nations U, 2017). Thus, new entrepreneurial initiatives sustain its attractiveness as a technology for investment. For instance, Synapto, an early stage medical technology venture founded by former students of the University of Maryland, uses portable EEG of OpenBCI to make Alzheimer's diagnosis more accessible and affordable (**Figure 6**). Synapto solutions are funded and validated by NIH (National Institutes of Health, 2017).

### Treatment, Rehabilitation, and Assistance

Beyond its functions as a prediction and diagnosis tool, EEG has spread as a biomarker for treatment of several clinical conditions. In particular, EEG biofeedback can be used for the treatment of patients suffering from addictions due to its direct correlation with drug dependency (Pritchep et al., 1996; Trudeau, 2005). Furthermore, it can also be applied as a potential therapy to help patients with Rett syndrome (Fabio et al., 2016) and for memory deficits recovery via neurofeedback (Rozelle and Budzynski, 1995; Kober et al., 2015). Although EEG does not provide complete relief in all cases, it can assist patients with managing their symptoms, thus affording them a better life quality.



**FIGURE 3 |** MJN-SERAS earphone EEG device for seizure prediction. Reprinted from International Epilepsy Day: Latest medical devices for epilepsy patients, by NS Medical Devices (2018), <https://www.nsmedicaldevices.com/news/international-epilepsy-day-devices-epilepsy/attachment/mjn-seras-epilepsia/>. Copyright 2018, by MJN Neuroserveis.

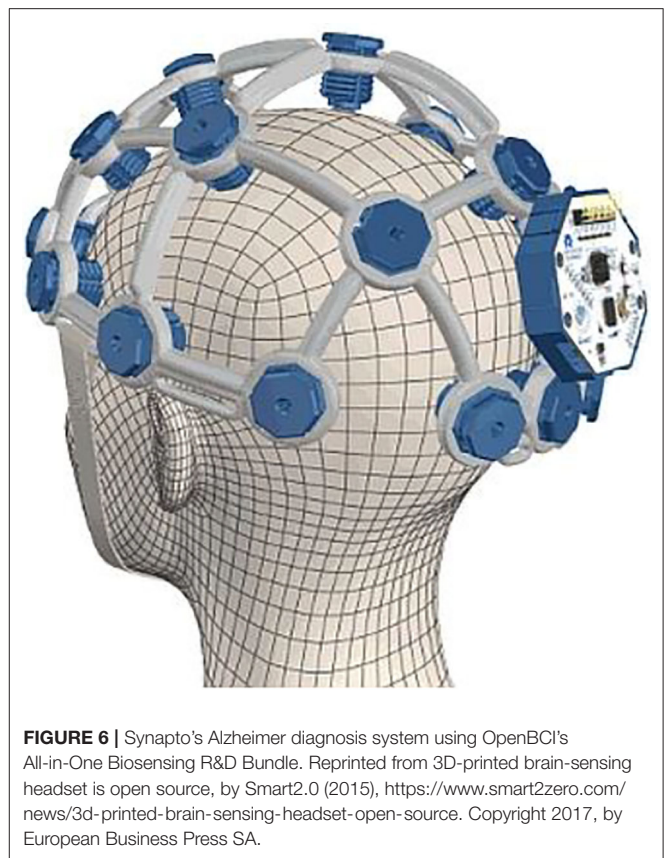


**FIGURE 4 |** mindBEAGLE system. Reprinted from mindBEAGLE Technical Specs and Features, by g.tec medical engineering GmbH (2018), <https://www.mindbeagle.at/Technical-Specs-and-Features>. Copyright 2018, by g.tec medical engineering GmbH.

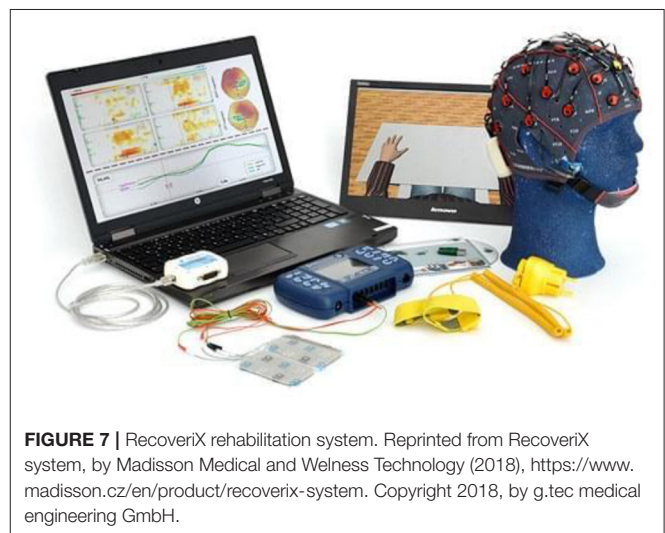


**FIGURE 5 |** BrainScope TBI assessment system. Reprinted from Our Solutions Brainscope, by Brainscope (2018), <https://www.brainscope.com/products>. Copyright 2018, by Brainscope.

On the other side, despite the superior capabilities of invasive methods, the viability of EEG for rehabilitation and restoration of lost functions cannot be ignored. In the light of overwhelming number of scientific evidence, EEG may be a feasible tool for the treatment of in lock-in syndrome (LIS) patients and patients with severe motor disabilities (Markand, 1976; Birbaumer and Cohen, 2007; Sellers et al., 2010; Zickler et al., 2011). It may be also a valuable bedside tool for neuro-motor rehabilitation on post-stroke patients (Markand, 1976; Birbaumer and Cohen, 2007; Ang et al., 2010; Sellers et al., 2010; Zickler et al., 2011; Comani et al., 2015). Here, EEG can be applied to regain previous levels of mobility or, at least, it can allow patients to



**FIGURE 6 |** Synapto's Alzheimer diagnosis system using OpenBCI's All-in-One Biosensing R&D Bundle. Reprinted from 3D-printed brain-sensing headset is open source, by Smart2.0 (2015), <https://www.smart2zero.com/news/3d-printed-brain-sensing-headset-open-source>. Copyright 2017, by European Business Press SA.



**FIGURE 7 |** RecoveriX rehabilitation system. Reprinted from RecoveriX system, by Madisson Medical and Wellness Technology (2018), <https://www.madisson.cz/en/product/recoverix-system>. Copyright 2018, by g.tec medical engineering GmbH.

better manage their dysfunctionalities. As stroke rehabilitation is a very active direction in this field, many products are being deployed for commercial purposes such as recoveriX (**Figure 7**), a g.tec solution which is currently being franchised in different treatment centers around the world, or nBETTER, a system created by the Singaporean company Neurostyle Pte Ltd. which detects visualized movements of stroke-affected limbs using





**FIGURE 8 |** IntendiX spelling system. Reprinted from Intendix, The Brain Computer Interface Goes Commercial, by Singularity Hub (2010), <https://singularityhub.com/2010/03/07/intendix-the-brain-computer-interface-goes-commercial-video/>. Copyright 2010, by g.tec medical engineering GmbH.

EEG-based neuro-feedback to provide visually engaging and mechanical feedback.

As for assistive purposes, EEG permits disabled people to communicate their opinions and ideas via a variety of methods such as spelling applications (Birbaumer and Cohen, 2007; Akcakaya et al., 2014; Birbaumer et al., 2014; Rezeika et al., 2018), semantic categorization (Stothart et al., 2017), or silent speech communication (Brumberg et al., 2010; Mohanchandra et al., 2015). This may facilitate advanced hands-free applications, which may provide disabled people ease and comfort. In this realm, the world's first personal EEG-based spelling system was introduced in 2010 by g.tec (Fazel-Rezai et al., 2012). Besides writing a text, the user can also interact with the system (IntendiX) to trigger an alarm, print out or copy texts into an e-mail, or send commands to external devices (Figure 8).

Likewise, Neuracle -a spinoff startup of Tsinghua University- developed a high-speed brain-controlled keyboards using WearableSensing's DSI24 headset (Figure 9), which has achieved high spelling rates up to 60 characters (~12 words) per minute (Chen et al., 2015).

Other companies offering diverse EEG solutions for medical applications are listed below (Table 1). The list ranks several hardware companies according to their number of publications, as found from Google Scholar. While it is not an exhaustive list, it represents an overview of some of the most important key players.

## Neuroergonomics and Smart Environments

The use of EEG is also widely extended ( $N = 41$ ) for the design of safer and more efficient operational environments in relation to neuroscience principles (Karwowski et al., 2003). This area of research has been called neuroergonomics (Parasuraman, 2003) and it is applicable to different contexts of usage.

One of the most attractive applications of neuroergonomics are smart environments. As a consequence of the progress in sensors and information technology, it has been identified



**FIGURE 9 |** Neuracle's brain-controlled keyboard using DSI24 headset. Reprinted from DSI 24 Dry Electrode EEG Headset, by Wearable Sensing (2018), <https://wearablesensing.com/products/dsi-24/>. Copyright 2018, by Wearable Sensing.

**TABLE 1 |** EEG key-players.

Company	Number of publications	Main product
NeuroScan	15.200	"Quick Caps" headsets up to 256 electrodes
BioSemi	8.800	"HeadCap" headset up to 256 channels
Brain products	6.690	"BrainCap" headsets up to 160 channels
g.tec	6.260	"g.Nautilus" headset 64 channels
EGI	5.000	"Geodesic EEG System 400" up to 256 sensors

that the feasibility of these environments is being gradually consolidated (Kameas and Calemis, 2010; Kosmyna et al., 2016). This new paradigm may enable human interaction with digital environments that are sensitive, adaptive, and responsive. In this line, several authors have reported that BCI assistive technologies related to automation and control of ubiquitous devices may have a promising impact on such intelligent settings (Pfurtscheller et al., 2006; Navarro et al., 2011). The next generation of human-compatible systems, powered by EEG-based BCI and ubiquitous computing, may not only help despaired people to regain higher standards of autonomy but may also drive the expansion of the living conditions of people, thus ensuring great comfort along with the intelligent usage of resources (Domingo, 2012; Lee et al., 2013; Corralejo et al., 2014; Kosmyna et al., 2016). Although some authors have reported the difficulty of building EEG systems for smart environments given the current state-of-the-art (Aloise et al., 2011; Su et al., 2011; Mehta and Parasuraman, 2013),

significant initiatives can be found in this field. For instance, BrainAble, an ongoing European Seventh Framework Program (FP7) financed project, aims to develop a multimodal neuronal interface with affective computing and virtual environments to restore and improve functional independence of patients with motor disabilities in their activities of daily living. The project also attempts to connect a human-computer interface with adapted social networks services in order to improve the life quality of the patient (Carmichael and Carmichael, 2014).

Neuroergonomic principles can be also employed in workplace environments. Here, neuroergonomics focuses on designing and controlling physical tasks to ensure that work demands are adapted to the physical, cognitive, and affective capabilities and limitations of the operator (Venthur et al., 2010; Garcia-Molina et al., 2013). Thus, EEG systems can be potentially used for cognitive real-time monitoring of workers mental workload in order to alert them to trigger certain behaviors. In the automotive sector, several studies have investigated the use of EEG during driving simulations for assessing driving performance and inattentiveness, and for detecting needs of emergency brakes before the braking onset (Dong et al., 2011; Karthaus et al., 2018). By doing so, authors have identified that distraction and fatigue are two main sources for driver's inattention, which in turn is considered as a strong cause for most traffic accidents (Dong et al., 2011). Those insights may be useful for technology transfer purposes, which may eventually propel the emergence of new companies as a result of the new advances in neuroergonomics. Deayea, a Chinese Shanghai-based company, is reportedly using EEG sensors in the caps of train drivers on the high-speed rail line between Beijing and Shanghai to monitor their concentrations levels and to identify thoughts of anger, anxiety, and sadness (Figure 10) (Chan, 2018). In the aviation sector, initial steps have also been taken toward assistive technologies for prevention of accidents, particularly in air traffic control and aircraft piloting (Fricke et al., 2014; Aricò et al., 2016; Vecchiato et al., 2016). By expanding these technologies, a new generation of wearables that enhance human performance or fully adapt user interfaces to different environments may be achieved. These wearables could be ultimately used as a tool to prevent the risk of error in operational environments.

Along the same line, advances in neuroergonomics may not only foster EEG solutions in workplace environments but also in the vast consumer markets. As EEG enables the identification of attention levels while doing a certain task, the future of driving could be disrupted. For instance, Nissan is developing a way to help drivers execute evasive maneuvers faster by using EEG technology. The project, called Brain-to-Vehicle, attempts to recognize the mental and emotional states of the driver in order to help semi-autonomous cars begin evasive actions between 0.2 and 0.5 s faster. Although it is at the moment in the experimental phase, it aims to develop practical applications within 5 to 10 years (O'Kane, 2018).

## Self-Regulation

A growing body of evidence ( $N = 26$ ) indicates that self-regulation through tracking devices plays an important role



**FIGURE 10 |** Deayea's driver headsets. Reprinted from Smart headset, by Shanghai Diyi Technology Co., Ltd. (2018), [http://www.deayea.cn/page98?product\\_id=4](http://www.deayea.cn/page98?product_id=4). Copyright 2018, by Shanghai Diyi Technology Co., Ltd.

in the voluntary control of mental and physiological processes (Lomas et al., 2015; Tang et al., 2015). In this manner, self-regulation through EEG has been claimed to be beneficial for wellbeing and emotional balance, especially in mindfulness meditation (Lutz et al., 2006, 2008; Rodina et al., 2017). Thanks to its efficacy as a brain activity tracking tool device, EEG is experiencing a steady growth in these kinds of market applications. Its most paradigmatic uses are being developed for meditation, focus, and sleep purposes.

In the meditation sector, the Canadian company InteraXon launched in 2014 the wearable headset Muse (Li et al., 2015), which measures user's brain activity and converts the EEG signal into audio feedback that is fed to the user via headphones, thus guiding the user during the whole meditation process (Figure 11). Muse also tracks users' progress and sets goals to keep them motivated.

Further, for focus purposes, the company Melon, which was crowdfunded in 2011 in Kickstarter, has developed an algorithm which identifies the attention levels of the user in relation to its activities and behaviors (Melon, 2016). By doing so, they aim to develop a neural tracking tool solution to improve user's productivity (Figure 12).

In the sleep sector, smart sleeping masks have been developed to improve the sleeping habits of consumers. Companies such as Entertech and Neuroon use these masks to track neural activity while napping (Figure 13). For instance, Entertech's mask Lunna recognizes rhythmic activities in the alpha range during the drowsiness period at sleep onset and in the rapid eye movement (REM) sleep stage in order to wake users up in the light sleep, thus preventing post naps to cloud the user's day (Lunna, 2018).

## Games and Entertainment

Games and entertainment are industries which will benefit extraordinarily from the deployment of portable and ergonomic EEG. In the academic sphere, the literature shows that most games and entertainment applications focus on multi-dimensional control using motor imagery-based EEG systems in virtual environments or in three-dimensional physical space ( $N = 25$ ). In virtual environment games, most research has concentrated on classification performances and user experience (Doud et al., 2011; Bonnet et al., 2013). Hence, Bonnet et al. created a multi-user game called BrainArena in which two users



**FIGURE 11 |** Muse's headband. Reprinted from Muse: the brain sensing headband, by Amazon (2018), <https://www.amazon.com/Muse-Brain-Sensing-Headband-Black/dp/B00LOQR37C>. Copyright 2018, by Muse.



**FIGURE 12 |** Melon's headband. Reprinted from Gadgets to help you relax in the new year, by ZDNET (2016), <https://www.zdnet.com/pictures/8-gadgets-to-help-you-relax-in-the-new-year/5/>. Copyright 2016, by Melon.

play football by means of EEG-based BCI (Bonnet et al., 2013). In three-dimensional physical space, LaFleur et al. presented a novel experiment of EEG-based BCI controlling a robotic quadcopter, which reported high control from remote distances with fast and accurate actuation (LaFleur and Nemec, 2013). In the commercial sphere, American companies such as NeuroSky and Emotiv are leading the industry of games and entertainment. NeuroSky's headset MindWave works with many gaming apps in the NeuroSky store, an in-house digital distribution platform which offers a wide variety of brain-controlled apps (**Figure 14**). One of the most popular games in this platform is BrainCopter, a game that allows users to command a virtual helicopter which should evade oncoming enemies by means of MindWave headset.

In physical space environments, Emotiv's EPOC+ and Insight headsets similarly enable users to control drones remotely (**Figure 15**) (Wang et al., 2018).

Other efforts done in this area focus on making virtual reality environments and video games more immersive by using EEG

as a control input (Lécuyer et al., 2008). In general, experiments conducted in this realm combine the use of different wearables. On the one hand, the user benefits from a virtual reality (VR) video game experience via VR headsets such as Oculus Rift (Doma, 2018). On the other hand, an EEG headset monitors the player's brain activities and digitizes it as a computer input for the VR video game.

Considering the integrative potential of both technologies, manufacturers are starting to incorporate eye-tracking and EEG sensors in the VR headsets to allow brain-controlled portable solutions. One of the most innovative products on the market is the mobile-powered VR headset LooxidLink (**Figure 16**). This wearable, designed by the Korean company Looxid Labs, integrates gold-plated EEG sensor capabilities into the VR components of traditional VR headsets, thus allowing the user to take advantage of the commands in the API to apply EEG into the VR environment. Looxid Labs won the Best of Innovation Award at Consumer Electronic Show 2018 (Jo, 2018).



**FIGURE 13** | Lunna headset. Reprinted from Ivation Luuna Brainwave Brain Sensing Bluetooth Smart Sleep Mask, by Amazon (2018), <https://www.amazon.com/Ivation-Brainwave-Bluetooth-Connection-Technology/dp/B07RYNBTJW>. Copyright 2018, by Entertech.

## Neuromarketing and Advertisement

Neuromarketing is an emerging interdisciplinary field located at the borderline between neuroscience psychology and marketing. The term neuromarketing was initially introduced by Ale Smidts in 2002 and is defined as “the study of the cerebral mechanism to understand the consumer’s behavior in order to improve the marketing strategies” (Boricean, 2009; Stasi et al., 2018). Neuromarketing focuses on assessing consumers’ cognitive and emotional responses to various marketing stimuli (Karmarkar, 2011). To achieve this purpose, neuromarketing studies can be conducted by means of different non-invasive techniques such as fMRI, MEG or PET.

The use of EEG has only recently been adopted in confluence with implicit associations’ test and other biometric techniques, such as eye-tracking, psychophysiological and electrodermal reactivity, or heart and respiratory rate (Calvert and Thensen, 2004; Kenning and Linzmajer, 2011; Morin, 2011). By means of EEG, effectiveness indicators such as emotional engagement, memory retention, awareness, and attention can be measured (Vecchiato et al., 2011; Sebastian, 2014). For instance, EEG evaluation has demonstrated remarkably results for TV commercials, where attention levels have been successfully measured, thus providing researchers with new methods for advertisement evaluation (Vecchiato et al., 2009; Nomura and Mitsukura, 2015; Wang et al., 2016). Several authors have reported that the analysis of these indicators is fundamental to discovering the factors that influence consumers’ purchase decisions (McClure et al., 2004). Also, they may contribute to the better understanding of consumers’ thoughts, emotions, feelings, needs, and motivations, as related to the purchasing process (Lindstrom and Underhill, 2010).

Although EEG is relatively a new consumer neuroscience technique, its application has hastily grown over the past years

( $N = 21$ ) (Plassmann et al., 2012; Smidts et al., 2014). Some of the most important milestones for EEG in the commercial arena include Yahoo’s assessment of consumers’ reactions to television commercials; Hyundai’s measurement of consumer neurological responses when viewing a sports car prototype; and Microsoft’s assessment of the degree of consumer engagement when using an Xbox video game (Flores et al., 2014). According to Plassmann et al., more than 300 companies are currently working worldwide in the field of neuromarketing (Plassmann et al., 2012). Among the vendors of these neuromarketing services are three American-based neuromarketing companies: NeuroFocus, a company absorbed by Nielsen Holdings, working with Hyundai, Google and Walt Disney Co.; EmSense, which counts Microsoft among its customers; and Sands Research, which collaborates with Chevron (Flores et al., 2014).

## Education

In the educational sector, EEG is mainly used to track student performance to improve the learning experience ( $N = 20$ ).

During the learning process, student’s attention and motivation during instruction generally influence the understanding of the contents (Saeed and Zyngier, 2012; Ning-Han et al., 2013). However, traditional teaching methods require teachers to visually detect students’ expressions in order to infer whether they are thoughtfully learning or not. Of course, this method poses a physical burden to the teachers and is not always infallible.

By applying neural technologies to provide instant feedback on the mental levels of students, the shortcomings of traditional teaching methods may be remedied. Several studies have corroborated this approach. For example, the feasibility of collecting useful information about cognitive processing and mental state using portable EEG monitoring devices has been



already assessed by Mostow et al. (2013). Also, the development of visual attention measurement systems based on EEG are under current development (Ko et al., 2017). These findings may set the basis for developing EEG systems capable of estimating the level of cognitive and visual attention during real classroom activities, thus enhancing the learning effectiveness (Corentin and Pascal, 2013).

Teachers may vastly benefit from this technology, which may alleviate their inaccuracy and reduce their burdens in measuring attention levels of learners (Slavin, 2008; Xu and Zhong, 2018).

A representative example of this methodology is Harvard Innovation Lab's incubated BrainCo. BrainCo has developed an EEG headband (FocusEDU) which aims at helping students cultivate efficient and focused habits through neurofeedback training (Figure 17).

By means of its accompanying app, which can be visualized on a tablet or a computer, FocusEDU can also be applied in the classroom to improve educators' teaching methods by tracking students' levels of engagement and attention. In 2017, BrainCo won the Most Innovative Award at the International Society for Technology in Education (ISTE) Conference (Smith, 2017).

## Security and Authentication

The use of EEG data as a biometric trait for security and authentication purposes has experienced a tremendous growth in cryptographic and biometric frameworks ( $N = 20$ ). Although many EEG-based authentication methods have been proposed, they have been roughly divided into two categories depending on the presence or absence of a stimulus. The former comprises both eyes-open/eyes-closed, whereas the latter includes visual evoked potentials, mental tasks, and emotional stimuli (Wu et al., 2018). In general terms, the use of EEG in these fields has been propelled due to the need for data security and authentication in numerous applications such as e-commerce, e-health, e-government, e-voting, or blockchain, among others (Damaševičius et al., 2018). More precisely, in cryptographic frameworks, security systems have shown to be vulnerable to several drawbacks such as simple insecure password, shoulder surfing, theft crime, and cancelable biometrics (Khalifa et al., 2012). One of the main concerns about these vulnerabilities is the absence of connections between verification strategies and the identity of the person (Karthikeyan and Sabarigiri, 2011). Thus, unlike cryptographic based authentication methods, cognitive biometrics can remedy these obstacles as they can uniquely identify a person based upon independent physical or behavioral characteristics (Svogor and Kisasondi, 2012; Ramzan and Shidlovskiy, 2018). Another motivation behind the exploration of bio-signals is that they cannot be casually acquired by external agents and they are present in every living being, which gives them advantages over other biometric-based authentication methods such as iris, fingerprints, face, palm, voice, and gait recognition (Revett et al., 2010). In addition, several studies have reported that cognitive-based biometric systems offer more resistance to spoofing attacks due to the difficulty of synthesizing EEG signals, and they have also tested covert warning messages when authorized users are in a condition of external forcing (Su et al., 2012).



**FIGURE 14 |** MindWave headset. Reprinted from NeuroSky MindWave Mobile BrainWave Starter Kit, by Amazon (2018), <https://www.amazon.in/NeuroSky-MindWave-Mobile-BrainWave-Starter/dp/B00B8BF4EM>. Copyright 2015, by NeuroSky.

As for the accuracy of these systems, research shows that the gamma-band of visually evoked potential signals and the neural network classifier could be used to identify individuals. Here, Palaniappan (Palaniappan, 2004) identified 20 individuals with an average accuracy of 99.06% and Hema et al. (2008) reached an average accuracy of 94.4 to 97.5% on 6 subjects. EEG signals have been also used in user context environments, such as simplified driving simulators, where they have been processed to verify the driver's identity on demand (Nakanishi et al., 2011). Likewise, several types of research have considered the authentication of EEG signals generated from driving behavior as part of smart driving systems. For example, EEG signals could be processed to characterized alcoholic drivers. As indicated by Murata et al., the deployment of these systems may help to prevent fatal incidents (Murata et al., 2011).

In the commercial arena, analysts predict that the global EEG biometrics market is to expand at a compound annual growth rate of 12.37% during the period 2016–2020 (Damaševičius et al., 2018). Meanwhile, efforts have been also made to create open-source authentication communities such as NeurotechX, who is currently developing an EEG biometric authentication system called Brainlock based on N400 (Swaine-Simon, 2017).

## ETHICAL ASPECTS

The review collected sources revealed that ethical issues are also broadly discussed across the literature. It was found that



**FIGURE 15 |** Emotiv EPOC+. Reprinted from Emotiv EPOC+, by EMOTIV (2018), <https://www.emotiv.com/epoc/>. Copyright 2018, by EMOTIV.



**FIGURE 16 |** LooxiiLink headset. Reprinted from Looxii Labs, by Seamless (2018), <https://shiropen.com/2017/09/19/28240/>. Copyright 2018, by Seamless.

ethical aspects may be treated whether as the subject matter of the paper or as a related subsection of an engineering study. Furthermore, it was noted that most of the articles deal with more than one ethical issue in depth and mention several other ethical aspects. The most frequently cited issues include safety and risk-benefit balance ( $N = 33$ ), agency ( $N = 28$ ), identity ( $N = 24$ ), enhancement ( $N = 21$ ), and privacy and data protection ( $N = 15$ ) (Figure 18). Thus, the same depicted order will be observed in this section.

### Safety and Risk-Benefit Balance

Among all the concerns surveyed in the literature, the most commonly cited problems involve the safety of EEG devices and their related balance of risks and benefits ( $N = 33$ ). These dimensions of concern are in accordance with the intrinsic

hazards of any biomedical device. It was also determined that safety and risk-benefit balance mainly refer to their medical and non-medical consequences.

With regards to the medical hazards, authors assert that non-invasive devices may pose serious risks of harm (Tamburrini and Mattia, 2011). Their main concerns relate to the negative side effects in brain plasticity when EEG devices are long term applied in developing children and adults (Tamburrini and Mattia, 2011). They also fear the unknown reversibility of these side-effects if the wearable is removed. However, no conclusive results have been appointed in this area.

Non-medical safety issues are more extensively mentioned and addressed in the literature. In this case, authors suggest that intense training and cognitive concentration could lead to potentially serious harms for EEG users, particularly in

communication and control contexts, where cognitive planning and attention can lead to frustration (Glannon, 2014). Also, the need for regular and challenging training sessions may impose physical, emotional, and financial burdens on the users and their family (Fenton and Alpert, 2008). In addition, as users become increasingly dependent on technology, device failure and errors can similarly place users in dangerous situations (Hildt, 2011). This could endanger the life of its users in specific contexts. For example, an EEG wheelchair failing as its user is crossing a street or an EEG driven car causing an accident could lead to fatal consequences.

Another non-medical concern in this area relates to the vulnerability of commercial applications of BCI. Here, it has been demonstrated that deliberately-designed tiny perturbations templates for target attacks can manipulate EEG-based BCI speller to output anything the attacker wants with high success rate (Zhang et al., 2020). If these attacks may be targeted in other scenarios such as automatic driving, wheelchair control, or exoskeleton control, where the feedback plays an important role and the cost of one step mistake can have a big impact on the user, the security of EEG commercial applications should be reconsidered before deployment.

Since EEG is regarded as an inherently risky technology, which may lead to negative social outcomes, further studies should be conducted to clarify the acceptable expectations of benefit and risk. Nonetheless, several scholars suggest that this analysis may not yet be possible due to scientific uncertainty and lack of validated knowledge (Haselager et al., 2009).

## Agency

Agency is understood by ethicists as the ability of the individual to choose its own actions. The agency problem is frequently discussed by scholars from a two-fold perspective ( $N = 28$ ). On a positive note, assistive technologies could lead to an increased agency via empowerment. On a negative note, the use of BCI could lead to an impairment of self-determination.

As an empowerment tool, several authors concur that EEG assistive technologies will allow patients greater independence (Mercer and Trothen, 2014; Zehr, 2015). This may enable patients to express their thoughts and behaviors, as well as to interact more independently with their environments, thus leading to higher standards of autonomy and human dignity. The increased agency conception acquires a greater significance in life-sustaining care contexts, where the informed consent plays an important role in end-of-life decision making. In this area, Glannon suggests that a weaker threshold version of understanding in decision-making about care would be justified for minimally conscious patients with a higher level of awareness and cognitive function who can clearly express their preferences about life-sustaining care through BCI-mediated binary responses (Glannon, 2016). This posture should be confronted with the general consensus in medical ethics about a high level of understanding for life-sustaining treatment with high probability of death (Drane, 1984; Appelbaum and Grisso, 1988; Jox, 2013; Peterson et al., 2013).

As an impairment tool, the actual threat to the social acceptance of mind-reading technologies lies in their potential

capacity to “understand” consumer decision-making processes. This debate has been extensively addressed by public policy and academia, especially in the field of neuromarketing (Murphy et al., 2008). The scientific community is openly divided between researchers and practitioners who welcome this field (Garcia and Saad, 2008; Perrachione and Perrachione, 2008) and its detractors, including the general media (Blakeslee, 2004; Arussy, 2009). In most cases, the assumptions of these discussions have an economic substrate. As neuroscience and behavioral economics are proving to challenge “rational consumer” theories and their rational spending patterns, new approaches to the importance of marketing and advertising are emerging. In this sense, the use of neuroscience to understand the subconscious minds of consumers and, eventually, to alter their purchase decisions is an ethical concern widely disseminated in the literature (McDowell and Dick, 2013). Some authors believe that by measuring consumer's brain activity and developing effective communication techniques, corporations will be able to discover the “buy button” in consumers' brains. Thereby, they will be able to learn how to better trigger consumers' attention, which may ultimately lead to unprecedented levels of manipulation (Kelly, 1979; Wilson et al., 2008).

## Identity

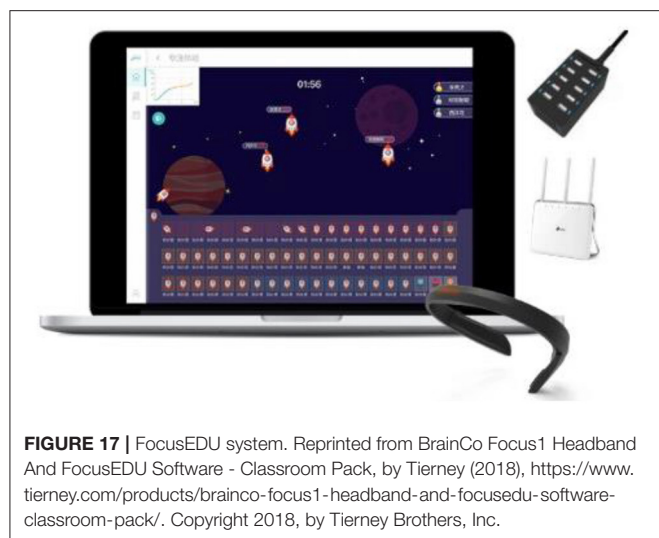
The concept of identity is overarching in the literature as most scholars think that neurotechnologies could clearly disrupt the physical and mental integrity of the individual ( $N = 24$ ).

In essence, the main concerns about identity are raised by invasive BCI. For instance, several studies have reported personality or behavioral changes leading to impulsivity, hypersexuality, mania, and gambling (Agid et al., 2006; Gisquet, 2008; Glannon, 2009). Alienation and estrangement have been also recounted in various treatments, where patients have stated that they “fe[el] like a robot”, “an electric doll” or as if they were under “remote control” (Schüpbach et al., 2006; Goering et al., 2017). However, these changes do not occur in all cases and its origin still remains unclear in the scientific community (Johansson et al., 2014; Goering et al., 2017). As mentioned above, although these statements derive from neurosurgical interventions, the question remains open as to whether similar results could be envisaged when EEG is applied for motor recovery or permanent motor replacement. From what has been identified, there is an absence of preliminary research and pronouncements in this area.

## Enhancement

EEG permits direct communication between brains and computers. In the current state-of-the-art, EEG is clearly in an early stage of development for prediction, diagnosis, and restoration of functions, as previously mentioned in section Commercial Aspects. Notwithstanding, as technology advances, future qualitative leaps could allow superior functional enhancement ( $N = 21$ ) (Hildt, 2011). This progression raises a number of questions about the nature of the human being.

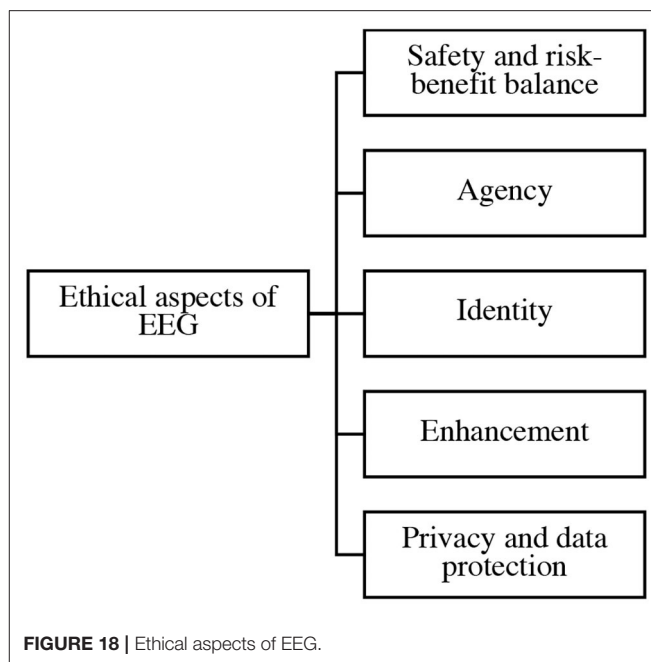
As soon as people begin to incorporate their body schemes with enhancing neurotechnologies, which may allow them



to radically expand their endurance and their sensory and mental capacities, authors like Hildt suggest that the notion of human being could be disrupted (Hildt, 2011). In particular, the extension of human limitations beyond the normal takes the debate on an ethical realm in which BCI users could become “cyborgs.” To this extent, Zehr believes that the development of sophisticated technologies that greatly enhance human intellect and physiology could transform the human condition (Zehr, 2015). As a result, *homo sapiens sapiens* could overcome its limitations and evolve into a *homo sapiens technologicus*, who takes advantage of the technology to improve its functioning (Zehr, 2015). This reassessment of the entire human predicament, as traditionally conceived, has been called “transhumanism” (Bostrom, 2005), and it is likely to change social norms, raise concerns about equitable access, and generate new forms of discrimination (Mercer and Trothen, 2014). Dystopian settings such as a class society, in which humans would coexist with enhanced humans, may come to fruition and create social stratification (Vlek et al., 2012). Likewise, nullifying equal access to resources as a consequence of unequal access to technology can aggravate social competence and unfairness among co-workers, thus generating new forms of discrimination (Kein et al., 2015). Of course, not all authors are convinced that these concerns are exclusive to BCIs or even possible. However, they arise with new vitality by virtue of advanced EEG-based BCI (McGee and Maguire, 2007).

## Privacy and Data Protection

The potential widespread use of EEG wearables raises a final set of issues that cluster around research ethics and the law ( $N = 15$ ). As new ways of connecting to the brain emerge, new potential violations of user privacy might flare up. As enshrined in the General Data Protection Regulation (GDPR), which entered into force in 2018, brain data qualifies as sensitive data, thus triggering higher protection standards than those for personal data. This means that the grounds for processing sensitive data under the



GDPR have become stricter and should comply with higher security standards. The legal basis of these restrictions is found in the greater impact that the misuse of such information could have on the life of the individual. As previously introduced in section Commercial Aspects, EEG devices could reveal a variety of information about the natural person, ranging from health and mental diseases and disorders, to psychological traits and mental states, creating potential problems such as discrimination based on neural information (Vlek et al., 2012). Indeed, some scholars suggest that because the EEG is capable of directly extracting sensitive information from the brain, a subject may be “unaware of the extent of information that is being obtained from his or her brain” (Vlek et al., 2012). Therefore, authors such as Farisco et al. note that in the biomedical sector, informed consent must respect (1) the disclosure of all needed information, (2) the capacity to understand it, and (3) the voluntariness to undergo the treatment (Farisco et al., 2015). In addition, in EEG-based commercial applications, companies and manufacturers must obtain a valid consent of the consumer by providing specific, informed and unambiguous information on the processing of his sensitive data. Some of the data that must be provided according to the GDPR are the identity of the controllers, the purpose of the processing, and the processing activities which may be carried out.

With regards to the processing activities to be carried out, a second privacy-related concern is the management of the extracted information. Here, scientists and the private sector have different interests. On the one side, the purpose of scientists is to uncover the objective truth and bring it among the public. On the other side, companies reluctantly give away their know-how as this is part of a highly competitive environment driven by profit maximization goals (Stanton et al., 2017). At this point, major ethical concerns



arise when it comes to the sharing of this confidential data (Flores et al., 2014). The legislation on privacy and data protection guarantees that the information extracted will be kept confidential in a database, and its results should only be shared on scientific grounds and in an anonymous way to ensure the privacy of the research subject (Slowther and Kleinman, 2009). Failure to maintain the privacy of this sensitive data will be considered a violation of any ethical research practice and should result in the appropriate legal sanctions. Under the current European framework for privacy and data protection, violators can be fined up to 4% of their global turnover, or € 20 million.

Although there have not yet been any major scandals in the European Union regarding the processing and sharing of brainwave datasets, it has been reported fraudulent sharing of scientific research output in the United States. Consumer groups have claimed that Emory University and Baylor School of Medicine violated the Belmont Report's principle of beneficence -which entails an obligation to protect individual subjects against risk of harm and the societal benefits that might be gained from the research- by partnering with neuromarketing companies (Fisher et al., 2010; Pop and Iorga, 2012; Ulman et al., 2015; Stanton et al., 2017). This situation has led to the modification of national legislations worldwide. For instance, France, which faced protests against neuroscience research, banned the use of brain-imaging methods for commercial purposes in 2011. The government argued that the processing of consumer brain signals might constitute an invasion of privacy and they should be solely processed for medical or scientific purposes (Ulman et al., 2015).

Taking all these facts into consideration, privacy and data protection are deemed as extremely important aspects to be considered for a peaceful transition into a BCI society.

## DISCUSSIONS AND CONCLUSIONS

The present scoping review provides a holistic view of EEG-based market applications, as well as identifies the most relevant ethical questions arising from the existing literature. Yet before discussing these issues, several limitations of this study should be considered. Although the study was conducted using different databases, most of the articles found were solely based on biomedical applications of BCI. By the same means, the ethical debate revolving around neural technologies was thus primarily focused on a biomedical approach. We consider that the limited number of articles that evaluated EEG from other non-biomedical research domains hampers the purpose of the present review. In order to draw more precise conclusions about the subject-matter of this study, more research should be conducted from a non-biomedical scope. This may emphasize different ethical connotations and present this technology through alternative methodological lenses. More broadly, we also identified that most of the ethical considerations were asserted in a general BCI context, specially by taking into consideration invasive BCI. Despite the fact that invasive and non-invasive methods might foreseeably share a large number

of identical ethical concerns, more scientific effort should be made on specific non-invasive risks in order to legitimize the discourse surrounding EEG applications. Another limitation of this review is that most of the literature addresses the ethical problems from an advanced technology-based perspective instead of focusing on the present state-of-the-art. Since one of the main duties of ethicists is to anticipate the new scenarios and living conditions implicit in the relentless progress of technology, we are prone to think that this approach may enhance the existing technological capabilities and provide a distorted view of reality. For this reason, we consider that the ethical findings obtained in this review might be treated with a small dose of scientific skepticism. Furthermore, the present review addresses only those issues that were recurrently cited across the coded articles with brief reference of other seldom detected topics. Commercial applications and ethical problems that were rarely cited, though underrepresented in this review, may be just as significant as the categories described above. Despite these limitations, there are several features of the literature sample that can be highlighted here.

## Commercial Aspects

There is no doubt that the overlap of science and markets is inevitable, and EEG has the potential to revolutionize these spaces. As stated, the applications of EEG are wide and can be employed in different sectors and industries. Hitherto, EEG solutions have been mostly explored in the medical sector for prediction and diagnosis of various health conditions, as well as for treatment, rehabilitation and assistance ( $N = 74$ ). They have been used as a rehabilitation tool for motor recovery after spinal cord injury, as spellers for individuals who have no other way to communicate; and as a means to control the environment of people who are locked-in or paralyzed. Other industries in which EEG has been successfully implemented are neuroergonomics, smart tracking devices, video games, neuromarketing, education, and authentication systems, among others. However, before EEG becomes widely accepted as a useful and reliable tool in the commercial sphere, several shortcomings need to be corrected.

First, EEG may be technologically questioned, so it should be treated with a degree of caution given the actual limitations of the current state-of-the-art. Secondly, for EEG technologies to be mass marketed, some breakthroughs must be found. Thirdly, from a cost-benefit standpoint, EEG may not be the best option to invest at the moment due to its minimal commercial viability. Fourth, for EEG to become satisfactory end-products, they should also focus on a user-friendly design.

## Limitations of EEG

Although a considerable amount of experimental evidence supports the notion that EEG techniques can provide relevant insights into the dynamic processes of the brain, authors also point out that their numerous benefits could be questioned (Lopes Da Silva, 2013). Currently, neuroscience research is limited not only by revealing what is occurring in the brain, but also by explaining why it occurs, thus making reliability a difficult aspect to improve. It should be noted that EEG is still a relatively

new technology and further advances should be made before the dynamics of the cognitive processes are completely unraveled.

As far as consumer EEG devices are concerned, they may be additionally distrusted due to several restraints. For instance, Leitão & Campos argue that the number of electrodes on consumer wearables is limited compared to the clinical-grade devices. Also, the electrodes are usually focused on a specific area of the brain and their resolution is lower compared with those of high-clinical density (Leitão and Campos, 2017). Swati et al. discuss that any eye movement, muscular activity or electronic devices in the vicinity of such commercial devices introduce artifacts to the signal that can disrupt the measurement of actual brain waves (Vaid et al., 2015). They also claim that numerous possible features with minimal computation and over-specification are still a key problem when considering recognition performance of the signal (Vaid et al., 2015). Spapé et al. recognize that the validity of classification algorithms for commercial EEG applications cannot be confidently assessed due to brand opacity and trade-secrets (Spapé et al., 2015). Finally, Poldrack suggests that the inferential methods used to study cognitive processes, which may be predictable to some extent, could be unreliable with respect to reverse inference (Poldrack, 2006). This, alongside with the low signal-to-noise ratio (SNR) of consumer consumer-grade devices, questions their validity as reliable neuroscience solutions.

Since EEG should then be regarded with some degree of doubt and the future of this technology is still uncertain, attention and scientific rigor shall be applied when formulating proposals about its future potentials. As several authors have already pointed out, a greater debate should be generated on the real effects of mind-reading technologies in order to prevent the naïve misconceptions that the information media can instill in the general public (Kenning, 2008; Weisberg et al., 2008; Spapé et al., 2015). These false assumptions about the objectivity and trustworthiness of consumer neuroscience solutions visibly magnify their real capacities, which are still far from their forecasts. Indeed, actual consumer-grade devices may well-satisfy consumers, but from a scientific point of view their reliability and effects still remain unclear.

## Technological Breakthroughs

Even if the natural limitations of EEG could be remedied, there still remains the need for technological disruptions to ensure the reliability of the device. As part of this approach, a growing body of evidence shows that EEG is clearly observing an asymptotic trend in the accuracy for cognitive state or intent estimation that converges to a significant error rate of 5–20% depending on the targeted cognitive variable (Makeig et al., 2012). It is possible that this trend may not be significantly curved by the sole action of incremental improvements alone. Disruptive innovations should take place in order to allow for the scaling up of both the amount of integrated information and the amount of offline and online computing (Kurzweil, 2001). For example, such innovations may arrive in the form of better electrophysiological sensor technologies, possibly via extremely high channel-count and signal-to-noise-ratio non-invasive systems. The combination of these systems with sufficient computational resources could

conceivably allow the modeling of brain activity at a range of spatial-temporal scales, as well as considerably reduce measuring errors, as postulated by Vaid et al. (2015). Additionally, to reach this level of information density, safer and more efficient procedures should be developed to enable closer-to-brain source measurements (Liao et al., 2012; Hoodgar et al., 2013). Thus, for EEG wearables to become as useful as computer mice and touch screens, technological breakthroughs are required that exceed the marginal improvements of current information processing techniques. Recent entrepreneurial initiatives are attempting to achieve these goals. In the field of communication and control, Facebook's purpose is to accelerate mobile device communication using non-invasive techniques to reach brain typewriting speeds of 100 words per minute (Strickland, 2017). However, at the present time there is still no pronouncement on the success of this type of initiatives.

## Cost-Benefit Trade-Offs

Aside from the limitations and technological breakthroughs that have been highlighted, another commercial issue that needs to be examined is the economic viability of EEG solutions to become satisfactory consumer-grade devices.

As previously mentioned, the present scoping review has determined that medical applications of EEG represent its most prominent uses. Indeed, EEG has been used as an assistive technology in the biomedical realm by default. The fact that EEG is mostly applied in the medical field and its solutions are primarily targeted at particular users, such as people with motor disabilities and LIS patients, has a high impact on its business prospects. This user population barrier has already been recognized by several authors, who believe that the high specificity of EEG users limits the market niche to which EEG solutions are directed (Nijboer, 2015). Having thus a reduced number of users, the market entry barriers for EEG investment are relatively high, and the expected reimbursement for commercial commitment tends to be low, as suggested by Nijboer (2015). This is the fundamental reason why BCI development is at the moment primarily subsidized by the European Commission (€ 11 million in FP6 and € 34 million in FP7), as its dimensions are not likely to attract the attention of the industry (Nijboer, 2015).

Despite this fact, as EEG-based pBCI applications begin to be deployed for purposes other than traditional aBCI applications, i.e., they start to be used as smart tracking solutions in diverse sectors such as those identified in the literature, their attractiveness could be increased. Consequently, novel EEG applications may expand their initial tailored group to wider user populations, thus increasing investment in EEG.

## User-Friendly Design and Experience

Finally, for EEG to become satisfactory end-products, they should also focus on design for usability. As some authors have stated, most of the current EEG prototypes are evaluated on the basis of speed and accuracy, rather than on usability (Moghimi et al., 2012), and they have argued that EEG engineers should integrate ergonomic factors and human-computer interaction principles into the design of their products (Bos et al., 2010;

Pasqualotto et al., 2012). Here, one of the most critical concerns for EEG wearables is the inconvenience to wear them in large-scale samples for extended periods of time (Xu and Zhong, 2018). If these problems could be solved in the near future, for example, by building more adaptive and portable wearables, EEG would be more widely used. In the same vein, the aesthetics of the device may be as important to users in everyday life, if not more so, than the technology itself. These can be key factors for the success of EEG products and services.

Furthermore, consumer experience is also an issue that has been extensively addressed. At an individual level, the use of EEG in sectors such as self-regulation frequently becomes either boring or frustrating over time (Nafus and Sherman, 2014). When, however, it is elevated to a collaborative level, some authors postulate that better results are achieved (Lupton, 2013). Most likely, the future of EEG-based pBCI lies in collaborative endeavors. Since human beings are inherently social creatures, advanced EEG technologies could foster their interactions. For example, consumers could be empowered and motivated by bringing them into large-scale interactive projects or programs in which users may communicate within the legal constraints. In addition, the user experience may be greatly improved by detecting users' affective states to adapt individual and collaborative features. In this sense, by mobilizing a new generation of EEG headsets focused on user-friendly experience, this technology could be brought on board pervasively (Swan, 2016).

## Ethical Aspects

Overall, the results of this review show that EEG sparks concern over many ethical problems and questions that should be addressed, particularly in the literature of biomedical ethics. It seems that further attention on the social impact of neural technologies in the following fields should be paid.

## Safety and Risk-Benefit Analysis

The most frequently cited problem in the literature concerns safety in medical and non-medical settings ( $N = 33$ ).

In the first case, it has been noted that there is lack of literature handling this concrete ethical problem for non-invasive applications such as EEG. Although there is a predominance of discussion on the potential negative side effects in brain plasticity of EEG wearables, the results are inconclusive and the hazards have not yet been validated. Given that EEG technology is currently being assessed without direct acknowledgment of the above concern, ethicists deliberating on this topic may need to wait until more robust conclusions about the real side effects of long-term uses of EEG devices are presented. Nevertheless, as these devices are easily accessible over the internet and can be expected to be worn ubiquitously in the future, medical hazards remain important issues for which some consideration must be given.

In the second case, non-medical risks, such as frustration, have been broadly mentioned in the literature as problems that justify improvements in EEG wearables. These advances could come in the form of psychologically adaptive EEG. Such devices may interact with user mental states, leading to a reduction in

training frustration and in users' physical and emotional burdens. Several authors have proposed overt adaptive EEGs that would be automatically deactivated when extremely low attention levels are detected or reactivated when the user's attention has returned (Fairclough, 2009). It has also been suggested the development covert adaptive devices which would autonomously modify their classification algorithm to adapt to changes in the users' mental states (Fairclough, 2009). This would allow more sensible and dynamic wearables as well as an increase of user experience. Device failure and algorithmic vulnerability are also critical issues highlighted by several authors. In these cases, we expect improvements to arrive as soon as technological breakthroughs appear, which allow EEG processing capabilities to be more robust and precise as well as more cybersecure.

Since safety is thus a critical issue, more extensive high-level discussions should be held on the relative risks and benefits of EEG devices. These discussions should highlight the importance of elaborating risk-benefit assessments by comparing EEG solutions with alternative assistive technologies, as stated by some authors (Tamburrini, 2014).

## Agency

There are a remarkable number of articles in the literature dealing with the ethical implications of agency through the use of neural technologies ( $N = 28$ ). Here, the main highlighted issues were related to the increased/decreased agency, as mentioned above.

Regarding the positive effects of EEG, authors suggest that the possibility of increased agency via EEG assistive applications is one the most important benefits of this technology. Here, the empowerment of functionally diverse individuals has been extensively addressed, and there is agreement about the decrease of social stigma that neural technologies may lead to. As neural technologies start being included in patients and consumers daily-life activities, they may enhance their lost agency capacity as well as return them the necessary confidence to autonomously interact with their environment. This can be of great relevance in contexts where patients' autonomous decision-making may enable them to achieve higher standards of living and dignity, especially in end-of-life situations. Regarding the negative effects, it has been identified that the incorporation of EEG technologies into the body-schemes of consumers could lead to several downsides, such as new forms of manipulation which may limit user's agency.

Bearing in mind the trade-offs of EEG, the key issue that remains to be identified is patient's preferences. It is essential to balance the interference and support of EEG systems in the user's daily activities. Thus, it could be possible that users may be willing to sacrifice some level of exposure in favor of having a greater capacity to do what they want to do or not. Understanding what would count as a reasonable balance for the user must be part of the design process, and it might seem that a system that offers options to the user would be preferable (Gilbert, 2015; Hoppe et al., 2015). This may have a profound impact on the incorporation of EEG assistive tools into the "body schemas" (Heersmink, 2013) and "structures of decision-making and acting" of patients (Clausen, 2008), as well as on the deployment of EEG in the consumer markets. In any case,

the practical implications of the agency debate are of the utmost importance, as they could challenge the social acceptance of this technology.

## Identity

In contrast to the agency issue, the identity problem has been less extensively validated through the literature. Notwithstanding, there are still a notable number of articles in the literature dealing with the ethical implications of identity ( $N = 24$ ). These concerns are eminently raised in invasive contexts of use. Here, more empirical research should be conducted in the area of non-invasive devices in order to draw well-founded conclusions. Beyond this preliminary debate, it should be further examined whether these types of changes should be understood as threats to identity *per se* or as simple alterations that may be beneficial or detrimental to the individual (Schermer, 2009; Baylis, 2013). To this extent, some scholars have already pointed out that the interpretation of the concept of identity as something fixed or mutable over time constitutes the premise of this debate (Goering et al., 2017). Therefore, a broader debate about the concept of identity should be conducted, as well as it should be evaluated *ex ante* whether or not these changes in personal identity may be a real problem that could have an impact on technological development and access to EEG.

## Enhancement

Enhancement through neural technologies poses several concerns as identified in the literature ( $N = 21$ ). We consider that these propositions should be treated from a broad perspective and, in any case, as long-term assumptions. Indeed, research shows that the technology stage is still premature to perceive the ethical implications of augmentation as present real-life problems. What should be noted is that public engagement, ethical deliberation, and legal frameworks shall be developed in order to accomplish a peaceful transition toward ubiquitous EEG. Since the ultimate goal of scientific research is social welfare, the deployment of neural technologies should obey the ethical and legal standards agreed upon by society. Therefore, involving the public in the debate and discussion on new emerging technologies is an essential requirement for this transition. Particularly, actions should be undertaken to inform, educate, and shape public policy regarding the use of neural technologies. As Heidegger indicates, the key to transitioning to a future of greater human-technology integration in an empowering manner is to consider the public opinion and tolerance, as well as to maintain “the right relationship with technology” (Heidegger, 1997). This relationship is an interaction in which technology enables but does not enslave.

## Privacy and Data Protection

Lastly, the findings of this review indicate that with the deployment of EEG wearables as consumer-grade devices, large amounts of sensitive data about the data subject will be collected

and processed ( $N = 15$ ). Consequently, private and public entities shall ensure transparency in relation to the processing of these pieces of data, as well as the appropriate security and confidentiality of the personal data relating to the data subjects. In addition, institutions shall stay updated to avoid any possible data breaches, and develop strong cyber hygiene practices and secure products. For example, communications between wearable sensors and processing or storage units shall be based on encrypted protocols to ensure appropriate security levels. Likewise, firewalls and domain name server-based security solutions should be kept updated to prevent unauthorized access and protect devices when they are exposed in everyday contexts.

On the other hand, any entity that keeps sensitive information will have to engage with industry and government standard's bodies to establish and steward technology norms as features. This would entail safe and secure processes, including a consent procedure that clearly specifies who will use the data, for what purposes and for how long. Consumers and patients should be assured that information and results concerning them will be kept confidential in a database, and that results shall be shared only on scientific grounds and anonymously to maintain their privacy rights.

## DATA AVAILABILITY STATEMENT

The original contributions presented in the study are included in the article/**Supplementary Material**, further inquiries can be directed to the corresponding author/s.

## AUTHOR'S NOTE

Certain legal implications of SECTION IV, *D. Privacy and data protection*, were not part of the scoping review and are provided for explanatory purposes only.

## AUTHOR CONTRIBUTIONS

CF made the literature review and wrote the paper. GL edited the paper. DZ is the supervisor, who conceived this study and edited the paper. All authors contributed to the article and approved the submitted version.

## FUNDING

This work was supported by the National Natural Science Foundation of China under Grant Nos. 61761166006 and 91848112.

## SUPPLEMENTARY MATERIAL

The Supplementary Material for this article can be found online at: <https://www.frontiersin.org/articles/10.3389/fnins.2020.611130/full#supplementary-material>



## REFERENCES

- Abdulkader, S. N., Atia, A., and Mostafa, M. S. M. (2015). Brain computer interfacing: applications and challenges. *Egypt. Inform. J.* 16, 213–230. doi: 10.1016/j.eij.2015.06.002
- Agid, Y., Schnupbach, M., Gargiulo, M., Mallet, L., Houeto, J. L., Behar, C., et al. (2006). Neurosurgery in Parkinson's disease: the doctor is happy, the patient less so? *J. Neural Transmission* 70, 409–14. doi: 10.1007/978-3-211-45295-0\_61
- Akçakaya, M., Peters, B., Moghadamfalahi, M., Mooney, A., Orhan, U., and Oken, B. (2014). Noninvasive brain-computer interfaces for augmentative and alternative communication. *IEEE Rev. Biomed. Eng.* 7, 31–49. doi: 10.1109/RBME.2013.2295097
- Aloise, F., Schettini, F., Aricò, P., Salinari, S., Guger, C., Rinsma, J., et al. (2011). Asynchronous P300-based brain-computer interface to control a virtual environment: initial tests on end users. *Clin. EEG Neurosci.* 42, 219–24. doi: 10.1177/155005941104200406
- Ang, K., Guan, C. K., Sui Geok Chua, K., Ang, B., and Kuah, C. (2010). "Clinical study of neurorehabilitation in stroke using EEG-based motor imagery brain-computer interface with robotic feedback," in *2010 Annual International Conference of the IEEE Engineering in Medicine and Biology* (Buenos Aires), 5549–5552. doi: 10.1109/IEMBS.2010.5626782
- Appelbaum, P. S., and Grisso, T. (1988). Assessing patients' capacities to consent to treatment. *N. Engl. J. Med.* 319, 1635–1638. doi: 10.1056/NEJM19881223192504
- Aricò, P., Borghini, G., Di Flumeri, G., Colosimo, A., Bonelli, S., Golfetti, A., et al. (2016). Adaptive automation triggered by EEG-based mental workload index: a passive brain-computer interface application in realistic air traffic control environment. *Front. Hum. Neurosci.* 10:539. doi: 10.3389/fnhum.2016.00539
- Aricò, P., Borghini, G., Flumeri, G. D., Bonelli, S., Golfetti, A., Graziani, I., et al. (2017). Human factors and neurophysiological metrics in air traffic control: a critical review. *IEEE Rev. Biomed. Eng.* 10, 250–263. doi: 10.1109/RBME.2017.2694142
- Aricò, P., Borghini, G., Flumeri, G. D., Sciaraffa, N., and Babiloni, F. (2018). Passive BCI beyond the lab: current trends and future directions. *Inst. Phys. Eng. Med.* 39:08TR02. doi: 10.1088/1361-6579/aad57e
- Arksey, H., and O'Malley, L. (2005). Scoping studies: towards a methodological framework. *Int. J. Soc. Res. Methodol.* 8, 19–32. doi: 10.1080/1364557032000119616
- Arussy, L. (2009). Neuromarketing is not marketing. *CRM Mag.* 13:12.
- Baylis, F. (2013). 'I am who I am': on the perceived threats to personal identity from deep brain stimulation. *Neuroethics* 6, 513–526. doi: 10.1007/s12152-011-9137-1
- Birbaumer, N., and Cohen, L. (2007). Brain-computer interfaces: communication and restoration of movement in paralysis. *J. Physiol.* 579, 621–36. doi: 10.1113/jphysiol.2006.125633
- Birbaumer, N., Gallegos-Ayala, G., Wildgruber, M., Silvoni, S., and Soekadar, S. (2014). Direct brain control and communication in paralysis. *Brain Topogr.* 27, 4–11. doi: 10.1007/s10548-013-0282-1
- Blakeslee, S. (2004). If you have a buy button in your brain, what pushes it? *New York Times*.
- Blankertz, B., Acqualagna, L., Dähne, S., Haufe, S., Schultze-Kraft, M., Sturm, I., et al. (2016). The berlin brain-computer interface: progress beyond communication and control. *Front. Neurosci.* 10:530. doi: 10.3389/fnins.2016.00530
- Bonnet, L., Lotte, F., and Lecuyer, A. (2013). Two brains one game: design and evaluation of a multi-user bci video game based on motor imagery. *IEEE Trans. Comput. Intell. AI Games* 5, 185–198. doi: 10.1109/TCAIG.2012.2237173
- Boriceanu, V. (2009). *Brief History of Neuromarketing 14–15th*. Bucharest: ICEA–FAA. 119p.
- Bos, D. P. O., Reuderink, B., van de Laar, B., Gürkök, H., Mühl, C., Poel, M., et al. (2010). "Human-computer interaction for BCI games: usability and user experience," in *2010 International Conference on Cyberworlds (CW)*, (IEEE: Singapore). doi: 10.1109/CW.2010.22
- Bostrom, N. (2005). A history of transhumanist thought. *J. Evol. Technol.* 14, 1–30. doi: 10.5840/jpr\_2005\_26
- Brumberg, J., Nieto-Castanon, A., Kennedy, P. R., and Guenther, F. (2010). Brain-computer interfaces for speech communication. *Speech Commun.* 52, 367–79. doi: 10.1016/j.specom.2010.01.001
- Burwell, S., Sample, M., and Eric, R. (2017). Ethical aspects of brain computer interfaces: a scoping review. *BMC Med Ethics* 18:60. doi: 10.1186/s12910-017-0220-y
- Calvert, G., and Thensen, T. (2004). Multisensory integration: methodological approaches and emerging principles in the human brain. *J. Psychol.* 98, 191–205. doi: 10.1016/j.jphysparis.2004.03.018
- Carmichael, C., and Carmichael, P. (2014). BNCI systems as a potential assistive technology: ethical issues and participatory research in the BrainAble project. *Disabil. Rehabil. Assist. Technol.* 9, 41–47. doi: 10.3109/17483107.2013.867372
- Chan, T. F. (2018). *China is Monitoring Employees' Brain Waves and Emotions*. New York, NY: Business Insider.
- Chen, X., Wang, Y., Nakanishi, M., Gao, X., Jung, T. P., and Gao, S. (2015). High-speed spelling with a noninvasive brain-computer interface. *Proc. Natl. Acad. Sci. U.S.A.* 112, E6058–E6067. doi: 10.1073/pnas.1508080112
- Clarke, A. R., Barry, R. J., Dupuy, F. E., Heckel, L. D., McCarthy, R., and Selikowitz, M. (2011). Behavioural differences between EEG-defined subgroups of children with attention-deficit/hyperactivity disorder. *Clin. Neurophysiol.* 122, 1333–1341. doi: 10.1016/j.clinph.2010.12.038
- Clausen, J. (2008). Moving minds: ethical aspects of neural motor prostheses. *Biotechnol. J.* 3, 1493–1501. doi: 10.1002/biot.200800244
- Comani, S., Schinaia, L., Tamburro, G., Velluto, L., Sorbi, S., Conforto, S., et al. (2015). "Assessing neuro-motor recovery in a stroke survivor with high-resolution EEG, robotics and Virtual Reality," in *2015 37th Annual International Conference of the IEEE Engineering in Medicine and Biology Society (EMBC)* (Milan), 3925–3928. doi: 10.1109/EMBC.2015.7319252
- Corentin, G., and Pascal, H. (2013). Apports de l'électroencéphalographie à la compréhension de la mémoire. *Rev. Neuropsychol.* 5, 243–254. doi: 10.1684/nrp.2013.0280
- Corralejo, R., Nicolas-Alonso, L., Alvarez, D., and Hornero, R. (2014). P300-based braincomputer interface aimed at operating electronic devices at home for severely disabled people. *Med. Biol. Eng. Comput.* 52, 861–872. doi: 10.1007/s11517-014-1191-5
- Damaševičius, R., Maskeliunas, R., and Wozniak, M. (2018). Combining cryptography with EEG biometrics. *Comput. Intell. Neurosci.* 2018:1867548. doi: 10.1155/2018/1867548
- Daudt, H. M. L., van Mossel, C., and Scott, S. J. (2013). Enhancing the scoping study methodology: a large, inter-professional team's experience with arksey and O'Malley's framework. *BMC Med. Res. Methodol.* 13:48. doi: 10.1186/1471-2288-13-48
- Doma, O. O. (2018). "EEG as an input for virtual reality," in *Encyclopedia of Computer Graphics and Games*, ed. N. Lee (Springer). doi: 10.1007/978-3-319-08234-9\_176-1
- Domingo, M. (2012). An overview of the internet of things for people with disabilities. *J. Netw. Comput. Appl.* 35, 584–96. doi: 10.1016/j.jnca.2011.10.015
- Dong, Y., Hu, Z., Uchimura, K., and Murayama, N. (2011). Driver inattention monitoring system for intelligent vehicles: a review. *Intell. Transport Syst. IEEE Trans.* 12, 596–614. doi: 10.1109/TITS.2010.2092770
- Doud, A. J., Lucas, J. P., Pisansky, M. T., and He, B. (2011). Continuous three-dimensional control of a virtual helicopter using a motor imagery based brain-computer interface. *PLoS ONE* 6:e26322. doi: 10.1371/journal.pone.0026322
- Drane, J. (1984). Competency to give informed consent: a model for making clinical assessments. *JAMA* 252, 925–927. doi: 10.1001/jama.1984.03350070043021
- Enriquez-Geppert, S., Huster, R. J., and Herrmann, C. S. (2017). EEG-neurofeedback as a tool to modulate cognition and behavior: a review tutorial. *Front. Hum. Neurosci.* 11:51. doi: 10.3389/fnhum.2017.00051
- Fabio, R. A., Billeci, L., Crifaci, G., Troise, E., Tortorella, G., and Pioggia, G. (2016). Cognitive training modifies frequency EEG bands and neuropsychological measures in rett syndrome. *Res. Dev. Disabil.* 53–54, 73–85. doi: 10.1016/j.ridd.2016.01.009
- Fairclough, S. H. (2009). Fundamentals of physiological computing. *Interact. Comput.* 21, 133–145. doi: 10.1016/j.intcom.2008.10.011
- Farisco, M., Laureys, S., Evers, K. (2015). "Externalization of consciousness. Scientific possibilities and clinical implications," in *Ethical Issues in Behavioral Neuroscience. Current Topics in Behavioral Neurosciences*, Vol. 19, eds G. Lee, J. Illes, and F. Ohl (Berlin; Heidelberg: Springer). doi: 10.1007/97854\_2014\_338

- Fazel-Rezai, R., Allison, B. Z., Guger, C., Sellers, E. W., Kleih, S. C., and Kübler, A. (2012). P300 brain computer interface: current challenges and emerging trends. *Front. Neuroeng.* 5:14. doi: 10.3389/fneng.2012.00014
- Fenton, A., and Alpert, S. (2008). Extending our view on using BCIs for locked-in syndrome. *Neuroethics* 1, 119–32. doi: 10.1007/s12152-008-9014-8
- Fisher, C., Chin, L., and Klitzman, R. (2010). Defining neuromarketing: practices and professional challenges. *Harvard Rev. Psychiatry* 18, 230–237. doi: 10.3109/10673229.2010.496623
- Flores, J., Baruca, A., and Saldivar, R. (2014). Is neuromarketing ethical? Consumers say yes. Consumers say no. *J. Legal Ethical Regul.* 17, 77–91.
- Fricke, T., Zander, T. O., Gramann, K., Holzapfel, F. (2014). First Pilot- in-the-loop Experiments on Brain Control of Horizontal Aircraft Motion, in *Deutscher Luft- und Raumfahrtkongress*. Augsburg.
- García Bellón, M., and Soria Bretones, C. (2013). Electroencefalografía en cuidados críticos. *Revista Electrón. Anestesia* 5:3. doi: 10.30445/rear.v5i2.284
- García, J. R., and Saad, G. (2008). Evolutionary neuromarketing: darwinizing the neuroimaging paradigm for consumer behavior. *J. Consum. Behav.* 7, 397–414. doi: 10.1002/cb.259
- García-Molina, G., Tsoneva, T., and Nijholt, A. (2013). Emotional braincomputer interfaces. *Int. J. Auton. Adapt. Commun. Syst.* 6, 9–25. doi: 10.1504/IJAACS.2013.050687
- Gilbert, F. (2015). A threat to autonomy? The intrusion of predictive brain implants. *AJOB Neurosci.* 6, 4–11. doi: 10.1080/21507740.2015.1076087
- Gisquet, E. (2008). Cerebral implants and Parkinson's disease: a unique form of biographical disruption? *Soc. Sci. Med.* 67, 1847–1851. doi: 10.1016/j.socscimed.2008.09.026
- Glannon, W. (2009). Stimulating brains, altering minds. *J. Med. Ethics* 35, 289–292. doi: 10.1136/jme.2008.027789
- Glannon, W. (2014). Neuromodulation, agency and autonomy. *Brain Topogr.* 27, 46–54. doi: 10.1007/s10548-012-0269-3
- Glannon, W. (2016). Brain-computer interfaces in end-of-life decision-making. *J. Brain Comput. Interfaces* 3, 133–139. doi: 10.1080/2326263X.2016.1207496
- Goering, S., Klein, E., Dougherty, D. D., and Widge, A. S. (2017). Staying in the loop: relational agency and identity in next-generation DBS for psychiatry. *AJOB Neurosci.* 8, 59–70. doi: 10.1080/21507740.2017.1320320
- Gola, M., Magnuski, M., Szumska, I., and Wrobel, A. (2013). EEG beta band activity is related to attention and attentional deficits in the visual performance of elderly subjects. *Int. J. Psychophysiol.* 89, 334–341. doi: 10.1016/j.ijpsycho.2013.05.007
- Guger, C., Spataro, R., Pellas, F., Allison, B. Z., Heilinger, A., Ortner, R., et al. (2018). Assessing command-following and communication with vibro-tactile P300 brain-computer interface tools in patients with unresponsive wakefulness syndrome. *Front. Neurosci.* 12:423. doi: 10.3389/fnins.2018.00423
- Hanley, D., Pritchep, L. S., Bazarian, J., Huff, J. S., Naunheim, R., Garrett, J., et al. (2017). Emergency department triage of traumatic head injury using a brain electrical activity biomarker: a multisite prospective observational validation trial. *Acad. Emerg. Med.* 24, 617–627. doi: 10.1111/ace.13175
- Haselager, P., Vlek, R., Hill, J., and Nijboer, F. (2009). Note on ethical aspects of BCI. *Neural Netw.* 22, 1352–1357. doi: 10.1016/j.neunet.2009.06.046
- Heersmink, R. (2013). Embodied tools, cognitive tools and brain-computer interfaces. *Neuroethics* 6, 207–219. doi: 10.1007/s12152-011-9136-2
- Heidegger, M. (1997). *Question Concerning Technology, Other Essays*. New York, NY: Harper Torchbooks.
- Hema, C. R., Pulraj, M. P., and Kaur, H. (2008). “Brain signatures: a modality for biometric authentication,” in *2008 International Conference on Electronic Design*, (Penang) 1–4. doi: 10.1109/ICED.2008.4786753
- Hildt, E. (2011). Brain-computer interaction and medical access to the brain: individual, social and ethical implications. *Sci. Eng. Ethics* 4, 2326–2621. doi: 10.2202/1941-6008.1143
- Hinchliffe, T. (2018). *MJN Neuroserveis Raises €750,000 to Roll Out Device Predicting Epileptic Seizures*. Available online at: <https://novobrief.com/predicting-epileptic-seizures/6097/> (accessed December 15, 2018).
- Hoodgar, M., Mehrani, M., Mehranzade, A., and Forootan, F. (2013). Proposing an effective feature extraction model for eeg signals to enhance quality of hand's motion detection. *J. Acad. Appl. Stud.* 3, 1–19.
- Hoppe, C., Feldmann, M., Blachut, B., Surges, B. R., Elger, C. E., and Helmstaedter, C. (2015). Novel techniques for automated seizure registration: patients' wants and needs. *Epilepsy Behav.* 52, 1–7. doi: 10.1016/j.yebeh.2015.08.006
- Houmani, N., Vialatte, F., Gallego-Jutglà, E., Gérard, D., Vi-Huong, N.-M., Jean, M., et al. (2018). Diagnosis of Alzheimer's disease with electroencephalography in a differential framework. *PLoS ONE* 13:e0193607. doi: 10.1371/journal.pone.0193607
- Jackson, A., and Bolger, D. (2014). The neurophysiological bases of EEG and EEG measurement: a review for the rest of us. *Psychophysiology* 51, 1061–1071. doi: 10.1111/psyp.12283
- Jaeseung, J. (2004). EEG dynamics in patients with Alzheimer's disease. *Clin. Neurophysiol.* 115, 7, 1490–1505. doi: 10.1016/j.clinph.2004.01.001
- Jo, A. (2018). Looxid Labs Wins a CES. *Best of Innovation Awards in Virtual Reality*. New York, NY: Business Insider.
- Johansson, V., Garwicz, M., Kanje, M., Halldenius, L., and Schouenborg, J. (2014). Thinking ahead on deep brain stimulation: an analysis of the ethical implications of a developing technology. *AJOB Neurosci.* 5, 24–33. doi: 10.1080/21507740.2013.863243
- Jox, R. (2013). Interface cannot replace interlocution: why the reductionist concept of neuroimaging-based capacity determination fails. *AJOB Neurosci.* 4, 15–17. doi: 10.1080/21507740.2013.827279
- Kameas, A., and Calemis, I. (2010). “Pervasive systems in health care,” in *Handbook of Ambient Intelligence and Smart Environments*, eds H. Nakashima, H. Aghajan, and J. C. Augusto (Boston, MA: Springer). doi: 10.1007/978-0-387-93808-0\_12
- Karmarkar, U. R. (2011). Note on neuromarketing. *Harvard Bus. Sch. Market. Unit Case*. 512–031.
- Karthus, M., Wascher, E., and Getzmann, S. (2018). Proactive vs. reactive car driving: EEG evidence for different driving strategies of older drivers. *PLoS ONE* 13:e0191500. doi: 10.1371/journal.pone.0191500
- Karthikeyan, D., and Sabarigiri, B. (2011). Enhancement of multi-modal biometric authentication based on iris and brain neuro image coding. *Int. J. Biometr. Bioinform.* 5, 249–56.
- Karwowski, W., Siemionow, W., and Gielo-Perczak, K. (2003). Physical neuroergonomics: the human brain in control of physical work activities. *Theor. Issues Ergon. Sci.* 4, 175–199. doi: 10.1080/1463922021000032339
- Kein, E., Brown, T., Sample, M., Truitt, A., and Goering, S. (2015). Engineering the brain: ethical issues and the introduction of neural devices. *Hast. Cent. Re* 45, 26–35. doi: 10.1002/hast.515
- Kelly, S. (1979). Subliminal embeds in print advertising: a challenge to advertising ethics. *J. Advertising* 8, 20–24. doi: 10.1080/00913367.1979.10673284
- Kenning, P. (2008). What advertisers can do and cannot do with neuroscience. *J. Advertising Int.* 27, 472–473.
- Kenning, P., and Linzmajer, M. (2011). Consumer neuroscience: an overview of an emerging discipline with implications for consumer policy. *J. Verbrauchers. Lebensmittelsicherheit* 6, 111–125. doi: 10.1007/s00003-010-0652-5
- Khalifa, W., Salem, A., Roushdy, M., and Revett, K. (2012). “A survey of EEG based user authentication schemes,” in *8th International Conference Informatics and Systems* (Cairo: INFOS).
- Ko, L.-W., Komarov, O., Hairston, W. D., Jung, T., and Lin, C.-T. (2017). Sustained attention in real classroom settings: an EEG study. *Front. Hum. Neurosci.* 11:388. doi: 10.3389/fnhum.2017.00388
- Kober, S. E., Schweiger, D., Witte, M., Reichert, J. L., Grieshofer, P., Neuper, C., et al. (2015). Specific effects of EEG based neurofeedback training on memory functions in post-stroke victims. *J. NeuroEng. Rehabil.* 12:107. doi: 10.1186/s12984-015-0105-6
- Kosmyna, N., Tarpin-Bernard, F., Bonnefond, N., and Rivet, B. (2016). Feasibility of BCI control in a realistic smart home environment. *Front. Hum. Neurosci.* 10:416. doi: 10.3389/fnhum.2016.00416
- Kupfer, D. J., Foster, F. G., Coble, P., McPartland, R. J., and Ulrich, R. F. (1978). The application of EEG sleep for the differential diagnosis of affective disorders. *Am. J. Psychiatry* 135, 69–74. doi: 10.1176/ajp.135.1.69
- Kurzweil, R. (2001). *The Law of Accelerating Returns, Kurzweil Accelerating Intelligence*. Available online at: <https://www.kurzweilai.net/the-law-of-accelerating-returns> (accessed November 20, 2018).
- LaFleur, K. M., and Nemec, E. C. 2nd. (2013). Quadcopter control in three-dimensional space using a noninvasive motor imagery-based brain-computer interface. *J. Neural. Eng.* 10:e046003. doi: 10.1088/1741-2560/10/4/046003
- Lazar, E. A. (2018). Improving the performance of empirical mode decomposition via Tsallis entropy: application to Alzheimer EEG analysis. *Biomed. Mater. Eng.* 29, 551–566. doi: 10.3233/BME-181008

- Lécuyer, A., Lotte, F., Reilly, R. B., Leeb, R., Hirose, M., and Slater, M. (2008). Brain-computer interfaces, virtual reality, and videogames. *Computer* 41, 66–72. doi: 10.1109/MC.2008.410
- Lee, W. T., Nisar, H., Malik, A. S., and Yeap, K. H. (2013). “A brain computer interface for smart home control,” in *2013 IEEE 17th International Symposium on Consumer Electronics (ISCE)* (Zhubei: Sheraton Hsin-Chu).
- Leitão, J., and Campos, T. (2017). “Muse headband: measuring tool or a collaborative gadget?,” in *Studies on Entrepreneurship, Structural Change and Industrial Dynamics* (New York, NY: Springer).
- Levac, D., Colquhoun, H., and O'Brien, K. (2010). Scoping studies: advancing the methodology. *Implement Sci.* 5:69. doi: 10.1186/1748-5908-5-69
- Li, Z., Xu, J., and Zhu, T. (2015). Recognition of Brain Waves of Left and Right Hand Movement Imagery with Portable Electroencephalographs, *CoRR*, abs/1509.08257.
- Liao, L.-D., Lin, C.-T., McDowell, K., Wickenden, A. E., Gramann, K., Jung, T. P., et al. (2012). “Biosensor technologies for augmented brain-computer interfaces in the next decades,” in *Proceedings of the IEEE*, Vol. 100, 1553–1566. doi: 10.1109/JPROC.2012.2184829
- Lindstrom, M., and Underhill, P. (2010). *Buyology: Truth and Lies About Why We Buy*. New York, NY: Random House Digital Inc.
- Lomas, T., Ivtzan, I., and Fu, C. H. (2015). A systematic review of the neurophysiology of mindfulness on EEG oscillations. *Neurosci. Biobehav. Rev.* 57, 401–410. doi: 10.1016/j.neubiorev.2015.09.018
- Lopes Da Silva, F. (2013). EEG and MEG: relevance to neuroscience. *Neuron* 80, 1112–1128. doi: 10.1016/j.neuron.2013.10.017
- Lunna, K. (2018). *Entertech*. Available online at: <https://www.kickstarter.com/projects/987756376/luuna> (accessed October 15, 2018).
- Lupton, D. (2013). Quantifying the body: monitoring and measuring health in the age of mHealth technologies. *Crit. Public Health* 23, 393–403. doi: 10.1080/09581596.2013.794931
- Lutz, A., Dunne, J. D., and Davidson, R. J. (2006). “Meditation and the neuroscience of consciousness: an introduction,” in *The Cambridge Handbook of Consciousness*, eds M. Moscovitch, P. Zelazo, and E. Thompson (Cambridge: Cambridge University Press), 497–549.
- Lutz, A., Slagter, H. A., and Davidson, R. J. (2008). Attention regulation and monitoring in meditation. *Trends Cogn. Sci.* 12, 163–169. doi: 10.1016/j.tics.2008.01.005
- Makeig, S., Kothe, C., Mullen, T., Bigdely-Shamlo, N., Zhang, Z., and Kreutz-Delgado, K. (2012). Evolving signal processing for brain-computer interfaces. *IEEE* 100, 1567–1583. doi: 10.1109/JPROC.2012.2185009
- Markand, O. N. (1976). Electroencephalogram in locked-in syndrome. *Clin. Neurophysiol.* 40, 529–534. doi: 10.1016/0013-4694(76)90083-3
- Marzbani, H., Marateb, H. R., and Mansourian, M. (2016). Neurofeedback: a comprehensive review on system design, methodology and clinical applications. *Basic Clin. Neurosci.* 7, 143–158. doi: 10.15412/J.BCN.03070208
- McClure, S. M., Li, J., Tomlin, D., Cypert, K. S., Montague, L. M., and Montague, R. (2004). Neural correlates of behavioral preference for culturally familiar drinks. *Neuron* 44, 379–387. doi: 10.1016/j.neuron.2004.09.019
- McDowell, W. S., and Dick, S. J. (2013). The marketing of neuromarketing: brand differentiation strategies employed by prominent neuromarketing firms to attract media clients. *J. Media Bus. Stud.* 10, 25–40. doi: 10.1080/16522354.2013.11073558
- McGee, E. M., Maguire, G. Q. Jr. (2007). Becoming borg to become immortal: regulating brain implant technologies. *Camb. Q. Healthc. Ethics* 16, 291–302. doi: 10.1017/S0963180107070326
- Mehta, R. K., and Parasuraman, R. (2013). Neuroergonomics: a review of applications to physical and cognitive work. *Front. Hum. Neurosci.* 7:889. doi: 10.3389/fnhum.2013.00889
- Melon, K. (2016). *Headband and Mobile App to Measure Your Focus Melon*. 19 December (2016). Available online at: <https://www.kickstarter.com/projects/806146824/melon-a-headband-and-mobile-app-to-measure-your-focus> (accessed October 12, 2018).
- Mercer, C., and Trothen, T. J. (2014). *Religion and Transhumanism: The Unknown Future of Human Enhancement*. Santa Barbara, CA: Praeger.
- Moghim, S., Kushki, A., Guerguerian, A. M., and Chau, T. (2012). A review of EEG-based brain-computer interfaces as access pathways for individuals with severe disabilities. *Assist. Technol.* 25, 99–110. doi: 10.1080/10400435.2012.723298
- Mohanchandra, K., Saha, S., and Lingaraju, G. (2015). EEG based brain computer interface for speech communication: principles and applications. *Intell. Syst. Refer. Library* 74, 273–293. doi: 10.1007/978-3-319-10978-7\_10
- Morin, C. (2011). Neuromarketing: the new science of consumer behavior. *Society* 48, 131–135. doi: 10.1007/s12115-010-9408-1
- Mormann, F., Lehnertz, K., David, P., and Elger, C. E. (2000). Mean phase coherence as a measure for phase synchronization and its application to the EEG of epilepsy patients. *Phys. D Nonlinear Phenomena* 144, 358–369. doi: 10.1016/S0167-2789(00)00087-7
- Mostow, J., Chang, K.-M., and Nelson, J. (2013). Toward exploiting EEG input in a reading tutor. *Int. J. Artif. Intell. Educ.* 22, 19–38. doi: 10.1007/978-3-642-21869-9\_31
- Murata, K., Fujita, E., Kojima, S., Maeda, S., Ogura, Y., Kamei, T., et al. (2011). Noninvasive biological sensor system for detection of drunk driving. *Inform. Technol. Biomed. IEEE Tran.* 15, 19–25. doi: 10.1109/ITTB.2010.2091646
- Murphy, E., Illes, J., and Reiner, P. B. (2008). Neuroethics of neuromarketing. *J. Consum. Behav.* 7, 293–302. doi: 10.1002/cb.252
- Nafus, D., and Sherman, J. (2014). This one does not go up to 11: the quantified self movement as an alternative big data practice. *Int. J. Commun.* 8, 1784–1794.
- Nakanishi, I., Baba, S., and Li, S. (2011). “Evaluation of brain waves as biometrics for driver authentication using simplified driving simulator,” in *Biometrics and Kansei Engineering (ICBAKE) 2011 International Conference* (Tokyo: Institute of Electrical and Electronics Engineers). doi: 10.1109/ICBAKE.2011.27
- National Institutes of Health (2017). National Institutes of Health Disease diagnostics take top honors of DEBUT biomedical engineering design competition, National Institutes of Health, 25 August (2017). Available online at: <https://www.nih.gov/news-events/news-releases/disease-diagnostics-take-top-honors-debut-biomedical-engineering-design-competition> (accessed October 12, 2018).
- Nations U (2017). *World Population Prospects: The 2017 Revision, United Nations Department of Economic and Social*. New York, NY: Nations U.
- Navarro, A., Ceccaroni, L., Velickovski, F., Torrellas, S., Miralles, F., Allison, B., et al. (2011). “Context-awareness as an enhancement of brain-computer interfaces,” in *Ambient Assisted Living. (Lecture Notes in Computer Science)* (Berlin: Springer). doi: 10.1007/978-3-642-21303-8\_30
- Nijboer, F. (2015). Technology transfer of brain-computer interfaces as assistive technology: barriers and opportunities. *Ann. Phys. Rehabil. Med.* 58, 35–38. doi: 10.1016/j.rehab.2014.11.001
- Ning-Han, L., Cheng-Yu, C., and Hsuan-Chin, C. (2013). Recognizing the degree of human attention using EEG signals from mobile sensors. *Sensors* 13, 10273–10286. doi: 10.3390/s130810273
- Nomura, T., and Mitsukura, Y. (2015). EEG-based detection of TV commercials effects. *Proc. Comput. Sci.* 60, 131–140. doi: 10.1016/j.procs.2015.08.112
- O’Kane, S. (2018). *Nissan’s Future Cars May Read Your Brain to Prevent Accidents*, New York, NY: The Verge.
- Pai, A. (2015). *BrainScope raises \$2.5M for Concussion Assessment Wearable and App*. Mobihealthnews. Available online at: <https://www.mobihealthnews.com/46552/brainscope-raises-2-5m-for-concussion-assessment-wearable-and-app> (accessed December 23, 2018).
- Palaniappan, R. (2004). Method of identifying individuals using VEP signals and neural network. *IEEE Proc. Sci. Measure. Technol.* 151, 16–20. doi: 10.1049/ip-smt:20040003
- Parasuraman, R. (2003). Neuroergonomics: research and practice. *Theor. Issues Ergon. Sci.* 4, 5–2010. doi: 10.1080/146392202010199753
- Pasqualotto, E., Federici, S., and Belardinelli, M. (2012). Toward functioning and usable brain-computer interfaces (BCIs): a literature review. *Disabil. Rehabil. Assist. Technol.* 7, 89–103. doi: 10.3109/17483107.2011.589486
- Perrachione, T., and Perrachione, J. (2008). Brains and brands: developing mutually informative research in neuroscience and marketing. *J. Consum. Behav.* 7, 303–318. doi: 10.1002/cb.253
- Peterson, A., Graham, M., Weijer, C., Fernandez, D., Owen, A., and Naci, L. (2013). Assessing decisionmaking capacity in the behaviorally nonresponsive patient with residual covert awareness. *AJOB Neurosci.* 4, 3–14. doi: 10.1080/21507740.2013.821189
- Pfurtscheller, G., Müller-Putz, G., Schlögl, A., Graimann, B., Scherer, R., Leeb, R., et al. (2006). 15 years of BCI research at graz university of technology:



- current projects. *IEEE Trans. Neural Syst. Rehabil. Eng.* 14, 205–210. doi: 10.1109/TNSRE.2006.875528
- Plassmann, H., Ramsøy, T. Z., and Milosavljevic, M. (2012). Branding the brain: a critical review and outlook. *J. Consum. Psychol.* 22, 18–36. doi: 10.1016/j.jcps.2011.11.010
- Poldrack, R. (2006). Can cognitive processes be inferred from neuroimaging data? *Trends Cogn. Sci.* 10, 59–63. doi: 10.1016/j.tics.2005.12.004
- Pop, N., and Iorga, A. (2012). A new challenge for contemporary marketing neuromarketing. *Manag. Market. Challenges Knowl. Soc.* 7, 631–644.
- Prichet, L. S., Alper, K., Kowalik, S. C., and Rosenthal, M. (1996). Neurometric QEEG studies of crack cocaine dependence and treatment outcome. *J. Addict. Dis.* 15, 39–53. doi: 10.1300/J069v15n04\_03
- Ramzan, Q., and Shidlovskiy, S. (2018). “Evolution of the brain computing interface (BCI) and proposed electroencephalogram,” in *MATEC Web of Conferences*, Vol. 155 (Toms), 8. doi: 10.1051/mateconf/201815501006
- Revet, K., Deravi, F., and Sirlantzis, K. (2010). “Biosignals for user authentication-towards cognitive biometrics?,” in *Emerging Security Technologies (EST), 2010. International Conference*. doi: 10.1109/EST.2010.32
- Rezeika, A., Benda, M., Stawicki, P., Gemblar, F., Saboor, A., and Volosyak, I. (2018). Brain-computer interface spellers: a review. *Brain Sci.* 8:57. doi: 10.3390/brainsci8040057
- Rincón, M. (2017). *MJN Neuroserveis. Quality of Life for Everybody, X Patient Barcelona Congress*. Edition II. Barcelona.
- Rodina, E., Bornfleth, H., and Johnson, M. (2017). DC-EEG recordings of mindfulness. *Clin. Neurophysiol.* 128, 512–519. doi: 10.1016/j.clinph.2016.12.031
- Rozelle, G. R., and Budzynski, T. H. (1995). Neurotherapy for stroke rehabilitation: a single case study. *Biofeedback Self Regul.* 20, 211–28. doi: 10.1007/BF01474514
- Saeed, S., and Zyngier, D. (2012). How motivation influences student engagement: a qualitative case study. *J. Educ. Learn.* 1, 252–267. doi: 10.5539/jel.v1n2p252
- Schermer, M. (2009). Changes in the self: the need for conceptual research next to empirical research. *AJOB Neurosci.* 9, 45–47. doi: 10.1080/15265160902788744
- Schüpbach, M., Gargiulo, M., and Welter, M. L. (2006). Neurosurgery in parkinson disease: a distressed mind in a repaired body? *Neurology* 66, 1811–1816. doi: 10.1212/01.wnl.0000234880.51322.16
- Sebastian, V. (2014). Neuromarketing and evaluation of cognitive and emotional responses of consumers to marketing stimuli *Proc. Soc. Behav. Sci.* 127, 753–757. doi: 10.1016/j.sbspro.2014.03.349
- Sellers, E., Vaughan, T., and Wolpaw, J. (2010). A brain-computer interface for long-term independent home use. *Amyotroph Lateral Scler.* 11, 449–455. doi: 10.3109/17482961003777470
- Selvam, V., and Shenbagadevi, S. (2011). “Brain tumor detection using scalp EEG with modified waveletica and multi layer feed forward neural network,” in *2011 Annual International Conference of the IEEE Engineering in Medicine and Biology Society*, (IEEE: Boston). doi: 10.1109/IEMBS.2011.6091508
- Sharanreddy, M., and Kulkarni, P. K. (2013). Detection of primary brain tumor present in eeg signal using wavelet transform and neural network. *Int. J. Biol. Med. Res.* 4, 2855–2859.
- Sharmila, A., and Mahalakshmi, P. (2017). Wavelet-based feature extraction for classification of epileptic seizure EEG signal. *J. Med. Eng. Technol.* 41, 670–680. doi: 10.1080/03091902.2017.1394388
- Slavin, R. E. (2008). Perspectives on evidence-based research in education d what works? Issues in synthesizing educational program evaluations. *Educ. Res.* 37, 5–14. doi: 10.3102/0013189X08314117
- Slowther, A., and Kleinman, I. (2009). *Confidentiality. The Cambridge Textbook of Bioethics*. Cambridge: Singer & A. M. Viens. 43–48. doi: 10.1017/CBO9780511545566.008
- Smidts, A., Hsu, M., Sanfey, A. G., Boksem, M. A. S., Ebstein, R. B., and Huettel, S. A. (2014). Advancing consumer neuroscience. *Market. Lett.* 25, 257–267. doi: 10.1007/s11002-014-9306-1
- Smith, R. (2017). *‘Thought Control’ and Learning Game Start-Up Companies in the Winner’s Circle at the ISTE*. San Antonio: Pitch Fest Competition. ISTE.
- Solis-Vivanco, R., Rodríguez-Violante, M., Cervantes-Arriaga, A., Justo-Guillén, E., and Ricardo-Garcell, J. (2018). Brain oscillations reveal impaired novelty detection from early stages of Parkinson’s disease. *Neuroimage Clin.* J. 22, 923–931. doi: 10.1016/j.nicl.2018.03.024
- Spapé, M. M., Jacucci, G., Filetti, M., Eugster, M. J. A., Jacucci, G., and Ravaja, N. (2015). “Human computer interaction meets psychophysiology: a critical perspective,” in *Symbiotic Interaction. Symbiotic 2015. Lecture Notes in Computer Science*, Vol. 9359, eds B. Blankertz, G. Jacucci, L. Gamberini, A. Spagnoli, and J. Freeman (Cham: Springer). doi: 10.1007/978-3-319-24917-9\_16
- Spataro, R., Heilinger, A., Allison, B., Cicco, D. D., Marchese, S., Gregoret, C., et al. (2018). Preserved somatosensory discrimination predicts consciousness recovery in unresponsive wakefulness syndrome. *Clin. Neurophysiol.* 129, 1130–1136. doi: 10.1016/j.clinph.2018.02.131
- Stanton, S. J., Sinnott-Armstrong, W., and Huettel, S. A. (2017). Neuromarketing: ethical implications of its use and potential misuse. *J. Bus. Ethics* 144, 799–811. doi: 10.1007/s10551-016-3059-0
- Stasi, A., Songa, G., Mauri, M., Cicci, A., Diotallevi, F., Nardone, G., et al. (2018). Neuromarketing empirical approaches and food choice: a systematic review. *Food Res. Int.* 108, 650–664. doi: 10.1016/j.foodres.2017.11.049
- Stefan, S., Schorr, B., Lopez-Rolon, A., Kolassa, I., Shock, J., Rosenfelder, M., et al. (2018). Consciousness indexing and outcome prediction with resting-state EEG in severe disorders of consciousness. *Brain Topogr.* 31, 848–862. doi: 10.1007/s10548-018-0643-x
- Stothart, G., Quadflieg, S., and Milton, A. (2017). A fast and implicit measure of semantic categorisation using steady state visual evoked potentials. *Neuropsychologia* 102, 11–18. doi: 10.1016/j.neuropsychologia.2017.05.025
- Strickland, E. (2017). *Facebook Announces Typing-by-Brain Project, IEEE Spectrum*. Available online at: <https://spectrum.ieee.org/the-human-os/biomedical/bionics/facebook-announces-typing-by-brain-project> (accessed April 20, 2017).
- Stylianou, M., Murphy, N., Peraza, L., Graziadio, S., Cromarty, R., Killen, A., et al. (2018). Quantitative electroencephalography as a marker of cognitive fluctuations in dementia with Lewy bodies and an aid to differential diagnosis. *Clin. Neurophysiol.* 129, 1209–1220. doi: 10.1016/j.clinph.2018.03.013
- Su, F., Zhou, H., Feng, Z., and Ma, J. (2012). “A biometric-based covert warning system using EEG,” in *Biometrics (ICB), (2012). 5th IAPR International Conference*.
- Su, Y., Qi, Y., Luo, J. X., Wu, B., and Li, Y. (2011). A hybrid brain-computer interface control strategy in a virtual environment. *Front. Inform. Technol. Electron. Eng.* 12, 351–361. doi: 10.1631/jzus.C1000208
- Svigor, I., and Kisasondi, T. (2012). “Two factor authentication using eeg augmented passwords,” in *Information Technology Interfaces (ITI), 2012 34th International Conference*.
- Swaine-Simon, S. (2017). *Director, DEF CON 24 –NeuroTechX—Introduction to Brain Based Authentication*. Las Vegas. Retrieved from: <https://www.youtube.com/watch?v=frAhjtnvkqs>
- Swan, M. (2016). The future of brain-computer interfaces: blockchaining your way into a cloudmind. *J. Evol. Technol.* 26, 60–81.
- Tamburrini, G. (2014). *Philosophical Reflections on Brain-Computer Interface*. Dordrecht: Springer, 147–162. doi: 10.1007/978-94-017-8996-7\_13
- Tamburrini, G., and Mattia, D. (2011). Disorders of consciousness and communication. Ethical motivations and communication-enabling attributes of consciousness. *Funct. Neurol.* 26, 51–54.
- Tang, Y.-Y., Holzel, B., and Posner, M. (2015). The neuroscience of mindfulness meditation. *Nat. Rev. Neurosci.* 16, 213–225. doi: 10.1038/nrn3916
- Trudeau, D. L. (2005). EEG biofeedback for addictive disorders—the state of the art in 2004. *J. Adult Dev.* 12, 139–146. doi: 10.1007/s10804-005-7030-z
- Ulman, Y. I., Cakar, T., and Yildiz, G. (2015). Ethical issues in neuromarketing: “I consume, therefore I am!”. *Sci. Eng. Ethics* 21, 1271–1284. doi: 10.1007/s11948-014-9581-5
- Vaid, S., Singh, P., and Kaur, C. (2015). “EEG signal analysis for BCI interface: a review,” in *2015 Fifth International Conference on Advanced Computing & Communication Technologies (ACCT)*, (Haryana) 143–147. doi: 10.1109/ACCT.2015.72
- Vecchiato, G., Astolfi, L., Fallani, F. D. V., Salinari, S., Cincotti, F., Aloise, F., et al. (2009). The study of brain activity during the observation of commercial advertising by using high resolution EEG techniques. *Annu. Int. Conf. IEEE Eng. Med. Biol. Soc.* 2009, 57–60. doi: 10.1109/IEMBS.2009.5335045
- Vecchiato, G., Babiloni, F., Astolfi, L., Toppi, J., Cherubino, P., Dai, J., et al. (2011). “Enhance of theta EEG spectral activity related to the memorization of commercial advertisings in Chinese and Italian subjects,” in *2011 4th*



- International Conference on Biomedical Engineering and Informatics (BMEI)* (Shanghai), 1491–1494. doi: 10.1109/BMEI.2011.6098615
- Vecchiato, G., Borghini, G., Aricò P., Graziani, L., Maglione, A. G., Cherubino, P., Babiloni, F., et al. (2016). Investigation of the effect of EEG-BCI on the simultaneous execution of flight simulation and attentional tasks. *Med. Biol. Eng. Comput.* 54, 1503–1513. doi: 10.1007/s11517-015-1420-6
- Venthur, B., Blankertz, B., Gugler, M., and Curio, G. (2010). “Novel applications of BCI technology: psychophysiological optimization of working conditions in industry,” in *2010 IEEE International Conference on Systems, Man and Cybernetics*, (IEEE: Istanbul), 417–21. doi: 10.1109/ICSMC.2010.5641772
- Vlek, R., Steines, D., Szibbo, D., Kubler, A., Schneider, M. J., and Haselager, P. (2012). Ethical issues in brain-computer interface research, development, and dissemination. *J. Neurol. Phys. Ther.* 36, 94–99. doi: 10.1097/NPT.0b013e31825064cc
- Wang, M., Li, R., Zhang, R., Li, G., and Zhang, D. (2018). A wearable SSVEP-based BCI system for quadcopter control using head-mounted device. *IEEE Access* 6, 26789–26798. doi: 10.1109/ACCESS.2018.2825378
- Wang, R. W. Y., Chang, Y.-C., and Chuang, S.-W. (2016). EEG spectral dynamics of video commercials: impact of the narrative on the branding product preference. *Nat. Sci. Rep.* 6:36487. doi: 10.1038/srep36487
- Wei, L., Hong, Q., Yue, H., and Xi, C. (2010). “The research in a plantar pressure measuring system connected with EEG. Signal Processing (ICSP) 2010,” in *IEEE 10th International Conference*, 434–37. doi: 10.1109/ICOSP.2010.5655374
- Weisberg, D., Keil, F., Goodstein, J., Rawson, E., and Gray, J. (2008). The seductive allure of neuroscience explanations. *J. Cogn. Neurosci.* 20, 470–477. doi: 10.1162/jocn.2008.20040
- Wilson, R. M., Gaines, J., and Hill, R. (2008). Neuromarketing and consumer free will. *J. Consum. Aff.* 42, 389–410. doi: 10.1111/j.1745-6606.2008.00114.x
- Wolpaw, J. R., Millán, J. D. R., and Ramsey, N. F. (2020). Brain-computer interfaces: definitions and principles. *Handbook Clin. Neurol.* 168, 15–23. doi: 10.1016/B978-0-444-63934-9.00002-0
- Wu, Q., Zeng, Y., Zhang, C., Tong, L., and Yan, B. (2018). An EEG-based person authentication system with open-set capability combining eye blinking signals. *Sensors* 18:335. doi: 10.3390/s18020335
- Xu, J., and Zhong, B. (2018). Review on portable EEG technology in educational research. *Comput. Hum. Behav.* 81, 340–349. doi: 10.1016/j.chb.2017.12.037
- Zander, T., and Kothe, C. (2011). Towards passive brain-computer interfaces: applying brain-computer interface technology to human-machine systems in general. *J. Neural Eng.* 8:025005. doi: 10.1088/1741-2560/8/2/025005
- Zander, T. O., Kothe, C., Jatzev, S., and Gaertner, M. (2010). Enhancing human-computer interaction with input from active and passive brain-computer interfaces. *Brain Comput. Interfaces* 181–199. doi: 10.1007/978-1-84996-272-8\_11
- Zehr, E. (2015). The potential transformation of our species by neural enhancement. *J. Motor Behav.* 47, 73–78. doi: 10.1080/00222895.2014.916652
- Zhang, X., Wu, D., Ding, L., Luo, H., Lin, C. T., Jung, T. P., et al. (2020). Tiny noise, big mistakes: adversarial perturbations induce errors in Brain-Computer Interface spellers. *Natl. Sci. Rev.* doi: 10.1093/nsr/nwaa233
- Zickler, C., Riccio, A., Leotta, F., Hillian-Tress, S., Halder, S., Holz, E., et al. (2011). A brain-computer interface as input channel for a standard assistive technology software. *Clin. EEG Neurosci.* 42, 236–244. doi: 10.1177/155005941104200409

**Conflict of Interest:** The authors declare that the research was conducted in the absence of any commercial or financial relationships that could be construed as a potential conflict of interest.

Copyright © 2020 Fontanillo Lopez, Li and Zhang. This is an open-access article distributed under the terms of the Creative Commons Attribution License (CC BY). The use, distribution or reproduction in other forums is permitted, provided the original author(s) and the copyright owner(s) are credited and that the original publication in this journal is cited, in accordance with accepted academic practice. No use, distribution or reproduction is permitted which does not comply with these terms.



# Effects of Long-Term Meditation Practices on Sensorimotor Rhythm-Based Brain-Computer Interface Learning

Xiyuan Jiang<sup>1</sup>, Emily Lopez<sup>1</sup>, James R. Stieger<sup>1,2</sup>, Carol M. Greco<sup>3</sup> and Bin He<sup>1\*</sup>

<sup>1</sup> Department of Biomedical Engineering, Carnegie Mellon University, Pittsburgh, PA, United States, <sup>2</sup> Department of Biomedical Engineering, University of Minnesota, Minneapolis, MN, United States, <sup>3</sup> Department of Psychiatry, University of Pittsburgh, Pittsburgh, PA, United States

## OPEN ACCESS

### Edited by:

Mitsuhiro Hayashibe,  
Tohoku University, Japan

### Reviewed by:

Sangtae Ahn,  
Kyungpook National University,  
South Korea  
Léa Pillette,  
Ecole Centrale de Nantes, France  
Camille Jeunet,  
UMR 5287 Institut de Neurosciences  
Cognitives et Intégratives d'Aquitaine  
(INICIA), France

### \*Correspondence:

Bin He  
bhe1@andrew.cmu.edu

### Specialty section:

This article was submitted to  
Neural Technology,  
a section of the journal  
Frontiers in Neuroscience

**Received:** 14 August 2020

**Accepted:** 21 December 2020

**Published:** 21 January 2021

### Citation:

Jiang X, Lopez E, Stieger JR,  
Greco CM and He B (2021) Effects  
of Long-Term Meditation Practices on  
Sensorimotor Rhythm-Based  
Brain-Computer Interface Learning.  
Front. Neurosci. 14:584971.  
doi: 10.3389/fnins.2020.584971

Sensorimotor rhythm (SMR)-based brain-computer interfaces (BCIs) provide an alternative pathway for users to perform motor control using motor imagery. Despite the non-invasiveness, ease of use, and low cost, this kind of BCI has limitations due to long training times and BCI inefficiency—that is, the SMR BCI control paradigm may not work well on a subpopulation of users. Meditation is a mental training method to improve mindfulness and awareness and is reported to have positive effects on one's mental state. Here, we investigated the behavioral and electrophysiological differences between experienced meditators and meditation naïve subjects in one-dimensional (1D) and two-dimensional (2D) cursor control tasks. We found numerical evidence that meditators outperformed control subjects in both tasks (1D and 2D), and there were fewer BCI inefficient subjects in the meditator group. Finally, we also explored the neurophysiological difference between the two groups and showed that the meditators had a higher resting SMR predictor, more stable resting mu rhythm, and a larger control signal contrast than controls during the task.

**Keywords:** EEG, electroencephalogram, mindfulness, meditation, BCI, brain-computer interface

## INTRODUCTION

Decades of research have sought to find alternative methods of communication between the human brain and the outside world. With the ever-growing knowledge in the neuroscience field, scientists have designed the brain-computer interface (BCI) to achieve this goal (Wolpaw et al., 2002; He et al., 2020). A BCI attempts to recognize the user's intent by decoding her/his neurophysiological signals and then converts this intent into commands to control objects, such as a cursor on a computer screen (Wolpaw et al., 1991; Trejo et al., 2006), a quadcopter (LaFleur et al., 2013), or a robotic arm in space (Meng et al., 2016; Edelman et al., 2019).

One of the main goals for the BCI is to help people suffering from various kinds of neuromuscular diseases, such as amyotrophic lateral sclerosis, stroke, and spinal cord injury (Armour et al., 2016) to regain a certain degree of movement ability (Rebsamen et al., 2010; Ang et al., 2015). Despite the limited ability to move, cognitive ability in this population remains partially or fully intact. Therefore, it would be a significant improvement in the quality of life if these individuals could use a BCI to complete daily life tasks.

There are many types of BCI based on various recording techniques and signals extracted. In this work, we focus on the sensorimotor rhythm (SMR)-based BCI, which uses electroencephalogram (EEG) to detect scalp electrical signals and decode motor intention (Yuan and He, 2014; He et al., 2015). The EEG-based SMR BCI has multiple merits, such as non-invasiveness, ease of use, relatively low cost, and high temporal resolution (He et al., 2020). This is particularly true when only a few electrodes are used (Clerc et al., 2016). The SMR or mu rhythm in EEG is generated by the synchronized electrical brain activity over the motor cortex area and has a frequency range of around 8–12 Hz (Pfurtscheller et al., 2006; Bernier et al., 2007). In BCI applications, the frequency band centered at 12 Hz (Royer et al., 2010; Doud et al., 2011; Cassady et al., 2014; Meng et al., 2016, 2018; Stieger et al., 2020) was shown to be effective in SMR control. Event-related desynchronization (ERD) occurs when the amplitude of mu rhythm decreases in response to a person moving or imagining moving her/his body (Pfurtscheller and Aranibar, 1979). On the other hand, when a person stops moving or imagining moving, the amplitude of mu rhythm increases, which is called event-related synchronization (ERS). SMR based BCI is a well-established BCI modality, and it has been demonstrated that people can perform multidimensional cursor control (McFarland et al., 2010; Meng et al., 2018), drone control (Royer et al., 2010; Doud et al., 2011; LaFleur et al., 2013), wheelchair control (Galán et al., 2008; Huang et al., 2012), and robotic arm control (Meng et al., 2016; Edelman et al., 2019) with SMR BCI.

Despite the progress of SMR-based BCI, challenges exist. Two primary limitations of SMR-based BCI are the system's need for long training times and BCI inefficiency, where the SMR BCI control paradigm may not work on around 20% of the system's users (Blankertz et al., 2010). The latter could be further developed as a subject variability issue: there exists a large variability of SMR BCI performance among the population. Efforts have been made to investigate its cause and solution (Ahn and Jun, 2015; Jeunet et al., 2016). For instance, Guillot et al. (2008) found that good MI performers have an increased ability to recruit MI-related brain network, and Sannelli et al. (2008) found that BCI inefficient subjects usually have higher intrinsic noise, i.e., the noise in the data which can overshadow the class-related information; Ahn and Jun (2015) did a systematic review of literature on SMR BCI inefficiency and found that these subjects typically have less developed brain networks for motor skills; Jeunet et al. (2016) further summarized the factors influencing SMR BCI as a relationship to the technology, attention, and spatial abilities.

Attention has been focused on developing better decoding algorithms and recording techniques (Lotte and Guan, 2011) for SMR BCI, i.e., from the “computer” perspective of BCI. However, less attention has been drawn to enhancing people's ability to generate more decodable EEG signals, i.e., from the “brain” side. For the latter, the high-level goal is to determine, given the same BCI system, if there exists a subpopulation that is better able to control it and if a certain kind of training or intervention could be developed to equip neurotypical people with this BCI control ability.

In the search for optimal mental training methods to potentially improve SMR BCI control, meditation is of interest due to its ability to alter brain plasticity and influence spatial-temporal brain activity, which in turn, are important components of SMR BCI control (Chan and Woollacott, 2007; Tang et al., 2007; Moore and Malinowski, 2009; Debarnot et al., 2014). As summarized in Debarnot et al. (2014), one of the most important effects of meditation is enhanced attention control, such as orienting attention (van den Hurk et al., 2010) and conflict monitoring (Jha et al., 2007). In terms of the influence of meditation on brain rhythms, Halsband et al. (2009) found that in hypnotic and mindfulness meditation states, there exist a modulation of alpha, gamma, and theta band brain rhythms, including but not limited to the sensorimotor area, which indicates the ability of meditation to alter motor-related spatial-temporal brain activity. In Kerr et al. (2011a), mindfulness training was found to enhance MEG alpha power modulation in the primary somatosensory cortex (SI).

With growing evidence suggesting that meditation brings enhanced attention and brain rhythm control, it is reasonable to hypothesize that people with meditation experience would develop a better ability to control SMR-based BCI. Indeed, previous work has investigated the effect of meditation on SMR BCI cursor control (Cassady et al., 2014; Tan et al., 2014, 2015; Kober et al., 2017; Stieger et al., 2020) or just generating ERD/ERS without controlling a BCI system (Kerr et al., 2011a,b, 2013; Rimbart et al., 2019). Similar to what Tang et al. (2015) summarized for the neuroscience aspect of meditation studies, efforts to study the meditation effect on SMR BCI could be divided into two categories, longitudinal studies and cross-sectional studies:

1. Previous longitudinal studies separated meditation-naïve subjects into a meditation group and a control group, with the meditation group receiving meditation training and the control group receive either active control tasks or no specific task (Mahmoudi and Erfanian, 2006; Tan et al., 2014, 2015; Botrel and Kübler, 2019; Stieger et al., 2020). After that, BCI performance and/or neurophysiological difference between the two groups was assessed. For example, a series of studies by Tan et al. (2014, 2015) and Ramli et al. (2019) described the effect of 4 weeks mindfulness meditation on SMR BCI performance, that mindfulness meditation improved BCI performance and was correlated with activation in the frontal-parietal region in functional magnetic resonance imaging during motor imagery. In Mahmoudi and Erfanian (2006), the mental practice of MI and concentration procedures improved the offline classification of MI in multiple EEG electrodes, such as C3 in the primary motor cortex area and F3 in the frontal area. In Kerr et al. (2013), they discovered that an 8 weeks mindfulness-based stress reduction training served to optimize attentional modulation of 7–14 Hz alpha rhythm in the primary sensory neocortex. Rimbart et al. (2019) found that the hypnotic state changes the sensorimotor beta rhythm during the ERD period, whereas the ERS in the mu and beta band remains unchanged. In

Stieger et al. (2020), an 8 weeks MBSR class improved SMR BCI accuracy via modulation of the volitional resting-state high alpha EEG rhythm.

2. In contrast, cross-sectional studies have investigated the difference in BCI/neurofeedback learning between people who already have meditation experience and meditation naïve subjects (Cassady et al., 2014; Kober et al., 2017). In Cassady et al. (2014), the meditation group was shown to have better results compared with the control group in terms of performance, learning speed, and information transfer rate. However, most of the claims in this study focused on the behavior difference. A more in-depth analysis of the neurophysiological difference is needed. Another question left unanswered is whether meditators are also better at more complex tasks, such as two-dimensional (2D) cursor control. A typical 2D cursor control paradigm is achieved by having the subject use left/right (LR) motor imagery to control LR cursor movement, bilateral hand motor imagery to go up, and rest to go down. Successful 2D cursor control requires the subject to carefully balance the strength of LR motor imagery and, therefore, is more challenging than 1D control. Because meditators are trained to control their attention, it is of interest to see if the BCI learning difference between meditators and non-meditators in a 2D BCI task would be even larger compared with 1D tasks and if there is any difference between the LR and up/down (UD) within the 2D compared with the 1D version of LR and UD tasks. In another study, Kober et al. (2017) found that people who pray frequently had a higher ability to control the SMR, but the recording was limited to Cz electrode only, and the control dimension was limited to 1D.

Despite the abundance of literature reporting positive effects of meditation on SMR BCI control, there are also studies whose results only partially support (Stieger et al., 2020) or do not support such a hypothesis (Botrel and Kübler, 2019). For example, Stieger et al. (2020) found that after an 8 weeks mindfulness-based stress reduction training, subjects indeed had significant performance improvements in the UD task (both hands motor imagery to go up and rest to go down), but for the LR control task (LR-hand motor imagery) the effect was not significant. Botrel and Kübler (2019) found that week-long visuomotor coordination and relaxation training did not improve SMR-based BCI performance. One of the reasons for this kind of disagreement may be a dose-effect, meaning that it might take a longer meditation time to affect BCI learning in a significant manner.

With these questions in mind, we recruited experienced meditators and controls and investigated the difference in SMR BCI learning between these two groups in both 1D and 2D tasks. The aims for this cross-sectional study are as follows: First, to verify the conclusions in the pilot study (Cassady et al., 2014) that meditators had better learning in SMR BCI with an independent investigation; second, to explore the behavior difference between the two groups in a more complex 2D

task; and third, to investigate the neurophysiological difference between these two groups.

## MATERIALS AND METHODS

### Participants

The experimental procedures involving human subjects described in the current study were approved by the Institutional Review Board (IRB) of Carnegie Mellon University with study ID STUDY2017\_00000430, and all participants provided written informed consent. Subjects were recruited via flyers in the surrounding area and an email sent out to local mindfulness groups. We utilized a single-blind two-group experimental design, with a meditation group and a control group. The experimenters did not know the identity of the subject in relation to their meditation experience throughout the whole experiment. We achieved this blinding through the following: (1) we asked two other researchers at our lab to refer potential subjects (both meditators and controls) to an unblinded research assistant (screener) and not to the blinded experimenters; (2) these potential subjects were screened for inclusion/exclusion by this screener whose only involvement in the study was to conduct screening; (3) during the consent process and survey, the experimenter asked the subject to cover any information related to meditation experience when submitting the paperwork; thus, the experimenter only knew information unrelated to meditation (age, sex, name, etc.) about this subject after collecting these documents. (4) During the experiment, the experimenter remained unaware of the subjects' meditation status and avoided any conversation related to meditation with the subject throughout the entire six sessions.

The meditation group consisted of 16 healthy subjects (age =  $38.5 \pm 15.7$  years) with a history of meditation practice, as evaluated by a questionnaire regarding personal meditation practice completed before experimentation. To be accepted into the meditator group, individuals had to cite at least a year of frequent and consistent practice, with most subjects having 2 or more years of consistent practice. Most of the meditators' practices belong to the subgroup of Vipassana, Zen, Mindfulness, and Buddhism. The control group consists of 19 healthy individuals (age =  $25.6 \pm 9.4$  years) with no prior meditation experience. Both groups had no prior BCI experience. We continually asked participants to describe their motor imagery strategies. If these strategies diverged from the kinesthetic motor imagery they were asked to perform, we reminded them to focus on the sensations and intention behind the imagined motion of their hands. We excluded one subject (identity: meditator) from the analysis because she/he expressed resistance to performing the required motor imagery and was not able to provide a concrete strategy when asked. Subjects' demographic information is summarized in **Supplementary Table 1**.

### Surveys to Measure Mindfulness

In the first session, we asked subjects to fill out two surveys before the BCI experiment. Both surveys aim to measure one's level of mindfulness. The first survey is called the Freiburg



Mindfulness Inventory (FMI) (Walach et al., 2006), which has 14 statements, such as “I am open to the experience of the present moment.” The subject was asked to use a 1–4 scale to indicate how often she/he has such experience. The FMI score was calculated by summing up the answers to each question with a proper recode of one question (Walach et al., 2006). The second survey is called Day-to-Day Experiences (Brown and Ryan, 2003), which has 15 questions, such as “I find it difficult to stay focused on what’s happening in the present;” the subject was asked to use a 1–6 scale to indicate how often she/he has such experience. The Mindful Attention Awareness Scale (MAAS) was calculated by averaging answers to each question in this Day-to-Day Experiences survey. In both surveys, a higher score indicates a higher level of mindfulness.

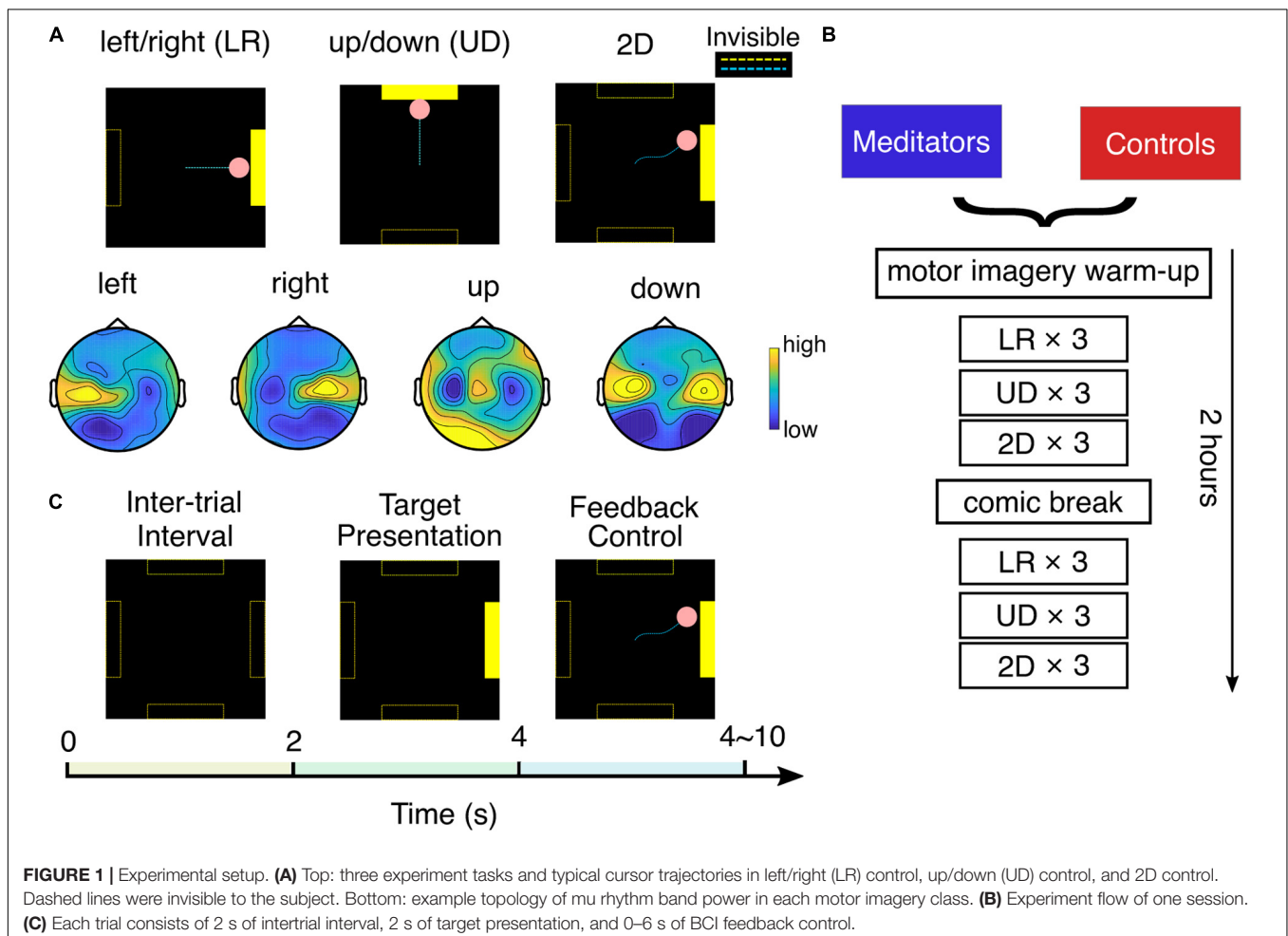
## Data Acquisition and Brain–Computer Interface Cursor Control Task

Subjects in both groups went through six sessions of BCI training within 4–6 weeks, with at least 1 session per week. Each experimental session lasted about 2 h, with a 9 min break in the middle. EEG data were recorded throughout the session using the Neuroscan SynAmps system with 64-channel EEG QuikCap

(Neuroscan Inc., Charlotte, NC). The sampling frequency was set to 1,000 Hz, and the impedance was kept below 5 k $\Omega$  during the preparation. The experimenter checked the impedance in the break to make sure it remained below 5 k $\Omega$ . In addition, to minimize the influence of artifact on the EEG data, we monitored the behavior of the subject and the recorded waveform. We restarted this run if we found the subject moved a lot or the real-time EEG signal became noisy.

The experiment setup is shown in **Figure 1**. Each session began with a 5 min warmup task, where the subject was instructed to perform left- or right-hand motor imagery by focusing on imagining the sensations and intention of opening/closing the LR hand.

After that, the subject was asked to perform BCI cursor control of three different tasks: LR, UD, and 2D, by moving the cursor to the corresponding bar with motor imagery. This experiment flow is detailed in **Figures 1A,B**. In the LR task, subjects were told to imagine opening/closing the LR hand as they practiced in the warm-up to move the cursor to the LR, to hit a bar that appears randomly at the right or left side of the screen. The vertical position of the cursor was fixed in the middle of the screen in the LR task. After subjects performed three runs of LR BCI, with each run consisting of 25 trials, a similar explanation was given for the



**FIGURE 1 |** Experimental setup. **(A)** Top: three experiment tasks and typical cursor trajectories in left/right (LR) control, up/down (UD) control, and 2D control. Dashed lines were invisible to the subject. Bottom: example topology of mu rhythm band power in each motor imagery class. **(B)** Experiment flow of one session. **(C)** Each trial consists of 2 s of intertrial interval, 2 s of target presentation, and 0–6 s of BCI feedback control.

UD BCI task, except they were instructed to imagine both hands simultaneously opening and closing to move the cursor up, and to rest, in other words, try to clear their minds to move the cursor down. The cursor's horizontal position was fixed at the middle of the screen in the UD task. After subjects performed three runs of UD BCI, they moved onto the 2D task, in which the same instructions were implemented to move the cursor up, down, left, or right according to which bar appeared on the screen. In the 2D task, the cursor is free to move in any direction within the screen boundary. After one block (three runs) each of LR, UD, and 2D BCI, the subjects were given a 9 min break in which they were instructed to read and rate comics by pressing a key on the keyboard. This standard "break task" ensures that subjects use the same approach to relax. After the break, they completed one more block each of LR, UD, and 2D BCI. In total, at each session, a subject completes six runs (25 trials each run, takes ~3 min each run) of LR, UD, and 2D tasks.

We used the standard cursor task in BCI2000 (Schalk et al., 2004) to conduct the SMR BCI experiment mentioned earlier. The technical details of the classifier are presented as follows: The spectral amplitude of the small Laplacian filtered C3 and C4 electrodes were estimated using autoregressive (AR) methods in a 3 Hz bin (Stieger et al., 2020) surrounding 12 Hz (Meng et al., 2016, 2018). After that, for the horizontal motion, a control signal was calculated by taking the AR amplitude difference between two electrodes ( $C4 - C3$ ), and for the vertical motion, it was calculated by summing up the AR amplitude of two electrodes ( $C4 + C3$ ). This control signal was further subtracted by an offset and multiplied with a gain value to make the normalized control signal zero mean and unit variance. The pink cursor acted as the feedback to the subject; the normalized control signal determined its speed, and its position was updated every 40 ms. The gain and offset values were reset when performing a new task (LR, UD, and 2D) and after the break. As shown in **Figure 1C**, each trial starts with a 2 s intertrial interval where the screen was black; then, the yellow target bar appears randomly at one of the possible locations for 2 s; after that, the subject was able to use MI to control the cursor (bar still visible). The length of the feedback control varied between 0 and 6 s and depended on if and when the cursor hits the bar. There could be three possible outcomes for each trial: the cursor hits the correct bar (hits, the cursor turns yellow), the cursor hits the incorrect bar (misses, the cursor does not change color), or the cursor does not contact any target within 6 s (timeout, the cursor does not change color).

## Performance Metric

We quantify the performance using percent valid correct (PVC) (Cassady et al., 2014; Meng et al., 2016; Edelman et al., 2019), which is the ratio between the number of hit trials and number of hit trials plus the number of missed trials. To reduce the influence of large subject variability in SMR BCI, in the analysis, we excluded outlier subjects: we compute the averaged percent valid correct (PVC) across the six sessions for a subject as the performance, for LR, UD, and 2D, respectively. After that, for each task (LR, UD, and 2D), we identified any subjects that are  $\pm 2.5$  median absolute deviations from the median of the whole sample (Leys et al., 2013). Finally, we took the

union of subjects identified in the three tasks as the excluded subjects. With this criterion, we identified one meditator and four controls as outliers. Together with the subject excluded due to not following the MI guideline (one meditator), the number of subjects involved in the analysis is 14 meditators and 15 controls. The information regarding the median performance and outlier subjects' performance is shown in **Supplementary Table 2**.

## Offline Electroencephalogram Data Analysis

We bandpass filtered the EEG data using a Hamming window as a finite impulse response filter with the passband set between 1 and 100 Hz, then downsampled to 250 Hz. We identified and rejected noisy channels with high impedance by visual inspection; then, these channels were spherically interpolated. The EEG data were re-referenced to a common average. We attempted to remove potential eye blinking artifacts using independent component analysis and a template matching procedure. In addition, we also visually inspected trials with high data variance and excluded these trials in the analysis, as these trials have a higher probability of containing muscle artifact. After that, complex Morlet wavelet convolution was used to extract the power of the mu frequency band (3 Hz bin centered at 12 Hz).

The neurophysiological predictor or SMR predictor measures the difference between mu band power and the  $1/f$  noise floor in a power-frequency plot for C3 and C4 (Blankertz et al., 2010). Concretely, the EEG power spectrum at rest could be fitted with the sum of a  $1/f$  noise floor,  $n(f; \lambda, k_n)$  and two Gaussian distributions, centered at mu rhythm and beta rhythm,  $g_\alpha(f; \mu_\alpha, \sigma_\alpha)$  and  $g_\beta(f; \mu_\beta, \sigma_\beta)$ . In this study, the power spectral density is equal to the mean of C3 and C4 band power after small Laplacian spatial filtering during the intertrial resting state, combining LR conditions and UD conditions.

$$\widehat{PSD}(f; \lambda, \sigma, k) = n(f; \lambda, k_n) + g_\alpha(f; \mu_\alpha, \sigma_\alpha) + g_\beta(f; \mu_\beta, \sigma_\beta)$$

$$n(f; \lambda, k_n) = k_{n1} + \frac{k_{n2}}{f^\lambda}$$

$$g_\alpha(f; \mu_\alpha, \sigma_\alpha) = k_\alpha N(f; \mu_\alpha, \sigma_\alpha)$$

$$g_\beta(f; \mu_\beta, \sigma_\beta) = k_\beta N(f; \mu_\beta, \sigma_\beta)$$

The SMR predictor (dB) is calculated individually for C3 and C4 electrode mu rhythm band power after small Laplacian spatial filtering.

$$Predictor = 10 \cdot \log_{10} \frac{PSD(mu)}{n(mu)}$$

In the case where the algorithm could not find a curve to fit, we manually selected 5–10 representative data points to describe the  $1/f$  noise floor function by following the trend of the PSD curve and fitted these points using  $n(f; \lambda, k_n)$ . We discard a subject and session pair if the PSD does not follow a  $1/f$  decrease trend. The percentage of data points discarded was 10.5%.

We designed a method to calculate the control signal during task execution to be as close to the real condition as possible.

Concretely, we first calculated the C3 and C4 electrode frequency band power after small Laplacian spatial filtering, denoted  $P_{C3}$  and  $P_{C4}$ . Then, the raw control signal was calculated using the following equation:

$$CS_{raw,LR} = P_{C4} - P_{C3}$$

$$CS_{raw,UD} = P_{C4} + P_{C3}$$

Then, we applied a similar z-scored procedure to the raw control signal as the BCI 2000 platform,

$$CS_{real} = G \times (CS_{raw} - offset)$$

where  $G$  and  $offset$  are set to make the  $CS_{real}$  zero mean and unit variance. The difference between this offline z-score and the online approach is that the latter is causal and adaptive, i.e.,  $G$  and  $offset$  is calculated via past 30 s of a window and change as time goes on. As shown in **Supplementary Figure 1**, we found that the control signal under this definition could better explain the variability of performance than the ERD/ERS method, i.e., band power during task execution divided by resting-state band power.

We quantify the contrast between two contexts in a task (e.g., left trials and right trials in LR task) using the Fisher score (Perdikis et al., 2018).

$$FS = \frac{|\mu_1 - \mu_2|}{\sqrt{s_1^2 + s_2^2}}$$

where  $\mu_1$  and  $\mu_2$  are the means and  $s_1^2$  and  $s_2^2$  are the variance of context 1 and context 2's band power in one session. The Fisher score is calculated independently for each channel, and its topology was obtained using FieldTrip (Oostenveld et al., 2010) toolbox; data in between-electrodes space are interpolated in a linear fashion.

When evaluating the statistical difference between the two groups, we noticed some outliers in subjects' neurophysiological metrics (SMR predictor and control signal contrast); therefore, we identified and excluded these outliers from analysis with the same method mentioned in section "Performance Metric." We did not find outliers when analyzing SMR predictor; we found additional two meditators and one control outlier when analyzing the resting-state EEG stability; we found an additional one meditator and one control outlier when analyzing the LR control signal; we found an additional one control outlier when analyzing the UD control signal. The results obtained in **Figure 5B** are obtained after excluding these additional outliers.

## Statistical Analysis

We performed linear mixed-effects models per type of performance and neurophysiological measures to investigate the session, group, and interaction effect. lme4 package (1.1-25) in R (4.0.3) was used to generate the linear mixed-effects models, and  $p$ -values were computed using lmerTest package (3.1-3), using Satterthwaite approximation for degrees of freedom (Kuznetsova et al., 2017). Each BCI performance and neurophysiological measure were modeled over time with a fixed

effect of session (six levels) and group (two levels, meditator and control). Random effects include within-subject factors of the session. Models were initially fit with the interaction of group and time, and then, fixed effects were reduced stepwise by excluding non-significant interaction terms/predictors and compared using ANOVA ratio tests until this smaller model explained the data significantly worse than the larger model (significant Chi-squared test) (Kuznetsova et al., 2017). Other statistical tests used in this work include rank-sum test, linear regression, and Chi-squared tests; the details of these tests will be explained wherever it appears in section "Results."

## RESULTS

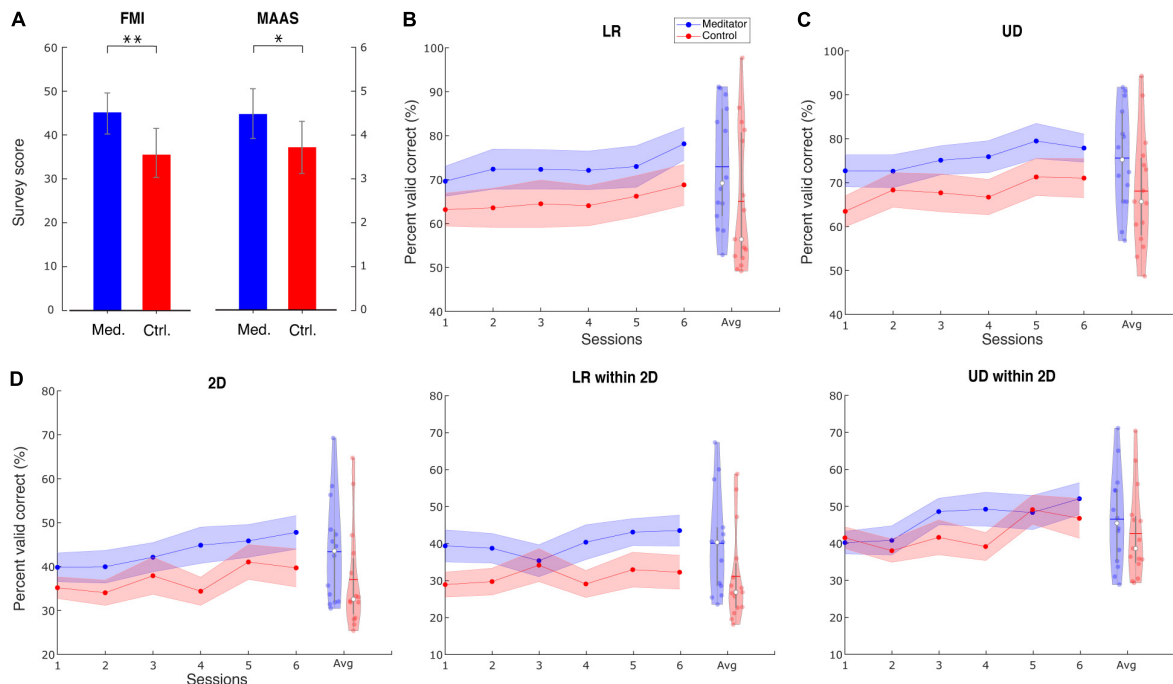
### Survey Results

In both surveys, we found meditators had higher scores than control subjects. Concretely, the FMI score for meditators is  $44.5 \pm 4.5$ , whereas, for control subjects, it is  $36.6 \pm 6.7$ . The difference is significant (Wilcoxon rank-sum test,  $Z = 3.15$ ,  $p < 0.01$ ). The MAAS score for meditators is  $4.42 \pm 0.81$ , whereas, for control subjects, it is  $3.73 \pm 0.67$ . The difference is significant (Wilcoxon rank-sum test,  $Z = 2.53$ ,  $p < 0.05$ ). Bar plots for the two groups' scores are shown in **Figure 2A**. The same observation also holds when including outlier subjects. These results serve as additional support, apart from the self-reported meditation experiences, that the meditators had higher levels of mindfulness than the control group. In addition to the group difference, we also calculated the correlation between these survey results and performance. We used baseline PVC as performance because this session is when the surveys were filled out. The correlation between survey results and UD PVC turned out to be significant. Specifically, for FMI,  $r(27) = 0.42$ ,  $p < 0.05$ , and for MAAS,  $r(27) = 0.41$ ,  $p < 0.05$ .

### Group Averaged Performance

We found that meditators achieved numerically better performance (PVC) compared with control subjects, and this difference was consistent throughout the six sessions. The group averaged performance in the baseline, and the final session is shown in **Supplementary Table 3**, and the averaged performance for all sessions is shown in **Figure 2**.

We used a linear mixed-effects model (see section "Materials and Methods") to investigate the statistical difference between the two groups in terms of group, session, and group-session interaction effect. The session effect indicates if BCI learning occurs for a specific task. We found a significant learning effect in all three tasks [LR:  $t(144) = 2.98$ ,  $p < 0.01$ ; UD:  $t(28) = 2.22$ ,  $p < 0.05$ ; 2D:  $t(28) = 2.84$ ,  $p < 0.01$ ]. The difference in dimensionality is due to the difference in the final model when performing the stepwise reduction (see section "Materials and Methods"). However, the group effect did not show significance [LR:  $F(1, 27) = 2.01$ ,  $p = 0.16$ ; UD:  $F(1, 27) = 2.71$ ,  $p = 0.11$ ; 2D:  $F(1, 27) = 1.79$ ,  $p = 0.19$ ], indicating that there is only a numerical superiority of meditators' BCI performance. We also did not find significance in the learning speed difference between the two groups, indicated by the interaction effect [LR:  $F(1, 143) = 0.1$ ,



**FIGURE 2 |** Survey results and group averaged performance and learning. **(A)** Survey results of FMI and MAAS show that meditators have a higher level of mindfulness than controls. Data are shown as mean  $\pm$  SD. Med. is meditator, Ctrl. is control. **(B)** Line plot describes the group LR averaged PVC  $\pm$  SEM for meditators and controls. Violin plot describes session-averaged performance distribution, with blue horizontal line indicating mean and white dot indicating median. **(C)** For UD task, **(D)** for 2D task, LR within the 2D task, and 2D within the 2D task. \* Indicates group difference with  $p < 0.05$ , and \*\* indicates  $p < 0.01$ , same for subsequent plots.

$p = 0.75$ ; UD:  $F(1, 27) = 0.001$ ,  $p = 0.97$ ; 2D:  $F(1, 27) = 0.32$ ,  $p = 0.57$ ].

Given that the 2D task is the combination of LR and UD, we next separated the LR and UD tasks within the 2D. Interestingly, we found that within the 2D task, meditators had a numerically higher baseline of LR, but for the UD, these two groups were at the same level. Further, the learning curve showed that meditators had numerically better learning compared with controls in the UD within 2D. Statistical analysis using linear mixed-effects model shows that learning effect of UD within the 2D is significant, whereas LR within the 2D is not [LR within 2D:  $F(1, 28) = 2.58$ ,  $p = 0.11$ ; UD within 2D:  $t(28) = 2.92$ ,  $p < 0.01$ ]. We did not find the group effect to be significant [LR within 2D:  $F(1, 27) = 3.11$ ,  $p = 0.08$ ; UD within 2D:  $F(1, 27) = 0.45$ ,  $p = 0.50$ ], as well as the interaction effect [LR within 2D:  $F(1, 27) = 0.21$ ,  $p = 0.64$ ; UD within 2D:  $F(1, 27) = 0.28$ ,  $p = 0.60$ ].

## Competency Curve

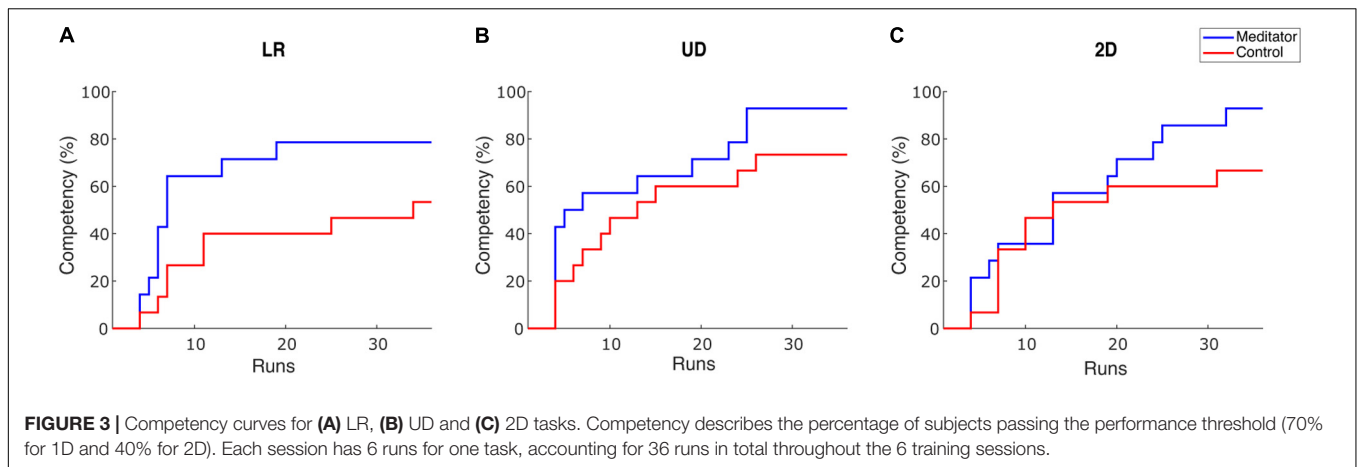
Although group averaged PVC is a good indicator of performance, there are several drawbacks. First, it only provides information on the overall trend of performance during BCI learning; we still do not know how many subjects remain BCI inefficient. Second, it does not provide information regarding within-session learning.

To intuitively show how learning occurs in the two groups, we plotted competency, the percentage of subjects whose PVC passed the BCI inefficiency threshold as sessions go on. We set

the threshold as 70% for 1D control and 40% for 2D control (Combrisson and Jerbi, 2015), but we obtain similar results under varied thresholds. To cope with potential fluctuation of performance, a subject passes the threshold if she/he meets one of the following criteria: achieving an averaged PVC  $>$  threshold in three consecutive runs or achieving an averaged PVC  $>$  threshold in one single session (Cassady et al., 2014). The result is shown in Figure 3.

There are two observations from this plot. First, after six sessions of learning, the percentage of subjects passing the BCI inefficiency threshold appears to be higher in meditators. The percentage of non-BCI inefficient subjects is 78.5% (53.3%), 92.8% (73.3%), and 92.8% (66.7%) for meditators (controls), in LR, UD, and 2D tasks, respectively. Therefore, in all three tasks, meditators indeed had numerically less BCI inefficient subjects after six sessions or 36 runs of learning, but Chi-squared tests did not reveal a significant difference for the competency between two groups [ $X^2(1, N = 29) = 2.04, 1.93, 3.02$ ,  $p = 0.15, 0.16$  and  $0.08$  for LR, UD, and 2D]. Second, regarding the speed of learning, the LR and the UD plot showed a steeper decline during the initial six runs, i.e., the baseline session. This means that the learning speed of meditators appears to be faster than the control subjects. Besides, although previous studies showed that BCI learning occurs on a session-by-session basis (Meng et al., 2016), our results showed that learning could also occur within a 2 h session. We also noticed that compared with 1D tasks (LR and UD), both groups in the 2D task showed a similar





learning curve in the first 20 runs, i.e., in the first three sessions. After that, meditators showed a numerically better learning speed compared with control subjects. This observation is consistent with the previous group average performance in the sense that in UD within the 2D task, meditators had numerically larger improvement starting from the third session. In addition, it also shows that 2D control is indeed more difficult than 1D control, requiring more training time.

### Group Averaged Topology During Task

Figure 4 shows the LR and UD task Fisher score topology (Perdikis et al., 2018) for meditators and controls. From the plot, a gradual increase of motor cortex area high alpha power could be seen in both groups, indicating that both groups were able to increase the contrast of two opposite conditions through voluntary motor imagery as learning progresses. However, this plot did not provide quantitative information regarding whether meditators had a higher baseline of C3 and C4 high alpha power or exhibited better learning. We also did not find electrode clusters with a significant difference between the two groups with cluster-based permutation tests (Stieger et al., 2020). To further investigate the effect of meditation experience on these quantities, we looked into the SMR predictor during the intertrial resting state, mu power variability at rest, and control signal contrast during task execution.

### Neurophysiological Predictor

Blankertz et al. (2010) found that in the resting state power spectral density plots of C3 and C4 electrodes, the difference between mu rhythm peak and noise level baseline is a significant predictor of the BCI performance. Here, we tried to investigate the difference in SMR predictor between meditators and controls. As shown in Figure 5A, we first fit a linear regression model between the SMR predictor and PVC. We found that in the LR task, the correlation coefficient between SMR predictor and PVC is  $r(153) = 0.13$ ,  $p = 0.11$ , and in the UD task,  $r(153) = 0.20$  with  $p < 0.05$ . Our correlation coefficient was smaller than that of Blankertz et al. (2010). The difference might be due to the task design, subject variability, or it could be due to the fact that Blankertz et al. (2010) recorded a 2 min resting state,

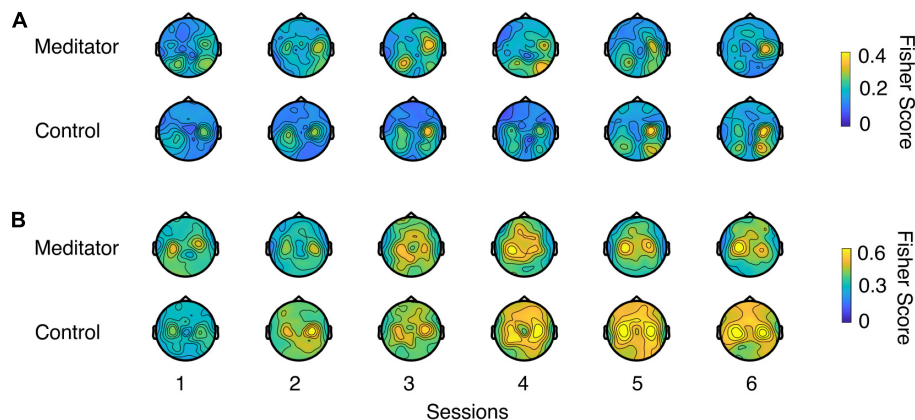
whereas, here, we used multiple short pretrial segments. We next asked if the session, group, and interaction effects exist in the SMR predictor. We found that the session effect is significant [ $t(125) = 2.42$ ,  $p < 0.05$ ], but we did not find the group and interaction effects to be statistically different between meditators and controls [group effect:  $F(1, 27) = 3.29$ ,  $p = 0.08$ ; interaction:  $F(1, 124) = 0.001$ ,  $p = 0.96$ ]. However, as shown in Figure 5B, a numerical difference between the meditator group and the control could be observed.

### Variability of Resting Electroencephalogram Mu Rhythm

Another perspective of investigating the resting state difference between meditators and controls is the stability of the EEG pattern, i.e., the mu rhythm in the SMR BCI setting. Sannelli et al. (2008) pointed out that BCI inefficient subjects usually have higher intrinsic noise. Specifically, this means that the presentation of noise in EEG band power overshadows the useful information. In our study, a relevant measurement of noise could be the variability or stability of EEG mu rhythm, and we hypothesize that this is related to the performance. Here, we used the coefficient of variation (CV) (Brown, 1998) to measure variability: the ratio of intertrial resting-state EEG mu power standard deviation and its mean. The lower the value, the more stable the EEG pattern is. We indeed found that the stability is negatively correlated with the performance [LR:  $r(172) = -0.19$ ,  $p < 0.05$ , UD:  $r(172) = -0.18$ ,  $p < 0.05$ ], when excluded potential outlier points, the relationship between LR PVC and stability is still significant [LR:  $r(154) = -0.17$ ,  $p < 0.05$ ], whereas for UD, it is not [UD:  $r(154) = -0.13$ ,  $p = 0.11$ ], indicating that the correlation is weak, especially for UD task. This CV did not show session, group, or interaction effect [session effect:  $F(1, 129) = 0.34$ ,  $p = 0.55$ ; group effect:  $F(1, 24) = 1.36$ ,  $p = 0.25$ ; interaction:  $F(1, 128) = 0.63$ ,  $p = 0.42$ ]. These results are shown in Figures 5C,D.

### Control Signal Baseline and Learning

Given the behavior difference described in the previous section, the next question to ask is whether meditators exhibit better



**FIGURE 4 |** Fisher score topology for meditators and controls during **(A)** LR and **(B)** UD task as session goes on. Fisher score describes the mu rhythm contrast between two opposite contexts in a task (e.g., left trials and right trials in LR task, or up trials and down trials in UD task).

overall performance and learning of  $\Delta$ control signal. Like the online scenario (see section “Materials and Methods”), we computed the control signal as the difference of z-scored C4 power and C3 power (for LR) or summation of z-scored C4 power and C3 power. The  $\Delta$ control signal is the difference of control signal between two opposite trial types (LR and UD). **Figures 5E,F** show the group averaged  $\Delta$ control signal as sessions go on. We noticed a session effect in the UD  $\Delta$ control signal [ $t(27) = 2.05, p < 0.05$ ] but not the LR  $\Delta$ control signal [ $F(1,134) = 0.96, p = 0.32$ ]. However, we did not notice significance in group [LR:  $F(1,25) = 0.68, p = 0.41$ ; UD:  $F(1,26) = 1.26, p = 0.27$ ] or interaction effect [LR:  $F(1,133) = 0.71, p = 0.39$ ; UD:  $F(1,26) = 0.09, p = 0.75$ ].

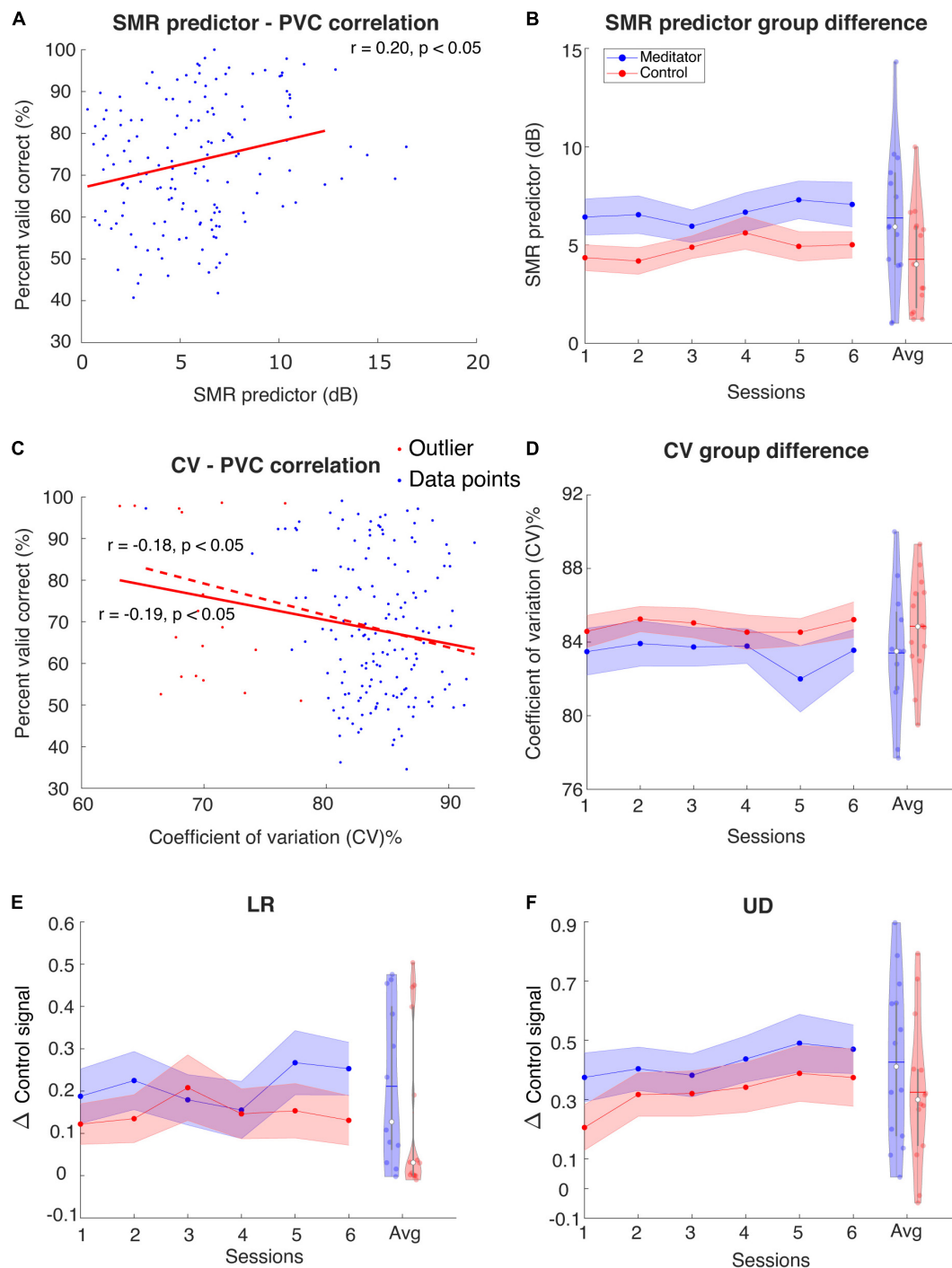
## DISCUSSION

Reducing the training time and BCI inefficiency is critical for the application of SMR-based BCI. Although prior studies have tried to solve this problem from the “brain” side of BCI by investigating the effect of meditation experience on SMR BCI learning, the relationship between these two is still not comprehensive. First, due to the large variability in the type and duration of meditation, more studies are needed to confirm the existence of such an effect. Second, it is still unclear whether and to what extent meditators are better able to do more complex tasks than 1D control. Third, a more thorough investigation of the neurophysiological difference between these two groups is needed.

Our results provide insights into the effect of long-term meditation experiences on SMR-based BCI. Concretely, we found that level of mindfulness is significantly correlated with the SMR BCI performance in the UD task, and experienced meditators had numerically higher overall BCI performance compared with meditation naïve subjects. We also found that there were numerically fewer BCI inefficient subjects remaining after six sessions of learning. As for task complexity, we extended the control paradigm to a more complex 2D cursor control task.

We found a similar trend when separating the LR and UD tasks within the 2D control, that meditators had numerically higher LR performance within the 2D task than controls. We also found that although meditators and controls started at approximately the same level of UD performance within the 2D task, numerically, meditators exhibited better learning and resulted in higher improvement than controls. Finally, neurophysiology analysis revealed a numerical difference between the SMR predictor, resting mu power stability, and UD control signal. Nevertheless, the statistical significance mainly lies in the learning of the task, i.e., subjects statistically improved their BCI performance after learning; we did not find that meditators statistically outperformed control subjects in terms of averaged performance and learning speed. As for the task difficulty and learning, we found that although the 1D version of LR and UD tasks both have a significant learning effect, in 2D, only the UD part showed significant learning. In terms of the  $\Delta$ control signal, we also found a significant learning effect of UD rather than LR. This observation is in agreement with Stieger et al. (2020) and suggests that the neurophysiological processes involved in learning the UD task (motor imagery vs. rest) could be easier to learn than the LR task (left motor imagery vs. right motor imagery).

It should be noted that our experimental task is consistent with prior work (Cassady et al., 2014) in terms of the platform (BCI 2000) and 1D BCI task design. However, there are several points that this prior work did not address: (1) Most of their claims were focused on the behavioral difference, including PVC and competency; the analysis on the neurophysiological difference between the two groups was limited. We added the electrophysiological topology, SMR predictor, mu stability, and control signal analysis to this framework, which could better explain the neurophysiological difference between the two groups. (2) Cassady and colleagues’ work did not implement 2D control tasks, which represents a more challenging task. Although by design, the 2D task is the combination of LR and UD control, in real-time BCI control, it is more challenging because subjects need to carefully maintain the cursor position while moving the cursor in the prompted direction. As meditators are better able



**FIGURE 5 | (A)** Regression between SMR predictor and PVC for UD task. Red line is regression line. For LR the correlation is not significant (plot not shown). **(B)** Group averaged SMR predictor for the meditator group and control group. Violin plot shows the session-averaged result. **(C)** Regression between resting-state stability and PVC for LR task. For UD task the correlation is only significant before excluding outliers (plot not shown). **(D)** Group averaged stability for the meditator group and control group. Violin plot shows the session-averaged result. **(E,F)** Group averaged  $\Delta$  control signal for **(E)** LR and **(F)** UD. Violin plot shows the session-averaged result.

to control their attention, they might perform even better than controls compared with 1D tasks. Currently, we are not aware of prior literature explicitly investigating the 2D cursor control

of long-term meditators and controls. Therefore, it is of interest to see if meditators would also be better at the 2D task, how much they outperform the controls, and if there is any difference

between the LR and UD within the 2D compared with the 1D version of LR and UD tasks. (3) It is known that there exists a large variability of SMR BCI performance in the population. Apart from the literature that reports the positive influence of meditation on SMR BCI control, we are also aware of literature that only partially supports or does not support the hypothesis that people with meditation experience would demonstrate better SMR BCI control (Botrel and Kübler, 2019; Stieger et al., 2020). Therefore, to make a claim more rigorous, it is important to show the replicability of results.

Our study serves to confirm and extend this finding by conducting experiments at a different location and time with independent subjects and experimenters. Specifically, although we generally found that meditators on average outperformed control subjects by 5–10% PVC, we did not find a statistical difference between the two groups in terms of overall performance (as shown in the group effect) and learning speed (as shown in the interaction effect), and the percentage of BCI inefficient subjects in these two groups was not statistically different (although the *p*-value was small). The difficulty of getting statistical significance could be due to the following two reasons: (1) Meditation experience is not the determining factor for generating SMR, and the effect is weak. (2) The variability among SMR BCI performance is large, thus requiring a larger sample size. For example, in Stieger et al. (2020), they implemented twice as large a sample size as us, but this requires much larger efforts to acquire. Therefore, our work updates the community about “how much” meditators perform better than meditation naïve people at SMR BCI and could serve as a reference for researchers who would like to recruit experienced meditators to obtain a better SMR BCI control.

Nevertheless, it is still of interest to discuss the potential cause of this meditation effect, as it could provide insight into what factors do influence BCI performance: The long-term meditation effect on SMR BCI could be due to the plasticity introduced by meditation experience. For example, one of the main benefits of mindfulness meditation is enhanced attentional control (MacLean et al., 2010). In the SMR BCI task, subjects are instructed to focus on or pay attention to the motor intention, which could be regarded as a specific type of attention control. Therefore, the prolonged meditation practices might serve as additional “training time” and cause the meditator group to have enhanced BCI performance. Future work along this line should investigate if neurotypical people are also able to improve SMR BCI control, apart from UD tasks (Stieger et al., 2020), with more extended meditation training.

An alternative explanation would be the preexisting difference in brain structure, personality, etc., for people who choose to meditate for years (Tang et al., 2015). In other words, the subpopulation who choose to meditate for years may have attributes that contribute to a successful SMR BCI control. Nevertheless, the research focusing on SMR BCI control ability for people with different characteristics is still limited, and future work on investigating the impact of these multidimensional and interrelated personal attributes might reveal more details of SMR BCI control.

The presence of BCI proficient subjects is also of importance to study. Multiple studies have shown that there exists a certain portion of subjects who are able to control the SMR BCI with very high accuracy the first time they use this technology (Edelman et al., 2019; Stieger et al., 2020). In our study, we quantified these subjects by the outlier exclusion criteria described in section “Materials and Methods.” See **Supplementary Table 2** for the details of these outliers’ performance. We found five subjects quantified as outliers; all were BCI proficient subjects. Interestingly, we found that there is only one meditator but four controls among them. This phenomenon is interesting because (1) it points out that meditation is not the determining factor of BCI proficiency, as a large portion of outliers are controls; (2) given that controls have numerically lower BCI performance and more BCI proficient subjects, larger variability might exist within the population with no meditation experience. Although more data are needed to validate this observation, it could be another perspective to investigate the effect of meditation on SMR BCI.

EEG resting mu rhythm variability and SMR BCI. In this study, we found that the resting EEG coefficient of variation (CV) is related to SMR BCI performance and could serve as an SMR BCI indicator, such as the SMR predictor (Blankertz et al., 2010). However, going back to the central question of finding a training paradigm to help prepare subjects for SMR BCI control, such an indicator is not optimal due to the lack of a clear training method, i.e., the training procedure of reducing resting EEG variance is not well established. We believe at least two potential research directions could be inspired by our work given the numerically more stable resting-state EEG signals of the meditator group: (1) Validation of the effect of resting-state EEG signal on SMR BCI performance by an independent investigator and BCI system; (2) A further investigation of the relationship between meditation training and resting-state EEG stability through a longitudinal perspective, i.e., if people could gain more stable resting-state EEG signal through meditation training. Research along this line could answer both “what causes the SMR BCI performance variation” and “how to improve SMR BCI,” which we believe is of high practical value.

Potential influence of presentation of the three tasks. In our study, the order of the three tasks is fixed for all subjects, i.e., LR followed by UD, followed by 2D. The fact that they are not randomized could influence the performance because subjects are usually more concentrated on the early phase of the experiment. Nevertheless, we believe the current study design is still of benefit to the question we are trying to address: if there exists a difference in learning within a task between meditators and controls. It would be fairer to compare the performance of a task given a similar level of tiredness. On the other hand, the randomized task design could be used to more rigorously investigate if the learning between different tasks is different, but it should also be noted that a larger sample size would be needed because of the randomized design.

Another concern regarding studying these two distinct groups is the effect of age and sex on our results. Although we tried our best to find age-matched controls for the meditators, the



meditators were on average 38.5 years old, and the controls were on average 24.8 years with a 13.7 years difference. One might argue that if meditators in our sample were more senior, this might affect our conclusion. However, we did not find evidence of significant correlations between age and performance, age and  $\Delta$ control signal, or age and SMR predictor (see **Supplementary Table 4**). These results suggest that the influence of age on our BCI system is not significant. As for sex, we have six females and eight males in the meditator group and 11 females and four males in the control group. Randolph (2012) found that females could be better at BCI tasks, but in our BCI setting, we did not find a significant difference in LR, UD, and 2D performance or SMR predictor between male and female subjects (see **Supplementary Table 4**). Nevertheless, this insignificance could also be due to the insufficient sample size, and future work along this line should either try to recruit a larger number of samples to validate the effect of age and sex or try to recruit subjects with a more balanced age and sex.

## CONCLUSION

In this study, we have examined the behavior and neurophysiological differences between experienced meditators and control subjects. We found evidence supporting that long-term meditation experiences could influence SMR BCI in terms of averaged performance, SMR predictor, resting-state mu stability, and control signal during task execution. This finding has implications on enhancing the “brain” side of SMR BCI and may help overcome the limitations of SMR BCI technology, such as long training time and BCI inefficiency.

## DATA AVAILABILITY STATEMENT

The data presented here are available upon reasonable request from the corresponding author.

## ETHICS STATEMENT

The studies involving human participants were reviewed and approved by the Institutional Review Board (IRB) of Carnegie Mellon University. The participants provided their written informed consent to participate in this study.

## REFERENCES

- Ahn, M., and Jun, S. C. (2015). Performance variation in motor imagery brain-computer interface: a brief review. *J. Neurosci. Methods* 243, 103–110. doi: 10.1016/j.jneumeth.2015.01.033
- Ang, K. K., Chua, K. S. G., Phua, K. S., Wang, C., Chin, Z. Y., Kuah, C. W. K., et al. (2015). A randomized controlled trial of EEG-Based motor imagery brain-computer interface robotic rehabilitation for stroke. *Clin. EEG Neurosci.* 46, 310–320. doi: 10.1177/1550059414522229
- Armour, B. S., Courtney-Long, E. A., Fox, M. H., Fredine, H., and Cahill, A. (2016). Prevalence and causes of paralysis—United States, 2013. *Am. J. Public Health* 106, 1855–1857. doi: 10.2105/AJPH.2016.303270

## AUTHOR CONTRIBUTIONS

XJ was involved in experiment conduction, data analysis, and manuscript writeup. EL was involved in experiment conduction and manuscript review. JS was involved in study design, experiment conduction, and manuscript review. CG was involved in study design, subject recruitment, and manuscript review. BH was involved in the conception, study design, supervision, and manuscript review. All authors contributed to the article and approved the submitted version.

## FUNDING

This work was supported in part by the National Institutes of Health (grants AT009263, MH114233, EB021027, NS096761, and EB008389).

## ACKNOWLEDGMENTS

We would like to thank Drs. David Creswell and Haiteng Jiang for useful discussions, Chang Liu and Kristie Lindblom for assistance in subject recruitment, and Olivia Fernau and Chalisa Udompanyawit for assistance in experimentation.

## SUPPLEMENTARY MATERIAL

The Supplementary Material for this article can be found online at: <https://www.frontiersin.org/articles/10.3389/fnins.2020.584971/full#supplementary-material>

**Supplementary Figure 1** | Comparison of two methods to compute the  $\Delta$ control signal during task execution. The traditional method to quantify how EEG band power changes during task execution is event-related desynchronization. Concretely, the control signal under the ERD definition would be band power normalized by the resting state alpha activity. Here we argue that the control signal using the z-score method would be a better metric by showing that it explains more performance variability. **(A)** in LR, the correlation coefficient for regression between  $\Delta$ control signal and PVC was 0.70 in the ERD method and 0.8 in the z-scored method,  $p < 0.05$ , **(B)** for UD it was 0.67 and 0.82,  $p < 0.05$ .

**Supplementary Figure 2** | Violin plot for performance and SMR. The violin plot provides more detailed information regarding the mean, median and distribution of the data. **(A)** for LR PVC, **(B)** for UD PVC, **(C)** for 2D PVC, **(D)** for SMR predictor, **(E,F)** for LR and UD  $\Delta$  control signal. The blue/red dots represent everyone's performance, the white dot indicates the median, the blue/red horizontal lines represent the mean, and the violin-like envelop represents the distribution density.

- Bernier, R., Dawson, G., Webb, S., and Murias, M. (2007). EEG mu rhythm and imitation impairments in individuals with autism spectrum disorder. *Brain Cogn.* 64, 228–237. doi: 10.1016/j.bandc.2007.03.004
- Blankertz, B., Sannelli, C., Halder, S., Hammer, E. M., Kübler, A., Müller, K.-R., et al. (2010). Neurophysiological predictor of SMR-based BCI performance. *NeuroImage* 51, 1303–1309. doi: 10.1016/j.neuroimage.2010.03.022
- Botrel, L., and Kübler, A. (2019). Week-long visuomotor coordination and relaxation trainings do not increase sensorimotor rhythms (SMR) based brain-computer interface performance. *Behav. Brain Res.* 372:111993. doi: 10.1016/j.bbr.2019.111993

- Brown, C. E. (1998). "Coefficient of variation," in *Applied Multivariate Statistics in Geohydrology and Related Sciences*, ed. C. E. Brown (Berlin: Springer), 155–157. doi: 10.1007/978-3-642-80328-4\_13
- Brown, K. W., and Ryan, R. M. (2003). The benefits of being present: mindfulness and its role in psychological well-being. *J. Pers. Soc. Psychol.* 84, 822–848. doi: 10.1037/0022-3514.84.4.822
- Cassady, K., You, A., Doud, A., and He, B. (2014). The impact of mind-body awareness training on the early learning of a brain-computer interface. *Technology* 2, 254–260. doi: 10.1142/S233954781450023X
- Chan, D., and Woollacott, M. (2007). Effects of level of meditation experience on attentional focus: is the efficiency of executive or orientation networks improved? *J. Alternat. Complementary Med.* 13, 651–658. doi: 10.1089/acm.2007.7022
- Clerc, M., Bougrain, L., and Lotte, F. (2016). *Brain-Computer Interfaces 1*. Hoboken, NJ: Wiley-ISTE.
- Combrisson, E., and Jerbi, K. (2015). Exceeding chance level by chance: the caveat of theoretical chance levels in brain signal classification and statistical assessment of decoding accuracy. *J. Neurosci. Methods* 250, 126–136. doi: 10.1016/j.jneumeth.2015.01.010
- Debarnot, U., Sperduti, M., Di Rienzo, F., and Guillot, A. (2014). Experts bodies, experts minds: how physical and mental training shape the brain. *Front. Hum. Neurosci.* 8:280. doi: 10.3389/fnhum.2014.00280
- Doud, A. J., Lucas, J. P., Pisansky, M. T., and He, B. (2011). Continuous three-dimensional control of a virtual helicopter using a motor imagery based brain-computer interface. *PLoS One* 6:e26322. doi: 10.1371/journal.pone.0026322
- Edelman, B. J., Meng, J., Suma, D., Zurn, C., Nagarajan, E., Baxter, B. S., et al. (2019). Noninvasive neuroimaging enhances continuous neural tracking for robotic device control. *Sci. Robot.* 4:aaw6844. doi: 10.1126/scirobotics.aaw6844
- Galán, F., Nutton, M., Lew, E., Ferrez, P. W., Vanacker, G., Philips, J., et al. (2008). A brain-actuated wheelchair: asynchronous and non-invasive Brain-computer interfaces for continuous control of robots. *Clin. Neurophysiol.* 119, 2159–2169. doi: 10.1016/j.clinph.2008.06.001
- Guillot, A., Collet, C., Nguyen, V. A., Malouin, F., Richards, C., and Doyon, J. (2008). Functional neuroanatomical networks associated with expertise in motor imagery. *NeuroImage* 41, 1471–1483. doi: 10.1016/j.neuroimage.2008.03.042
- Halsband, U., Mueller, S., Hinterberger, T., and Strickner, S. (2009). Plasticity changes in the brain in hypnosis and meditation. *Contemporary Hypnosis* 26, 194–215. doi: 10.1002/ch.386
- He, B., Baxter, B., Edelman, B. J., Cline, C. C., and Ye, W. W. (2015). Noninvasive brain-computer interfaces based on sensorimotor rhythms. *Proc. IEEE* 103, 907–925. doi: 10.1109/JPROC.2015.2407272
- He, B., Han, Y., Meng, J., and Gao, S. (2020). "Brain-Computer Interfaces," in *Neural Engineering*, 3rd Edn, ed. B. He (Berlin: Springer).
- Huang, D., Qian, K., Fei, D.-Y., Jia, W., Chen, X., and Bai, O. (2012). Electroencephalography (EEG)-Based Brain-Computer Interface (BCI): a 2-D virtual wheelchair control based on event-related desynchronization/synchronization and state control. *IEEE Trans. Neural Systems Rehabil. Eng.* 20, 379–388. doi: 10.1109/TNSRE.2012.2190299
- Jeunet, C., N'Kaoua, B., and Lotte, F. (2016). "Chapter 1 - Advances in user-training for mental-imagery-based BCI control: psychological and cognitive factors and their neural correlates," in *Progress in Brain Research Brain-Computer Interfaces: Lab Experiments to Real-World Applications*, ed. D. Coyle (Amsterdam: Elsevier), 3–35. doi: 10.1016/bs.pbr.2016.04.002
- Jha, A. P., Krompinger, J., and Baime, M. J. (2007). Mindfulness training modifies subsystems of attention. *Cogn. Affect. Behav. Neurosci.* 7, 109–119. doi: 10.3758/CABN.7.2.109
- Kerr, C. E., Jones, S. R., Wan, Q., Pritchett, D. L., Wasserman, R. H., Wexler, A., et al. (2011a). Effects of mindfulness meditation training on anticipatory alpha modulation in primary somatosensory cortex. *Brain Res. Bull.* 85, 96–103. doi: 10.1016/j.brainresbull.2011.03.026
- Kerr, C. E., Josyula, K., and Littenberg, R. (2011b). Developing an observing attitude: an analysis of meditation diaries in an MBSR clinical trial. *Clin. Psychol. Psychotherapy* 18, 80–93. doi: 10.1002/cpp.700
- Kerr, C. E., Sacchet, M. D., Lazar, S. W., Moore, C. I., and Jones, S. R. (2013). Mindfulness starts with the body: somatosensory attention and top-down modulation of cortical alpha rhythms in mindfulness meditation. *Front. Hum. Neurosci.* 7:12. doi: 10.3389/fnhum.2013.00012
- Kober, S. E., Witte, M., Ninaus, M., Koschutnig, K., Wiesen, D., Zaiser, G., et al. (2017). Ability to gain control over one's own brain activity and its relation to spiritual practice: a multimodal imaging study. *Front. Hum. Neurosci.* 11:271. doi: 10.3389/fnhum.2017.00271
- Kuznetsova, A., Brockhoff, P. B., and Christensen, R. H. B. (2017). lmerTest package: tests in linear mixed effects models. *J. Stat. Soft.* 82, 1–26. doi: 10.18637/jss.v082.i13
- LaFleur, K., Cassady, K., Doud, A., Shades, K., Rogin, E., and He, B. (2013). Quadcopter control in three-dimensional space using a noninvasive motor imagery-based brain-computer interface. *J. Neural Eng.* 10:046003. doi: 10.1088/1741-2560/10/4/046003
- Leys, C., Ley, C., Klein, O., Bernard, P., and Licata, L. (2013). Detecting outliers: do not use standard deviation around the mean, use absolute deviation around the median. *J. Exp. Soc. Psychol.* 49, 764–766. doi: 10.1016/j.jesp.2013.03.013
- Lotte, F., and Guan, C. (2011). Regularizing common spatial patterns to improve BCI designs: unified theory and new algorithms. *IEEE Trans. Biomed. Eng.* 58, 355–362. doi: 10.1109/TBME.2010.2082539
- MacLean, K. A., Ferrer, E., Aichele, S. R., Bridwell, D. A., Zanesco, A. P., Jacobs, T. L., et al. (2010). Intensive meditation training improves perceptual discrimination and sustained attention. *Psychol. Sci.* 21, 829–839. doi: 10.1177/0956797610371339
- Mahmoudi, B., and Erfanian, A. (2006). Electro-encephalogram based brain-computer interface: improved performance by mental practice and concentration skills. *Med. Bio Eng. Comput.* 44, 959–969. doi: 10.1007/s11517-006-0111-118
- McFarland, D. J., Sarnacki, W. A., and Wolpaw, J. R. (2010). Electroencephalographic (EEG) control of three-dimensional movement. *J. Neural Eng.* 7:036007. doi: 10.1088/1741-2560/7/3/036007
- Meng, J., Streitz, T., Gulachek, N., Suma, D., and He, B. (2018). Three-Dimensional brain-computer interface control through simultaneous overt spatial attentional and motor imagery tasks. *IEEE Trans. Biomed. Eng.* 65, 2417–2427. doi: 10.1109/TBME.2018.2872855
- Meng, J., Zhang, S., Bekyo, A., Olsoe, J., Baxter, B., and He, B. (2016). Noninvasive electroencephalogram based control of a robotic arm for reach and grasp tasks. *Sci. Rep.* 6:38565. doi: 10.1038/srep38565
- Moore, A., and Malinowski, P. (2009). Meditation, mindfulness and cognitive flexibility. *Consciousness Cogn.* 18, 176–186. doi: 10.1016/j.concog.2008.12.008
- Oostenveld, R., Fries, P., Maris, E., and Schoffelen, J.-M. (2010). FieldTrip: open source software for advanced analysis of meg, eeg, and invasive electrophysiological data. *Comput. Intell. Neurosci.* 2011:e156869. doi: 10.1155/2011/156869
- Perdikis, S., Tonin, L., Saeedi, S., Schneider, C., Millán, J., and del, R. (2018). The cybathlon BCI race: successful longitudinal mutual learning with two tetraplegic users. *PLoS Biol.* 16:e2003787. doi: 10.1371/journal.pbio.2003787
- Pfurtscheller, G., and Aranibar, A. (1979). Evaluation of event-related desynchronization (ERD) preceding and following voluntary self-paced movement. *Electroencephal. Clin. Neurophysiol.* 46, 138–146. doi: 10.1016/0013-4694(79)90063-90064
- Pfurtscheller, G., Brunner, C., Schlögl, A., Lopes, and da Silva, F. H. (2006). Mu rhythm (de)synchronization and EEG single-trial classification of different motor imagery tasks. *NeuroImage* 31, 153–159. doi: 10.1016/j.neuroimage.2005.12.003
- Ramli, N., Su Sim, K., Tan, L. K., Tan, Y. Q., Tan, L. F., Goh, K. J., et al. (2019). Effect of mindfulness meditation on brain-computer interface. *Neurol. Asia* 24, 343–353.
- Randolph, A. B. (2012). "Not all created equal: individual-technology fit of brain-computer interfaces," in *Proceedings of the 2012 45th Hawaii International Conference on System Sciences* (New York, NY: IEEE), 572–578. doi: 10.1109/HICSS.2012.451
- Rebsamen, B., Guan, C., Zhang, H., Wang, C., Teo, C., Ang, M. H., et al. (2010). A brain controlled wheelchair to navigate in familiar environments. *IEEE Trans. Neural Systems Rehabil. Eng.* 18, 590–598. doi: 10.1109/TNSRE.2010.2049862
- Rimbert, S., Zaepffel, M., Riff, P., Adam, P., and Bougrain, L. (2019). Hypnotic state modulates sensorimotor beta rhythms during real movement and motor imagery. *Front. Psychol.* 10:2341. doi: 10.3389/fpsyg.2019.02341
- Royer, A. S., Doud, A. J., Rose, M. L., and He, B. (2010). EEG control of a virtual helicopter in 3-dimensional space using intelligent control strategies. *IEEE*

- Trans. Neural Systems Rehabil. Eng.* 18, 581–589. doi: 10.1109/TNSRE.2010.2077654
- Sannelli, C., Braun, M., Tangermann, M., and Müller, K.-R. (2008). “Estimating noise and dimensionality in bci data sets: towards illiteracy comprehension,” in *Proceedings of the 4th International Brain-Computer Interface workshop and training course* (Graz: Verlag der Technischen Universität Graz).
- Schalk, G., McFarland, D. J., Hinterberger, T., Birbaumer, N., and Wolpaw, J. R. (2004). BCI2000: a general-purpose brain-computer interface (BCI) system. *IEEE Trans. Biomed. Eng.* 51, 1034–1043. doi: 10.1109/TBME.2004.827072
- Stieger, J. R., Engel, S., Jiang, H., Cline, C. C., Kreitzer, M. J., and He, B. (2020). Mindfulness improves brain–computer interface performance by increasing control over neural activity in the alpha band. *Cereb. Cortex* 31, 426–438. doi: 10.1093/cercor/bhaa234
- Tan, L. F., Dienes, Z., Jansari, A., and Goh, S.-Y. (2014). Effect of mindfulness meditation on brain–computer interface performance. *Consciousness Cogn.* 23, 12–21. doi: 10.1016/j.concog.2013.10.010
- Tan, Y.-Q., Tan, L.-F., Mok, S.-Y., and Goh, S.-Y. (2015). Effect of short term meditation on braincomputer interface performance. *J. Med. Bioeng.* 4, 135–138. doi: 10.12720/jomb.4.2.135-138
- Tang, Y.-Y., Hölzel, B. K., and Posner, M. I. (2015). The neuroscience of mindfulness meditation. *Nat. Rev. Neurosci.* 16, 213–225. doi: 10.1038/nrn3916
- Tang, Y.-Y., Ma, Y., Wang, J., Fan, Y., Feng, S., Lu, Q., et al. (2007). Short-term meditation training improves attention and self-regulation. *PNAS* 104, 17152–17156. doi: 10.1073/pnas.0707678104
- Trejo, L. J., Rosipal, R., and Matthews, B. (2006). Brain-computer interfaces for 1-D and 2-D cursor control: designs using volitional control of the EEG spectrum or steady-state visual evoked potentials. *IEEE Trans. Neural Systems Rehabil. Eng.* 14, 225–229. doi: 10.1109/TNSRE.2006.875578
- van den Hurk, P. A. M., Giommi, F., Gielen, S. C., Speckens, A. E. M., and Barendregt, H. P. (2010). Greater efficiency in attentional processing related to mindfulness meditation. *Q. J. Exp. Psychol.* 63, 1168–1180. doi: 10.1080/17470210903249365
- Walach, H., Buchheld, N., Büttenmüller, V., Kleinknecht, N., and Schmidt, S. (2006). Measuring mindfulness—the Freiburg Mindfulness Inventory (FMI). *Personal. Individ. Diff.* 40, 1543–1555. doi: 10.1016/j.paid.2005.11.025
- Wolpaw, J. R., Birbaumer, N., McFarland, D. J., Pfurtscheller, G., and Vaughan, T. M. (2002). Brain–computer interfaces for communication and control. *Clin. Neurophysiol.* 113, 767–791. doi: 10.1016/S1388-2457(02)00057-53
- Wolpaw, J. R., McFarland, D. J., Neat, G. W., and Forneris, C. A. (1991). An EEG-based brain-computer interface for cursor control. *Electroencephal. Clin. Neurophysiol.* 78, 252–259. doi: 10.1016/0013-4694(91)90040-B
- Yuan, H., and He, B. (2014). Brain–Computer interfaces using sensorimotor rhythms: current state and future perspectives. *IEEE Trans. Biomed. Eng.* 61, 1425–1435. doi: 10.1109/TBME.2014.2312397

**Conflict of Interest:** The authors declare that the research was conducted in the absence of any commercial or financial relationships that could be construed as a potential conflict of interest.

Copyright © 2021 Jiang, Lopez, Stieger, Greco and He. This is an open-access article distributed under the terms of the Creative Commons Attribution License (CC BY). The use, distribution or reproduction in other forums is permitted, provided the original author(s) and the copyright owner(s) are credited and that the original publication in this journal is cited, in accordance with accepted academic practice. No use, distribution or reproduction is permitted which does not comply with these terms.



# A Semi-active Exoskeleton Based on EMGs Reduces Muscle Fatigue When Squatting

Zhuo Wang<sup>1,2,3†</sup>, Xinyu Wu<sup>1,2,4†</sup>, Yu Zhang<sup>1,2,3</sup>, Chunjie Chen<sup>1,2,4\*</sup>, Shoubin Liu<sup>3</sup>, Yida Liu<sup>1,2,4</sup>, Ansi Peng<sup>1,2,4</sup> and Yue Ma<sup>1,2,4</sup>

<sup>1</sup> Chinese Academy of Sciences Key Laboratory of Human-Machine-Intelligence Synergic Systems, Shenzhen Institutes of Advanced Technology, Chinese Academy of Sciences, Shenzhen, China, <sup>2</sup> Guangdong Provincial Key Lab of Robotics and Intelligent System, Shenzhen Institutes of Advanced Technology, Chinese Academy of Sciences, Shenzhen, China, <sup>3</sup> School of Mechanical Engineering and Automation, Harbin Institute of Technology, Shenzhen, China, <sup>4</sup> ShenZhen College of Advanced Technology, University of Chinese Academy of Sciences, Shenzhen, China

## OPEN ACCESS

### Edited by:

Hong Cheng,  
University of Electronic Science and  
Technology of China, China

### Reviewed by:

Rui Huang,  
University of Electronic Science and  
Technology of China, China  
Wenbin Chen,  
Huazhong University of Science and  
Technology, China  
Haoyao Chen,  
Harbin Institute of Technology,  
Shenzhen, China

### \*Correspondence:

Chunjie Chen  
cj.chen@siat.ac.cn

<sup>†</sup> These authors contributed equally to  
this work

**Received:** 03 November 2020

**Accepted:** 01 March 2021

**Published:** 06 April 2021

### Citation:

Wang Z, Wu X, Zhang Y, Chen C,  
Liu S, Liu Y, Peng A and Ma Y (2021)  
A Semi-active Exoskeleton Based on  
EMGs Reduces Muscle Fatigue When  
Squatting.  
Front. Neurobot. 15:625479.  
doi: 10.3389/fnbot.2021.625479

In dynamic manufacturing and warehousing environments, the work scene made it impossible for workers to sit, so workers suffer from muscle fatigue of the lower limb caused by standing or squatting for a long period of time. In this paper, a semi-active exoskeleton used to reduce the muscle fatigue of the lower limb was designed and evaluated. (i) Background: The advantages and disadvantages of assistive exoskeletons developed for industrial purposes were introduced. (ii) Simulation: The process of squatting was simulated in the AnyBody.7.1 software, the result showed that muscle activity of the gluteus maximus, rectus femoris, vastus medialis, vastus lateralis, vastus intermedius, and erector spinae increased with increasing of knee flexion angle. (iii) Design: The exoskeleton was designed with three working modes: rigid-support mode, elastic-support mode and follow mode. Rigid-support mode was suitable for scenes where the squatting posture is stable, while elastic-support mode was beneficial for working environments where the height of squatting varied frequently. The working environments were identified intelligently based on the EMGs of the gluteus maximus, and quadriceps, and the motor was controlled to switch the working mode between rigid-support mode and elastic-support mode. In follow mode, the exoskeleton moves freely with users without interfering with activities such as walking, ascending and descending stairs. (iv) Experiments: Three sets of experiments were conducted to evaluate the effect of exoskeleton. Experiment one was conducted to measure the surface electromyography signal (EMGs) in both condition of with and without exoskeleton, the root mean square of EMGs amplitude of soleus, vastus lateralis, vastus medialis, gastrocnemius, vastus intermedius, rectus femoris, gluteus maximus, and erector spinae were reduced by 98.5, 97.89, 80.09, 77.27, 96.73, 94.17, 70.71, and 36.32%, respectively, with the assistance of the exoskeleton. The purpose of experiment two was aimed to measure the plantar pressure with and without exoskeleton. With exoskeleton, the percentage of weight through subject's feet was reduced by 63.94, 64.52, and 65.61% respectively at 60°, 90°, and 120° of knee flexion angle, compared to the condition of without exoskeleton. Experiment three was purposed to measure the metabolic cost at a speed of 4 and 5 km/h with and without exoskeleton. Experiment



results showed that the average additional metabolic cost introduced by exoskeleton was 2.525 and 2.85%. It indicated that the exoskeleton would not interfere with the movement of the wearer. Seriously in follow mode. (v) Conclusion: The exoskeleton not only effectively reduced muscle fatigue, but also avoided interfering with the free movement of the wearer.

**Keywords:** semi-active exoskeleton, industrial exoskeleton, lower-limb exoskeleton, human-robot collaboration, EMG signal

## 1. INTRODUCTION

Despite the on-going trend in automation and mechanization in the industry, many workers still suffer from work-related musculoskeletal disorders due to unnatural body postures (De Looze et al., 2016; Huang et al., 2019). For example, in dynamic manufacturing and warehousing environments, the work scene made it impossible for workers to seat, so workers suffered from muscle fatigue of the lower limb caused by standing or squatting for a long period of time. Exoskeleton was suggested as a potential method to reduce exposure to activities and avoid postures that increase the risk of knee injury (Reid et al., 2010). Meanwhile, exoskeleton was suitable for application in such a dynamic scenario, which was not only providing support for the wearer anywhere, but also would not affect the free movement of the wearer.

An exoskeleton could be defined as a wearable, external mechanical device that augmented the performance of an able-bodied wearer, and helped disabled people to retrieve some motion abilities (Dollar and Herr, 2008; Krut et al., 2010; Huang et al., 2018). Exoskeletons could be divided into active exoskeleton and (quasi) passive exoskeleton according to whether there was a power supply. An active exoskeleton was driven by one or more actuators (e.g., electrical motor, pneumatic artificial muscle and hydraulic cylinder), so active exoskeleton was able to provide larger assistance force (Bosch et al., 2016). For example, the ReWalk Personal 6.0 System (Esquenazi et al., 2012), which has been developed for spinal cord injured patients (Rupal et al., 2017), was actuated by DC motors at the hip and knee joints; Muscle Suit Power, which was able to provide up to 35.7 kgf assistive force, was actuated by four McKibben artificial muscles (Kobayashi, 2016); Ekso NR was actuated by hydraulic actuators and was designed to help patients to relearn to correctly stand and work after stroke (Bionics, 2015). However, the efficiency and operation range were negatively affected due to the introduction of the heavy actuators and external power supplies (van Dijk and Van der Kooij, 2014). A (quasi) passive exoskeleton was driven by any type of actuator, but rather applied elastic materials, springs or dampers to store energy harvested by human motion and to use this as required to support a posture or a motion (De Looze et al., 2016). LegX (6.2 kg) (Pillai et al., 2020) and the Chairless Chair (Spada et al., 2018) were passive exoskeletons, which were used to reduce the effort of muscles when the wearer was in a position (e.g., squatting and semi-squatting) and they wished to maintain the position for a long time. But the chairless chair required wearers to fix a position

by crouching down into the required position and pushing a button. And it was easy to interfere with the movement of the wearer because the joint axes of the Chairless Chair and wearer did not coincide.

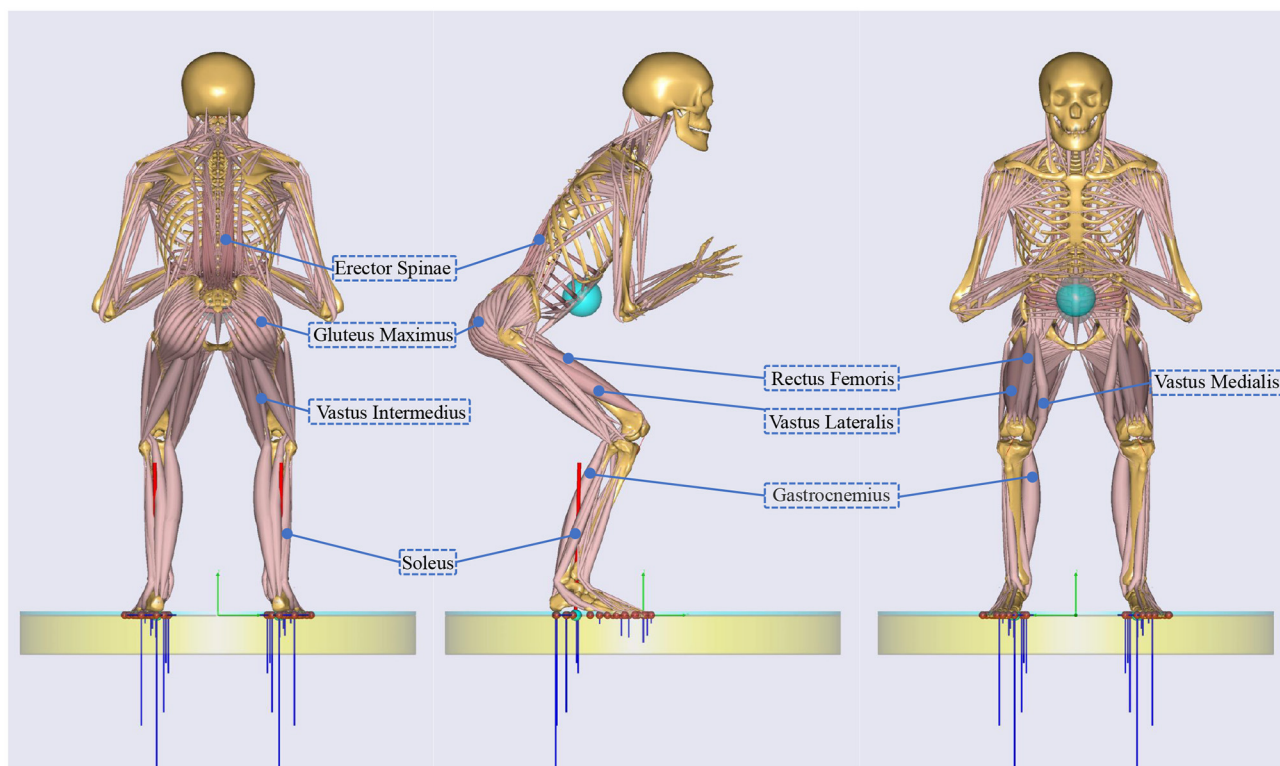
In this paper, a semi-active exoskeleton was developed. With respect to already existing devices (Collo et al., 2016), special emphasis was placed on its light weight as well as multi working modes. The weight of the semi-active exoskeleton developed by us was only 2.6 kg, which was only 42% of the weight of the LegX and 74% of the weight of the Chairless Chair. Meanwhile, it was easy to switch among three working modes: rigid-support mod, elastic-support mode and follow mode. In rigid-support mode, the weight of the wearer was supported by the exoskeleton like a chair, instead of just relying on the legs when the wearer was squatting and semi-squatting. Meanwhile, the locking angle was adjusted easily by ratchet and pawl according to the flexion angle ( $0^\circ \sim 135^\circ$ ) of the knee joint. Elastic-support mode was beneficial for working environments where the height of squatting varied frequently, which provided assist force depending on the deformation of the torsion spring. In follow mode, the passive exoskeleton moved simultaneously with the legs of the wearer.

The main structure of this paper was as follows: the process and results of simulating squat were demonstrated in detail in section 2. The design of the exoskeleton was described in section 3. The experiment and result were presented in section 4. The exoskeleton was discussed in section 5.

## 2. SIMULATION

Generally speaking, the locomotion system of humans was composed of skeletons, joints and muscles. The force generated by muscle contraction drove the skeleton to rotate around the joint (Nordin and Frankel, 2001; Neumann, 2013). Erector spinae, quadriceps femoris, gluteus maximus, and triceps surae are stretched when squatting, as shown in the **Figure 1**. Among them, quadriceps femoris included rectus femoris, vastus medialis, vastus medialis and vastus intermedius, triceps surae consisted of gastrocnemius and soleus. The force generated by stretched erector spinae compensated gravity to maintain a semi-squatting posture.

AnyBody (AnyBody.7.1, AnyBody Technology A/S, Aalborg, Denmark) was capable of analyzing the musculoskeletal system of humans (Damsgaard et al., 2006). To analyze the muscle activity of erector spinae, quadriceps femoris, gluteus maximus



**FIGURE 1 |** The main muscles involved in squatting.

and triceps surae during squatting, the process of squatting was simulated in the AnyBody software. The musculoskeletal modeling and simulation of squatting were based on the demo provided by AnyBody Technology (Wu et al., 2020). The parameters in the musculoskeletal model were modified according to the subjects' body (De Roeck et al., 2020): The time period of a squat cycle and frames per second for simulation were set to 3 s and 30, respectively, minimum and maximum knee flexion angle of a squat cycle were set as  $10^\circ$  and  $135^\circ$ , squat distance between toe medial nodes shoulder width ratio and squat angle foot rotation were set to 1.6 and  $5^\circ$  separately.

Changes in muscle activity of a squat cycle were shown in **Figure 2**. As the knee flexion angle gradually increased from  $10^\circ$  to  $135^\circ$ , the muscle activity of the gluteus maximus, rectus femoris, vastus medialis, vastus lateralis, vastus intermedius, and erector spinae first increased and then decreased, while the muscle activity of gastrocnemius and soleus decreased. The muscle activity of the gluteus maximus, rectus femoris, vastus medialis, vastus lateralis, vastus intermedius and erector spinae reached the maximum of 0.2598, 0.1904, 0.1264, 0.2, 0.091, and 0.2334, respectively, at the knee flexion angle of 115, 118, 54, 54, 96, and  $52^\circ$ . The higher the muscle activity value, the more intense the muscle contraction. So the function of the semi-active exoskeleton was aimed to reduce the muscle activity involved when squatting.

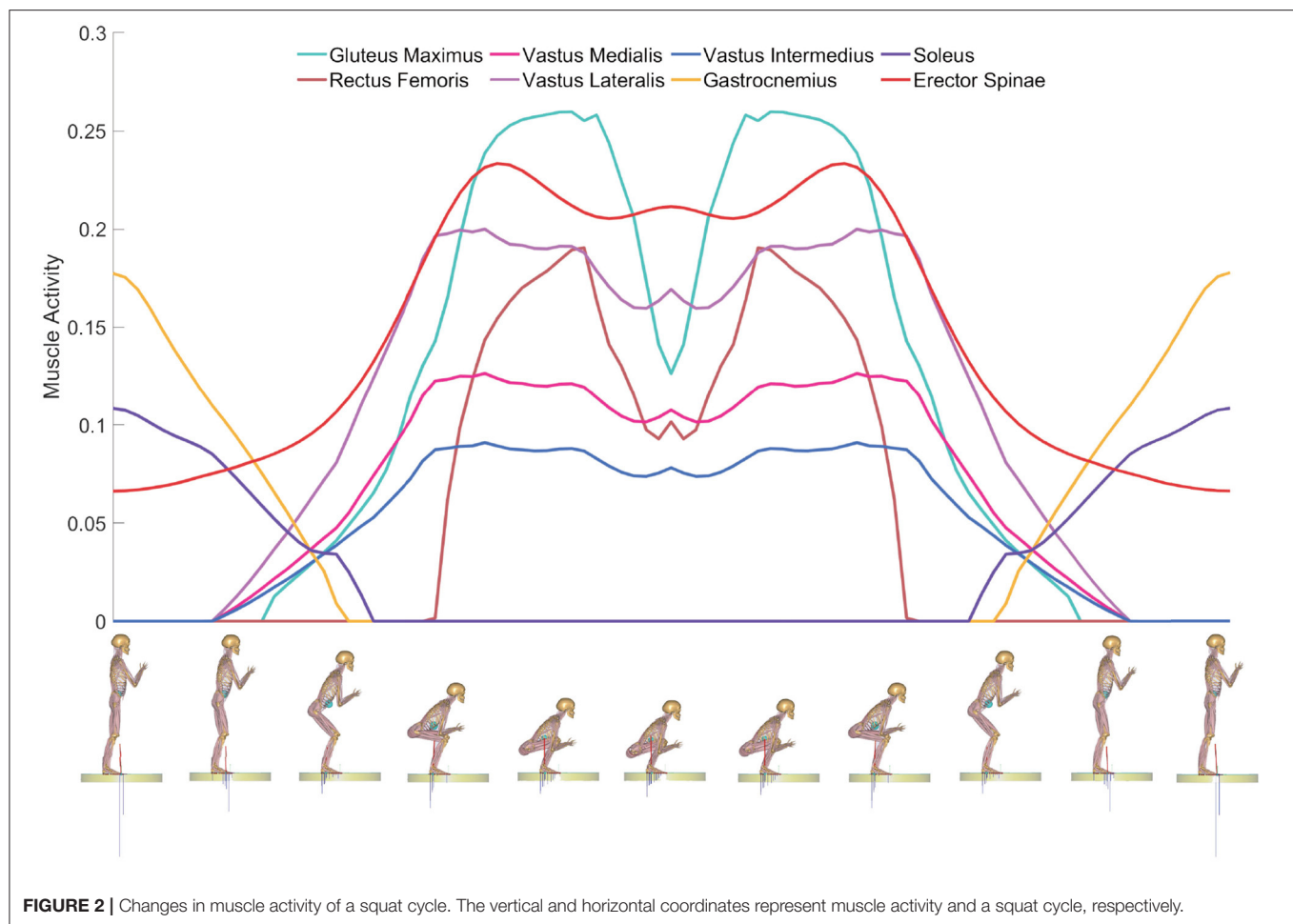
### 3. DESIGN OF THE EXOSKELETON

The assistive device presented in this work was used to provide support when the wearer was in a semi-squatting position for a long time and not interfere with movement when walking. So the special design was placed on its light weight as well as multi working modes.

#### 3.1. System Overview

As depicted in **Figure 3A**, the semi-active exoskeleton was mainly composed of belt, thigh linkage, motor, knee joint, wrap, calf linkage, and ankle joint. (i) the belt was adopted to fix the exoskeleton on the waist of the wearer and at transferred the weight of the body to the exoskeleton when squatting; (ii) thigh linkage and calf linkage made of carbon were tied on the lower limb by wraps and connected to a lockable knee joint; (iii) the knee joint could be locked when squatting and free to rotate within the range of  $0^\circ$  and  $135^\circ$  during walking; (iv) the ankle joint had two degrees of freedom, so it was able to rotate in sagittal plane and coronal plane. The total weight of our exoskeleton is 2,067 g. The weight of each component was given in **Table 1**.

The lockable knee joint was the main component, whose structure was shown in **Figure 3C**. The locking plate was adopted to adjust the angle of lockable knee joint according to the squatting position of wearer. In follow mode, the angle of the

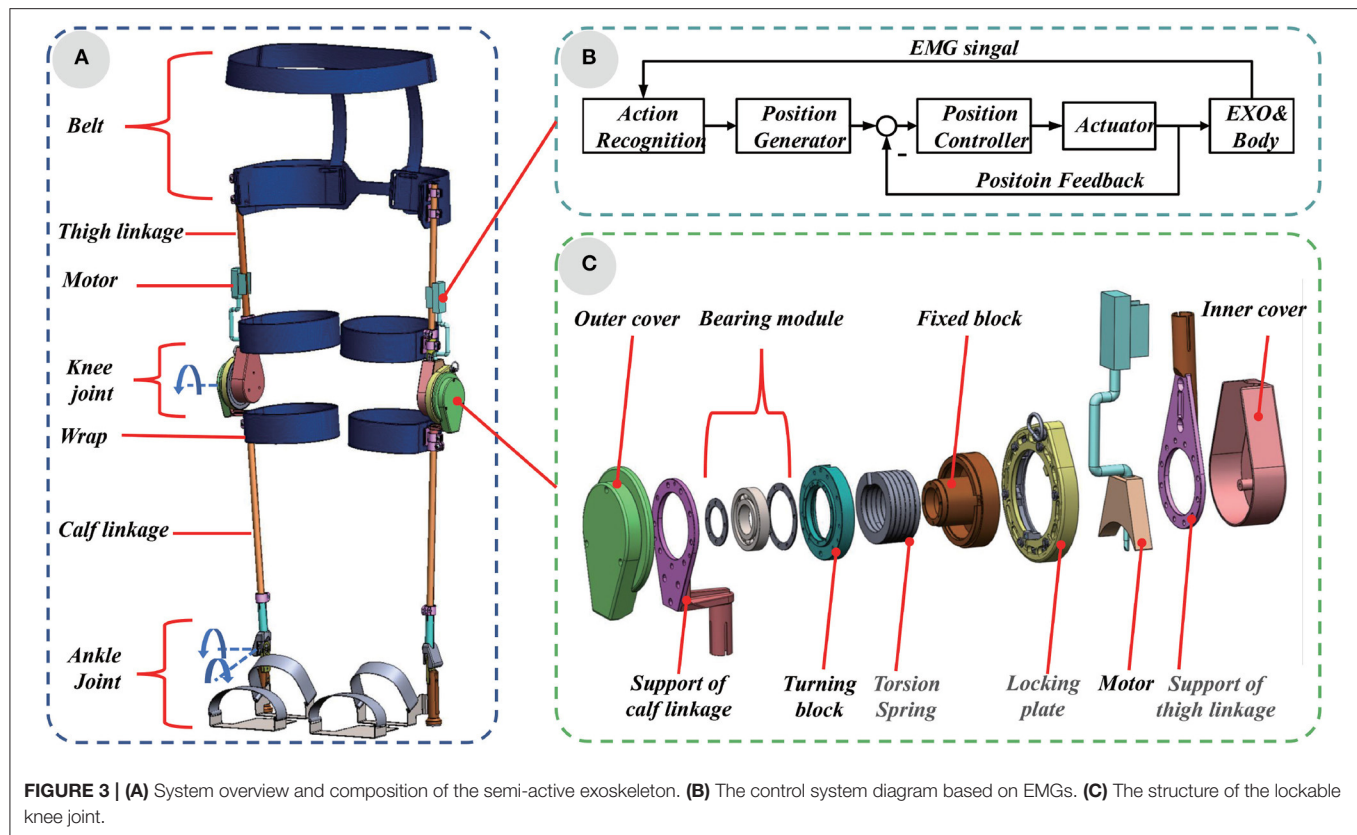


locking plate was adjusted to  $0^\circ$ , and the exoskeleton moves with the wearer without interfering with the daily activities such as normal walking, ascending and descending stairs and other daily activities. In the rigid-support mode, the angle of the locking plate was adjusted to the same angle as the angle of knee joint in any squatting position, the exoskeleton provided a comfortable support for the wearer. The linear motor was used to switch between rigid-support and elastic-support mode. When the height of the wearer's squatting posture changed frequently, the standard deviation of the EMGs of the gluteus maximus and quadriceps muscles increased more than 145 and 385 mv. Before calculating the standard deviation of the EMGs, which were filtered through 10 ~ 500Hz band pass filter and 50Hz notch filter (Neumann, 2013). When the standard deviation of the EMGs of the gluteus maximus and quadriceps muscle was greater than 145 and 385 mv, the linear motor was controlled to expand to limit the rotation of one end of the torsion spring. The exoskeleton worked in an elastic-support mode. Otherwise, the linear motor was controlled to contract, the torsion spring was not restricted. The exoskeleton worked in a rigid-support mode. At different squatting heights, the torsion spring was rotated at different angles, and assistance force was provided by the exoskeleton, the control system diagram was shown in **Figure 3B**.

### 3.2. Design

Theoretically speaking, it would be beneficial to improve assistance effect and comfort if the degree of freedom (DOF) of the exoskeleton was consistent with the DOF of the lower limbs of the human body. In general, the human lower limb could be taken as a structure with 7 DOFs. Three rotational DOFs at the hip, one rotation DOF at the knee, and three rotation DOFs at the ankle (Dollar and Herr, 2008). But the motion of squat mainly involved the flexions and extensions of the hip, knee, and ankle joints. In order to optimize the overall mechanical structure, knee joint capable of flexion and extension and ankle joint capable of flexion and extension, abduction and adduction were designed in the exoskeleton. The range of motion (ROM) of knee joint and ankle joint of the exoskeleton are set to match the ROM of humans during squatting. They are given in detail in **Table 2**. The ROM of exoskeleton was set between ROM at work and maximum ROM of human, which could protect the wearer's joint movement without interfering with the wearer's movement. At the same time, mechanical limit devices were designed at the end of the ROM of the knee and ankle joints to ensure the safety of the wearer.

According to the result of squatting simulation in the AnyBody software, the muscle activity of quadriceps femoris and

**TABLE 1 |** The weight of each component of our exoskeleton.

Component	Mass (g)	Number
Belt	305	1
Thigh linkage	91	2
Motor	205	2
Knee joint	326	2
Wrap	46	4
Calf linkage	33	2
Ankle joint	134	2
Total weight	2,067	-

**TABLE 2 |** Range of motion of knee joint and ankle joint of exoskeleton.

Joint	Motion	ROM at work(°)	Maximum ROM of human(°)	ROM of exoskeleton(°)
Knee joint	Flexion	100	145	120
	Extension	0	0	0
	Dorsiflexion	20	50	30
Ankle joint	Plantarflexion	7	30	30
	Abduction	10	30	15
	Adduction	10	30	15

gluteus maximus increased. The belt and wrap made of nylon, were fixed on the hip area and the quadriceps area of the thigh. They functioned to the exoskeleton to the wearer's lower limb and transmitted the weight of the wearer to the supporting linkage of the thigh.

The support linkages of thigh and calf, which were made of carbon fiber, were connected together by a lockable knee joint. They were the main frame of the exoskeleton. The structure of the exoskeleton was designed for people with heights from 1.5 to 1.85 m. According to human dimensions, the adjustable ranges of thigh length, calf length and ankle height were set at 380 ~ 550 mm, 300 ~ 450 mm, and 60 ~ 80 mm, respectively.

The structure of the lockable knee joint was shown in Figure 3C. The lockable knee joint was composed of outer cover, bearing module, turning block, torsion spring, fixed block, locking plate, motor, and inner cover. The outer cover and inner cover were made of resin materials to protect the internal structure of the lockable knee joint. The axis of support of calf linkage, bearing module and turning block were fixed together with screws to coincide, while the axis of torsion spring, fixed block, locking plate, motor, and support of thigh linkage coincide. The turning block and fixed block, which were made of GCr15, were connected together with bearing components, so the support of calf and support of thigh could rotate coincidentally. The motor was installed on the support of the thigh linkage with screws.



As depicted in **Figure 4B**. The locking plate was assembled by inner cover, pinion, positioning part, ratchet, spring holder, reset part, and outer cover. The inner cover and outer cover were made of resin materials, the pinion, positioning part, ratchet, and spring holder were made of Gcr15 and the reset part was made of aluminum alloy. Gear teeth were machined on the reset part, which was meshed with the pinion. Springs, torsional springs and pawls were installed in the spring holder. The engagement of the ratchet and the pawl ensure the positioning plate not only rotates in one direction around spring the holder. The rotation angle depended on the bosses of the inner ring of the ratchet and turning block. Adjusting the engagement of pinion and gear teeth on the reset part allows the ratchet to rotate in reverse.

The spring in the lockable knee joint was a customized torsional spring. The torsional spring was made of 60Si2MnA and its cross-section was rectangle, which was the long side in the radial direction and the short side in the axial direction. The stiffness of the torsional spring was  $0.8 \text{ N.m/}^\circ$ , which was calculated by Equation (1).

$$C_T = \frac{Ea^3b}{12 \times 180D_2n} \quad (1)$$

where  $E$  represented the elastic modulus of 60Si2MnA with a value of  $206 \text{ GPa}$ ;  $a$  and  $b$  were the length and width of section of spring steel wire, whose values were  $8$  and  $3.6 \text{ mm}$ , respectively;  $D_2$  and  $n$  represented the mean diameter and number of coils, whose values were  $40 \text{ mm}$  and  $5.5$ , respectively. According to the wearer's weight and applicable scenarios, torsion springs with different initial angles could be adjusted, so that the best elastic support can be obtained. One end of the torsion spring was fixed on the turning block. The torsion angle of the torsion spring was  $0^\circ$  when the knee joint was extended. However, the free end was restricted by motor, the torsion spring was twisted during the flexion of the knee joint. According to Equation (2), the energy storage of the torsion spring could be calculated.

$$E' = \int_0^\theta C_T \theta \, d\theta \quad (2)$$

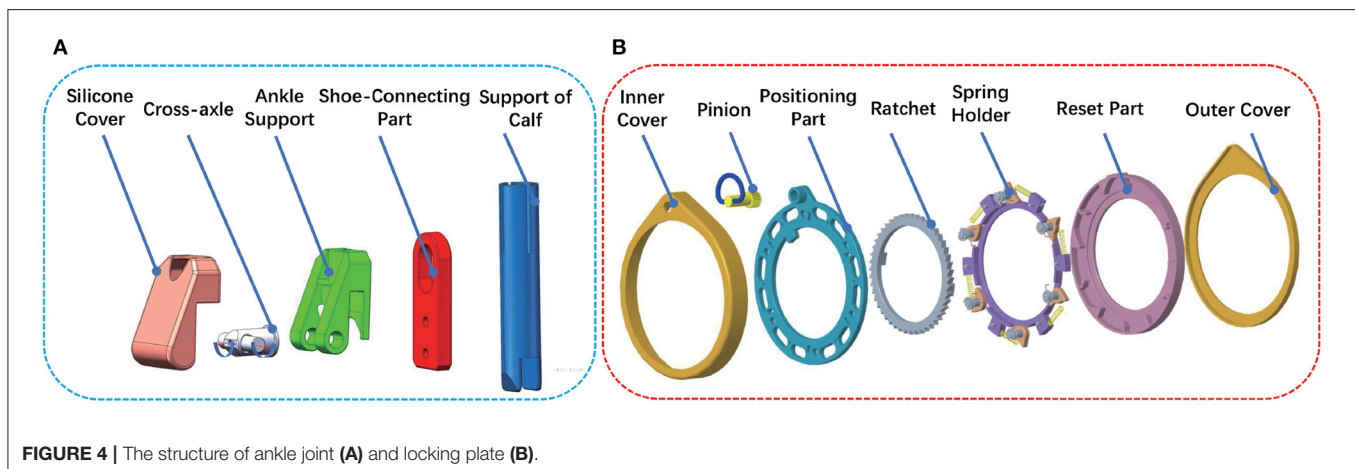
where  $E'$  represented the energy storage of the torsion spring,  $\theta$  was the torsion angle of spring, the physical quantity represented by  $C_T$  was the same as that in Equation (1). The energy was released to augment the muscle during knee extension.

The structure of the lockable ankle joint was depicted in **Figure 4A**. The lockable joint was mainly composed of silicon cover, cross-axle, ankle support, shoe-connecting part, and support of calf. The ankle support and shoe-connecting part were connected by cross-axle, allowing the shoe-connecting part to rotate in two directions around ankle support. In addition, cross-axes can slide slightly up and down along the chute on the shoe-connecting part. When the wearer's foot was off the ground, the shoe-connecting part slides down relative to cross-axle, which contributed to the dorsiflexion and plantarflexion, eversion and inversion, as shown in **Figure 5A**. When the wearer's feet were on the ground, especially in a squatting position, the shoe-connecting part slid upward relative to cross-axle, and the shoe-connecting part was restricted by the locking slot on the ankle support, which restricted eversion and inversion movement, as shown in **Figure 5B**. Since the ankle joint had no eversion and inversion movement, the exoskeleton can provide stable support.

## 4. EXPERIMENTS

In order to evaluate the performance of the exoskeleton, three different experiments were conducted. In the first experiment, the EMGs of muscles related to squatting were measured in both conditions of with and without exoskeleton, to validate whether the exoskeleton can relieve muscle fatigue. The second experiment was to test the effective support that the exoskeleton can provide under different weights and squatting positions. Experiment three was used to measure the additional metabolic cost introduced by the exoskeleton to wearer in follow mode. All experiments were performed in a laboratory at a stable indoor temperature of  $26^\circ\text{C}$ . Before each experiment, subjects were instructed to get familiar with exoskeleton and exoskeleton was adjusted accordingly.

Four healthy subjects, with no leg diseases, volunteered to participate in three experiments. The contents and impacts of



**FIGURE 4 |** The structure of ankle joint (A) and locking plate (B).

experiments were informed in detail to them and their contents were obtained. The human body's characteristics dimensions of subjects were detailed in **Table 3**.

Each experiment was divided into an experimental group and a control group. The experimental group was required to wear the exoskeleton, while the control group was not required to wear the exoskeleton. In order to avoid the influence of human muscle fatigue on the experiment, both the experimental group and the control group were conducted for 2 days, respectively. The experiment procedures of the control group and the experimental group were the same.

#### 4.1. EMGs Measurement

Surface myoelectric signal analysis has been proved effective for assessing the electrical manifestations of localized muscle fatigue (Pi et al., 2006). In order to accurately evaluate the effect of exoskeleton in reducing muscle fatigue, the EMGs of the muscle related to squatting with and without exoskeleton were measured in this experiment.

First of all, the skin was shaved, scrubbed, and cleaned with alcohol swab before the surface ENG sensors were applied (Bosch et al., 2016). Secondly, eight surface EMG sensors (SX230, Biometrics Limited, UK) were attached by EMG Sensor Tapes (T350) to the skins of soleus, vastus lateralis, vastus medialis, gastrocnemius, vastus intermedius, rectus femoris, gluteus maximus, and erector spinae. And then surface EMG Sensors were wrapped around the subject's limb by gauze to prevent it from falling and the reference electrode (R306), was wrapped on the wrist joint by elastic bands. Next, the surface EMG sensors and reference electrode were connected to an eight-channel DataLOG (MWX8), which transmitted real-time data to computers via Bluetooth Wireless link. Finally, subjects were instructed to use an electric drill to install screws on the board that simulating assembly works, whose process lasted for 2 min. Drilling different holes in the horizontal direction of the board to simulate the scene of squatting height stability (worked in a rigid-support mode), while drilling different holes in the vertical direction of the board to simulate the scene of squatting height

varied (worked in an elastic-support mode). According to the simulation results in AnyBody software, the muscle activity was higher when the knee flexion angle was  $120^\circ$ , so the surface EMGs were recorded at 500Hz when the knee flexion angle was  $120 \pm 10^\circ$ . The experiment setup was shown in **Figure 6A**.

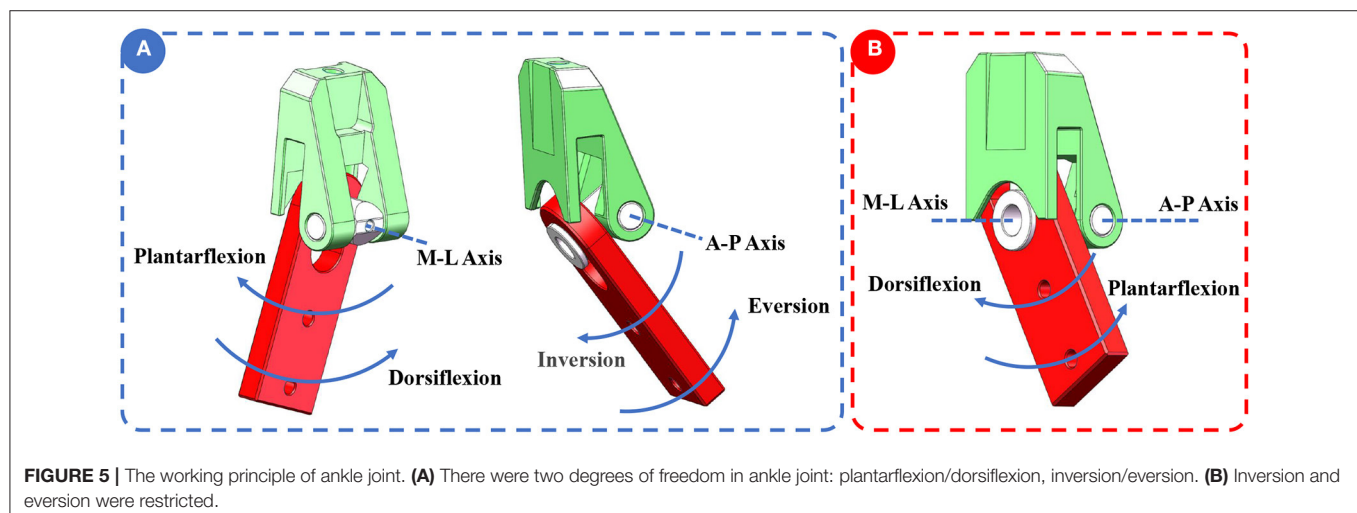
Average rectified value (ARV), integrated electromyogram (iEMG) and root mean square (RMS) of EMGs showed an upward trend during muscles fatigue (Viitasalo and Komi, 1977; Madeleine et al., 2002). Changes in these values were usually related to muscle contraction, but RMS could better reflect muscle fatigue under the same muscle contraction state (Jiang et al., 2017). After EMGs were filtered through 10 ~ 500Hz band pass filter and 50 Hz notch filter (Neumann, 2013), RMS was calculated according to Equation (3).

$$RMS = \sqrt{\frac{1}{N} \sum_{i=1}^N EMG^2(i)} \quad (3)$$

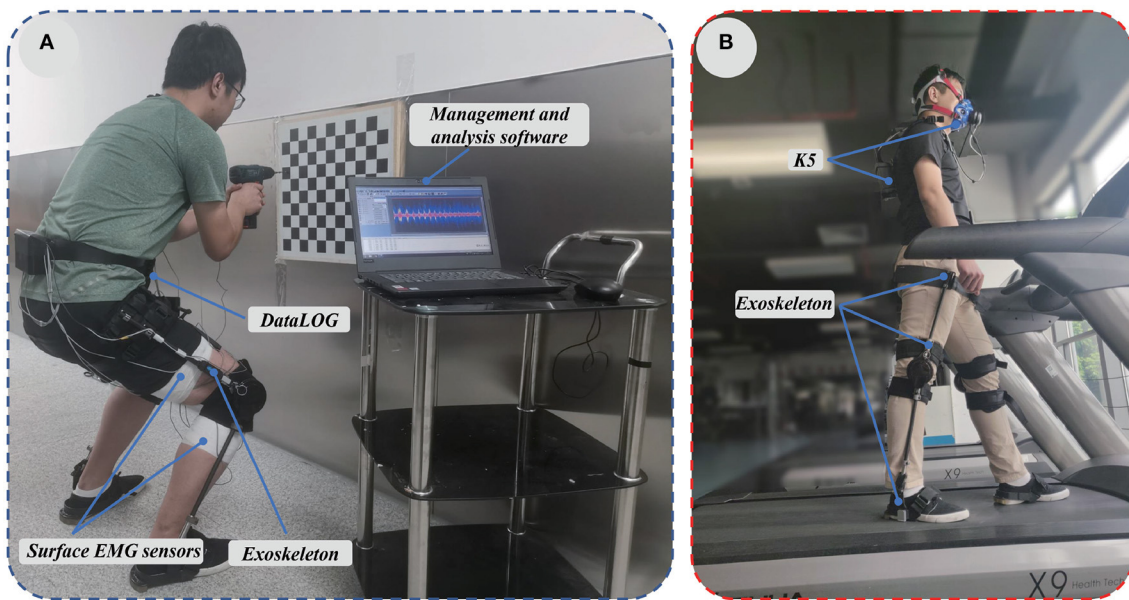
where RMS represented the root mean square of EMGs,  $N$  represented the number of EMGs collected within the sampling time,  $EMG(i)$  represented the amplitude of the  $i$ -th EMGs. The root mean square of EMGs amplitude of soleus, vastus lateralis, vastus medialis, gastrocnemius, vastus intermedius, rectus femoris, gluteus maximus, and erector spinae were

**TABLE 3 |** The human body's characteristics dimensions of subjects.

Subject	1	2	3	4
Gender	Woman	Man	Man	Man
Stature (cm)	160	176	177	183
Weight (kg)	48	67.5	80	70
Thigh length (mm)	435	483	480	540
Calf length (mm)	340	400	418	440
Ankle height (mm)	52	81	80	83
Shoes size (cm)	23	26	26.5	26.5



**FIGURE 5 |** The working principle of ankle joint. (A) There were two degrees of freedom in ankle joint: plantarflexion/dorsiflexion, inversion/eversion. (B) Inversion and eversion were restricted.



**FIGURE 6 | (A)** EMGs of the muscle related to squatting with and without exoskeleton were measured in this experiment. **(B)** The metabolic cost with and without exoskeleton was measured.

reduced by 98.5, 97.89, 80.09, 77.27, 96.73, 94.17, 70.71, and 36.32%, respectively with the assistance of the exoskeleton, which was shown in **Figure 7**. We can conclude that the exoskeleton was able to reduce muscle fatigue effectively.

## 4.2. Plantar Pressure Measurement

The working principle of the exoskeleton to reduce muscle fatigue was that the weight of wearer was transmitted to the ground by the exoskeleton and the lower limbs, rather than just by the lower limbs of wearer. To measure the support force provided by exoskeleton under different weights and squatting positions, the foot pressure was measured in this experiment.

Before the starting experiment, experiment acquisition system was designed, which was composed of two plantar pressure sensors (ZNX-01, Suzhou Leanstar Electronic Technology Co., Ltd., China) and bluean acquisition circuit board, which communicated with XCOM software (V2.2, download from <http://www.openedv.com/>) through a serial port at speed of 460800 bps, as shown in **Figure 8B**. To analyze the relationship between the weight and voltage of RFP pressure sensor, the subjects were required to carry additional loads, whose weight was increased from 0 to 5 kg with an increment of 0.5kg each time. The subjects were instructed to stand 30 s at different loads. As shown in **Figure 8A**, the splattering points were the average value of voltage of RFP pressure sensor and weight, the blue line was the fitted line as expressed by Equation (4).

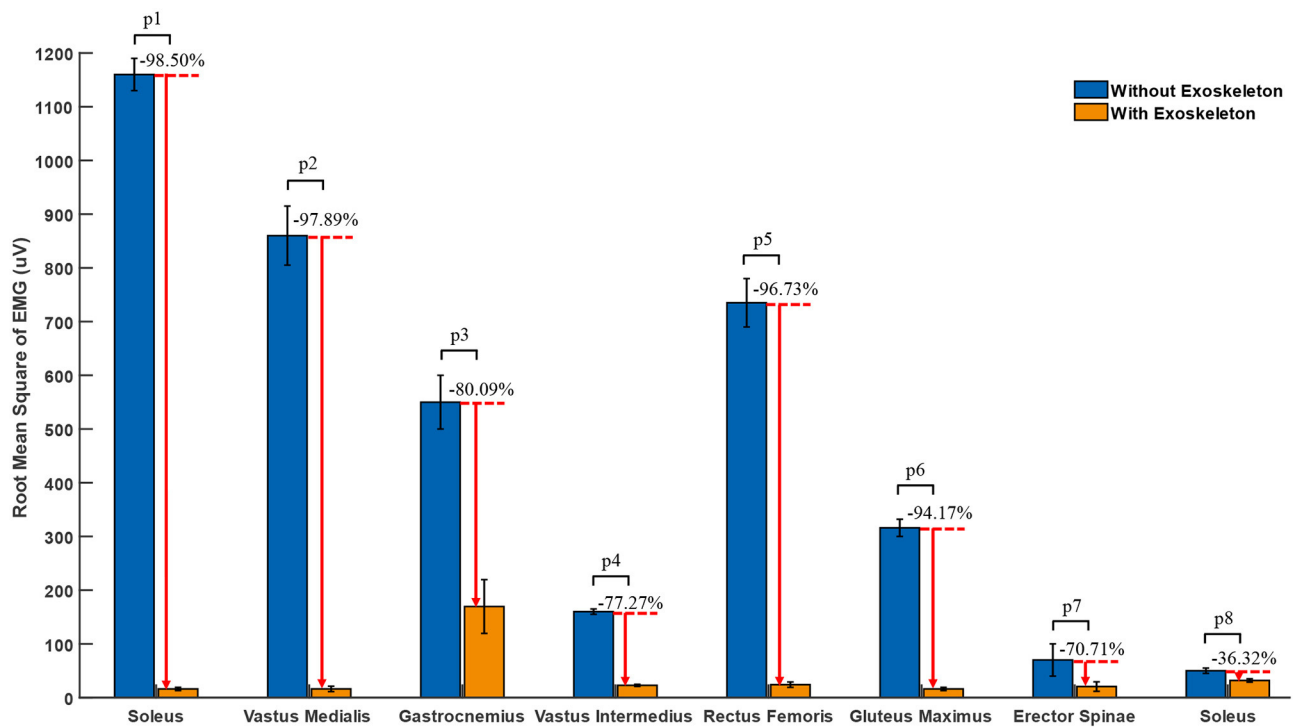
$$G = -162.3U + 1649.7 \quad (4)$$

where the  $G$  was the weight (the sum of weight of subject and additional load) of the subject and  $U$  represented the voltage value.

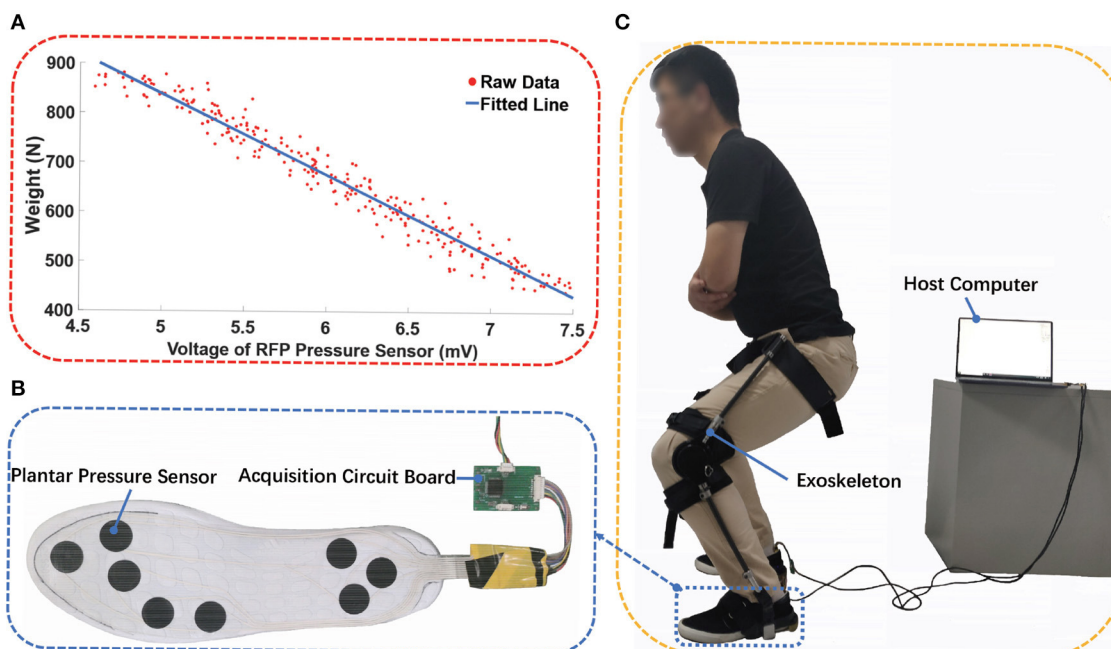
At first, the weight and voltage of RFP pressure sensor were recorded when the subjects were instructed to flex the knee without exoskeleton at 60°, 90°, and 120°, respectively. Each test lasted for 1 min and a 5-min rest was set. After the exoskeleton was adjusted to fit the subject, the same experiment was conducted again, as shown in **Figure 8C**. The exoskeleton worked in a rigid-support mode.

To eliminate the influence of unstable squatting posture, the data of the first 15 s and the last 15 s were removed, and only the data in between were selected for analysis. After the data was filtered by median filter, the plantar force of both conditions were calculated according to Equation (4). Taking into account the differences of subject, the plantar force was normalized using the weight of the subject, as shown in **Figure 9**. The reason why the percentage of body weight through subject feet at 60°, 90°, and 120° of knee flexion angle was less than 100% was that there was a difference in the pressure distribution on the soles of the feet when standing and squatting. In particular, parts of weight were transmitted to ground through the areas of arches of the foot, on which no RFP pressure sensor was installed. Comparing the percentage of weight of both conditions, wearing an exoskeleton reduces the weight through the subject's feet by 63.94, 64.52, and 65.61%, respectively at 60, 90, and 120° of knee flexion angle. Moreover, the assistive force provided by the exoskeleton increased as the angle of knee flexion increased, which can be attributed to the increase in the effective contact area between the belt and the subject.

**Table 4** showed a comparison between our exoskeleton and the Chairless Chair. The exoskeleton designed by us was only 2.1 kg, which was lighter than 3.5kg of the Chairless Chair. Meanwhile, only 29.3% of weight was supported by the subject's

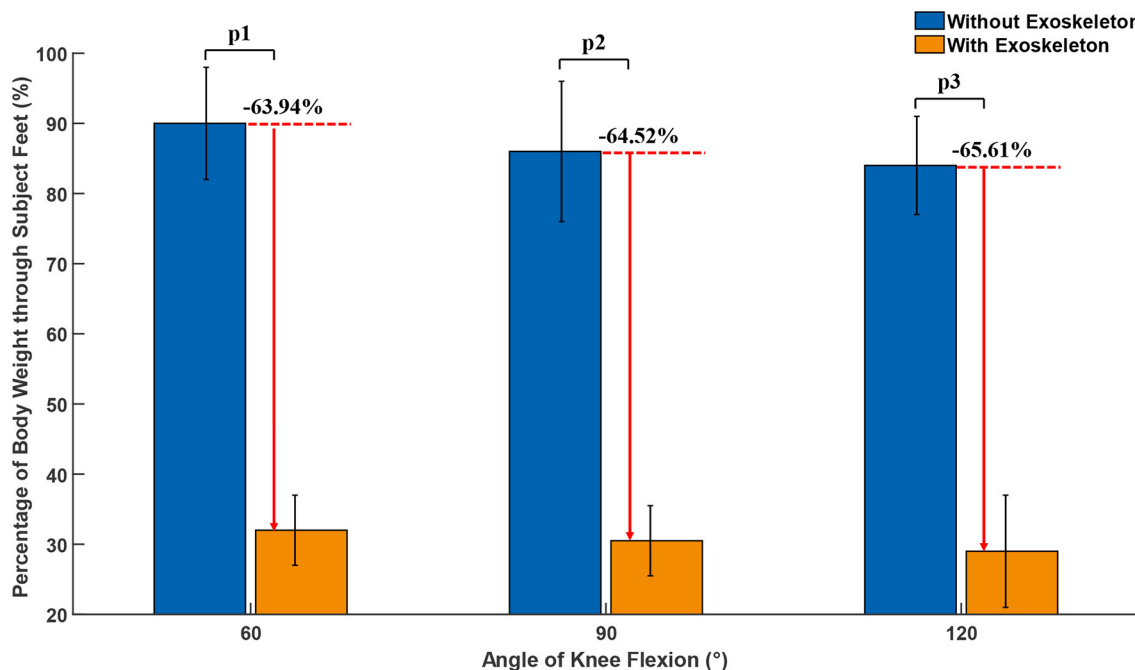


**FIGURE 7 |** The RMS of the EMGs of the knee joint at 120 degree flexion angle. p1, p2, p3, p4, p5, p6, p7, and p8 are the result of two-side *t*-tests, which are 0.0002, 0.0014, 0.0044, 0.0014, 0.0013, 0.0004, 0.1112, and 0.0131, respectively.



**FIGURE 8 |** Plantar pressure measurement. **(A)** The splatting was the raw data from experiment and the blue line is fitted line, **(B)** the plantar sensor and data acquisition circuit board, **(C)** the foot pressure experiment was conducted.





**FIGURE 9 |** Percentage of body weight through subject Feet at 60°, 90°, and 120° of knee flexion angle. p1, p2, and p3 are the result of two-side *t*-tests, which are 0.0018, 0.0036, and 0.0009, respectively.

**TABLE 4 |** Comparison with the chairless chair.

Exoskeleton	Weight (kg)	Percentage of body weight through subject feet (%)
Chairless Chair	3.5 (Spada et al., 2018)	33
This work	2.1	29.3

feet after wearing the exoskeleton, which was effectively the weight transmitted by the feet.

### 4.3. Metabolic Cost Measurement

In order to evaluate whether the exoskeleton interfered with the subjects' movement in the following mode, such as walking between the workbenches of the assembly line. The wearable metabolic system (K5, COSMED, Italy) was adopted to measure the concentration and volume of the exhaled pulmonary gas, which are mainly carbon dioxide and oxygen (Chen et al., 2020). In experiment, the metabolic cost under the conditions of with and without exoskeleton were measured when the subject was walking at the speed of 4 and 5 km/h on a treadmill (SH-5918, ShuHua Sports Co., Ltd., China).

Each experiment lasted for 20 min and was divided into three stages, which as shown in **Figure 6B**. First, the subject was asked to maintain a standing position for 5 min in order to measure the standing cost; Then, the subject walked for 10 min to obtain the walking metabolic cost; Finally, the subject was also instructed to maintain a standing position for 5 min.

The method of calculating the net metabolic cost was subtracting the standing metabolic cost from the walking metabolic. Taking into the unstable metabolic cost at the beginning and the transition from standing to walking, the data from the 3rd to the 5th min, the 7th to the 13th min, and the 17th to the 20th min in each experiment are selected to calculated based on Equation (5) (Garby and Astrup, 1987).

$$\Delta H = c_1 VO_2 + c_2 VCO_2 \quad (5)$$

where  $\Delta H$  was the energy rate (kJ/s), coefficients  $c_1$  and  $c_2$  were 16.04 and 4.94 kJ/L, respectively, the unit of  $VO_2$  and  $VCO_2$  was L/s. The result of metabolic cost measurement when the subject was walking at the speed of 4 and 5 km/h were shown in **Table 5**. The average additional metabolic cost introduced by exoskeleton was 2.525 and 2.85%. It means that the exoskeleton would not interfere with the movement of the wearer in follow mode.

## 5. DISCUSSION

A semi-active exoskeleton was designed in this work, used to reduce the muscle fatigue of the lower limb when squatting.

In order to analyze the muscle activity of each muscle in the process of squatting, so that the designed exoskeleton can effectively reduce muscle fatigue, the process of squatting was simulated in the AnyBody software. As the knee flexion angle gradually increased from 10° to 135°, the muscle activity of the gluteus maximus, rectus femoris, vastus medialis, vastus lateralis, vastus intermedius, and erector spinae first increased and then decreased, while the muscle activity of gastrocnemius and soleus

**TABLE 5 |** The result of metabolic cost measurement when the subject was walking at the speed of 4 and 5 km/h.

Subject	4 km/h			5 km/h		
	WOE (W/kg)	WE (W/kg)	AMC (%)	WOE (W/kg)	WE (W/kg)	AMC (%)
1 (female)	4.20	4.33	3.1	4.69	4.82	2.8
2 (male)	5.32	5.42	1.9	5.81	5.98	2.9
3 (male)	5.27	5.43	3.0	5.75	5.89	2.4
4 (male)	5.78	5.90	2.1%	5.82	6.01	3.3

Where WOE, WE, and AMC were the abbreviation of without exoskeleton, with exoskeleton and additional metabolic cost, respectively.

decreased. Therefore, the exoskeleton was designed to provide assistance force for the gluteus maximus, rectus femoris, vastus medialis, vastus lateralis, vastus intermedius and erector spinae.

The exoskeleton was applicable for users from 150 to 185 cm, which has the degree of freedom of flexion and extension of knee joint, dorsiflexion, plantarflexion, eversion and inversion of ankle joint. Because its parts were made of carbon fiber and aluminum alloy, the total weight of the exoskeleton was only 2,067 g, which was only 33.9% of Legx and 60% of the Chairless Chair. It was easy to switch among three working modes: follow mode, rigid-support mode and elastic-support mode. In the follow mode, the angle of the locking plate was adjusted to 0°, and the assist device can follow the wearer's movement without interfering with the daily activities such as normal walking, upstairs and down-stairs and other daily activities. In the rigid-support mode, the angle of the locking plate was adjusted to the same angle as the angle of the knee joint in any squatting position. The assistive device provided comfortable support for the wearer. In the elastic-support mode, the energy is harvested by a torsion spring during knee-flexion and was released during knee-extension, which was used to reduce the moment required for the knee joint during knee-extension.

In order to evaluate the performance of the exoskeleton, three different experiments were conducted, respectively. In the first experiment, the EMGs of the muscles related to squatting with and without exoskeleton was measured, the result showed that the mean EMGs amplitude of soleus, vastus lateralis, vastus medialis, gastrocnemius, vastus intermedius, rectus femoris, gluteus maximus, and erector spinae were reduced by 98.5, 97.89, 80.09, 77.27, 96.73, 94.17, 70.71, and 36.32%, respectively, with the assistance of the exoskeleton. The second experiment was to test the effective support that the exoskeleton can provide under different weights and squatting positions. Compared to the percentage of weight through subject's feet without and with exoskeleton, it was reduced by 63.94, 64.52, and 65.61%, respectively, at 60°, 90°, and 120° of knee flexion angle. Experiment three was used to measure the additional metabolic cost brought by the exoskeleton to wearer in follow mode. The average additional metabolic cost introduced by exoskeleton was 2.525 and 2.85%. Each kilogram added to the foot increases energy expenditure 7–10% (Knapik et al., 2004), which means the

average additional metabolic cost introduced by exoskeleton was less than that worn by safety shoes (the weight of the safety shoes was greater than 1 kg). Therefore, it means that the exoskeleton would not seriously interfere with the movement of the wearer in follow mode.

The exoskeleton not only effectively reduced muscle fatigue, but also did not interfere with the free movement of the wearer. In the future, the intelligent switcher will be designed, which will enable the exoskeleton to switch in three working modes intelligently according to the intention of wearer.

## DATA AVAILABILITY STATEMENT

The original contributions generated for the study are included in the article/supplementary material, further inquiries can be directed to the corresponding author/s.

## ETHICS STATEMENT

The studies involving human participants were reviewed and approved by the Medical Ethics Committee of Shenzhen Institutes of Advanced Technology. The participants provided their written informed consent to participate in this study.

## AUTHOR CONTRIBUTIONS

ZW and XW: conceptualization and writing—original draft preparation. ZW and AP: methodology. ZW and YZ: software. ZW, YZ, and AP: validation. ZW: formal analysis and data curation. AP and CC: investigation. CC and SL: resources. YL and YM: writing—review and editing. SL: visualization. CC: supervision. XW and CC: project administration and funding acquisition. All authors have read and agreed to the published version of the manuscript.

## FUNDING

This work was supported in part by Natural Science Foundation of China (U1913207), in part by the National Program of China (2017YFB1302303), in part by the Natural Science Foundation of Guangdong Province, China (2019A1515010782), in part by Guangdong Basic and Applied Basic Research Foundation (2019A1515110576), in part by Shenzhen Technology Research Project (JSGG20180507182901552), in part by the Science Technology and Innovation Committee of Shenzhen Municipality (SZSTI) Fundamental Research Project under Grant JCYJ20180302145539583), in part by Shandong Province Science and Technology Projects (2018CXGC0909), and in part by Key-Area R&D Program of Guangdong Province (2020B090925002).

## ACKNOWLEDGMENTS

The authors would like to thank all subjects who participated in experiments and the members of SIAT exoskeleton team.

## REFERENCES

- Bionics, E. (2015). Ekso bionics. *IEEE Spectr.* 49, 30–32.
- Bosch, T., van Eck, J., Knitel, K., and de Looze, M. (2016). The effects of a passive exoskeleton on muscle activity, discomfort and endurance time in forward bending work. *Appl. Ergon.* 54, 212–217. doi: 10.1016/j.apergo.2015.12.003
- Chen, C., Zhang, Y., Li, Y., Wang, Z., Liu, Y., Cao, W., et al. (2020). Iterative learning control for a soft exoskeleton with hip and knee joint assistance. *Sensors* 20:4333. doi: 10.3390/s20154333
- Collo, A., Bonnet, V., and Venture, G. (2016). “A quasi-passive lower limb exoskeleton for partial body weight support,” in *2016 6th IEEE International Conference on Biomedical Robotics and Biomechatronics (BioROB)* (Singapore: IEEE), 643–648. doi: 10.1109/BIOROB.2016.7523698
- Damsgaard, M., Rasmussen, J., Christensen, S. T., Surma, E., and De Zee, M. (2006). Analysis of musculoskeletal systems in the anybody modeling system. *Simul. Modell. Pract. Theory* 14, 1100–1111. doi: 10.1016/j.simpat.2006.09.001
- De Looze, M. P., Bosch, T., Krause, F., Stadler, K. S., and O’Sullivan, L. W. (2016). Exoskeletons for industrial application and their potential effects on physical work load. *Ergonomics* 59, 671–681. doi: 10.1080/00140139.2015.1081988
- De Roeck, J., Van Houcke, J., Almeida, D., Galibarov, P., De Roeck, L., and Audenaert, E. A. (2020). Statistical modeling of lower limb kinetics during deep squat and forward lunge. *Front. Bioeng. Biotechnol.* 8:233. doi: 10.3389/fbioe.2020.00233
- Dollar, A. M., and Herr, H. (2008). Lower extremity exoskeletons and active orthoses: challenges and state-of-the-art. *IEEE Trans. Robot.* 24, 144–158. doi: 10.1109/TRO.2008.915453
- Esquenazi, A., Talaty, M., Packel, A., and Saulino, M. (2012). The rewalk powered exoskeleton to restore ambulatory function to individuals with thoracic-level motor-complete spinal cord injury. *Am. J. Phys. Med. Rehabil.* 91, 911–921. doi: 10.1097/PHM.0b013e318269d9a3
- Garby, L., and Astrup, A. (1987). The relationship between the respiratory quotient and the energy equivalent of oxygen during simultaneous glucose and lipid oxidation and lipogenesis. *Acta Physiol. Scand.* 129, 443–444. doi: 10.1111/j.1365-201X.1987.tb10613.x
- Huang, R., Cheng, H., Guo, H., Lin, X., and Zhang, J. (2018). Hierarchical learning control with physical human-exoskeleton interaction. *Inform. Sci.* 432, 584–595. doi: 10.1016/j.ins.2017.09.068
- Huang, R., Cheng, H., Qiu, J., and Zhang, J. (2019). Learning physical human-robot interaction with coupled cooperative primitives for a lower exoskeleton. *IEEE Trans. Automat. Eng.* 16, 1566–1574. doi: 10.1109/TASE.2018.2886376
- Jiang, Y., Zou, R., and Liu, J. (2017). Research progress of muscle fatigue discrimination based on surface electromyography. *Chin. J. Bioinform.* 8, 120–126. doi: 10.3969/j.issn.1672-5565.20160622001
- Knapik, J. J., Reynolds, K. L., and Harman, E. (2004). Soldier load carriage: historical, physiological, biomechanical, and medical aspects. *Milit. Med.* 169, 45–56. doi: 10.7205/MILMED.169.1.45
- Kobayashi, H. (2016). Wearable power assist system “muscle suit”. *J. Japan Instit. Electron. Packaging* 19, 384–388. doi: 10.5104/jiep.19.384
- Krut, S., Benoit, M., Dombre, E., and Pierrot, F. (2010). “Moonwalker, a lower limb exoskeleton able to sustain bodyweight using a passive force balancer,” in *2010 IEEE International Conference on Robotics and Automation* (Anchorage, AK: IEEE), 2215–2220. doi: 10.1109/ROBOT.2010.5509961
- Madeleine, P., Farina, D., Merletti, R., and Arendt-Nielsen, L. (2002). Upper trapezius muscle mechanomyographic and electromyographic activity in humans during low force fatiguing and non-fatiguing contractions. *Eur. J. Appl. Physiol.* 87, 327–336. doi: 10.1007/s00421-002-0655-8
- Neumann, D. A. (2013). *Kinesiology of the Musculoskeletal System-e-Book: Foundations for Rehabilitation*. Amsterdam: Elsevier Health Sciences.
- Nordin, M., and Frankel, V. H. (2001). *Basic Biomechanics of the Musculoskeletal System*. Philadelphia, PA: Lippincott Williams and Wilkins.
- Pi, X. T., Chen, F., Peng, C. L., and Zheng, E. (2006). Methods applied to muscle fatigue assessment using surface myoelectric signals. *J. Biomed. Eng.* 23:225. doi: 10.1016/S1872-2075(06)60043-5
- Pillai, M. V., Van Engelhoven, L., and Kazerooni, H. (2020). Evaluation of a lower leg support exoskeleton on floor and below hip height panel work. *Hum. Fact.* 62, 489–500. doi: 10.1177/0018720820907752
- Reid, C. R., Bush, P. M., Cummings, N. H., McMullin, D. L., and Durrani, S. K. (2010). A review of occupational knee disorders. *J. Occupat. Rehabil.* 20, 489–501. doi: 10.1007/s10926-010-9242-8
- Rupal, B. S., Rafique, S., Singla, A., Singla, E., Isaksson, M., and Virk, G. S. (2017). Lower-limb exoskeletons: research trends and regulatory guidelines in medical and non-medical applications. *Int. J. Adv. Robot. Syst.* 14:1729881417743554. doi: 10.1177/1729881417743554
- Spada, S., Ghibaud, L., Carnazzo, C., Di Pardo, M., Chander, D. S., Gastaldi, L., et al. (2018). “Physical and virtual assessment of a passive exoskeleton,” in *Congress of the International Ergonomics Association* (Florence: Springer), 247–257. doi: 10.1007/978-3-319-96068-5\_28
- van Dijk, W., and Van der Kooij, H. (2014). Xped2: a passive exoskeleton with artificial tendons. *IEEE Robot. Automat. Mag.* 21, 56–61. doi: 10.1109/MRA.2014.2360309
- Viitasalo, J. H., and Komi, P. V. (1977). Signal characteristics of EMG during fatigue. *Eur. J. Appl. Physiol. Occupat. Physiol.* 37, 111–121. doi: 10.1007/BF00421697
- Wu, R., Wang, J., Chen, W., and Wang, P. (2020). Design of a transfer robot for the assistance of elderly and disabled. *Adv. Robot.* 35, 194–204. doi: 10.1080/01691864.2020.1819875

**Conflict of Interest:** The authors declare that the research was conducted in the absence of any commercial or financial relationships that could be construed as a potential conflict of interest.

The reviewer HC declared a shared affiliation, with no collaboration, with the authors ZW, YZ, SL to the handling editor at the time of the review.

Copyright © 2021 Wang, Wu, Zhang, Chen, Liu, Liu, Peng and Ma. This is an open-access article distributed under the terms of the Creative Commons Attribution License (CC BY). The use, distribution or reproduction in other forums is permitted, provided the original author(s) and the copyright owner(s) are credited and that the original publication in this journal is cited, in accordance with accepted academic practice. No use, distribution or reproduction is permitted which does not comply with these terms.



# A Real-Time Stability Control Method Through sEMG Interface for Lower Extremity Rehabilitation Exoskeletons

Can Wang<sup>1,2,3</sup>, Ziming Guo<sup>1,2,3</sup>, Shengcai Duan<sup>1,2,3</sup>, Bailin He<sup>1,2,3</sup>, Ye Yuan<sup>1,2,3</sup> and Xinyu Wu<sup>1,2,3,4,5\*</sup>

<sup>1</sup> Guangdong Provincial Key Lab of Robotics and Intelligent System, Shenzhen Institute of Advanced Technology, Chinese Academy of Sciences, Shenzhen, China, <sup>2</sup> Shenzhen Institute of Advanced Technology, University of Chinese Academy of Sciences, Shenzhen, China, <sup>3</sup> CAS Key Laboratory of Human-Machine Intelligence-Synergy Systems, Shenzhen Institute of Advanced Technology, Shenzhen, China, <sup>4</sup> Guangdong-Hong Kong-Macao Joint Laboratory of Human-Machine Intelligence-Synergy Systems, Shenzhen Institute of Advanced Technology, Chinese Academy of Sciences, Shenzhen, China, <sup>5</sup> Department of Mechanical and Automation Engineering, The Chinese University of Hong Kong, Hong Kong, Hong Kong

## OPEN ACCESS

### Edited by:

Hong Cheng,  
University of Electronic Science and  
Technology of China, China

### Reviewed by:

Xiaogang Xiong,  
Harbin Institute of Technology,  
Shenzhen, China  
Mingming Zhang,  
Southern University of Science and  
Technology, China

### \*Correspondence:

Xinyu Wu  
xy.wu@siat.ac.cn

### Specialty section:

This article was submitted to  
Neural Technology,  
a section of the journal  
Frontiers in Neuroscience

**Received:** 23 December 2020

**Accepted:** 26 February 2021

**Published:** 13 April 2021

### Citation:

Wang C, Guo Z, Duan S, He B,  
Yuan Y and Wu X (2021) A Real-Time  
Stability Control Method Through  
sEMG Interface for Lower Extremity  
Rehabilitation Exoskeletons.  
Front. Neurosci. 15:645374.  
doi: 10.3389/fnins.2021.645374

Herein, we propose a real-time stable control gait switching method for the exoskeleton rehabilitation robot. Exoskeleton rehabilitation robots have been extensively developed during the past decade and are able to offer valuable motor ability to paraplegics. However, achieving stable states of the human-exoskeleton system while conserving wearer strength remains challenging. The constant switching of gaits during walking may affect the center of gravity, resulting in imbalance of human-exoskeleton system. In this study, it was determined that forming an equilateral triangle with two crutch-supporting points and a supporting leg has a positive impact on walking stability and ergonomic interaction. First, the gaits planning and stability analysis based on human kinematics model and zero moment point method for the lower limb exoskeleton are demonstrated. Second, a neural interface based on surface electromyography (sEMG), which realizes the intention recognition and muscle fatigue estimation, is constructed. Third, the stability of human-exoskeleton system and ergonomic effects are tested through different gaits with planned and unplanned gait switching strategy on the SIAT lower limb rehabilitation exoskeleton. The intention recognition based on long short-term memory (LSTM) model can achieve an accuracy of nearly 99%. The experimental results verified the feasibility and efficiency of the proposed gait switching method for enhancing stability and ergonomic effects of lower limb rehabilitation exoskeleton.

**Keywords:** rehabilitation exoskeleton robot, real-time motion stability, gait switch, surface electromyography, motion intention recognition, muscle fatigue, ergonomic effects

## 1. INTRODUCTION

In recent years, powered lower limb exoskeleton robots have been proven to be particularly versatile and effective in the medical and military fields. Lower-limb exoskeleton robots can be roughly divided into two categories, including the auxiliary exoskeleton robot and the assisted exoskeleton robot. The auxiliary exoskeleton robot is used to aid the sick and the elderly in their normal daily



life functioning or medical rehabilitation. The assisted exoskeleton robot is utilized for strength augmentation in disaster rescues or auxiliary operations. The auxiliary exoskeleton is our discussed object in this investigation, although the mechanism design and manufacture, path planning, and high-level intent control for lower limb exoskeleton robot has been developed to a relatively sophisticated level. Unfortunately, achieving a stable gait switching during walking for lower limb exoskeleton robots is still a challenging research.

Research into exoskeleton robots has resulted in considerable development of lower limb rehabilitation exoskeleton robots. Auxiliary walking exoskeleton robots are mainly applied in the field of medical rehabilitation for patients with inferior legs and feet, such as the elderly and disabled. Some heterogeneous structure exoskeleton robots (Li et al., 2015; Parietti et al., 2015; Eguchi et al., 2018) are investigated in recent years. However, it was found that those exoskeleton robots take advantage of the heterogeneous structure with human lower limbs to gain walking stability, which may have some support strength but poor adaptability. As opposite of heterogeneous exoskeleton robots, most paraplegic rehabilitation exoskeleton robots have developed to be humanoid bipedal robots, and some of these exoskeletons are equipped with crutches to maintain better balance. Exoskeleton robots require the human interface to provide walking stability so that it may function as a flexible assistant. Such robots have been developed by commercial companies including Rewalk (Talaty et al., 2013), Ekso Bionics (Baunsgaard et al., 2018), Ailegs (Chen et al., 2018), and MaiBu BEAR H1. Exoskeleton robots especially require the walking stability as far as possible so as to provide flexible assistant. The Hybrid Assistive Limb (HAL) (Shimizu et al., 2019), which takes advantage of sEMG in control strategy, was designed by the robotics company Cyberdyne (Yilmaz et al., 2018).

Moreover, plenty of research institutes and universities are also actively developing humanoid exoskeletons. Sogang University in Korea developed a exoskeleton namely SUBAR (Chen et al., 2013; Hwang and Jeon, 2018), which could estimate the muscular torque of its wearer. Singapore's Nanyang Technological University (Mertz, 2012) and Harvard University (Abe et al., 2018) have also made solid progress in the development of assisted exoskeletons. The Chinese University of Science and Technology designed an exoskeleton robot driven by a servo motor (Li et al., 2019) and developed a fuzzy algorithm for lower extremity exoskeleton (Huang et al., 2016a). The exoskeleton team of H. C. from University of Electronic Science and Technology of China have developed exoskeletons for paraplegia (Huang et al., 2018), hemiplegia patients (Peng et al., 2020), and human-power augmentation (Huang et al., 2016b, 2019). The exoskeleton group at the Shenzhen Institutes of Advanced Technology of the Chinese Academy of Sciences has developed the fourth generation of the SIAT exoskeleton robot. With four degrees of freedom (DoFs), this exoskeleton robot has successfully enabled persons with disabilities to stand up and walk independently (Liu et al., 2017; Wang et al., 2018a).

The human-exoskeleton interaction is drawing more and more attention (Huang et al., 2016b,c; Lin et al., 2019). The

neural interface between the human and exoskeleton based on the brain computer interface (BCI) (Yuan et al., 2018) and sEMG has been a hot research topic. Brain-computer interfaces are relatively unstable (Wang et al., 2018b). Decoding sEMG signal is one of the important approaches for intention identification (Chu et al., 2007). The human-exoskeleton system is operated by the identified results of decoding sEMG signals, which can prevent the disadvantages of the operation with physical buttons. For instance, the pilot can focus on maintaining balance rather than pressing control button to operate exoskeleton at the same time, which may result in fatigue and instability. In addition, the sEMG is an intuitive and noninvasive way to real-time monitor the muscle states, which has proven to be an effective in muscle fatigue detection (Lin et al., 2019).

While investigating the existing exoskeleton control methods, we found very few studies that have examined the minimum force requirements into the control scheme by the wearer. We also found scarce consideration for the state of the wearer while operating a lower limb exoskeleton. In detail, the use of crutches can lead to walking instability, thereby impacting exoskeleton assistance, while also impacting the patients' overall rehabilitation. In this study, the usage of crutches and gait switching is investigated to gain the stability of human-exoskeleton system. This study could be applied to rehabilitation training in rehabilitation medical institutions, which is customized for each patient. An overview of the developed rehabilitation exoskeleton motion analysis system is presented in **Figure 1**. As shown in **Figure 1**, the gait model based on stability analysis and gait planning is first completed. Then intention recognition based on sEMG with machine learning is demonstrated. After that, the exoskeleton is driven with the control model. Finally, the exoskeleton motion analysis is demonstrated.

In this study, real-time gait conversion is achieved through neural interface and proposed gait switching method based on the SIAT exoskeleton rehabilitation robot. The gait switching method trying to make two crutch-supporting points and a supporting leg form an equilateral triangle base to increase the stability of human-exoskeleton system and enhance its ergonomic effects, including joints load bearing and less muscle fatigue. The main contributions of this paper are as follows:

- (1) The analysis of gait planning is demonstrated based on a human kinematics model and real-time motion stability based on the zero-moment point (ZMP).
- (2) A neural interface is constructed based on sEMG to achieve motion intention recognition and muscle fatigue estimation.
- (3) The stability of human-exoskeleton system and ergonomic effects of the proposed gait switching method are verified by the organized experiments.

The remainder of this paper is organized as follows. Section 2 provides methodology used in this research. Section 3 presents system setup. Section 4 details experimental works and results. Section 5 shows the conclusions and future work.

## 2. METHODOLOGY

### 2.1. Gait Analysis

#### 2.1.1. Gait Planning

In this study, the SIAT exoskeleton robot movement was achieved by the cooperation of the hip, knee, and ankle joints. We regard the lower limbs of the human body as a model of six connecting rods, as illustrated in **Figure 2**.

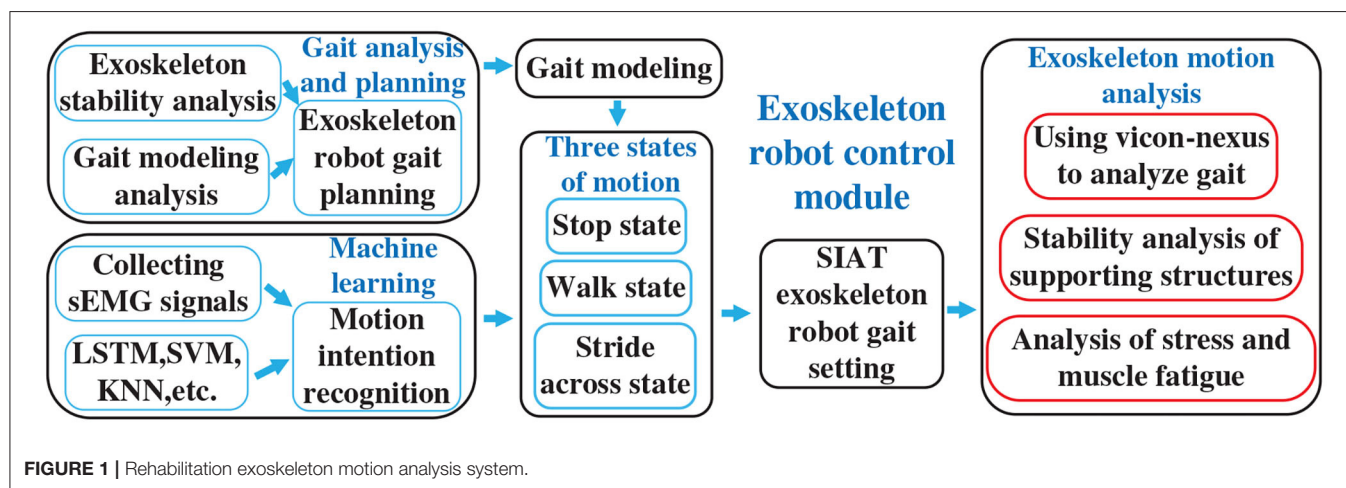
Taking the hip joint as the coordinate axis origin in the figure, the thigh, and calf are regarded as two straight rods in the sagittal plane. One end of the thigh is connected to the shank with the knee joint, and the foot is connected to the calf through the ankle joint. According to the angle relationship and adjacent coordinates, the Denavit–Hartenberg (DH) (Gillis et al., 2018) relationship between the hip, knee, and ankle joints can be determined, as indicated in **Table 1**. Through the DH relation, we can obtain the relational coordinate matrix as follows: where

$$\cos\theta_1 = b_1, \cos\theta_2 = b_2, \sin\theta_1 = c_1, \sin\theta_2 = c_2, \cos\alpha_1 = j_1, \cos\alpha_2 = j_2, \sin\alpha_1 = k_1, \sin\alpha_2 = k_2.$$

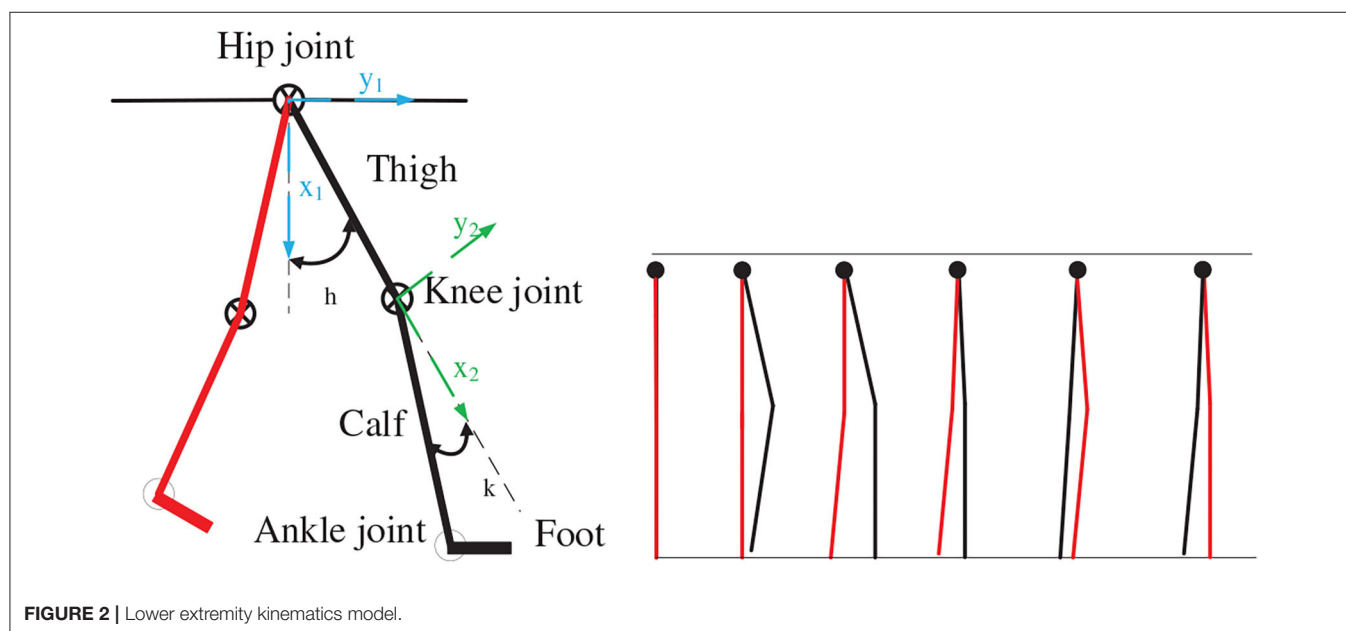
$$A_1 = \begin{bmatrix} b_1 & -c_1j_1 & c_1k_1 & a_1b_1 \\ c_1 & b_1j_1 & -b_1k_1 & a_1c_1 \\ 0 & k_1 & j_1 & d_1 \\ 0 & 0 & 0 & 1 \end{bmatrix} \quad (1)$$

**TABLE 1** | Denavit–Hartenberg relationship.

Link	$a_i$	$\alpha_i$	$d_i$	$\theta_i$
1	L1	0	0	$\theta_h$
2	L2	0	0	$-\theta_k$



**FIGURE 1** | Rehabilitation exoskeleton motion analysis system.



**FIGURE 2** | Lower extremity kinematics model.

$$A_2 = \begin{bmatrix} b_2 & -c_2j_2 & c_2k_2 & a_2b_2 \\ c_2 & b_2j_2 & -b_2k_2 & a_2c_2 \\ 0 & k_2 & j_2 & d_2 \\ 0 & 0 & 0 & 1 \end{bmatrix} \quad (2)$$

$$T = A_1 \times A_2 \quad (3)$$

$$T = \begin{bmatrix} b_1b_2 - c_1c_2j_1 & t_{01} & t_{02} & t_{03} \\ b_2c_1 + b_1c_2j_1 & t_{11} & t_{12} & t_{13} \\ c_2k_1 & t_{21} & t_{22} & t_{23} \\ 0 & 0 & 0 & 1 \end{bmatrix} \quad (4)$$

where  $t_{01} = c_1k_1k_2 - b_1c_2j_2 - b_2c_1j_1j_2$ ,  $t_{02} = b_1c_2k_2 + c_1j_2k_1 + b_2c_1j_1k_2$ ,  $t_{03} = a_1b_1 + a_2b_1b_2 + c_1d_2k_1 - a_2c_1c_2j_1$ ,  $t_{11} = b_1b_2j_1j_2 - b_1k_1k_2 - c_1c_2j_2$ ,  $t_{12} = c_1c_2k_2 - b_1j_2k_1 - b_1b_2j_1k_2$ ,  $t_{13} = a_1c_1 + a_2b_2c_1 - b_1d_2k_1 + a_2b_1c_2j_1$ ,  $t_{21} = j_1k_2 + b_2j_2k_1$ ,  $t_{22} = j_1j_2 - b_2k_1k_2$ ,  $t_{23} = d_1 + d_2j_1 + a_2c_2k_1$ . The homogeneous coordinate matrix  $T$  that demonstrates the relationship between angle of hip and angle of ankle can be easily obtained through the homogeneous coordinate matrix  $A_1$  and  $A_2$ . Based on the kinematics analysis of the exoskeleton robot, matrix relationships are used to calculate the positions of the hip and knee motors at each moment, which are converted into the motor rotation angle values.

The Vicon dynamic capture demonstrated that the joint exhibits a sinusoidal trajectory state when the human body moves. The SIAT rehabilitation exoskeleton has six DoFs: four actives and two passives. The hip and knee joints are initiative.

We initially treat these two joints as two points and draw the trajectories of these points during the walking process to determine the trajectory approximating the sine function (Chen et al., 2019), as illustrated in **Figure 3**.

The sine function,  $y = A \sin[(\omega x + \varphi) + k]$ , is used to express the joint movement trajectory of the human body. The hip joint is regarded as the coordinate 0 point, and the coordinate relationship is established according to the hip joint position. The length of the thigh is set to  $l_1$ , the length of the calf is set to  $l_2$ , and the number of sampling points is denoted by  $i$ . The sinusoidal relationship is used to obtain the hip joint abscissa  $x_0(i)$  and ordinate  $y_0(i)$ . In the same manner, the abscissa  $x_3(i)$  and ordinate  $y_3(i)$  of the left foot position are obtained by means of the sinusoidal relationship (Guo et al., 2019).

The left knee position is determined as follows:

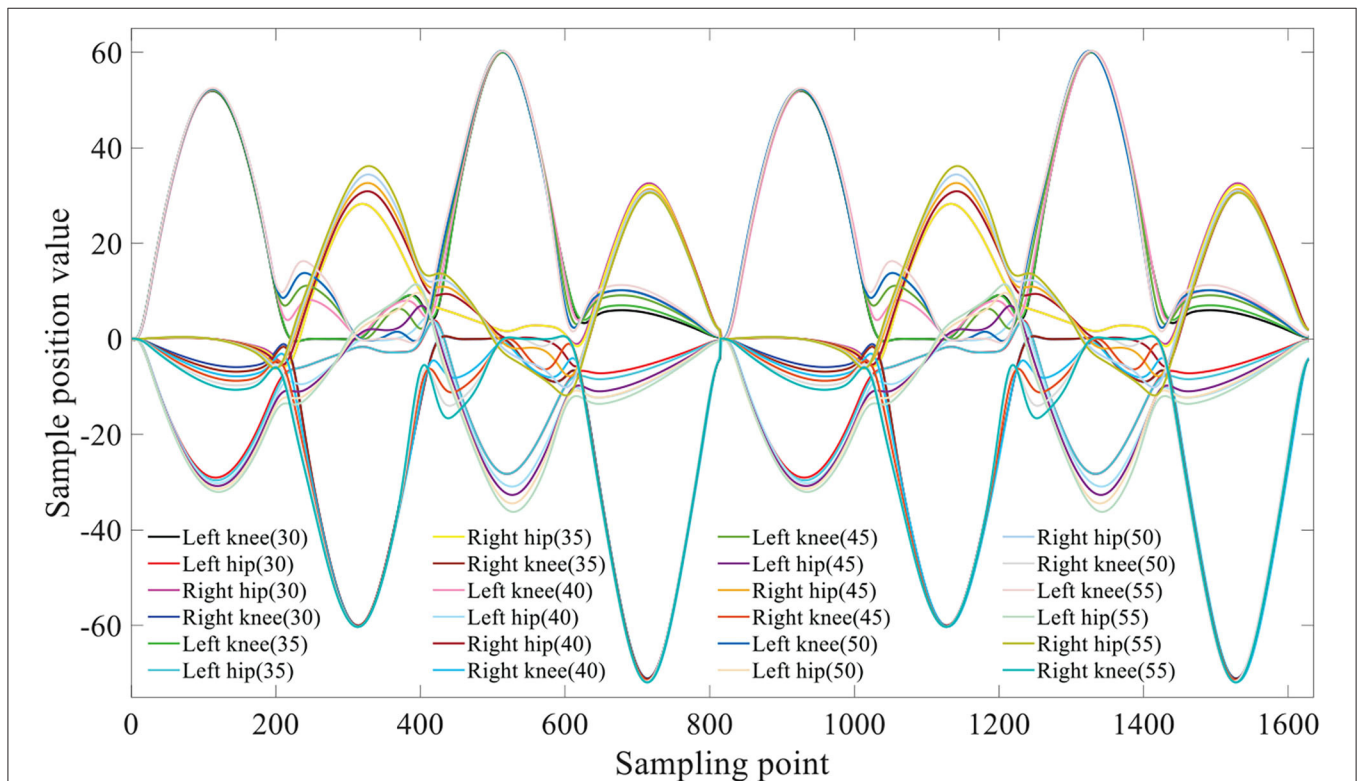
$$(x - x_3(i))^2 + (y - y_3(i))^2 = l_2^2 \quad (5)$$

$$(x - x_0(i))^2 + (y - y_0(i))^2 = l_1^2 \quad (6)$$

The maximum values of  $x$  and  $y$ , namely  $x_4(i)$  and  $y_4(i)$ , respectively, are used. In this manner, the angle value of each position can be reversed as follows:

Left hip:

$$Ahl(i) = \arctan \left( \frac{x_4(i) - x_0(i)}{y_0(i) - y_4(i)} \right) \quad (7)$$



**FIGURE 3 |** The motors gait trajectory.

Left knee: takes 0 when the value is  $<0$ :

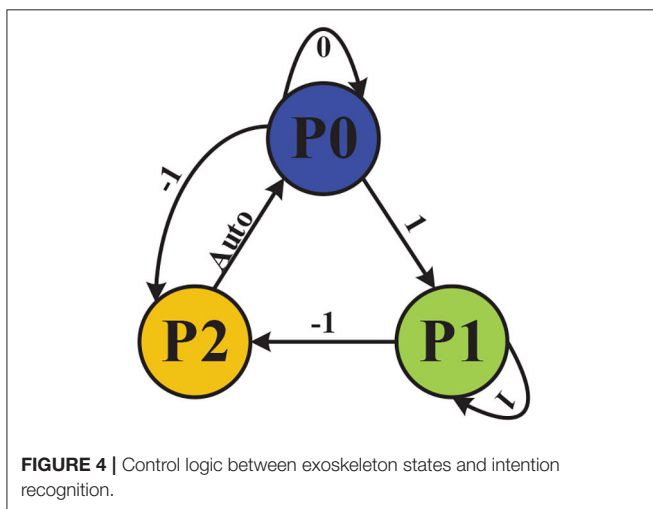
$$Akl(i) = \arctan\left(\frac{x_3(i) - x_4(i)}{y_4(i) - y_3(i)}\right) \quad (8)$$

Using the compilation algorithm, we determine the different positions of the motor at each moment, and these are combined into a complete motion cycle. The generated motor gait trajectory is illustrated in **Figure 3**. A parenthesis indicates the planning step size (in cm).

When compiling the control program, we set different step sizes, paces, and changed the motion states. The crutch support points were placed in different positions to form triangle support points of different shapes. In our previous experiments, we used the Tactilus<sup>®</sup> foot pressure insole to collect the pressure data and obtain the motion trajectory (Guo et al., 2019). It was verified that the stable triangle support point was more conducive to mastering balance. The present study uses the Vicon Nexus motion capture system in conjunction with the 3D force test runner to verify the results.

The control logic between exoskeleton states and intention recognition is illustrated in **Figure 4**. The three exoskeleton states are as follows: the quiescent state is set to P0 (stop), the walking state is set to P1 (walk), and step over an obstacle ( $21.5 \times 13.5 \times 10.5$  cm) state is set to P2 (stride across). The starting state is P0 (stop).

In order to operate the exoskeleton robot, we set the control instruction value of detected immobility to 0, the control instruction value of detected walking to 1, and the control instruction value of detected crossing obstacle to  $-1$ , which is then reset to its initial state of P0 (stop). When the identified results of sEMG signals is 1, the exoskeleton would run to the state P1 (walk); when identified results of sEMG signals is 0, the exoskeleton would run to the state P0 (stop); when the identified results of sEMG signals is  $-1$ , the exoskeleton would run to the state P2 (stride across). The exoskeleton would automatically run to the state P0 (stop) after the P2 (stride across) state.



The motion intention is recognized through sEMG, which will be demonstrated in section 2.2.1. Because of the continuity and density of the collected sEMG, control instructions are sent to the exoskeleton only when three consecutive identical recognition results are detected. If three consecutive signals are not detected, the exoskeleton remains static after completing the current motion.

### 2.1.2. Stability Analysis

To help paraplegic wearing the exoskeleton to master balance, a stable gait switch method based on the ZMP is proposed. For these patients, the lack of strength and sense of lower extremities means that they cannot rely on their legs to keep balance. Double crutches need to be added to ensure balance; hence, the exoskeleton exists in a quadruped state (Wu et al., 2018). By positioning the crutches to form a triangle base of support, additional stability is produced.

The walking process can be divided as follows: 40% of situations are supported by one leg, 20% of situations are supported by two legs, and the remaining 40% of situations are supported by one leg, the other is semi-supported. In order to evaluate the performance of the stable gait switch method, a real-time gait was divided into eight parts.

The entire movement process will only produce plantar pressure during the incomplete support stages. The main part of the full leg support stage is the forward force balance (Moraes et al., 2019). When the three supporting points form a triangle and the barycenter falls within the triangle, the stable state achieves at this time. The ZMP theory is used to calculate the overall pressure center point position of human-exoskeleton system during walking. The ground force is regarded as the discrete force set  $f_i \in S(i = 1, 2, \dots, N)$  acting on  $p_i$ , as indicated in **Figure 5**.

The moments around the point  $p$  are expressed as:

$$\tau = \sum_{i=1}^N (p_i - p) \times f_i \quad (9)$$

Because the equivalent moment of force for the ZMP is zero, the foot does not rotate around the ground vertical axis (does not cause slipping). At this time, the ZMP position is:

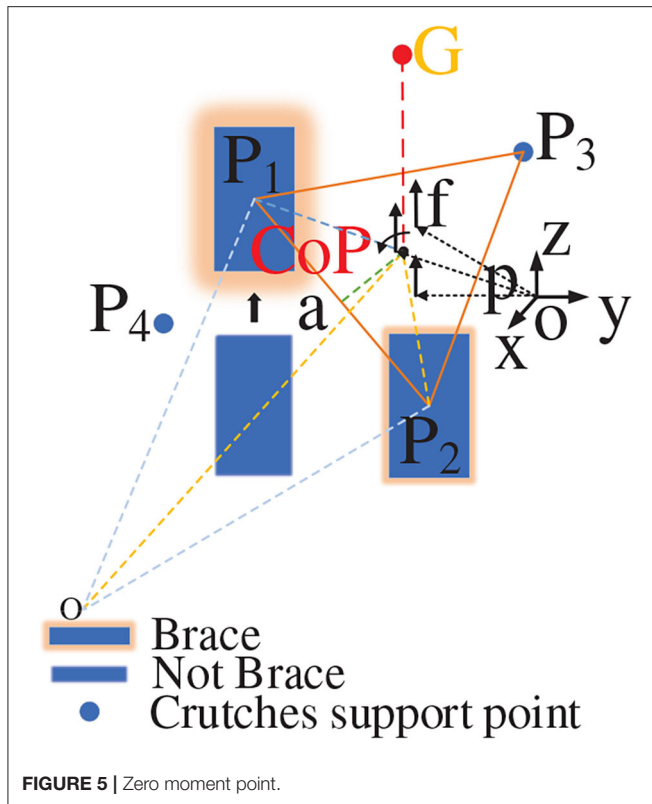
$$p = \frac{\sum_{i=1}^N p_i f_{iz}}{\sum_{i=1}^N f_{iz}} \quad (10)$$

In the formula, when  $f_{iz}$  is the case in which  $f_i$  forms a triangular support in the vertical direction of the  $z$  axis, the ZMP position is:

$$p = \frac{p_L f_L + p_R f_R + p_g f_g}{f_L + f_R + f_g} \quad (11)$$

In the above,  $p_L$ ,  $p_R$ , and  $p_g$  represent the ZMP position obtained by the left foot, right foot, and crutch, respectively. By means of calculation, the center of pressure (CoP) and ZMP are almost coincident or coincident. We measure the shortest distance from





**FIGURE 5 |** Zero moment point.

the CoP to triangle the support side. We list one of these here as follows:

$$\alpha_{Ca} = d_{C \perp P_1 P_2} \quad (12)$$

$$d_{C \perp P_1 P_2} = \left| \overrightarrow{OC} - \overrightarrow{OP_2} - \left( \overrightarrow{OP_1} - \overrightarrow{OP_2} \right) \cdot \left( \overrightarrow{OC} - \overrightarrow{OP_2} \right) \vec{e} \right| \quad (13)$$

In order to ensure stability of human-exoskeleton system, we analyzed the stability of different triangular support structures.

When the position of  $\tau$  falls within the triangle formed by the support points, the value of  $\alpha_{Ca}$  is  $>0$ , and stability is indicated. The barycenter will fall in the center of the triangle only when the vertical distance between each point of the CoP point and triangle is sufficiently small and all distances are equal, indicating that the three supporting points are evenly stressed, as shown in **Figure 6A**. When the three support points formed a normal acute triangle, as indicated in **Figure 6B**, the vertical distance between each point of the CoP point and the triangle is unequal, indicating that the force of the three support points is not uniform in this state. When the three support points form a right triangle, as indicated in **Figure 6C**, the force of the three support points is also uneven as the barycenter of the triangle falls on the oblique side, which constitutes a critical stable state. When the triangle formed by the three support points is an obtuse triangle, as indicated in **Figure 6D**, the barycenter of the triangle has fallen outside the triangle, constituting a tendency to dump. The stability threshold for walking at each step must be controlled within a safe range because an uneven force will

accelerate muscle fatigue and soreness, resulting in a decrease in stability and affecting the rehabilitation effect.

## 2.2. sEMG Interface

A neural interface is constructed based on sEMG, which aims to accomplish the intention recognition and muscle fatigue estimation. Because of the lack of sEMG in lower limb for paraplegics, the sEMG signals and angle signals from the upper limbs are collected. The sEMG and angle signal of the subject were simultaneously collected while the subject wearing the SIAT exoskeleton was normally walking or triggering the gait conversion. One of the planned motions was listed, with the right elbow joint bent at not  $<90^\circ$  as the triggering signal. This action is used as trigger because that paraplegics can perform this action fair easily in the standing posture. Moreover, considering that sEMG will be used for further intention recognition, this action will not conflict with other gait switching actions. The acquired joint angle was used as an auxiliary confirmation angle value to achieve more accurate intention recognition.

### 2.2.1. Motion Intention Recognition

To recognize the motion intention better, this research injected the LSTM deep learning model. A deep motion pattern identification model based on the LSTM structure is proposed to study the inherent characteristics of joint and sEMG from a time perspective (Miiikkulainen et al., 2019). The LSTM model contains input, forget, and output gates (Zeiler, 2012), as well as one or more self-connected memory cells, which allows the cells to reset data when the network needs to forget useless inputs (Chang and Lin, 2011). The LSTM memory cells can store and access information over long periods.

The most important component in the LSTM neural network is the state unit  $s_i^{(t)}$ :

$$s_i^{(t)} = f_i^{(t)} s_i^{(t-1)} + g_i^{(t)} \sigma \left( b_i + \sum_j U_{ij} x_j^{(t)} + \sum_j W_{ij} h_j^{(t-1)} \right) \quad (14)$$

The input of LSTM network is given as:

$$g_i^{(t)} = \sigma \left( b_i^g + \sum_j U_{ij}^g x_j^{(t)} + \sum_j W_{ij}^g h_j^{(t-1)} \right) \quad (15)$$

The forgetting layer output is given as:

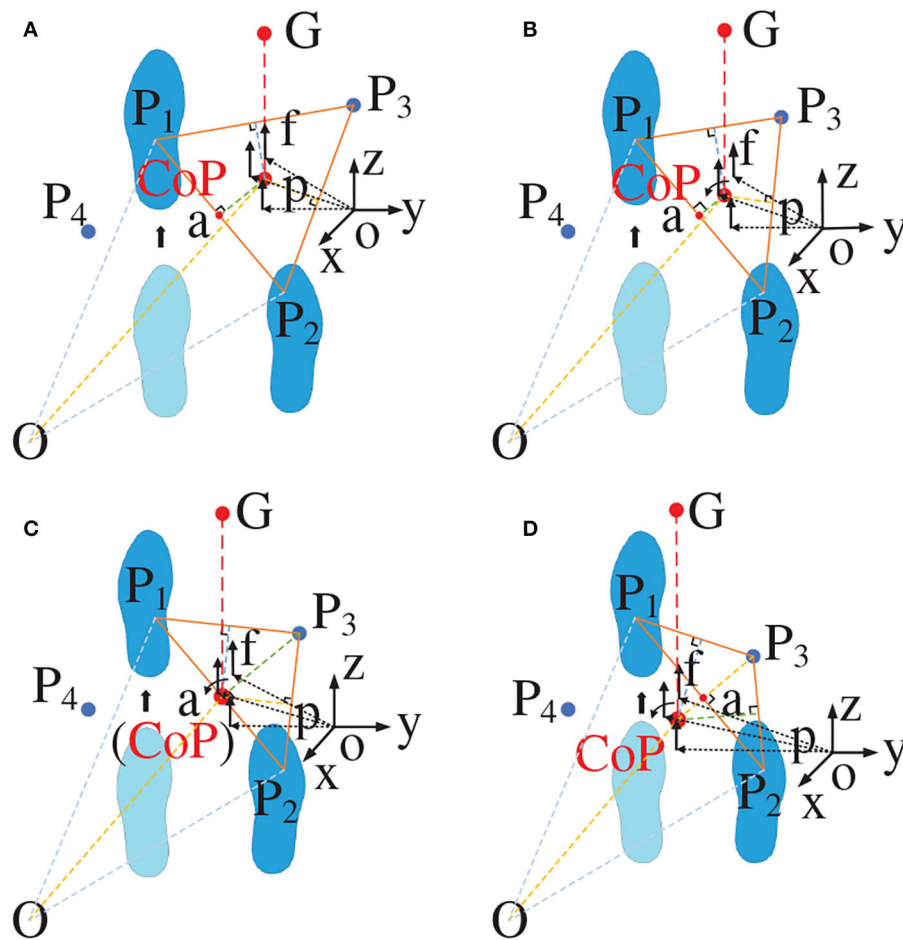
$$f_i^{(t)} = \sigma \left( b_i^f + \sum_j U_{ij}^f x_j^{(t)} + \sum_j W_{ij}^f h_j^{(t-1)} \right) \quad (16)$$

The LSTM network cell output is given as:

$$h_i^{(t)} = \tanh \left( s_i^{(t)} \right) q_i^{(t)} \quad (17)$$

The LSTM network output is given as:

$$q_i^{(t)} = \sigma \left( b_i^o + \sum_j U_{ij}^o x_j^{(t)} + \sum_j W_{ij}^o h_j^{(t-1)} \right) \quad (18)$$



**FIGURE 6 |** Triangular force analysis. **(A)** The barycenter falls in the center of the triangle; **(B)** The barycenter falls in the non-center of the triangle; **(C)** The barycenter falls in edge of the triangle; **(D)** The barycenter falls out of the triangle.

where  $b$ ,  $U$  and  $W$  are the offset weights of the LSTM cells, input weights, and forget gates, respectively. Moreover,  $x^{(t)}$  is the current input, while  $h^{(t)}$  is the current hidden layer vector containing the output of all LSTM cells.

The current memory is written as:

$$C'_t = \tanh \left( W_{ij}^c x_j^c + U_{ij}^c h_j^{(t-1)} + b_i^c \right) \quad (19)$$

The current value for the states of the memory cells is given as:

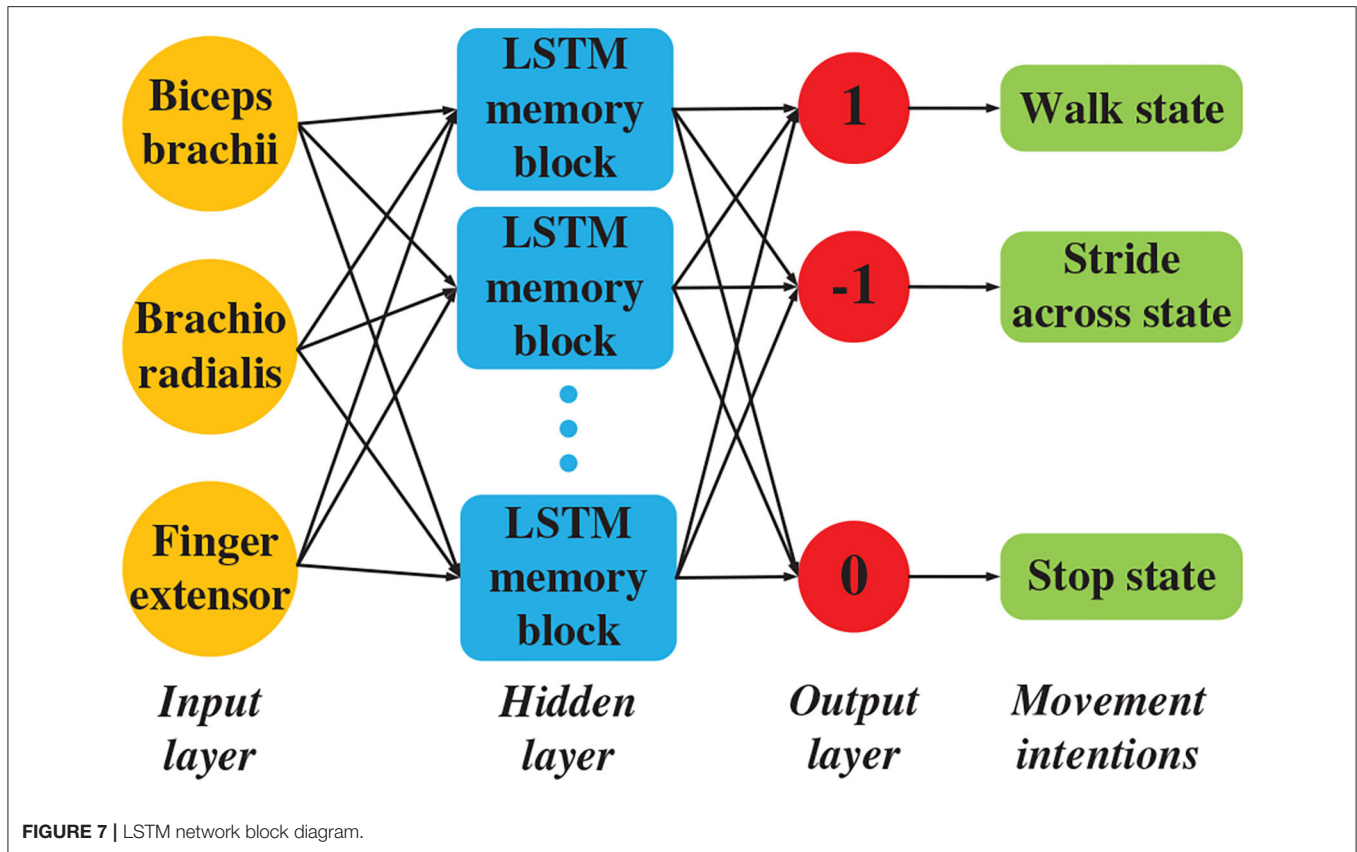
$$C_t = f_i^{(t)} C_{t-1} + g_i^{(t)} C'_t \quad (20)$$

The memory block output is given as:

$$h_j^{(t-1)} = q_i^{(t)} \tanh(C_t) \quad (21)$$

Based on the LSTM neural network framework, the neural network for motion intention recognition is constructed. Multiple LSTM cells can be stacked for more expressive power, as presented in **Figure 7**. In different states, the elbow joint angle

data and the sEMG signal of the selected muscles (the musculus biceps brachii, brachioradialis, and finger extensor) are collected. Based on the collected data, the movement intention is identified through the LSTM neural network model, which is built using TensorFlow<sup>®</sup>. The neural network model is trained and verified by the obtained data. The exoskeleton system is controlled by the optimal model through predicting the motion intention of wearer. The LSTM neural network structure consists of one input layer, two hidden layer, and one output layer. The input layer is composed of three nodes corresponding three selected muscles. The number of neuron nodes in hidden layer is 128, and the hidden layer uses ReLU as the activation function. The dropout probability of nodes is set to 0.5. Taking advantage of dropout can make the LSTM network model more robust and avoid the problem of over-fitting (Zeiler, 2012). In order to prevent gradient drop, the adaptive moment estimation algorithm and weighted average method are utilized in this research. The LSTM model achieves optimization by using the following paraments: train errors = 0.004583, train costs = 2.511049, valid errors = 0.001667, and valid costs = 0.198940. We explain the different



LSTM neural networks that are used for accuracy comparisons (Chu et al., 2007). The softmax layer is selected as the output layer. The output layer is composed of three nodes, which correspond with the three gait categories.

### 2.2.2. Muscle Fatigue Estimation

In this research, muscle fatigue is quantified based on sEMG through the neural interface and the wavelet packet energy entropy (WPEE) is utilized to quantify the muscle fatigue. WPEE not only has the advantages of wavelet transform but also tests the overall representation of the signal from the perspective of the system. The complexity of the frequency component signal and the dynamic characteristics of the signal are given. The wavelet packet decomposition and composition are completed with daubechies wavelet basis function (db1), which have good smoothness and compactness (Nakashima and Kushida, 2019).

After wavelet packet decomposition, the reconstructed signal energy of  $(i, j)$  is calculated as:

$$E_i^j = \sum_{k=1}^M |d_{i,j}^k|^2 \quad (22)$$

where  $d_{i,j}^k$  denotes the coefficient of the  $k$ th decomposition node  $(i, j)$ , and  $M$  presents the number of points in the decomposed signal sequence. Then, the relative value of energy in single frequency band, which presents the each band energy

distribution of signals in overall frequency range, can be acquired by normalizing the energy:

$$P_i^j = \frac{E_i^j}{\sum_{j=0}^{2^i-1} E_i^j} \quad (23)$$

where  $j \in [0, 2^i - 1]$ . The probability is also called relative wavelet packet energy. Combining the energy distribution of wavelet packet decomposition coefficient with information entropy, the WPEE is defined as:

$$\text{WPEE} = - \sum_{j=0}^{2^i-1} P_i^j \ln P_i^j \quad (24)$$

WPEE can quantitatively measure the order and disorder of sEMG frequency distribution. If the sEMG energy is concentrated in one sub-band, the WPEE is 0, that is, the sEMG is orderly; on the contrary, if the sEMG energy is randomly dispersed in each sub-band, the sEMG is disorderly. Therefore, if muscles are more fatigue, the frequency of sEMG is more compressed to low frequency (Guan et al., 2017; Nakashima and Kushida, 2019), contributing to a decrease in WPEE. The values of WPEE are first normalized and then statistically stratified to support visualization and comparison of the muscle fatigue quantitative results.

### 3. SYSTEM SETUP

The main equipment in this research includes SIAT Exoskeleton, Biometrics sEMG acquisition system and Vicon Nexus motion capture system, as illustrated in **Figure 8**.

#### 3.1. SIAT Exoskeleton

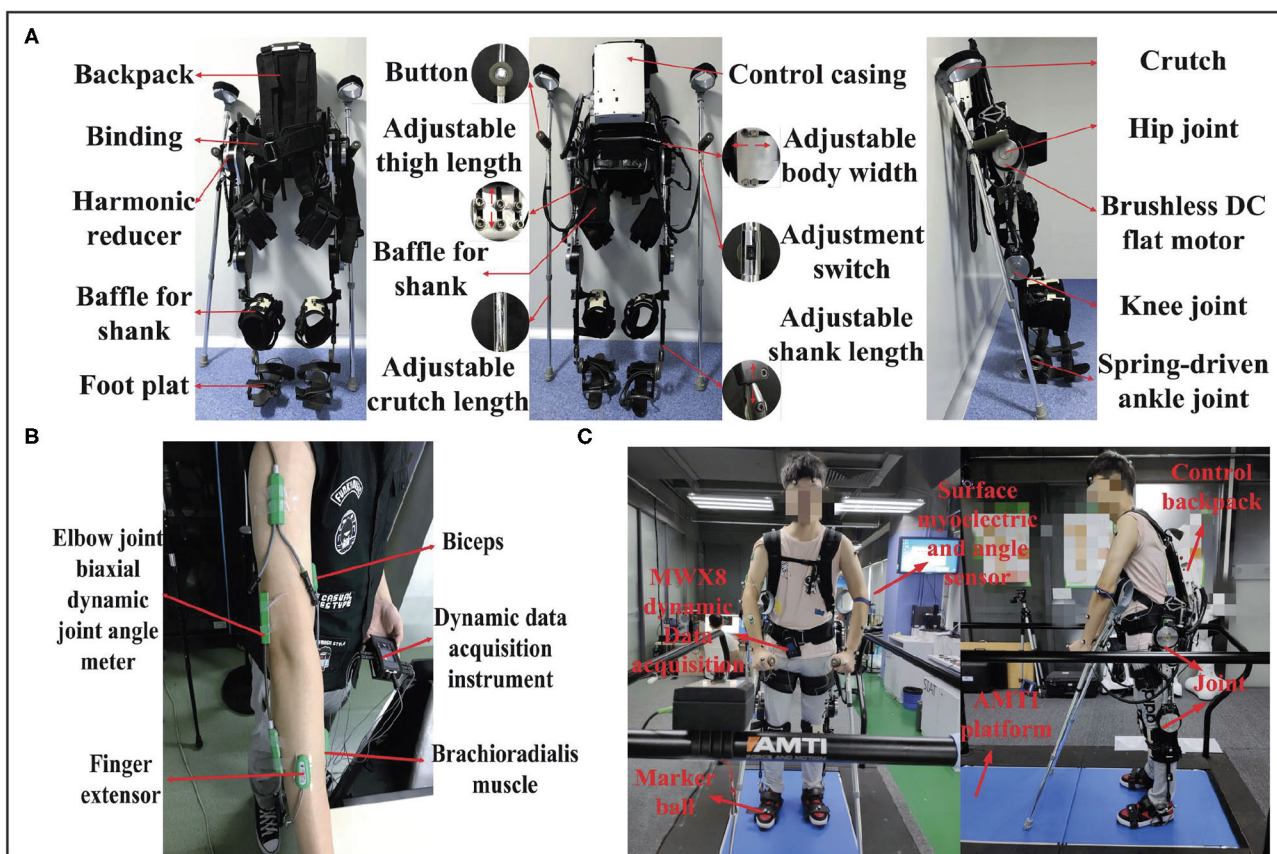
The SIAT exoskeleton robot, which is driven with two geared brushless motors for each leg, is designed for the disabled. This robot was developed by the Shenzhen Institutes of Advanced Technology, Chinese Academy of Sciences. The SIAT lower-limb rehabilitation exoskeleton robot is illustrated in **Figure 8A**. The SIAT exoskeleton robot includes hip, and knee joints, with a total of four DoFs. It can provide assistance to the hip and knee joints in the sagittal plane. Furthermore, the ankle joint is equipped with a spring mechanism to ensure a maximum contact area between the sole and ground to maintain stability. The encoders can obtain the angle of the hip and knee joints and crutches are used to ensure overall balance of the exoskeleton.

The SIAT exoskeleton consists of a mechanical frame, drive system, control system, and sensing system. The total weight is approximately 15 kg. The control unit is a Windows

microcomputer that is placed in a white backpack on the back. The use of the microcomputer offers numerous advantages including the ability to optimize software specifically for the exoskeleton robot, while in use or copied to the microcomputer for direct use (Yan et al., 2018).

#### 3.2. Biometrics

The portable sEMG signal acquisition system (Biometrics PS850) includes a signal acquisition device (DataLog) and management software that is specifically designed for sEMG measurements. The sEMG acquisition device includes eight independent programmable analog channels and two digital channels. The used sampling rate is set to 500 Hz in this research. Using the DataLog data acquisition memory, the collected signal records can be stored and analyzed. Three analogy channels are used to collect sEMG and a wired twin-axis goniometer is utilized to collect angle signal. The surface myoelectric collectors were attached to three selected muscles (musculus biceps brachii, brachioradialis, and finger extensor on the right arm), and the angle sensor was attached to the elbow joint. The sEMG acquisition system and selected muscles are illustrated in **Figure 8B**.



**FIGURE 8 |** System setup: **(A)** SIAT Lower-limb Rehabilitation Exoskeleton Robot; **(B)** sEMG acquisition system and selected muscles; **(C)** VICON BONITA 10 environment, including Vicon camera, Vicon sole, and AMTI platform.



### 3.3. Vicon Nexus

The full set of equipment (Vicon BONITA 10) from Vicon Nexus is utilized for motion data acquisition and verification. The center of gravity movement trajectory and movement pressure of the exoskeleton robot during the walking process were detected by the pressure-measuring device on the running platform. The Vicon motion capture system captured the real-time motion of the exoskeleton robot wearer, detected the motion posture, and determined the wearer's center of gravity movement trajectory.

Vicon is a 3D optical motion capture system developed by Oxford Metrics Limited in the United Kingdom. VICON BONITA 10 environment includes Vicon cameras, a Vicon sole, and the AMTI platform, as shown in **Figure 8C**. Every part of the 3D optical motion capture system are connected via a network to provide real-time optical data, and it can be used for real-time online or off-line motion capture and analysis. The working principle is based on a reflective capture system, which requires reflective balls (markers) on the wearer. When the Vicon camera emits red light onto the reflective ball, the reflective ball will reflect red light of the same long wavelength to the camera. Therefore, the capture camera can determine the two-dimensional coordinates of each reflective ball. Following Vicon's control software processing, the 3D coordinates and the trajectory of each reflective ball can be obtained. In this study, we used six cameras to capture the motion pose.

## 4. EXPERIMENTAL WORKS AND RESULTS

Three healthy male subjects participated in the experiments of this work and voluntarily signed an informed consent form, which was approved by the Medical Ethics Committee of Shenzhen Institutes of Advanced Technology [(SIAT)-IRB-170315-H0142].

### 4.1. Experimental Design

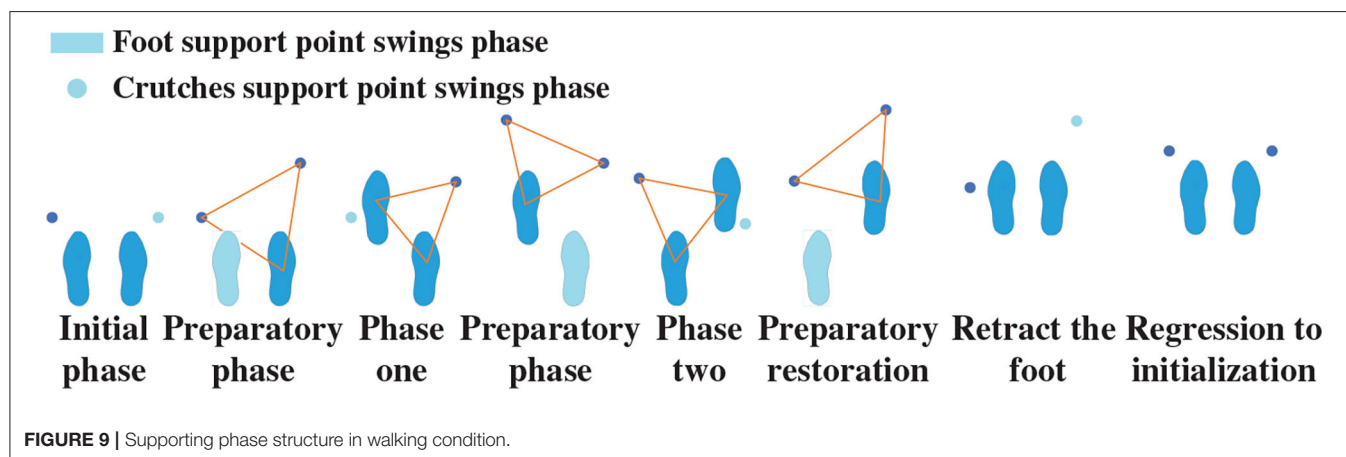
When people with disabilities in the lower limb suddenly stand up with exoskeleton, it is difficult for them to master balance. Moreover, paraplegic patients do not trust the exoskeleton robot when they wear the exoskeleton for the first time. In this case, the support point position of the crutches is particularly important.

During one movement cycle, the crutches are regarded as support points. Therefore, the human–exoskeleton system forms a quadruped state. During a gait cycle, the right crutch is first moved while lifting the left leg. With the left crutch as the support point, the right leg is lifted. Then, as the right crutch is moved to become the support point, the left leg is lifted. Finally, the crutches are retracted on the right-hand side to complete a periodic gait. It is necessary to form a three-point steady state during the movement and a four-point steady state in the stopping phase. Under normal circumstances, it is difficult to guarantee balance in the walking condition, and it is necessary to form a stable triangular support point. As shown in **Figure 9**, one complete period gait consists of a series of gait phases and states. Two-crutch points and supporting feet are required to form an equilateral triangle in the transition phase to maintain the stability of the human–exoskeleton system.

In experiments, the subject was attached to the exoskeleton through soft bandages. While the human exoskeleton was walking, the weight was transmitted to the supporting legs and crutches. Walking with different gaits was performed on the Vicon 3D force-measuring platform. In total, 10 datasets were collected for each gait group.

To control exoskeleton robot based on motion intention of the subject in real time, the sEMG of selected muscles are simultaneously collected. The gait of the exoskeleton robot is then switched according to the identified results derived from the optimized LSTM model. A real-time communication connection between the intention recognition and the exoskeleton robot is constructed. We use Visual Studio (VS) to establish the exoskeleton Windows presentation foundation (WPF) control interface, establish intention recognition based on the LSTM model on MATLAB®, build a real-time communication connection between the sEMG signal acquisition system and MATLAB® to make it run simultaneously, and use the IP address and port to establish a real-time communication connection with the exoskeleton WPF control interface.

Real-time training is conducted through machine learning by collecting sEMG signals of stopping, walking, and stride across states. The recognized signal is then transmitted to the VS program through real-time communication interface.

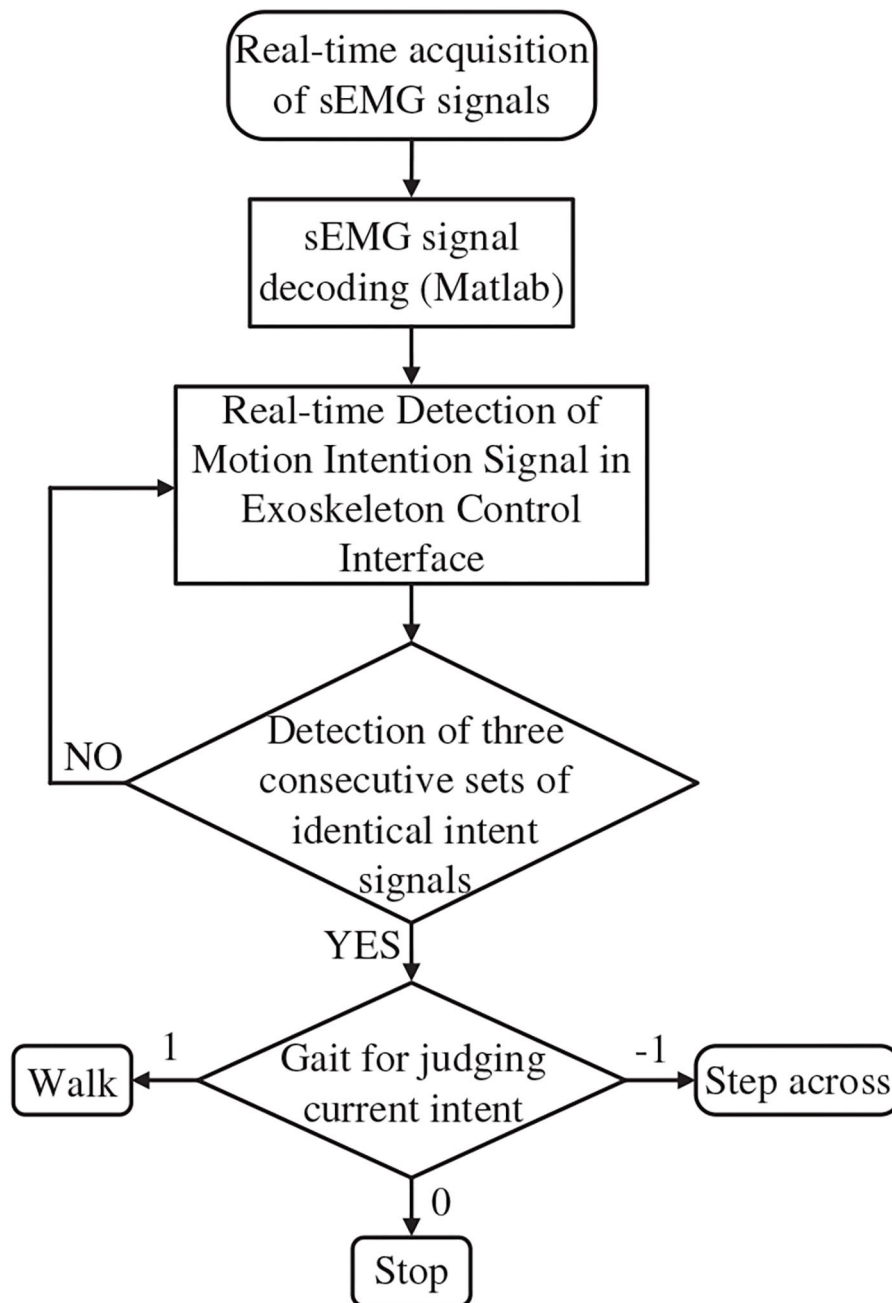


The real-time intention recognition flowchart is shown in **Figure 10**.

The pressure data were monitored in real time through the 3D force measuring treadmill and the real-time motion trajectory of the subject was determined through the Vicon dynamic capture system, as illustrated in **Figure 3**. Eight different gaits in this experiment, and planned and unplanned walking were performed in each gait. The equilateral triangle support structure

is considered as the planned gait and the rest of the triangle support structure as the unplanned gait. The data were collected and compared to verify that it is more stable in the planned walking state.

In addition, muscle fatigue experiments are conducted to demonstrate the advantage of our proposed gait switch method further. Each subject wearing the exoskeleton robot walks for 12 min (2 sessions  $\times$  6 min) using planned and unplanned gait



**FIGURE 10 |** The flowchart of real-time intention recognition.

switching method, respectively. The subject would have enough rest between each walking test to reduce the fatigue impact from prior test.

## 4.2. Results and Analysis

The CoP trajectories of different gaits based on the Vicon 3D force-measurement treadmill are compared. The comparison of each CoP trajectory is illustrated in **Figure 11**. It is found that stability is better while walking with the planned path. Under the planned gait switching method condition, the deviation between the similar wave peaks and the wave valleys is smaller in the different gait trajectories, the gait is smoother, and the center of gravity movement trajectory is smaller.

Through the reverse derivation of the human load bearing using the Vicon 3D force-measuring treadmill, the load bearing sizes of the ankle, knee, hip, and waist can be obtained. The gait with 28, 32, 36, 40, 44, and 48 cm steps size, and the gait of step over obstacle (stride cross) are utilized to be tested. Each subject walk with these gaits, and the average results deriving from each group of gaits are indicated in **Table 2**. By comparing the forces, we can observe that the planned gait results in greater conservation of strength. This is further verified by the muscle fatigue estimation results.

After the sEMG is collected, the power frequency interference at 50 Hz had to be eliminated (Kim et al., 2019). Bandpass filtering of 10–500 Hz was also required after the interference was removed by infinite impulse response. We collected 214,000 sample points as training data for the collected samples, and each motion covered 40 datasets with a length of 1,000. The feature vectors were extracted from the sEMG data using the root mean

square (RMS):

$$RMS = \sqrt{\frac{\sum_{i=1}^N |x(i)|^2}{N}} = \sqrt{\frac{x_1^2 + x_2^2 + \dots + x_N^2}{N}} \quad (25)$$

The extracting feature causes the features between different signals to be more prominent and improve accuracy. The data could be mapped nonlinearly to a high-dimensional space to solve the linearity of the original space.

The objective function is expressed as:

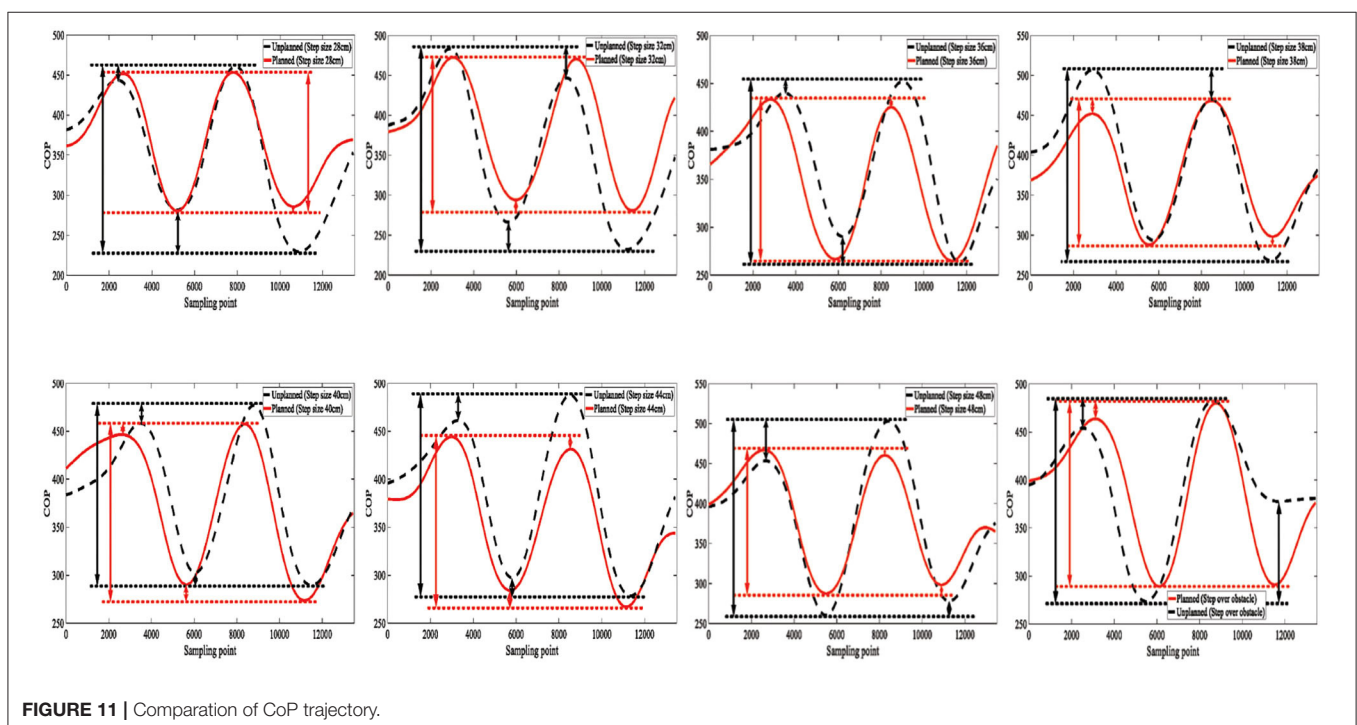
$$\max_{\alpha_i \geq 0} \min_{w, b} L(w, b, \alpha) = p^* \quad (26)$$

where  $p^*$  represents the optimal value.

The corresponding classification function is given as:

$$f(x) = \sum_{i=1}^n \alpha_i y_i K(x_i, x) + b \quad (27)$$

where  $K(x, z)$  represents the construction kernel function. The extracted feature vector was affixed with the corresponding motion pattern tags and placed in the neural network as datasets for processing. Note that 80% of the data were used as the test set, and the remaining 20% were used as the verification set. The correct rate was verified via cross-validation of different folds. The common machine learning method, including Supporting Vector Machine (SVM), Multiple Layers Perception Neural Networks (MLPNN), K-Nearest Neighbor (KNN), and Linear Discriminant Analysis (LDA), are compared with the LSTM



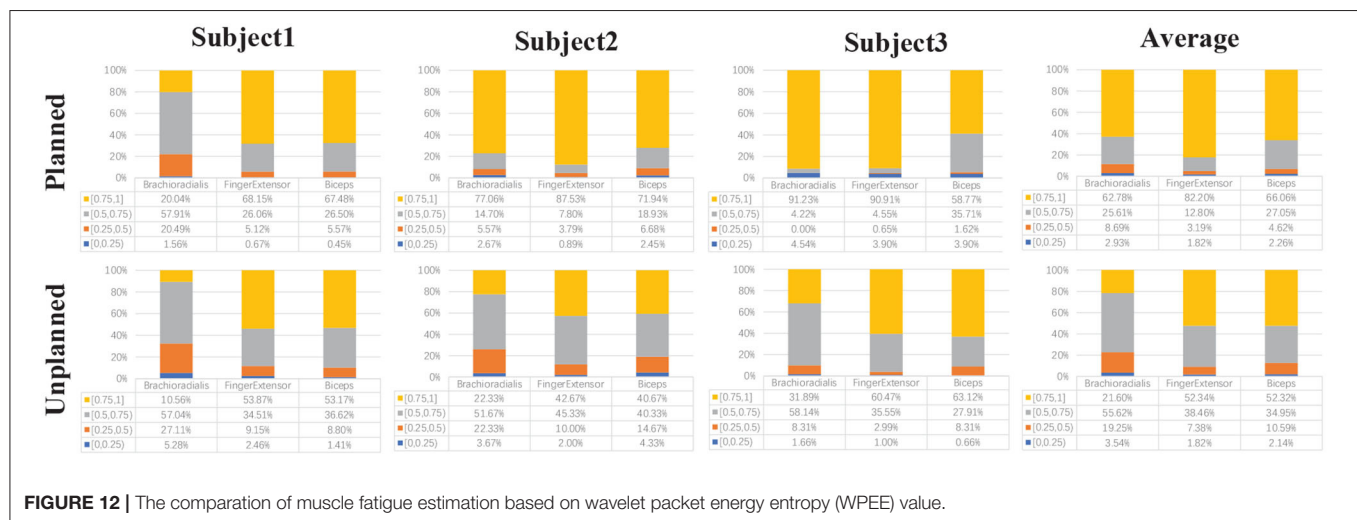
**FIGURE 11 |** Comparison of CoP trajectory.

**TABLE 2 |** Joints load bearing comparison between in planned and unplanned gait.

Parameter	28 cm	32 cm	36 cm	40 cm	44 cm	48 cm	Stride cross
Ankle joint force (N/kg) (Planned)	5.549	5.463	5.221	4.506	5.092	5.571	5.628
Knee joint force (N/kg) (Planned)	4.076	4.288	3.397	3.049	3.665	3.798	4.828
Hip joint force (N/kg)(Planned)	5.094	5.312	4.410	4.056	4.646	4.810	5.836
Waist force (N/kg)(Planned)	6.675	5.757	5.210	4.565	5.674	5.934	6.603
Wrist force (N/kg)(Planned)	4.192	4.256	4.680	4.265	4.141	4.396	4.376
Ankle joint force (N/kg) (Unplanned)	7.755	7.205	6.265	7.152	6.327	6.335	6.882
Knee joint force (N/kg) (Unplanned)	6.286	5.054	4.623	4.318	4.901	5.446	6.885
Hip joint force (N/kg)(Unplanned)	7.267	6.123	5.645	5.336	6.243	6.472	7.171
Waist force (N/kg)(Unplanned)	7.673	7.467	7.322	6.801	6.850	6.723	7.702
Wrist force (N/kg)(Unplanned)	5.343	5.301	6.052	6.138	5.445	5.354	5.536

**TABLE 3 |** Intention recognition rate comparison.

Method	2-Fold (%)	4-Fold (%)	6-Fold (%)	8-Fold (%)	10-Fold (%)	12-Fold (%)	14-Fold (%)
LSTM	96.5	98.0	99.2	99.4	99.4	99.5	99.5
SVM	94.0	95.0	95.0	95.3	96	96.5	96.5
KNN	85.5	90.0	91.7	92.4	90.1	90.0	89.5
MLPNN	91.0	91.3	92.5	93	93.9	97.0	94
LDA	86.4	85.6	90.1	87.9	85.0	86.4	86.4

**FIGURE 12 |** The comparison of muscle fatigue estimation based on wavelet packet energy entropy (WPEE) value.

model. The comparison of intention recognition rate is indicated in Table 3.

During the muscle fatigue experiments, the gaits in different size are utilized to test. The subject wearing the exoskeleton robot walks back and forth in an open area about 10 m long and 3 m wide. The subject crosses an obstacle (21.5 × 13.5 × 10.5 cm) two times and turns around at the end of the path. The subjects are asked to move the body weight forward as much as possible to imitate the paraplegic. The muscle fatigue estimation results and analysis in gait with 36 cm are demonstrated as in Figure 12. The normalized WPEE value is divided into four layers and statistics are completed. The lower the WPEE value, the more severe the muscle fatigue. It is obvious that the proportion of high value

WPEE in planned gait switching condition is more than that in unplanned gait switching condition. Therefore, we may safely claim that the muscle is more fatigue using the unplanned gait switch method.

## 5. CONCLUSIONS

In this research, an adjustable real-time stable gait switching strategy with a neural interface for the lower extremity exoskeleton robot is proposed. The gaits planning and stability analysis based on the human kinematics model for the SIAT lower limb exoskeleton are first demonstrated. A neural interface



based on sEMG that realizes the intention recognition and muscle fatigue estimation is constructed. The stability of human-exoskeleton system and muscle fatigue of the wearers with the exoskeleton robot were tested through different gaits. The intention recognition accuracy based on the LSTM model was approximately 99%. The feasibility and efficiency of the proposed gait switching method is verified using the experimental results.

Although the proposed real-time gait switching strategy has shown advantages, several limitations of this study should be noted. First, the real-time gait switching method was only trained and tested using healthy subjects, and paraplegic patients may generate different locomotion features. Second, the most steady-state gait needs to be adjusted by online real-time gait feedback compensation. Moreover, the sEMG function of paraplegic patients may be incomplete and not easily obtainable. In future work, real-time gait feedback compensation adjustment should be considered to enable the exoskeleton robots to adapt to different walking environments.

## DATA AVAILABILITY STATEMENT

The raw data supporting the conclusions of this article will be made available by the authors, without undue reservation.

## ETHICS STATEMENT

The studies involving human participants were reviewed and approved by the Medical Ethics Committee of Shenzhen Institutes of Advanced Technology. The patients/participants

provided their written informed consent to participate in this study.

## AUTHOR CONTRIBUTIONS

CW and ZG conceived the research project. CW and XW developed the SIAT exoskeleton. ZG, SD, BH, and YY designed and performed the experiments. ZG and SD preformed the data processing and analysis and wrote the paper. CW, XW, BH, and YY performed supports and discussions. All authors reviewed and approved the submitted paper.

## FUNDING

This work was partly supported by the National Key Research and development Program of China (2017YFB1302303), National Natural Science Foundation-Shenzhen Joint Research Program (U2013213), and the Key R&D Program of Guangdong Province, China (2018B030339001).

## ACKNOWLEDGMENTS

The authors would like to thank all subjects who participate in the experiments and the partners from the Center for Intelligent and Biomimetic Systems, SIAT.

## REFERENCES

- Abe, T., Koizumi, S., Nabae, H., Endo, G., and Suzumori, K. (2018). "Muscle textile to implement soft suit to shift balancing posture of the body," in *2018 IEEE International Conference on Soft Robotics (RoboSoft)* (Livorno), 572–578. doi: 10.1109/ROBOSOFT.2018.8405387
- Baunsgaard, C. B., Nissen, U. V., Brust, A. K., Frotzler, A., Ribeill, C., Kalke, Y.-B., et al. (2018). Gait training after spinal cord injury: safety, feasibility and gait function following 8 weeks of training with the exoskeletons from Ekso bionics. *Spinal Cord* 56, 106–116. doi: 10.1038/s41393-017-0013-7
- Chang, C.-C., and Lin, C.-J. (2011). LIBSVM: A library for support vector machines. *ACM Trans. Intell. Syst. Technol.* 2, 1–27. doi: 10.1145/1961189.1961199
- Chen, B., Zi, B., Wang, Z., Qin, L., and Liao, W.-H. (2019). Knee exoskeletons for gait rehabilitation and human performance augmentation: a state-of-the-art. *Mech. Mach. Theory* 134, 499–511. doi: 10.1016/j.mechmachtheory.2019.01.016
- Chen, G., Chan, C. K., Guo, Z., and Yu, H. (2013). A review of lower extremity assistive robotic exoskeletons in rehabilitation therapy. *Crit. Rev. Biomed. Eng.* 41, 343–363. doi: 10.1615/CritRevBiomedEng.2014010453
- Chen, S., Li, J., Shuai, M., Wang, Z., Jia, Z., Huang, X., et al. (2018). First multicenter clinical trial of china's domestically designed powered exoskeleton-assisted walking in patients with paraplegia. *Ann. Phys. Rehabil. Med.* 61:e495. doi: 10.1016/j.rehab.2018.05.1152
- Chu, J.-U., Moon, I., Lee, Y.-J., Kim, S.-K., and Mun, M.-S. (2007). A supervised feature-projection-based real-time EMG pattern recognition for multifunction myoelectric hand control. *IEEE/ASME Trans. Mechatron.* 12, 282–290. doi: 10.1109/TMECH.2007.897262
- Eguchi, Y., Kadone, H., and Suzuki, K. (2018). Standing mobility device with passive lower limb exoskeleton for upright locomotion. *IEEE/ASME Trans. Mechatron.* 23, 1608–1618. doi: 10.1109/TMECH.2018.2799865
- Gillis, N., Mehrmann, V., and Sharma, P. (2018). Computing the nearest stable matrix pairs. *Numer. Linear Algeb. Appl.* 25:e2153. doi: 10.1002/nla.2153
- Guan, S. Y., Sugi, M., Yokoi, H., Arai, T., Kato, R., and Ota, J. (2017). Quantification of muscle fatigue using surface electromyography for isometric handgrip task. *J. Telecommun. Electron. Comput. Eng.* 9, 205–209.
- Guo, Z., Wang, C., Yan, Z., Zhang, L., Ma, X., and Wu, X. (2019). "Stable control gait planning strategy for a rehabilitation exoskeleton robot," in *2019 IEEE International Conference on Mechatronics and Automation (ICMA)* (Tianjin), 1265–1270. doi: 10.1109/ICMA.2019.8816513
- Huang, R., Cheng, H., Chen, Y., Chen, Q., Lin, X., and Qiu, J. (2016a). Optimisation of reference gait trajectory of a lower limb exoskeleton. *Int. J. Soc. Robot.* 8, 223–235. doi: 10.1007/s12369-015-0334-7
- Huang, R., Cheng, H., Guo, H., Chen, Q., and Lin, X. (2016b). "Hierarchical interactive learning for a human-powered augmentation lower exoskeleton," in *2016 IEEE International Conference on Robotics and Automation (ICRA)* (Stockholm), 257–263. doi: 10.1109/ICRA.2016.7487142
- Huang, R., Cheng, H., Guo, H., Lin, X., Chen, Q., and Sun, F. (2016c). "Learning cooperative primitives with physical human-robot interaction for a human-powered lower exoskeleton," in *2016 IEEE/RSJ International Conference on Intelligent Robots and Systems (IROS)* (Daejeon), 5355–5360. doi: 10.1109/IROS.2016.7759787
- Huang, R., Cheng, H., Qiu, J., and Zhang, J. (2019). Learning physical human-robot interaction with coupled cooperative primitives for a lower exoskeleton. *IEEE Trans. Autom. Sci. Eng.* 16, 1566–1574. doi: 10.1109/TASE.2018.2886376
- Huang, R., Peng, Z., Cheng, H., Hu, J., Qiu, J., Zou, C., et al. (2018). "Learning-based walking assistance control strategy for a lower limb exoskeleton with hemiplegia patients," in *2018 IEEE/RSJ International Conference on Intelligent Robots and Systems (IROS)*, 2280–2285. Madrid: IEEE. doi: 10.1109/IROS.2018.8594464

- Hwang, B., and Jeon, D. (2018). Estimation of the user's muscular torque for an over-ground gait rehabilitation robot using torque and insole pressure sensors. *Int. J. Control Autom. Syst.* 16, 275–283. doi: 10.1007/s12555-016-0545-1
- Kim, J., Kang, I., El-Khamy, M., and Lee, J. (2019). *System and Method for Higher Order Long Short-Term Memory (LSTM) Network*. US Patent 10,241,684. Washington, DC: Official Gazette of the United States Patent and Trademark Office.
- Li, L., Hoon, K. H., Tow, A., Lim, P., and Low, K. (2015). "Design and control of robotic exoskeleton with balance stabilizer mechanism," in *2015 IEEE/RSJ International Conference on Intelligent Robots and Systems (IROS)* (Hamburg), 3817–3823. doi: 10.1109/IROS.2015.7353913
- Li, Z., Liu, H., and Ficuciello, F. (2019). Guest editorial special issue on bioinspired embodiment for intelligent sensing and dexterity in fine manipulation. *IEEE Trans. Indus. Inform.* 15, 1141–1143. doi: 10.1109/TII.2018.2885814
- Lin, T.-C., Krishnan, A. U., and Li, Z. (2019). "Physical fatigue analysis of assistive robot teleoperation via whole-body motion mapping," in *2019 IEEE/RSJ International Conference on Intelligent Robots and Systems (IROS)* (Macau), 2240–2245. doi: 10.1109/IROS40897.2019.8968544
- Liu, D.-X., Wu, X., Du, W., Wang, C., Chen, C., and Xu, T. (2017). Deep Spatial-Temporal Model for rehabilitation gait: optimal trajectory generation for knee joint of lower-limb exoskeleton. *Assembly Automat.* 37, 369–378. doi: 10.1108/AA-11-2016-155
- Mertz, L. (2012). The next generation of exoskeletons: lighter, cheaper devices are in the works. *IEEE Pulse* 3, 56–61. doi: 10.1109/MPUL.2012.2196836
- Miikkulainen, R., Liang, J., Meyerson, E., Rawal, A., Fink, D., Francon, O., et al. (2019). "Evolving deep neural networks," in *Artificial Intelligence in the Age of Neural Networks and Brain Computing*, eds R. Kozma, C. Alippi, Y. Choe, and F. Carlo Morabito (Cambridge, MA: Elsevier), 293–312. doi: 10.1016/B978-0-12-815480-9.00015-3
- Moraes, C., Junior, E. A., Lucena, R., Cavalcanti, É., and Rodrigues, M. (2019). "Human gait cycle analysis using an adapted mechanical prosthesis," in *XXVI Brazilian Congress on Biomedical Engineering*, eds A. V. Alvarenga, R. Costa-Felix, and J. C. Machado (Armacao de Buzios: Springer), 241–248. doi: 10.1007/978-981-13-2119-1\_38
- Nakashima, K., and Kushida, D. (2019). "Estimation of muscle fatigue time based on electromyography during isotonic contraction," in *2019 IEEE 1st Global Conference on Life Sciences and Technologies (LifeTech)* (Osaka), 65–69. doi: 10.1109/LifeTech.2019.8883992
- Parietti, F., Chan, K. C., Hunter, B., and Asada, H. H. (2015). "Design and control of supernumerary robotic limbs for balance augmentation," in *2015 IEEE International Conference on Robotics and Automation (ICRA)* (Seattle, WA), 5010–5017. doi: 10.1109/ICRA.2015.7139896
- Peng, Z., Luo, R., Huang, R., Hu, J., Shi, K., and Cheng, H. (2020). Data-driven optimal assistance control of a lower limb exoskeleton for hemiplegic patients. *Front. Neurobot.* 14:37. doi: 10.3389/fnbot.2020.00037
- Shimizu, Y., Kadone, H., Kubota, S., Suzuki, K., Saotome, K., Ueno, T., et al. (2019). Voluntary ambulation using voluntary upper limb muscle activity and hybrid assistive limb®(hal®) in a patient with complete paraplegia due to chronic spinal cord injury: a case report. *J. Spinal Cord Med.* 42, 460–468. doi: 10.1080/10790268.2017.1423267
- Talaty, M., Esquenazi, A., and Briceno, J. E. (2013). "Differentiating ability in users of the rewalk tm powered exoskeleton: an analysis of walking kinematics," in *2013 IEEE 13th International Conference on Rehabilitation Robotics (ICORR)* (Seattle, WA), 1–5. doi: 10.1109/ICORR.2013.6650469
- Wang, C., Wu, X., Ma, Y., Wu, G., and Luo, Y. (2018a). A flexible lower extremity exoskeleton robot with deep locomotion mode identification. *Complexity* 2018:5712108. doi: 10.1155/2018/5712108
- Wang, C., Wu, X., Wang, Z., and Ma, Y. (2018b). Implementation of a brain-computer interface on a lower-limb exoskeleton. *IEEE Access* 6, 38524–38534. doi: 10.1109/ACCESS.2018.2853628
- Wu, C.-H., Mao, H.-F., Hu, J.-S., Wang, T.-Y., Tsai, Y.-J., and Hsu, W.-L. (2018). The effects of gait training using powered lower limb exoskeleton robot on individuals with complete spinal cord injury. *J. Neuroeng. Rehabil.* 15, 1–10. doi: 10.1186/s12984-018-0355-1
- Yan, Z., Li, N., Long, X., Ren, H., and Wu, X. (2018). "Bionic mechanical design and stair ascending/descending gait planning of a lower-limb exoskeleton robot," in *2018 IEEE International Conference on Cyborg and Bionic Systems (CBS)* (Shenzhen), 155–160. doi: 10.1109/CBS.2018.8612274
- Yilmaz, E., Fisahn, C., Mayadev, A., Kobota, K., Cambier, Z., et al. (2018). Functional neurorehabilitation using the hybrid assistive limb (HAL): a first experience in the united states. *Int. J. Neurorehabil.* 5, 2376–0281. doi: 10.4172/2376-0281.1000306
- Yuan, Y., Su, W., Li, Z., and Shi, G. (2018). Brain-computer interface-based stochastic navigation and control of a semiautonomous mobile robot in indoor environments. *IEEE Trans. Cogn. Dev. Syst.* 11, 129–141. doi: 10.1109/TCDS.2018.2885774
- Zeiler, M. D. (2012). Adadelta: an adaptive learning rate method. *arXiv [Preprint]. arXiv:1212.5701*.

**Conflict of Interest:** The authors declare that the research was conducted in the absence of any commercial or financial relationships that could be construed as a potential conflict of interest.

Copyright © 2021 Wang, Guo, Duan, He, Yuan and Wu. This is an open-access article distributed under the terms of the Creative Commons Attribution License (CC BY). The use, distribution or reproduction in other forums is permitted, provided the original author(s) and the copyright owner(s) are credited and that the original publication in this journal is cited, in accordance with accepted academic practice. No use, distribution or reproduction is permitted which does not comply with these terms.



# Dual-Threshold-Based Microstate Analysis on Characterizing Temporal Dynamics of Affective Process and Emotion Recognition From EEG Signals

Jing Chen<sup>1</sup>, Haifeng Li<sup>1\*</sup>, Lin Ma<sup>1</sup>, Hongjian Bo<sup>2</sup>, Frank Soong<sup>3</sup> and Yaohui Shi<sup>4</sup>

<sup>1</sup> School of Computer Science and Technology, Faculty of Computing, Harbin Institute of Technology, Harbin, China,

<sup>2</sup> Shenzhen Academy of Aerospace Technology, Shenzhen, China, <sup>3</sup> Speech Group, Microsoft Research Asia, Beijing, China,

<sup>4</sup> Heilongjiang Provincial Hospital, Harbin, China

## OPEN ACCESS

### Edited by:

Zhan Li,

University of Electronic Science  
and Technology of China, China

### Reviewed by:

Hansheng Xue,

Australian National University,  
Australia

Yanshuo Chu,

University of Texas MD Anderson  
Cancer Center, United States

Sunaina Soni,

All India Institute of Medical Sciences,  
India

### \*Correspondence:

Haifeng Li

lihaifeng@hit.edu.cn

### Specialty section:

This article was submitted to  
Neural Technology,  
a section of the journal  
Frontiers in Neuroscience

**Received:** 01 April 2021

**Accepted:** 14 June 2021

**Published:** 14 July 2021

### Citation:

Chen J, Li H, Ma L, Bo H,  
Soong F and Shi Y (2021)

Dual-Threshold-Based Microstate  
Analysis on Characterizing Temporal  
Dynamics of Affective Process  
and Emotion Recognition From EEG  
Signals. *Front. Neurosci.* 15:689791.  
doi: 10.3389/fnins.2021.689791

Recently, emotion classification from electroencephalogram (EEG) data has attracted much attention. As EEG is an unsteady and rapidly changing voltage signal, the features extracted from EEG usually change dramatically, whereas emotion states change gradually. Most existing feature extraction approaches do not consider these differences between EEG and emotion. Microstate analysis could capture important spatio-temporal properties of EEG signals. At the same time, it could reduce the fast-changing EEG signals to a sequence of prototypical topographical maps. While microstate analysis has been widely used to study brain function, few studies have used this method to analyze how brain responds to emotional auditory stimuli. In this study, the authors proposed a novel feature extraction method based on EEG microstates for emotion recognition. Determining the optimal number of microstates automatically is a challenge for applying microstate analysis to emotion. This research proposed dual-threshold-based atomize and agglomerate hierarchical clustering (DTAAHC) to determine the optimal number of microstate classes automatically. By using the proposed method to model the temporal dynamics of auditory emotion process, we extracted microstate characteristics as novel temporospatial features to improve the performance of emotion recognition from EEG signals. We evaluated the proposed method on two datasets. For public music-evoked EEG Dataset for Emotion Analysis using Physiological signals, the microstate analysis identified 10 microstates which together explained around 86% of the data in global field power peaks. The accuracy of emotion recognition achieved 75.8% in valence and 77.1% in arousal using microstate sequence characteristics as features. Compared to previous studies, the proposed method outperformed the current feature sets. For the speech-evoked EEG dataset, the microstate analysis identified nine microstates which together explained around 85% of the data. The accuracy of emotion recognition achieved 74.2% in valence and 72.3% in arousal using microstate sequence characteristics as features. The experimental results indicated that microstate characteristics can effectively improve the performance of emotion recognition from EEG signals.

**Keywords:** EEG, dual-threshold-based AAHC, microstate characteristics, auditory emotion process, emotion recognition

## INTRODUCTION

To make a human-machine interaction more natural, emotion recognition should play an important role. Interest in emotion recognition from different modalities (e.g., face, speech, body posture, and physiological responses) has risen in the past decades. Physiological signals could measure the changes in physiological responses to emotional stimulus. They have advantages on eliminating social masking or factitious emotion expressions to obtain a better understanding of underlying emotions (Jang et al., 2015). Among the various types of physiological signals, an electroencephalogram (EEG) shows a direct measure of the electrical activity of the brain. It has been used in cognitive neuroscience to investigate the regulation and processing of emotion (Dennis and Solomon, 2010; Thiruchselvam et al., 2011). With the rapid development of dry EEG electrode techniques, EEG-based emotion recognition has received increasing applications in different fields such as affective brain-computer interaction (Atkinson and Campos, 2016; Chen et al., 2021), healthcare (Hossain and Muhammad, 2019), emotional companionship, and e-learning (Ali et al., 2016).

Early work on emotion recognition from EEG goes back as far as 1997 (Musha et al., 1997). In the past several years, various signal processing methods have been proposed to improve the EEG-based emotion recognition. Previous studies (Jenke et al., 2014; Alarcao and Fonseca, 2017) provided a comprehensive overview of the existing works in emotion recognition based on EEG signals. Feature extraction is a critically significant step in EEG-based emotion recognition framework. Basically, features from EEG can be distinguished in time domain, frequency domain, and time-frequency domain. The time domain features aim to identify and detect the temporal information in the brain activity. Frantzidis et al. (2010) used amplitude and latency of event-related potentials (ERPs) as features for EEG-based emotion classification. However, it is difficult to detect ERPs related to emotions since the onset is usually unknown. Other features, such as Hjorth features (Mehmood and Lee, 2015), fractal dimension (Sourina and Liu, 2011; Liu and Sourina, 2013), and higher-order crossings (Petrantonakis and Hadjileontiadis, 2009) have been used to characterize EEG time series. The frequency-domain feature aims to capture the relative amplitude and phase information of specific oscillation frequency. The most popular frequency-domain features are band power (Rozgić et al., 2013) and high-order spectra (Hosseini et al., 2010). These features could be extracted from different frequency bands, e.g., delta (1–3 Hz), theta (4–7 Hz), alpha (8–13 Hz), beta (14–30 Hz), and gamma (31–49 Hz). With this kind of method, it is not possible to determine when a particular frequency occurs. The time-frequency domain features bring up the temporal information by considering the dynamical changes of spectrum. The most commonly used time-frequency analyses for feature extraction were short-time Fourier transform (Lin et al., 2010), wavelet transform (Mohammadi et al., 2017), and Hilbert–Huang transform (Zong and Chetouani, 2009).

However, some limitations still exist on traditional feature sets. As EEG is an unsteady and rapidly changing voltage signal,

the feature extracted from EEG usually changes dramatically, whereas emotion states change gradually (Wang et al., 2014). This leads to bigger differences among EEG features, even with the same emotion state in adjacent time. Most existing feature extraction approaches do not consider these differences between EEG and emotion. In this study, the authors proposed a feature extraction method based on EEG microstates for emotion recognition. Microstate analysis treats multichannel EEG as a series of momentary quasi-stable scalp electric potential topographies (Pascual-Marqui et al., 1995). These quasi-stable potential topographies are referred to as microstates, so brain electrical activity could be modeled as being composed of a time sequence of non-overlapping microstates. Microstate sequences could capture the important spatio-temporal properties of an EEG signal. At the same time, it can reduce the fast-changing EEG signals to a sequence of prototypical topographical maps. Characterizing the dynamics of brain neuronal activity through EEG microstate patterns could provide novel information for improving EEG-based emotion recognition.

Microstate analysis has been used to study the resting state of the human brain based on the topography of the EEG signals (Van de Ville et al., 2010; Khanna et al., 2015; Michel and Koenig, 2018). The greater part of the literature acknowledges four standard microstate maps on healthy subjects at rest. In addition, the characteristics of microstate sequences have been proven to offer a potential biomarker for some diseases, such as mood and anxiety disorders (Al Zoubi et al., 2019), autism spectrum disorder (D'Croz-Baron et al., 2019), and schizophrenia (Soni et al., 2018, 2019; da Cruz et al., 2020; Kim et al., 2021). Baradits et al. (2020) created a specified feature set to represent microstate characteristics. These features were used to classify patients with schizophrenia and healthy controls.

While microstate analysis has been widely used to study brain function, few studies have used this method to analyze how the brain responds to emotional auditory stimuli. There are some challenges when applying microstate analysis to emotion process. Considering the complex emotion process, how to determine the optimal number of microstates automatically is a subject worthy of study. The modified K-means and K-medoids had been used to determine the microstate classes in many studies (Von Wegner et al., 2018). However, these methods need pre-set K cluster centers, and the clusters are sensitive to the initialization. Emotional response is a complex cognitive process so that it is difficult to predict the number of microstate classes subjectively. Atomize and agglomerate hierarchical clustering (AAHC) algorithm is specifically proposed for the microstate analysis of EEG (Murray et al., 2008). It is a hierarchical clustering that can offer more optional clustering results. The method initializes with a large number of clusters and then reduces the number of clusters by one during each iteration step. It stops when only one single final cluster is obtained, but the best partition from numerous clustering results is subjectively determined.

To overcome this limitation, this study proposes a dual threshold-based atomize and agglomerate hierarchical clustering (DTAAHC) which can determine the optimal number of microstate classes automatically. For microstate analysis,



microstates are expected to be distinct and could explain the original EEG topographies as much as possible. Therefore, two optimization criteria are used to estimate the quality of the candidate microstates during iterations. Compared with AAHC, in addition to global explained variance (GEV) contribution, the proposed algorithm also considers the microstate topographic similarity. Global map dissimilarity (GMD) is used to measure the topographic differences of candidate microstates. In addition, the iteration stops when the criterion GEV reaches the threshold. Although we made a minor alteration to the AAHC algorithm, the new method could identify the optimal microstate classes automatically and reduce the computational cost. By using the proposed method to model the temporal dynamics of the auditory emotion process, we extract microstate characteristics as novel temporospatial features for improving the performance of emotion recognition from EEG signals. The schema of the present study is shown in **Figure 1**.

## MATERIALS AND METHODS

This section provides details of the experimental tasks and datasets used in this study. In addition, we describe the proposed DTAHC and the temporal parameters of microstate sequences for emotion recognition.

### Datasets

Speech, music, and ambient sound events carry emotional information in human communication. In the present study, we focused on the emotional response induced by speech and music. Two independent datasets were available for analysis.

#### Dataset 1: Speech-Evoked Emotion Cognitive Experiment

##### Participants

Nineteen healthy participants (8 females and 11 males) with normal hearing participated in the experiment. The mean age of the 19 subjects was 22.4 (SD = 5.4; range, 18–27) years. All subjects were self-reported right-handers. All subjects had no personal history of neurological or psychiatric illness. The subjects were undergraduate and graduate students at Harbin Institute of Technology. The participants must exhibit enough proficiency in English. The ethics committee of Heilongjiang Provincial Hospital accepted the study. The concept was explained to the subjects, and written informed consent was obtained.

##### Stimuli selection

There are two unique models for signifying emotions: the categorical model and the dimensional model. In the former, emotions are recognized with the help of words denoting emotions or class tags. In the dimensional model, the representation is based on a set of quantitative measures using multidimensional scaling. One of the classical and widely used categorical models is six basic emotion classes, namely, anger, disgust, fear, joy, sadness, and surprise (Ekman et al., 1987). Various dimensional models have also been proposed (Schlosberg, 1954; Russell and Mehrabian, 1977; Russell, 1980). In this work, we use the valence–arousal scale of Russell (1980),

which is widely used in research on affect, to quantitatively describe emotions. In this scale, each emotional state can be placed on a two-dimensional plane with arousal and valence as the horizontal and vertical axes, respectively. In the present research, we first selected stimuli by categorical model. After selection, we rated the valence–arousal scales for each stimulus online using Self-Assessment Manikin (SAM).

Considering the six basic emotions, we collected 20 pairs of audio clips for each emotion category. Each pair of clips was the same slice of a film in two languages (original English version vs. Chinese-dubbed version).

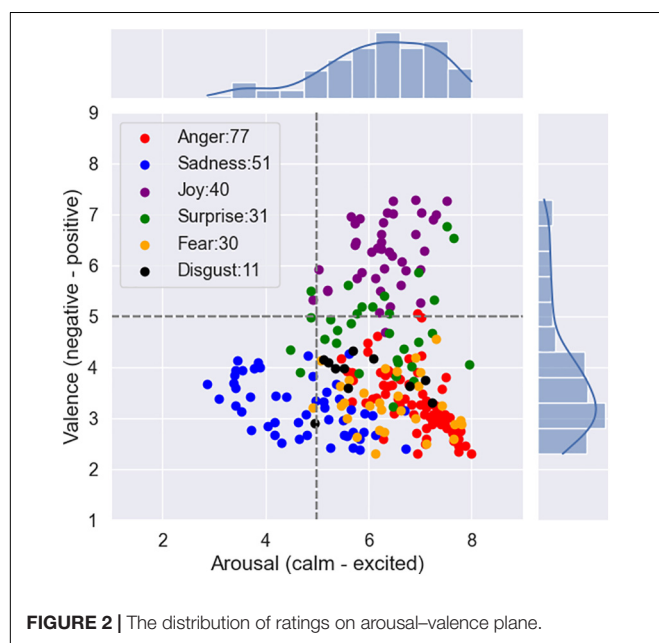
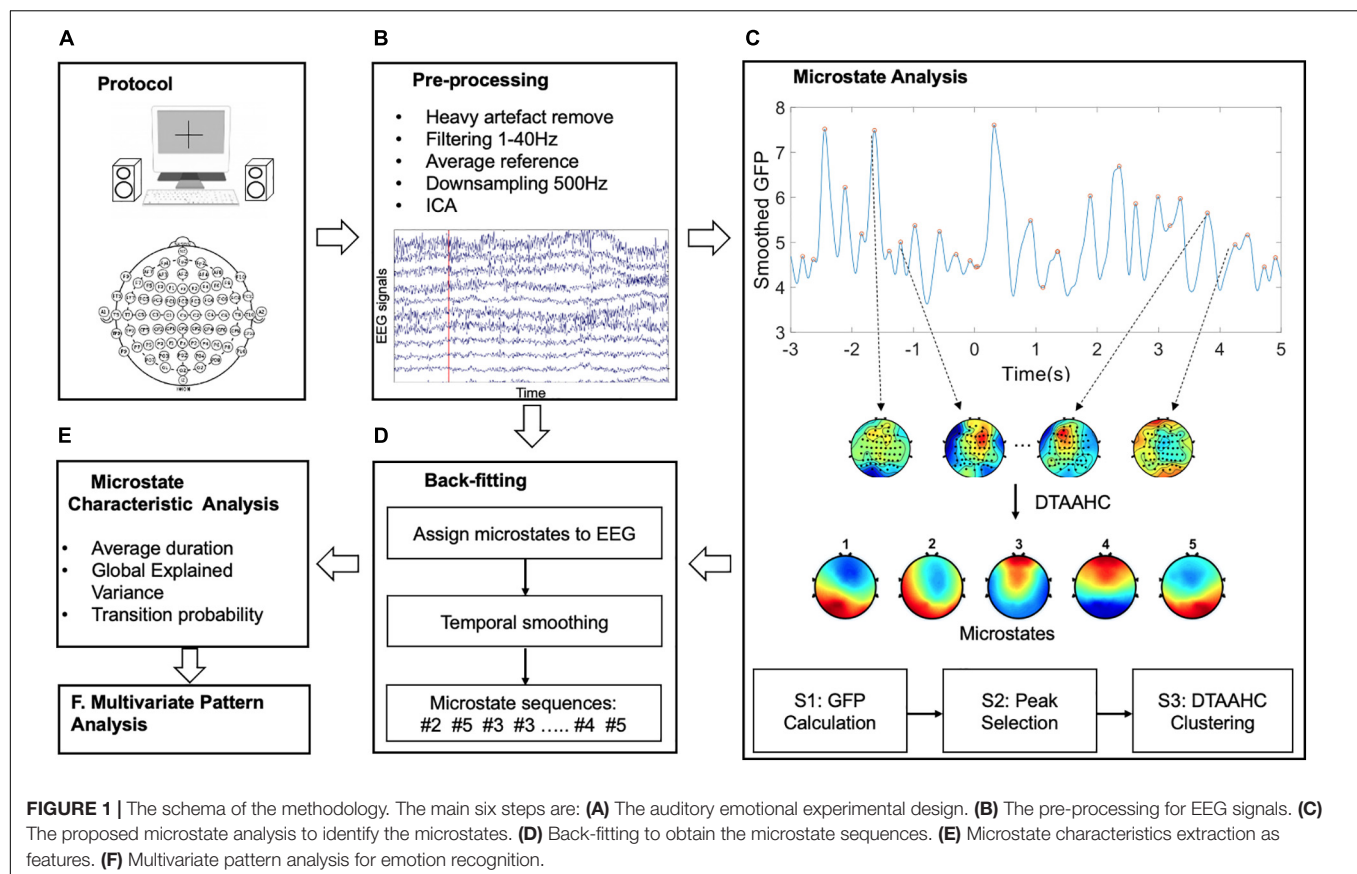
The stimuli used in the experiment were selected in three steps. First, we selected the raw films by watching a range of films for 1 month. The principles considered in the raw film selection are listed below: (A) The films display relatively strong emotions; (B) The films should have an original English version and a Chinese-dubbed version; and (C) The Chinese-dubbed version matches the original version to the greatest extent. We finally selected 40 films as raw sources. Second, we need to select emotional clips from the films. This step is carried out manually. The selection requirements are as follows: (A) Each segment should contain the speech of only one speaker; (B) Each segment expresses a single desired target emotion; (C) Each segment lasts for 5 s and contains at least a complete utterance; and (D) The background sound should not be too obvious. We finally selected 158 pairs of clips. We extracted soundtracks from these film clips. Third, all the audio clips were manually rechecked to guarantee the quality of emotional expression by 10 subjects. Some clips with ambiguous emotions were removed. We finally selected 20 pairs of clips for each emotion category which maximize the strength of elicited emotions. The list of the film clips is shown in **Supplementary Table 1**.

To obtain reliable emotional labels of these clips, we utilized Amazon's Mechanical Turk service to collect data from native English-speaking and native Chinese (Mandarin)-speaking subjects. We initially started with a target goal of 40 repetitions per clip. The subjects were allowed to classify as many of the 240 possible audio clips as they wish. There was no expectation for a single subject to complete all 240 audio exemplars. In the event that a subject completes only a portion of the 240 audio clips, we will continue to solicit additional subjects until we have achieved the required number of responses.

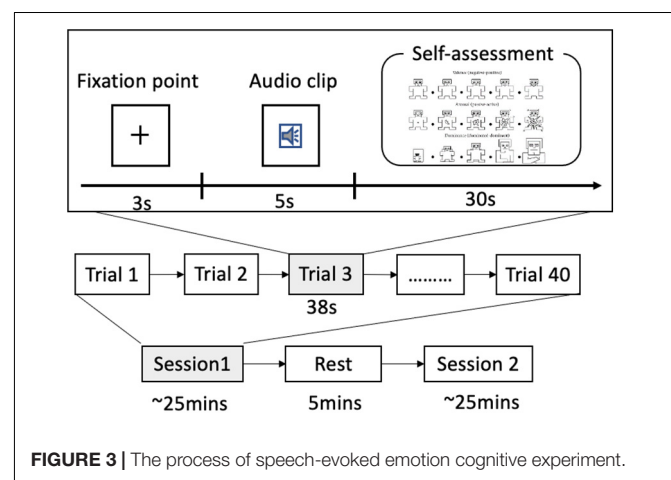
We presented subjects with selected audio clips and asked them to rate the emotional content of what they just heard and how they arrived at that decision. Discrete affective label and dimensional emotional annotation (arousal–valence) with 1–9 scales related to a single audio clip were obtained. **Figure 2** shows the mean locations of the stimuli on the arousal–valence plane.

##### Experimental protocol

Before the experiment, the subjects were given a set of instructions to help them understand the experiment protocol. When the instructions were clear, the participants were led into the experiment room with sensors placed on their heads. After that, an experimenter explained the meaning of the different scales of SAM. The SAM is a non-verbal pictorial assessment technique that directly measures the valence, arousal, and dominance associated with the affective reaction of a person



to a wide variety of stimuli. The arousal dimension ranges from a relaxed, sleepy figure to an excited, wide-eyed figure. The valence dimension ranges from a frowning, unhappy figure to a smiling, happy figure. The dominance–submissiveness scale represents



the controlling and dominant vs. controlled or submissive one feels: a prominent figure indicates maximum control in the situation. The participants could perform three practice trials to familiarize themselves with the experiment.

The subjects were instructed to keep their eyes open for the entire duration of the experiment. The process of our experiment is depicted in **Figure 3**. In this experiment, each subject performed two sessions of around 25 min each. They can

have a 5-min break after one session is finished. Each session consisted of 40 trials.

Audio clips inducing different emotional states were presented in random order. Each trial consists of the following steps:

- (a) a 3-s baseline recorded, during which the subjects were instructed to watch a fixation cross presented on a computer monitor,
- (b) a 5-s audio clip played, during which the subjects were instructed to listen attentively and watch a central visual fixation, and
- (c) a 30-s self-assessment for arousal, valence, and dominance, during which the subjects used a computer keyboard to rate the SAM on a scale of 1–9.

The experiment was programmed using Psychophysics Toolbox of Matlab. **Table 1** summarizes the number of trials for high/low valence and arousal and the average rating for the four conditions.

### EEG acquisition

The EEG signals were continuously recorded using a 64-channel EEG system (64-channel Quik-Cap and Neuroscan Synamp2 Amplifier). The cap had 64 electrodes and two integrated bipolar which led for vertical and horizontal electrooculography (EOG). During recording, two EOGs and two mastoid electrodes (M1 and M2) were not placed. Each electrode impedance should be less than 10 k $\Omega$ . The sampling rate was 1,000 Hz. The electrodes were placed over the scalp according to the international 10–20 system.

### EEG pre-processing

The EEG signal pre-processing was performed to reduce unwanted noise and artifacts that compromise the quality of the signal. First, four signals from two EOGs and two mastoid electrodes were removed. Sixty-two remaining signals were used for the processing and analysis of the next step. Then, the EEG signals were average-referenced, down-sampled to 500 Hz, and filtered with 1–35 Hz to obtain the desired frequency range and remove the electrical line noise. After that, the eye blinks and muscular artifacts were excluded using independent component analysis (ICA). For each group, each participant, and each trial, EEG signal from 3-s baseline before the audio clip was removed to correct stimulus-unrelated variations. The pre-processing was performed using EEGLAB of Matlab.

## Dataset 2: Music-Evoked Emotion Cognitive Experiment

Music is a powerful method for emotional communication and can evoke genuine basic emotions in the listener (Daly

et al., 2015). Physiological measurements can be used to identify personal emotional responses to music. A popular public database, Dataset for Emotion Analysis using Physiological signals (DEAP), has been widely used to analyze affective states (Koelstra et al., 2011). DEAP is a multimodal dataset, including EEG, MEG, galvanic skin resistance, electrooculography, blood volume pressure, skin temperature, and respiration pattern. A total of 32 subjects participated in the data collection, and 40 carefully pre-selected 1-min-long music videos were used as the stimulus to elicit emotions for each subject. Before each video is displayed, a 5-s baseline is recorded. Each participant was requested to finish a self-assessment for arousal, valence, and dominance on a scale of 1–9 after watching.

In this research, we used 32-channel EEG original signals for emotion recognition based on microstate analysis. The raw EEG data can be downloaded from <http://www.eecs.qmul.ac.uk/mmv/datasets/deap/>. During pre-processing, the EEG data was average-referenced, down-sampled to 128 Hz, and filtered with a 1–35-Hz cutoff, and eye artifacts were removed with ICA. The 5-s baseline before the stimuli was used to correct the data for stimulus-unrelated variations. There is a total of 1,280 trials for analysis.

## The Proposed Dual-Threshold-Based Microstate Analysis

The principles of microstate analysis are the quasi-stable periods of topographies, which is demonstrated in previous studies. More particularly, the changes of electric field configurations can be described by a limited number of microstate classes, which remain stable for around 80–120 ms before abruptly transitioning to another configuration. EEG microstates might represent and characterize the dynamic neuronal activity of conscious contents.

### Global Field Power

Global field power (GFP) is calculated to find a series of dominant template topographies. GFP constitutes a single, reference-independent measure of response strength at a global level (Lehmann and Skrandies, 1980). GFP is simply the standard deviation of all electrodes at a given time. What GFP tells the researcher is, on average across the electrode montage, how strong is the potential being recorded. It is often used to measure the global brain response to an event or to characterize the rapid changes in brain activity.

For each subject, GFP was calculated for each sample time according to Eq. 1, where  $N$  denotes the number of electrodes,  $u_i(t)$  is the measured voltage of a specific electrode at time  $t$ , and  $\bar{u}(t)$  is the average voltage of the  $N$  electrodes at the respective sample time  $t$ .

$$GFP(t) = \sqrt{\frac{\sum_{i=1}^N (u_i(t) - \bar{u}(t))^2}{N}} \quad (1)$$

The local maxima of the GFP curve represent high global neuronal synchronization (Skrandies, 2007) and are considered with the highest signal-to-noise ratio. The topographies around these peaks remain stable and are submitted to the clustering

**TABLE 1** | Database summary.

Condition	Valence		Arousal	
	High	Low	High	Low
Number of trials	790	583	815	558
Rating	5.9 $\pm$ 0.8	3.3 $\pm$ 0.5	6.4 $\pm$ 0.7	3.7 $\pm$ 0.3

algorithm. For each participant, the GFP of each trial is calculated. After smoothing the GFP with a Gaussian-weighted moving average of 50 time points, topographies at GFP peaks were collected and fed into a DTAHC clustering algorithm to identify the microstates.

### The Proposed Dual-Threshold-Based AAHC

AAHC is a bottom-up hierarchical clustering wherein the number of clusters is initially large and progressively diminishes. Classical agglomerative hierarchical clustering would eventually disintegrate the short-duration period of stable topography. These short-duration periods would be designated to other clusters even if they contribute a high GEV (Murray et al., 2008). In AAHC, clusters are given priority according to their GEV contributions. In this way, short-duration periods are conditionally maintained. Specifically, during each iteration, AAHC frees the cluster with the lowest GEV and then re-assigns these “free” maps to the surviving clusters by calculating spatial correlation. The iterations stop when only one single final cluster is obtained. An important next step is the choice of the number of desired output clusters. Unfortunately, there is no definitive solution. The more clusters one identifies, the higher the quality of the clustering but the lower the data reduction. Five criteria to decide on the amount of microstate clusters have been described by Poulsen et al. (2018). GEV is used to measure the percentage of data that can be explained by microstate classes. The cross-validation criterion is related to the residual noise. Dispersion ( $W$ ) is a measure of the average distance between members of the same cluster. However, it is not a suitable measure of fitting for polarity-invariant methods such as modified K-means and AAHC. Krzanowski-Lai criterion and normalized Krzanowski-Lai criterion are based on dispersion ( $W$ ).

Here we propose DTAHC to determine the optimal number of microstate classes automatically during clustering. Compared with AAHC, in addition to GEV contribution, the proposed algorithm also considers the microstate topographic similarity. For microstate analysis, microstates are expected to be distinct and could explain the original EEG topographies as much as possible. Therefore, two optimization criteria are used to estimate the quality of the topographical maps of microstate classes during iterations. First, the cluster with the lowest GEV is freed and re-assigned to the surviving clusters. Second, the clusters are merged if the GMD between the candidate microstate classes is lower than 0.1. In addition, the iteration stops when the criterion GEV reaches the threshold. Although we made a minor alteration to the AAHC algorithm, the new method could identify the optimal microstate classes automatically and reduce the computational cost. The detailed introduction of this method is discussed below.

GMD is used to measure the topographic differences of microstate maps, independent of electric strength. It is defined as follows:

$$\text{GMD} = \sqrt{\frac{1}{N} \sum_{i=1}^N \left( \frac{u_i - \bar{u}}{\text{GFP}_u} - \frac{v_i - \bar{v}}{\text{GFP}_v} \right)^2} \quad (2)$$

where  $u_i$  and  $v_i$  are the voltages of two specified microstates, and  $\bar{u}$  and  $\bar{v}$  are the average voltages of the  $N$  electrodes. GMD ranges

from 0 to 2, where 0 indicates topographic homogeneity and 2 indicates topographic inversion.

GEV measures the percentage of data that can be explained by microstate classes. It is frequently used to quantify how well the microstate classes describe the whole data. The higher GEV, the better. It is influenced by the dimensionality of the data. The total GEV is the sum of the GEV values over all microstate classes:

$$\text{GEV} = \sum_l \text{GEV}_l \quad (3)$$

The  $\text{GEV}_l$  value for a specific microstate class with label  $l$  is:

$$\text{GEV}_l = \frac{\sum_t \text{GFP}_t^2 \cdot C_{V_t, M_l}^2 \cdot \delta_{l, L_t}}{\sum_t \text{GFP}_t^2} \quad (4)$$

$$\delta_{l, L_t} = \begin{cases} 1 & \text{if } l = L_t \\ 0 & \text{if } l \neq L_t \end{cases} \quad (5)$$

$$C_{V_t, M_l} = \frac{\sum_i V_{ti} M_{li}}{\sqrt{\sum_i V_{ti}^2} \cdot \sqrt{\sum_i M_{li}^2}} \quad (6)$$

The spatial correlation  $C_{V_t, M_l}$  between instantaneous EEG topography  $V_t$  and the candidate microstate class  $M_l$  can be calculated by Eq. 6, where  $V_{ti}$  is the voltage of  $i$ th electrode of instantaneous EEG at time  $t$  (local peak index), and  $M_{li}$  denotes the topography of the microstate class  $l$ .

In this study, DTAHC is performed on the EEG topographies at local peaks of GFP. During initialization, each topography map is considered as a unique cluster. Upon subsequent iterations, the spatial correlation  $C_{V_t, M_l}$  between each instantaneous EEG topography  $V_t$  and the candidate microstate class  $M_l$  will be calculated by Eq. 6, merging the clusters which have maximum spatial correlation. The groups of the centroid of maps are defined as the candidate microstate class for that cluster. Then, two optimization criteria are applied. The  $\text{GEV}_l$  for a specific microstate class with label  $l$  is calculated by Eq. 4. The cluster with the lowest GEV is removed and re-assigned to the most similar cluster during each iteration step. The GMDs between the candidate microstate classes are calculated. The clusters are merged if the GMD is lower than the threshold. The iterations stop when the GEV is higher than the threshold. In the present work, the threshold of GEV is set to 85% (Lehmann et al., 2005; Michel and Koenig, 2018; D’Croz-Baron et al., 2019). The threshold of GMD is set to 0.1 (Murray et al., 2008). Table 2 shows the DTAHC procedure.

### Microstate Sequence Characteristics

After microstate classes are identified, the original individual EEG data can be labeled as a microstate sequence, with fitting back of these microstate classes to topographies at sample point. Temporal parameters can be extracted as features for further analysis and can also be compared between different experimental conditions or between groups of subjects.

### Backfitting

Microstate classes are assigned to EEG at each time frame (or index of GFP peaks) considering the highest spatial correlation



**TABLE 2 |** Pseudocode for dual-threshold-based atomize and agglomerate hierarchical clustering (DTAAHC).**Algorithm:** DTAAHC

**Inputs:** set of  $n$  topographies  $D = \{S_1, S_2, S_3, \dots, S_n\}$ ;  
the spatial correlation  $C$ ;  
 $Th_{GEV}$ : threshold of global explained variance (GEV)  
 $Th_{GMD}$ : threshold of global map dissimilarity

**Procedure:**

- 1: **for**  $i = 1, 2, \dots, n$  **do**
- 2:    $Cluster_i \leftarrow \{S_i\}$
- 3: **end for**
- 4: **repeat**
- 5:   **for**  $i = 1, 2, \dots, n$  **do**
- 6:     **for**  $j = 1, 2, \dots, n$  **do**
- 7:        $C_{Cluster_i, Cluster_j} = C(Cluster_i, Cluster_j)$
- 8:     **end for**
- 9:   **end for**
- 10:   merge two clusters  $Cluster_{i^*}$  and  $Cluster_{j^*}$ , which have maximum spatial correlation  $\max(C_{Cluster_i, Cluster_j})$
- 11:   define the centroid (mathematical average) as the template map for that cluster
- 12:   calculate the  $GEV_i$  between each template map and samples
- 13:   the cluster with the min ( $GEV_i$ ) is atomized, and each sample in this cluster is independently re-assigned to the surviving cluster with the highest spatial correlation
- 14:   calculate the GMD for each pair of template map
- 15:   merge clusters if the GMD is lower than  $Th_{GMD}$
- 16: **until**  $\sum (GEV_i) > Th_{GEV}$

**Outputs:** Cluster  $\{Cluster_1, Cluster_2, Cluster_3, \dots, Cluster_k\}$

(see Eq. 5). The maximum spatial correlation determines the microstate label  $L_t$ . In the fitting process, temporal smoothing (Pascual-Marqui et al., 1995; Poulsen et al., 2018) is applied to avoid interruptions in spontaneous EEG sequences with a lot of unwanted noise—that is, class assignments are based on topographical similarity with microstate classes and the microstate labels of samples prior to and following the EEG sample. Different temporal parameters and statistical analyses will be performed after class assignments for every subject.

### Temporal Parameters

EEG microstate sequences (EEG-MS) are symbolic time series related to potential neurophysiological relevance. The temporal dynamic characteristics of EEG-MS can be described by the following parameters. These statistical parameters mainly represent the activation strength, the spatial configuration, and the temporal attributes of microstates:

- (1) Duration (ms): This refers to the average length of continuous sequences belonging to a given microstate class.
- (2) Occurrence: This indicates the average frequency in which a microstate class is present per second. It is computed by taking the number of segments belonging to a microstate class divided by the whole analysis duration (in seconds).
- (3) Time coverage (%): This represents the proportion of a specified microstate that is active during the whole analysis time.

GEV (%): This parameter is the percentage of explained variation of a given microstate class, described in Eq. 4.

### Transition Probabilities

Transition probabilities can be derived to quantify the probabilities of a certain class switched to other classes. The transition probability between two states is given as  $T_{ij} = P(X_{t+1} = S_j | X_t = S_i)$ . A Markov chain describes the probability distribution of the system either remaining in that state or transitioning to a different state for the next time point. In this study, separate transition probabilities are computed and compared for each of the four conditions (high vs. low valence and high vs. low arousal).

### Statistical Analysis

Statistical analyses were performed by using in-house scripts. Each microstate parameter was compared on the valence and arousal dimension separately. The trial is labeled as “high” group if its dimension value is higher than 4.5 and “low” group if its dimension value is lower than 4.5. To evaluate group differences in the microstate parameters mentioned above, we used Wilcoxon rank-sum statistic test for comparisons (Musaeus et al., 2019; Chu et al., 2020). The Wilcoxon rank-sum test is a nonparametric approach. It allows us to compare two populations where the underlying distributions are not normal but that do have similar shapes.

## RESULTS

### Microstate Class Spatial Topographies Microstate Classes

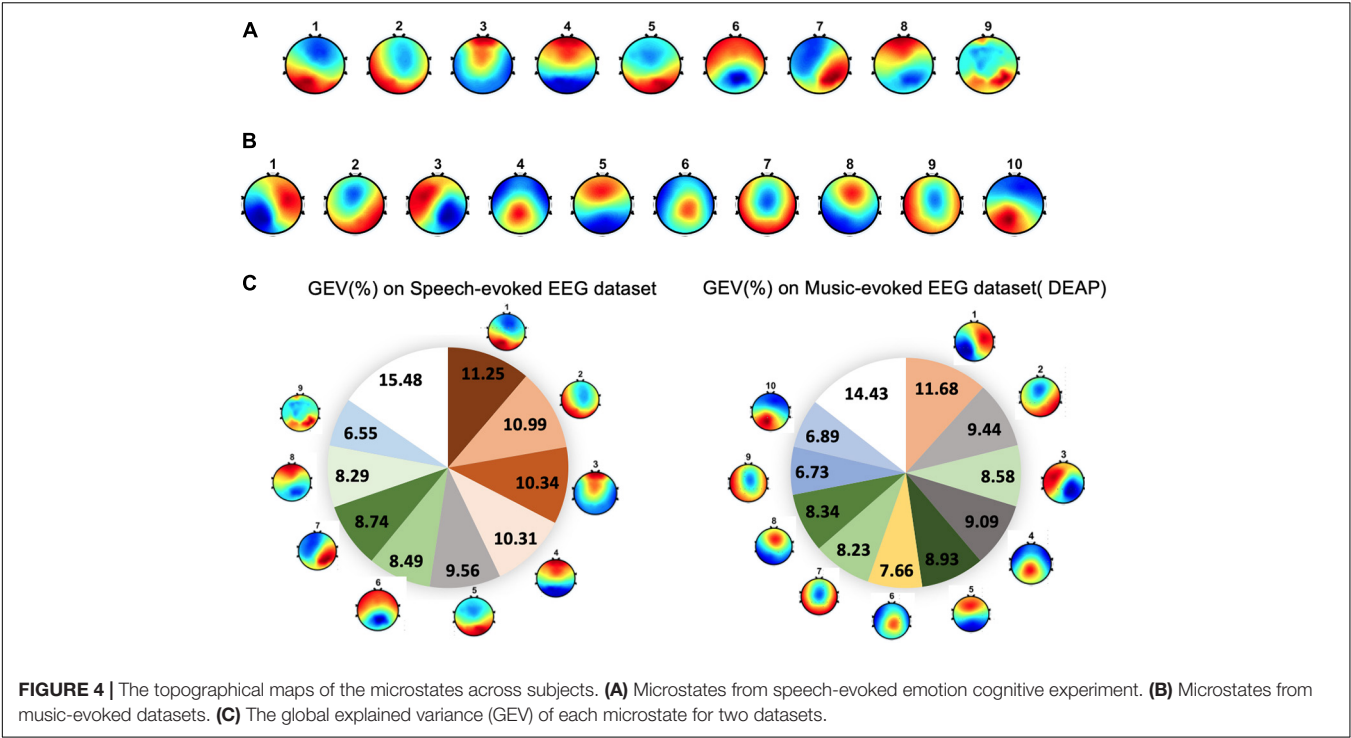
For dataset 1, the group-level clustering revealed nine optimal microstate classes for emotional speech-evoked EEG. These nine microstate topography templates are illustrated in **Figure 4A**. The topographies are labeled as #1–9. For dataset 2, the microstate analysis identified 10 microstates for emotional music video-evoked EEG (see **Figure 4B**).

### Global Explained Variance

The performance of the microstate segmentation algorithm is reported in terms of the GEV, which estimates the portion of EEG point topography that can be explained by microstates. For dataset 1, the nine EEG microstate classes together explained around 85% of the data in global field power peaks. The GEV of each microstate class ranged from 6.55 to 11.25% (see **Figure 4C**). For dataset 2, ten microstates explained 86% of the variance of all global field power peaks. Correspondingly, the GEV of each microstate class fluctuates between 6.73 and 11.68%.

### Global Map Dissimilarity

GMD is calculated as a measure of topographic differences of microstate maps. For dataset 1, the GMD matrix across different microstates is shown in **Table 3**. The GMD ranged from 0.10 to 0.25 (mean = 0.18,  $SD = 0.06$ ). **Table 4** presents the GMD between different microstates of dataset 2. The average GMD is 0.25 ( $SD = 0.08$ ). The range of the GMD is 0.10–0.34.



**TABLE 3 |** The global map dissimilarity (GMD) between different microstates of dataset 1.

GMD		Microstates from dataset 1								
		#1	#2	#3	#4	#5	#6	#7	#8	#9
Microstates from dataset 1	#1	0	0.11	0.23	0.25	0.12	0.23	0.15	0.23	0.10
	#2	0.11	0	0.23	0.23	0.14	0.21	0.17	0.21	0.11
	#3	0.23	0.23	0	0.11	0.24	0.11	0.23	0.12	0.23
	#4	0.25	0.23	0.11	0	0.25	0.11	0.22	0.10	0.24
	#5	0.12	0.14	0.24	0.25	0	0.23	0.10	0.24	0.10
	#6	0.23	0.21	0.11	0.11	0.22	0	0.23	0.10	0.23
	#7	0.15	0.17	0.23	0.22	0.10	0.23	0	0.24	0.10
	#8	0.23	0.21	0.12	0.10	0.24	0.10	0.24	0	0.23
	#9	0.10	0.11	0.23	0.24	0.10	0.23	0.10	0.23	0

**TABLE 4 |** The GMD between different microstates of dataset 2 (Dataset for Emotion Analysis using Physiological signals, DEAP).

GMD		Microstates from DEAP									
		#1	#2	#3	#4	#5	#6	#7	#8	#9	#10
Microstates from DEAP	#1	0	0.25	0.29	0.30	0.18	0.24	0.28	0.14	0.31	0.33
	#2	0.25	0	0.33	0.19	0.34	0.22	0.11	0.33	0.16	0.16
	#3	0.29	0.33	0	0.30	0.14	0.32	0.28	0.20	0.23	0.28
	#4	0.30	0.19	0.30	0	0.33	0.11	0.24	0.31	0.25	0.11
	#5	0.18	0.34	0.14	0.33	0	0.30	0.32	0.10	0.30	0.34
	#6	0.24	0.22	0.32	0.11	0.30	0	0.29	0.26	0.31	0.17
	#7	0.28	0.11	0.28	0.24	0.32	0.29	0	0.33	0.11	0.19
	#8	0.14	0.33	0.20	0.31	0.10	0.26	0.33	0	0.33	0.34
	#9	0.31	0.16	0.23	0.25	0.30	0.31	0.11	0.33	0	0.194
	#10	0.33	0.16	0.28	0.11	0.34	0.17	0.19	0.34	0.19	0

## Temporal Parameters

It is controversial whether the first-order Markov model can capture the complex temporal dependencies for a longer time series of minutes (von Wegner et al., 2017). The duration of one trial in DEAP is 60 s. The duration is 5 s in the emotional speech-evoked cognitive experiment. Therefore, the microstate sequence characteristics are evaluated on the speech-evoked EEG dataset. We compared the temporal parameters of microstates in valence and arousal dimensions separately. We divided the trials into two groups based on the valence or arousal level. The trial is labeled as “high” group if its valence (or arousal) value is higher than 4.5 and as “low” group if it is lower than 4.5.






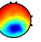

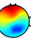
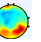
The comparison results are shown in **Table 5**. For the valence dimension, the mean duration, occurrence, time coverage, and GEV are investigated for the high valence and the low valence groups. The Wilcoxon rank-sum statistic test was used to identify statistically significant

differences between high/low conditions for each microstate class in every temporal parameter. The significance level is set to 5%. The significant group differences are marked with an asterisk. The result revealed that the duration of microstate #3 is significantly increased during the response to a high valence stimulus ( $p = 0.02$ ). No significant differences in occurrence, time coverage, and GEV between the groups are found.

For the arousal dimension, microstates #3 and #6 had a striking increase in duration for high arousal ( $p = 0.05$ ). On the other hand, the occurrence, temporal coverage, and GEV of microstate #7 slumped during the same period for high arousal.




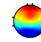
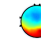
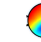





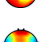







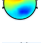
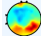






Further tests examined the model of transition probabilities for valence and arousal, respectively. **Table 6** depicted the statistically significant differences ( $p$ -value) of directions of transitions between high- vs. low-level groups. For valence, the statistical analysis unraveled the significant differences between high and low groups in five transitions: from

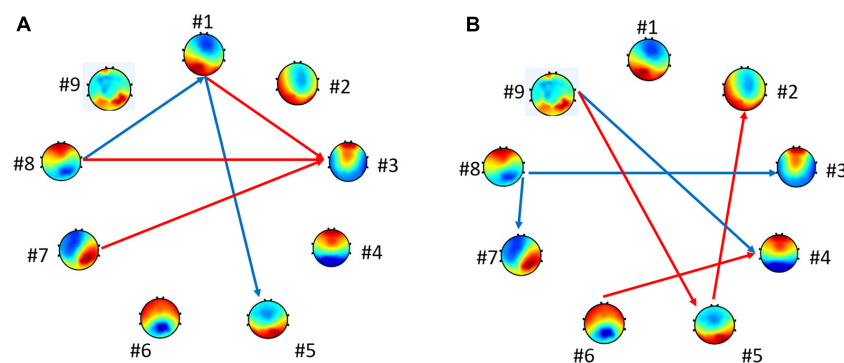
**TABLE 5 |** Means for all microstate parameters of speech-evoked EEG signals.

		Microstate classes								
Temporal parameters		#1	#2	#3	#4	#5	#6	#7	#8	#9
										
<b>Mean duration, ms (SD)</b>										
Valence	High	97.58 (17.4)	106.33 (21.0)	110.73 (22.5)	74.12 (15.6)	87.19 (19.3)	107.06 (23.9)	104.96 (20.8)	83.89 (16.8)	69.03 (28.1)
	Low	98.98 (19.6)	107.26 (19.5)	102.80 (21.8)	73.85 (17.5)	82.46 (17.0)	105.71 (22.5)	103.66 (19.5)	80.56 (18.6)	67.27 (227.5)
	<i>P</i> -value	0.53	0.22	<b>0.02*</b>	0.83	0.86	0.77	0.51	0.79	0.79
Arousal	High	98.32 (19.0)	106.77 (20.1)	105.21 (22.8)	73.82 (16.8)	83.18 (17.5)	106.64 (23.3)	103.86 (19.7)	81.60 (18.4)	67.66 (27.8)
	Low	102.72 (23.9)	110.36 (17.2)	98.90 (18.9)	75.19 (22.8)	89.18 (24.3)	98.55 (20.1)	105.45 (18.3)	78.48 (13.1)	68.32 (30.5)
	<i>P</i> -value	0.11	0.09	<b>0.05*</b>	0.64	0.52	<b>0.05*</b>	0.49	0.79	0.73
<b>Frequency of occurrence, counts/s (SD)</b>										
Valence	High	1.20 (0.6)	1.51 (0.6)	1.30 (0.6)	0.46 (0.3)	0.67 (0.4)	1.30 (0.6)	1.44 (0.5)	0.78 (0.5)	0.47 (0.2)
	Low	1.23 (0.6)	1.55 (0.5)	1.35 (0.7)	0.45 (0.3)	0.68 (0.4)	1.31 (0.6)	1.45 (0.5)	0.74 (0.5)	0.51 (0.2)
	<i>P</i> -value	0.52	0.50	0.49	0.93	0.86	0.56	0.84	0.64	0.27
Arousal	High	1.22 (0.6)	1.54 (0.6)	1.34 (0.7)	0.45 (0.3)	0.68 (0.4)	1.31 (0.6)	1.43 (0.5)	0.75 (0.5)	0.51 (0.2)
	Low	1.31 (0.6)	1.57 (0.5)	1.25 (0.6)	0.43 (0.3)	0.65 (0.3)	1.31 (0.8)	1.62 (0.6)	0.71 (0.4)	0.44 (0.2)
	<i>P</i> -value	0.20	0.62	0.39	0.55	0.72	0.76	<b>0.04*</b>	0.70	0.74
<b>Ratio of time coverage, % (SD)</b>										
Valence	High	12.11 (6.4)	16.57 (8.0)	15.84 (9.3)	4.13 (2.7)	6.48 (3.5)	14.29 (6.9)	15.53 (6.6)	7.26 (4.8)	7.74 (1.6)
	Low	12.79 (6.6)	17.02 (7.0)	15.22 (9.3)	4.02 (2.5)	6.37 (3.8)	14.59 (8.2)	15.16 (6.1)	7.12 (4.7)	7.67 (1.8)
	<i>P</i> -value	0.45	0.37	0.78	0.97	0.92	0.65	0.82	0.64	0.58
Arousal	High	12.52 (6.5)	16.85 (7.3)	15.51 (9.4)	4.06 (2.5)	6.36 (3.7)	14.61 (8.0)	15.10 (6.2)	7.21 (4.8)	7.73 (1.8)
	Low	14.02 (6.8)	17.64 (5.4)	13.59 (7.4)	3.88 (2.6)	6.88 (3.9)	13.27 (7.8)	17.13 (6.6)	6.49 (3.7)	7.07 (1.7)
	<i>P</i> -value	0.09	0.32	0.20	0.71	0.87	0.25	<b>0.05*</b>	0.58	0.68
<b>Global explained variance, % (SD)</b>										
Valence	High	6.35 (4.3)	6.38 (3.8)	9.22 (6.8)	3.65 (2.9)	3.82 (2.3)	6.01 (4.3)	4.87 (2.7)	4.84 (3.9)	3.06 (0.6)
	Low	6.53 (4.5)	6.79 (4.0)	9.08 (7.2)	3.27 (2.2)	3.64 (2.2)	6.16 (4.0)	4.82 (2.5)	4.58 (3.5)	2.90 (0.5)
	<i>P</i> -value	0.78	0.21	0.91	0.67	0.93	0.69	0.93	0.68	0.47
Arousal	High	6.42 (4.4)	6.62 (4.0)	9.21 (7.1)	3.38 (2.4)	3.65 (2.3)	6.20 (4.1)	4.76 (2.5)	4.71 (3.7)	2.97 (0.5)
	Low	7.37 (4.0)	7.59 (2.5)	7.97 (6.4)	3.19 (2.7)	4.13 (1.6)	5.16 (3.6)	5.65 (2.5)	3.78 (2.8)	2.67 (0.5)
	<i>P</i> -value	0.12	0.08	0.39	0.71	0.72	0.32	<b>0.03*</b>	0.54	0.92

The asterisk indicates significant difference ( $p \leq 0.05$ ).

**TABLE 6 |** The differences ( $p$ -value) of transition probabilities between high and low valence or arousal.

→	Dimensions									
	Valence	–	0.99	0.09	0.47	0.003	0.97	0.47	0.87	0.78
	Arousal	–	0.54	0.56	0.48	0.77	0.42	0.65	0.61	0.94
	Valence	0.29	–	0.48	0.49	0.10	0.80	0.29	0.75	0.88
	Arousal	0.76	–	0.98	0.86	0.20	0.98	0.12	0.64	0.86
	Valence	0.66	0.83	–	0.79	0.66	0.12	0.20	0.93	0.57
	Arousal	0.91	0.43	–	0.18	0.26	0.94	0.45	0.61	0.19
	Valence	0.72	0.41	0.75	–	0.31	0.28	0.66	0.48	0.08
	Arousal	0.44	0.53	0.91	–	0.46	0.12	0.41	0.74	0.38
	Valence	0.10	0.70	0.72	0.76	–	0.07	0.67	0.98	0.83
	Arousal	0.29	0.08	0.21	0.64	–	0.51	0.13	0.37	0.26
	Valence	0.29	0.19	0.43	0.12	0.20	–	0.23	0.24	0.24
	Arousal	0.42	0.48	0.23	0.09	0.40	–	0.37	0.36	0.76
	Valence	0.99	0.34	0.06	0.28	0.32	0.89	–	0.32	0.48
	Arousal	0.12	0.87	0.68	0.43	0.92	0.52	–	0.43	0.70
	Valence	0.04	0.72	0.06	0.51	0.68	0.22	0.96	–	0.26
	Arousal	0.21	0.46	0.04	0.77	0.60	0.98	0.0002	–	0.71
	Valence	0.74	0.84	0.65	0.93	0.97	0.98	0.91	0.92	–
	Arousal	0.67	0.65	0.12	0.01	0.08	0.23	0.78	0.21	–

**FIGURE 5 |** Connections with the statistically significant difference between groups. The blue arrows represent  $p < 0.05$ . The red arrows represent  $p < 0.10$  for **(A)** high vs. low valence groups and for **(B)** high vs. low arousal groups.

microstate #1 to #3, #7 to #3, and #8 to #3 ( $p < 0.10$ ) and from microstate #1 to #5 and #8 to #1 ( $p < 0.05$ ). For arousal, six transitions have significant differences: from microstate #9 to #5, #5 to #2, and #6 to #4 ( $p < 0.10$ ) and from #9 to #4, #8 to #3, and #8 to #7 ( $p < 0.05$ ). **Figure 5** highlights the directions of transitions that show significant differences.

## Emotion Recognition Results

In order to verify the effectiveness of our feature sets, we firstly captured the EEG data from the public DEAP dataset to validate our framework. Then, the proposed feature extraction was applied to the speech-evoked EEG dataset.

A fivefold cross-validation method is adopted to evaluate the performance: the dataset is split into fivefolds. In each iteration, onefold is used to test the model, and the rests serve as the training set. The process is repeated until each fold has been used as the training set.

For the two-class classification problem, the accuracies are measured using

$$\text{Accuracy} = \frac{TP + TN}{TP + TN + FN + FP} \quad (7)$$

where TP, TN, FP, and FN denote true positive, true negative, false positive, and false negative, respectively.

## Performance on DEAP Dataset

The dataset is separated into high–low classes by valence or arousal dimension. Each class is determined by the positivity of arousal and valence ratings. Valence and arousal levels higher than 4.5 are high and *vice versa*.

Considering temporal dependencies more complex than the first Markov models, von Wegner et al. (2017) suggested that the geometric distribution of microstate durations for short EEG time series was up to a duration of 16 s. In DEAP, the duration of EEG signals is 60 s. Therefore, we segment each signal using



**TABLE 7 |** The classification accuracies of different feature sets on dataset 2 (Dataset for Emotion Analysis using Physiological signals, DEAP).

References	Feature set	Classifier	Accuracy	
			Valence (%)	Arousal (%)
Mert and Akan (2018)	MEMD, PSD, Entropy, Hjorth, IMF energy, energy ratios	k-NN	67.0	51.0
		ANN	72.7	75.0
Zhuang et al. (2017)	EMD, TSD, PD, NE	SVM	69.1	71.9
Daimi and Saha (2014)	DT-CWPT	SVM	65.3	66.9
	Temporal parameters	SVM	72.5	72.1
This study	Transition probabilities	SVM	74.4	73.9
	Temporal parameters + transition probabilities	SVM	<b>75.8</b>	<b>77.1</b>

DT-CWPT, dual-tree complex wavelet packet transform time–frequency features; PSD, power spectral density; EMD, empirical mode decomposition.

a moving window with a length of 5 s to evaluate short-time identifiability.

We perform three experiments on the microstate-related feature sets. We first use four temporal parameters (duration, occurrence, time coverage, and GEV) as features to obtain accuracies for the valence and arousal dimensions and later use transition probabilities as features to obtain the accuracies. Finally, we combine temporal parameters and transition probabilities as a feature set to measure performance. The extracted features are fed into the support vector machine (SVM) for classification. SVM is widely used for emotion recognition, which has promising properties in many fields. We also carry out comparisons of other features that exist in the works of literature.

The accuracy results of high/low valence and arousal are given in **Table 7**. The four temporal parameters with SVM yield accuracy rates of 72.5 and 72.1% for high/low valence and high/low arousal, while the transition probabilities have scores of 74.4 and 73.9%, respectively. The highest scores of 75.8% for valence and 77.1% for arousal are obtained by combining temporal parameters and transition probabilities. Our methods are compared to other states-of-the-art which use the DEAP dataset. According to the comparison table, our study has higher accuracy rates than the previous studies. The results demonstrate that the parameters derived from microstate sequences are promising features for characterizing the dynamics of neural activity and recognizing emotion from EEG signals.

### Performance on Speech-Evoked EEG Signals

In this section, the performances of microstate characteristic features are evaluated on the emotional speech-evoked EEG dataset.

Three different classifiers are applied to three feature sets—that is, SVM, random forest, and artificial neural network (ANN).

**TABLE 8 |** The classification accuracies of different feature sets on speech-evoked EEG signals.

Dataset	Feature set	Classifier	Accuracy	
			Valence (%)	Arousal (%)
This study	Temporal parameters	Support vector machine (SVM)	71.8	68.8
		Random forest (RF)	72.0	67.9
		Artificial neural network (ANN)	72.3	69.5
	Transition probabilities	SVM	69.9	70.5
		RF	68.5	68.3
		ANN	70.4	69.8
	Temporal parameters + transition probabilities	SVM	<b>74.2</b>	71.9
		RF	73.1	70.7
		ANN	73.9	<b>72.3</b>

From **Table 8**, there is no significant difference among the three classifiers. The performance of the features extracted in this research is not affected by the type of classifiers. The highest accuracy is obtained by combining temporal parameters and transition probabilities as the feature set for valence and arousal. In valence recognition, the highest accuracy is 74.2% with the SVM classifier. For arousal, it is 72.3% with ANN.

## DISCUSSION

In this study, we applied the microstate analysis to the emotional auditory response. Our proposed method DTAHC revealed that nine template maps best described the entire dataset, explaining ~85% of the global variance for speech-evoked EEG. For music-evoked EEG, 10 template maps explain ~86% of the data. In previous visual research, Gianotti et al. (2008) studied the temporal dynamics of the neural activity that responded to emotional words and picture stimulus using ERP microstate analysis. In the emotional word experiment, 11 sequential microstates were identified. Among the 11 microstates, four of them were valence-sensitive and two of them were arousal-sensitive. In the emotional picture experiment, the microstate analysis identified 15 sequential microstates. Five of the fifteen and two of the fifteen microstates were valence-sensitive and arousal-sensitive, respectively. Although four prototypical microstate classes were useful to compare or complement results across different studies, several studies also suggested that the number of microstate classes was explicitly driven by the data. Muthukrishnan et al. (2016) performed the microstate analysis in a visuospatial working memory task. The optimal number of clusters was determined by the cross-validation criterion without prior assumptions. D'Croz-Baron et al. (2019) investigated that six template microstate maps can best describe the dataset across the autism spectrum disorder and neurotypical controls. In research of schizophrenia (Soni et al., 2018, 2019), four to six microstate maps were clustered, which related to the conditions of the experiments. Michel and Koenig (2018) discussed a meta-criterion for the optimal number of clusters. They suggested

that the most appropriate choice was a pragmatic compromise between the needs for specificity and generalizability.

The four prototypical microstates exhibited highly similar topographies across studies and were consistently labeled as class A, B, C, and D. Microstate A exhibits a left–right orientation, map B exhibits a right–left orientation, map C exhibits an anterior–posterior orientation, and map D exhibits a fronto-central maximum (Michel and Koenig, 2018). In terms of the orientation of the electrical axis, we relate some microstates of our study to four prototypical microstates. Here we mark maxima as “+” and minima as “-.” In our emotional speech-evoked cognitive experiment, three microstates (#3, #4, and #8) are characterized by fronto-central orientation of the maxima which are similar to map D (Santarnecchi et al., 2017; da Cruz et al., 2020). Some studies suggest that microstate D is associated with attention network activity (Britz et al., 2010; Milz et al., 2016). For the music-evoked EEG dataset, microstates #5 and #8 exhibit fronto-central maximum.

In the speech-evoked emotion experiment, microstates #1, #2, and #5 have an anterior(-)-posterior(+) orientation which is consistent with map C (Santarnecchi et al., 2017; Seitzman et al., 2017; Al Zoubi et al., 2019). Microstate #6 has an anterior(+)-posterior(-) orientation which is consistent with map C in some studies (Hernandez et al., 2016; Pipinis et al., 2017; da Cruz et al., 2020). In the music-evoked cognitive experiment, microstates #2 and #10 have an anterior(-)-posterior(+) orientation which is somewhat alike to map C.

In the speech-evoked emotion experiment, microstate #7 shows a left anterior (-)–right posterior (+) location of the extrema. It is similar to map B (Khanna et al., 2014; Santarnecchi et al., 2017). In the music-evoked cognitive experiment, microstate #3 has a left anterior (+)–right posterior (-) orientation which is alike to map B in some studies (Milz et al., 2017; Pipinis et al., 2017; da Cruz et al., 2020).

In the music-evoked cognitive experiment, microstate #1 has a left posterior (-)–right anterior (+) orientation which is consistent with map A in the studies (Tomescu et al., 2015; Pipinis et al., 2017; da Cruz et al., 2020).

We also identify some microstates which have significant differences with prototypical microstates. In the speech-evoked emotion experiment, microstate #9 has a local extremum in posterior (+). In the music-evoked emotion experiment, microstates #4 and #6 exhibit local maxima in posterior. Microstates #7 and #9 show local minima at the axis center.

For future research, the relationship between microstates and brain functions can be explored using source localization. Some computational approaches, e.g., distributed linear inverse solution (LAURA) (de Peralta Menendez et al., 2004), can help understand the brain source activation in terms of intracranial generators.

We further delved into the temporal characteristics of microstates for emotional speech perception. The Wilcoxon rank-sum test was used to analyze the statistical differences of the microstate parameters between different groups. For the valence dimension, the results indicated that the mean duration of microstate #3 (active prefrontal cortex) in the high group was longer than that in the low group. For arousal dimension,

three microstates had significant differences between high and low group. Specifically, the mean duration of microstates #3 and #6 (active frontal lobe) in the high group was longer than those in the low group. The occurrence, coverage, and GEV of microstate #7 (active temporal lobe) had significant differences between the high and low groups. In previous research, Gianotti et al. (2008) found that five of the 15 microstates were different for pleasant vs. unpleasant pictures, and two of the 15 microstates were different for high- vs. low-arousing pictures. However, it was difficult to compare this work with our study directly since visual and auditory information activated different cortices.

## CONCLUSION

The main purpose of this study is to extract novel features based on EEG microstates for emotion recognition. Determining the optimal number of microstates automatically is a challenge for applying microstate analysis to emotion. To overcome the limitation, this research proposed DTAHC. The proposed method identified 10 microstates on a public music-evoked EEG dataset (DEAP) and nine microstates on our recorded emotional speech-evoked EEG dataset. Subsequently, the microstate sequence characteristics were compared in the aspect of high/low valence or arousal conditions. Finally, these characteristics were fed into the classifier for emotion recognition. All the findings in this work suggested that the microstate sequence characteristics can effectively improve the performance of emotion recognition from EEG signals. We hope this work will stimulate future research to propose novel algorithms to reduce the limitation of microstate analysis and uncover more interesting mechanisms of the affective process, e.g., linking the source localization of microstates to brain functions can help understand the functional significance of these states.

## DATA AVAILABILITY STATEMENT

The raw data supporting the conclusions of this article will be made available by the authors, without undue reservation.

## ETHICS STATEMENT

The studies involving human participants were reviewed and approved by the Heilongjiang Provincial Hospital. The patients/participants provided their written informed consent to participate in this study.

## AUTHOR CONTRIBUTIONS

JC was involved in the conduct of the experiment, data analysis, and writing of the manuscript. HL, LM, and FS were involved in the conception, supervision, and manuscript review.

HB was involved in the study design and conduct of the experiment. YS was involved in the study design and subject recruitment. All authors contributed to the article and approved the submitted version.

## FUNDING

This research was supported by the National Natural Science Foundation of China (U20A20383), National Key Research and Development Program of China (2018YFC0806800 and 2020YFC0833204), Shenzhen Key Laboratory of Innovation Environment Project (ZDSYS201707311437102), Shenzhen Foundational Research Funding (JCYJ20180507183608379

and JCYJ20200109150814370), Funds for National Scientific and Technological Development, Project funded by China Postdoctoral Science Foundation (2020T130431), Basic and Applied Basic Research of Guangdong (2019A151511179 and 2021A1515011903), and Open Funding of State Key Laboratory of Robotics and System, Heilongjiang Touyan Team.

## SUPPLEMENTARY MATERIAL

The Supplementary Material for this article can be found online at: <https://www.frontiersin.org/articles/10.3389/fnins.2021.689791/full#supplementary-material>

## REFERENCES

- Al Zoubi, O., Mayeli, A., Tsuchiyagaito, A., Misaki, M., Zotev, V., Refai, H., et al. (2019). EEG microstates temporal dynamics differentiate individuals with mood and anxiety disorders from healthy subjects. *Front. Hum. Neurosci.* 13:56. doi: 10.3389/fnhum.2019.00056
- Alarcao, S. M., and Fonseca, M. J. (2017). Emotions recognition using EEG signals: a survey. *IEEE Trans. Affect. Comput.* 10, 374–393. doi: 10.1109/taffc.2017.2714671
- Ali, M., Mosa, A. H., Al Machot, F., and Kyamakya, K. (2016). “EEG-based emotion recognition approach for e-healthcare applications,” in *Paper Presented at the 2016 8th International Conference on Ubiquitous and Future Networks (ICUFN)*, Vienna.
- Atkinson, J., and Campos, D. (2016). Improving BCI-based emotion recognition by combining EEG feature selection and kernel classifiers. *Exp. Syst. Appl.* 47, 35–41. doi: 10.1016/j.eswa.2015.10.049
- Baradits, M., Bitter, I., and Czobor, P. (2020). Multivariate patterns of EEG microstate parameters and their role in the discrimination of patients with schizophrenia from healthy controls. *Psychiatry Res.* 288:112938. doi: 10.1016/j.psychres.2020.112938
- Britz, J., Van De Ville, D., and Michel, C. M. (2010). BOLD correlates of EEG topography reveal rapid resting-state network dynamics. *Neuroimage* 52, 1162–1170. doi: 10.1016/j.neuroimage.2010.02.052
- Chen, C., Yu, X., Belkacem, A. N., Lu, L., Li, P., Zhang, Z., et al. (2021). EEG-based anxious states classification using affective BCI-based closed neurofeedback system. *J. Med. Biol. Eng.* 41, 155–164. doi: 10.1007/s40846-020-00596-7
- Chu, C., Wang, X., Cai, L., Zhang, L., Wang, J., Liu, C., et al. (2020). Spatiotemporal EEG microstate analysis in drug-free patients with Parkinson's disease. *Neuroimage Clin.* 25, 102132. doi: 10.1016/j.nicl.2019.102132
- da Cruz, J. R., Favrod, O., Roinishvili, M., Chkonia, E., Brand, A., Mohr, C., et al. (2020). EEG microstates are a candidate endophenotype for schizophrenia. *Nat. Commun.* 11, 1–11.
- Daimi, S. N., and Saha, G. (2014). Classification of emotions induced by music videos and correlation with participants' rating. *Exp. Syst. Appl.* 41, 6057–6065. doi: 10.1016/j.eswa.2014.03.050
- Daly, I., Williams, D., Hallowell, J., Hwang, F., Kirke, A., Malik, A., et al. (2015). Music-induced emotions can be predicted from a combination of brain activity and acoustic features. *Brain Cogn.* 101, 1–11. doi: 10.1016/j.bandc.2015.08.003
- D'Croz-Baron, D. F., Baker, M., Michel, C. M., and Karp, T. (2019). EEG microstates analysis in young adults with autism spectrum disorder during resting-state. *Front. Hum. Neurosci.* 13:173. doi: 10.3389/fnhum.2019.00173
- de Peralta Menendez, R. G., Murray, M. M., Michel, C. M., Martuzzi, R., and Andino, S. L. G. (2004). Electrical neuroimaging based on biophysical constraints. *Neuroimage* 21, 527–539. doi: 10.1016/j.neuroimage.2003.09.051
- Dennis, T. A., and Solomon, B. (2010). Frontal EEG and emotion regulation: electrocortical activity in response to emotional film clips is associated with reduced mood induction and attention interference effects. *Biol. Psychol.* 85, 456–464. doi: 10.1016/j.biopsycho.2010.09.008
- Ekman, P., Friesen, W. V., O'sullivan, M., Chan, A., Diacoyanni-Tarlatzis, I., Heider, K., et al. (1987). Universals and cultural differences in the judgments of facial expressions of emotion. *J. Pers. Soc. Psychol.* 53, 712–717. doi: 10.1037/0022-3514.53.4.712
- Frantzidis, C. A., Bratsas, C., Papadelis, C. L., Konstantinidis, E., Pappas, C., and Bamidis, P. D. (2010). Toward emotion aware computing: an integrated approach using multichannel neurophysiological recordings and affective visual stimuli. *IEEE Trans. Inform. Technol. Biomed.* 14, 589–597. doi: 10.1109/titb.2010.2041553
- Gianotti, L. R., Faber, P. L., Schuler, M., Pascual-Marqui, R. D., Kochi, K., and Lehmann, D. (2008). First valence, then arousal: the temporal dynamics of brain electric activity evoked by emotional stimuli. *Brain Topogr.* 20, 143–156. doi: 10.1007/s10548-007-0041-2
- Hernandez, L. D., Rieger, K., Baenninger, A., Brandeis, D., and Koenig, T. (2016). Towards using microstate-neurofeedback for the treatment of psychotic symptoms in schizophrenia. A feasibility study in healthy participants. *Brain Topography* 29, 308–321. doi: 10.1007/s10548-015-0460-4
- Hossain, M. S., and Muhammad, G. (2019). An audio-visual emotion recognition system using deep learning fusion for a cognitive wireless framework. *IEEE Wirel. Commun.* 26, 62–68. doi: 10.1109/mwc.2019.1800419
- Hosseini, S. A., Khalilzadeh, M. A., Naghibi-Sistani, M. B., and Niazmand, V. (2010). “Higher order spectra analysis of EEG signals in emotional stress states,” in *Paper Presented at the 2010 2nd International Conference on Information Technology and Computer Science*, Kiev.
- Jang, E.-H., Park, B.-J., Park, M.-S., Kim, S.-H., and Sohn, J.-H. (2015). Analysis of physiological signals for recognition of boredom, pain, and surprise emotions. *J. Physiol. Anthropol.* 34:25.
- Jenke, R., Peer, A., and Buss, M. (2014). Feature extraction and selection for emotion recognition from EEG. *IEEE Trans. Affect. Comput.* 5, 327–339. doi: 10.1109/taffc.2014.2339834
- Khanna, A., Pascual-Leone, A., and Farzan, F. (2014). Reliability of resting-state microstate features in electroencephalography. *PLoS One* 9:e114163. doi: 10.1371/journal.pone.0114163
- Khanna, A., Pascual-Leone, A., Michel, C. M., and Farzan, F. (2015). Microstates in resting-state EEG: current status and future directions. *Neurosci. Biobehav. Rev.* 49, 105–113. doi: 10.1016/j.neubiorev.2014.12.010
- Kim, K., Duc, N. T., Choi, M., and Lee, B. (2021). EEG microstate features for schizophrenia classification. *PLoS One* 16:e0251842. doi: 10.1371/journal.pone.0251842
- Koelstra, S., Muhl, C., Soleymani, M., Lee, J.-S., Yazdani, A., Ebrahimi, T., et al. (2011). Deap: a database for emotion analysis; using physiological signals. *IEEE Trans. Affect. Comput.* 3, 18–31. doi: 10.1109/t-affc.2011.15
- Lehmann, D., Faber, P. L., Galderisi, S., Herrmann, W. M., Kinoshita, T., Koukkou, M., et al. (2005). EEG microstate duration and syntax in acute, medication-naïve, first-episode schizophrenia: a multi-center study. *Psychiatry Res.* 138, 141–156. doi: 10.1016/j.psychres.2004.05.007
- Lehmann, D., and Skrandies, W. (1980). Reference-free identification of components of checkerboard-evoked multichannel potential fields.

- Electroencephalogr. Clin. Neurophysiol.* 48, 609–621. doi: 10.1016/0013-4694(80)90419-8
- Lin, Y.-P., Wang, C.-H., Jung, T.-P., Wu, T.-L., Jeng, S.-K., Duann, J.-R., et al. (2010). EEG-based emotion recognition in music listening. *IEEE Trans. Biomed. Eng.* 57, 1798–1806.
- Liu, Y., and Sourina, O. (2013). “Real-time fractal-based valence level recognition from EEG,” in *Transactions on Computational Science XVIII*, eds M. L. Gavrilova, C. J. K. Tan, and A. Kuijper (Berlin: Springer), 101–120. doi: 10.1007/978-3-642-38803-3\_6
- Mehmood, R. M., and Lee, H. J. (2015). EEG based emotion recognition from human brain using Hjorth parameters and SVM. *Int. J. Bio Sci. Bio Technol.* 7, 23–32. doi: 10.14257/ijbsbt.2015.7.3.03
- Mert, A., and Akan, A. (2018). Emotion recognition from EEG signals by using multivariate empirical mode decomposition. *Pattern Anal. Appl.* 21, 81–89. doi: 10.1007/s10044-016-0567-6
- Michel, C. M., and Koenig, T. (2018). EEG microstates as a tool for studying the temporal dynamics of whole-brain neuronal networks: a review. *Neuroimage* 180, 577–593. doi: 10.1016/j.neuroimage.2017.11.062
- Milz, P., Faber, P. L., Lehmann, D., Koenig, T., Kochi, K., and Pascual-Marqui, R. D. (2016). The functional significance of EEG microstates—associations with modalities of thinking. *Neuroimage* 125, 643–656. doi: 10.1016/j.neuroimage.2015.08.023
- Milz, P., Pascual-Marqui, R. D., Achermann, P., Kochi, K., and Faber, P. L. (2017). The EEG microstate topography is predominantly determined by intracortical sources in the alpha band. *Neuroimage* 162, 353–361. doi: 10.1016/j.neuroimage.2017.08.058
- Mohammadi, Z., Frounchi, J., and Amiri, M. (2017). Wavelet-based emotion recognition system using EEG signal. *Neural Comput. Appl.* 28, 1985–1990. doi: 10.1007/s00521-015-2149-8
- Murray, M. M., Brunet, D., and Michel, C. M. (2008). Topographic ERP analyses: a step-by-step tutorial review. *Brain Topogr.* 20, 249–264. doi: 10.1007/s10548-008-0054-5
- Musaeus, C. S., Salem, L. C., Kjaer, T. W., and Waldemar, G. (2019). Microstate changes associated with Alzheimer's disease in persons with down syndrome. *Front. Neurosci.* 13:1251. doi: 10.3389/fnins.2019.01251
- Musha, T., Terasaki, Y., Haque, H. A., and Ivamitsky, G. A. (1997). Feature extraction from EEGs associated with emotions. *Artif. Life Robot.* 1, 15–19. doi: 10.1007/bf02471106
- Muthukrishnan, S.-P., Ahuja, N., Mehta, N., and Sharma, R. (2016). Functional brain microstate predicts the outcome in a visuospatial working memory task. *Behav. Brain Res.* 314, 134–142. doi: 10.1016/j.bbr.2016.08.020
- Pascual-Marqui, R. D., Michel, C. M., and Lehmann, D. (1995). Segmentation of brain electrical activity into microstates: model estimation and validation. *IEEE Trans. Biomed. Eng.* 42, 658–665. doi: 10.1109/10.391164
- Petrantonakis, P. C., and Hadjileontiadis, L. J. (2009). Emotion recognition from EEG using higher order crossings. *IEEE Trans. Inform. Technol. Biomed.* 14, 186–197. doi: 10.1109/titb.2009.2034649
- Pipinis, E., Melynyte, S., Koenig, T., Jarutyte, L., Linkenkaer-Hansen, K., Ruksenas, O., et al. (2017). Association between resting-state microstates and ratings on the amsterdam resting-state questionnaire. *Brain Topogr.* 30, 245–248. doi: 10.1007/s10548-016-0522-2
- Poulsen, A. T., Pedroni, A., Langer, N., and Hansen, L. K. (2018). Microstate EEGlab toolbox: an introductory guide. *bioRxiv* [Preprint] bioRxiv: 289850,
- Rozgić, V., Vitaladevuni, S. N., and Prasad, R. (2013). “Robust EEG emotion classification using segment level decision fusion,” in *Paper Presented at the 2013 IEEE International Conference on Acoustics, Speech and Signal Processing*, Vancouver, BC.
- Russell, J. A. (1980). A circumplex model of affect. *J. Pers. Soc. Psychol.* 39, 1161–1178. doi: 10.1037/h0077714
- Russell, J. A., and Mehrabian, A. (1977). Evidence for a three-factor theory of emotions. *J. Res. Pers.* 11, 273–294. doi: 10.1016/0092-6566(77)90037-x
- Santaronechi, E., Khanna, A. R., Musaeus, C. S., Benwell, C. S., Davila, P., Farzan, F., et al. (2017). EEG microstate correlates of fluid intelligence and response to cognitive training. *Brain Topogr.* 30, 502–520. doi: 10.1007/s10548-017-0565-z
- Schlossberg, H. (1954). Three dimensions of emotion. *Psychol. Rev.* 61, 81–88. doi: 10.1037/h0054570
- Seitzman, B. A., Abell, M., Bartley, S. C., Erickson, M. A., Bolbecker, A. R., and Hetrick, W. P. (2017). Cognitive manipulation of brain electric microstates. *Neuroimage* 146, 533–543. doi: 10.1016/j.neuroimage.2016.10.002
- Skrandies, W. (2007). The effect of stimulation frequency and retinal stimulus location on visual evoked potential topography. *Brain Topogr.* 20, 15–20. doi: 10.1007/s10548-007-0026-1
- Soni, S., Muthukrishnan, S. P., Samanchi, R., Sood, M., Kaur, S., and Sharma, R. (2019). Pre-trial and pre-response EEG microstates in schizophrenia: an endophenotypic marker. *Behav. Brain Res.* 371:111964. doi: 10.1016/j.bbr.2019.111964
- Soni, S., Muthukrishnan, S. P., Sood, M., Kaur, S., and Sharma, R. (2018). Hyperactivation of left inferior parietal lobule and left temporal gyri shortens resting EEG microstate in schizophrenia. *Schizophr. Res.* 201, 204–207. doi: 10.1016/j.schres.2018.06.020
- Sourina, O., and Liu, Y. (2011). “A fractal-based algorithm of emotion recognition from EEG using arousal-valence model,” in *Paper Presented at the International Conference on Bio-inspired Systems and Signal Processing*, Rome.
- Thiruchselvam, R., Blechert, J., Sheppes, G., Rydstrom, A., and Gross, J. J. (2011). The temporal dynamics of emotion regulation: an EEG study of distraction and reappraisal. *Biol. Psychol.* 87, 84–92. doi: 10.1016/j.biopsycho.2011.02.009
- Tomescu, M. I., Rihis, T. A., Roinishvili, M., Karahanoglu, F. I., Schneider, M., Menghetti, S., et al. (2015). Schizophrenia patients and 22q11. 2 deletion syndrome adolescents at risk express the same deviant patterns of resting state EEG microstates: a candidate endophenotype of schizophrenia. *Schizophr. Res. Cogn.* 2, 159–165. doi: 10.1016/j.scog.2015.04.005
- Van de Ville, D., Britz, J., and Michel, C. M. (2010). EEG microstate sequences in healthy humans at rest reveal scale-free dynamics. *Proc. Natl. Acad. Sci. U.S.A.* 107, 18179–18184. doi: 10.1073/pnas.1007841107
- Von Wegner, F., Knaut, P., and Laufs, H. (2018). EEG microstate sequences from different clustering algorithms are information-theoretically invariant. *Front. Comput. Neurosci.* 12:70. doi: 10.3389/fncom.2018.00070
- von Wegner, F., Tagliazucchi, E., and Laufs, H. (2017). Information-theoretical analysis of resting state EEG microstate sequences-non-Markovianity, non-stationarity and periodicities. *Neuroimage* 158, 99–111. doi: 10.1016/j.neuroimage.2017.06.062
- Wang, X.-W., Nie, D., and Lu, B.-L. (2014). Emotional state classification from EEG data using machine learning approach. *Neurocomputing* 129, 94–106. doi: 10.1016/j.neucom.2013.06.046
- Zhuang, N., Zeng, Y., Tong, L., Zhang, C., Zhang, H., and Yan, B. (2017). Emotion recognition from EEG signals using multidimensional information in EMD domain. *BioMed Res. Int.* 2017:8317357.
- Zong, C., and Chetouani, M. (2009). “Hilbert-Huang transform based physiological signals analysis for emotion recognition,” in *Paper Presented at the 2009 IEEE International Symposium on Signal Processing and Information Technology (ISSPIT)*, Ajman.

**Conflict of Interest:** FS was employed by company Microsoft Research Asia.

The remaining authors declare that the research was conducted in the absence of any commercial or financial relationships that could be construed as a potential conflict of interest.

Copyright © 2021 Chen, Li, Ma, Bo, Soong and Shi. This is an open-access article distributed under the terms of the Creative Commons Attribution License (CC BY). The use, distribution or reproduction in other forums is permitted, provided the original author(s) and the copyright owner(s) are credited and that the original publication in this journal is cited, in accordance with accepted academic practice. No use, distribution or reproduction is permitted which does not comply with these terms.





# Evaluation of Multilevel Surgeries in Children With Spastic Cerebral Palsy Based on Surface Electromyography

Sujiao Li<sup>1,2</sup>, Xueqin Luo<sup>1,2</sup>, Song Zhang<sup>3,4</sup>, Yuanmin Tang<sup>1,2</sup>, Jiming Sun<sup>3</sup>, Qingyun Meng<sup>5</sup>, Hongliu Yu<sup>1,2\*</sup> and Chengyan Sun<sup>3\*</sup>

<sup>1</sup> Institute of Rehabilitation Engineering and Technology, School of Medical Device and Food Engineering, University of Shanghai for Science and Technology, Shanghai, China, <sup>2</sup> Shanghai Engineering Research Center of Assistive Devices, University of Shanghai for Science and Technology, Shanghai, China, <sup>3</sup> Department of Functional Neurosurgery, Shanghai Punan Hospital, Shanghai Eber Medical Group, Shanghai, China, <sup>4</sup> Department of Pediatric Neurosurgery, Xinhua Hospital, Shanghai JiaoTong University School of Medicine, Shanghai, China, <sup>5</sup> College of Rehabilitation Sciences, Shanghai University of Medicine and Health Sciences, Shanghai, China

## OPEN ACCESS

### Edited by:

Zhan Li,  
University of Electronic Science and  
Technology of China, China

### Reviewed by:

Josep M. Font-Llagunes,  
Universitat Politècnica de  
Catalunya, Spain

Lizhi Pan,  
Tianjin University, China

### \*Correspondence:

Chengyan Sun  
chengyansun@hotmail.com  
Hongliu Yu  
YHL98@hotmail.com

### Specialty section:

This article was submitted to  
Neural Technology,  
a section of the journal  
Frontiers in Neuroscience

**Received:** 15 March 2021

**Accepted:** 25 May 2021

**Published:** 15 July 2021

### Citation:

Li S, Luo X, Zhang S, Tang Y, Sun J,  
Meng Q, Yu H and Sun C (2021)  
Evaluation of Multilevel Surgeries in  
Children With Spastic Cerebral Palsy  
Based on Surface Electromyography.  
*Front. Neurosci.* 15:680645.  
doi: 10.3389/fnins.2021.680645

The root mean square (RMS) of the surface electromyography (sEMG) signal can respond to neuromuscular function, which displays a positive correlation with muscle force and muscle tension under positive and passive conditions, respectively. The purpose of this study was to investigate the changes in muscle force and tension after multilevel surgical treatments, functional selective posterior rhizotomy (FSPR) and tibial anterior muscle transfer surgery, and evaluate their clinical effect in children with spastic cerebral palsy (SCP) during walking. Children with diplegia ( $n = 13$ ) and hemiplegia ( $n = 3$ ) with ages from 4 to 18 years participated in this study. They were requested to walk barefoot at a self-selected speed on a 15-m-long lane. The patient's joints' range of motion (ROM) and sEMG signal of six major muscles were assessed before and after the multilevel surgeries. The gait cycle was divided into seven phases, and muscle activation state can be divided into positive and passive conditions during gait cycle. For each phase, the RMS of the sEMG signal amplitude was calculated and also normalized by a linear envelope (10-ms running RMS window). The muscle tension of the gastrocnemius decreased significantly during the loading response, initial swing, and terminal swing ( $p < 0.05$ ), which helped the knee joint to get the maximum extension when the heel is on the ground and made the heel land smoothly. The muscle force of the gastrocnemius increased significantly ( $p < 0.05$ ) during the mid-stance, terminal stance, and pre-swing, which could generate the driving force for the human body to move forward. The muscle tension of the biceps femoris and semitendinosus decreased significantly ( $p < 0.05$ ) during the terminal stance, pre-swing, and initial swing. The decreased muscle tension could relieve the burden of the knee flexion when the knee joint was passively flexed. At the terminal swing, the muscle force of the tibial anterior increased significantly ( $p < 0.05$ ), which could improve the ankle dorsiflexion ability and prevent foot drop and push forward. Thus, the neuromuscular function of cerebral palsy during walking can be evaluated by the muscle activation state and the RMS of the sEMG signal, which showed that multilevel surgical treatments are feasible and effective to treat SCP.

**Keywords:** sEMG signal, muscle activity, cerebral palsy, gait analysis, multilevel surgery

## INTRODUCTION

Cerebral palsy (CP) refers to a group of persistent motor and postural developmental disorder syndrome that leads to restricted mobility, which is caused by non-progressive brain damage to the developing fetus or infant (Bell et al., 2002). Spastic cerebral palsy (SCP) is the most common type of CP, accounting for ~60–70% of all children with CP. SCP represents a series of neurofunctional disorders, involving joint stiffness, decreased physical activity, tendon hyperreflexia, strong flexor reflex, and strong resistance when muscle is passively stretched (Gage and Novacheck, 2001). Many studies have shown that the gait cycle of patients with SCP presented an abnormal pattern (Winters et al., 1987; Perry and Davids, 1992; Crenna, 1998). Information on different gait patterns could improve early treatment in children with bilateral CP before abnormal gait patterns are fully established (Domagalska-Szopa and Szopa, 2019). Abnormal gait not only affects the patient's joints but also modifies muscle activity and activation patterns (Patikas et al., 2005).

Significant progress has been made in the treatments for CP, especially SCP. To date, the clinical methods for treating SCP mainly include functional training, surgical treatment, physical therapy, acupuncture and massage, and drug therapy (Chin et al., 2020). Comparing these methods, surgical treatment is a very efficient method for patients with severe movement disorders (Buddhdev et al., 2017). The key purpose of surgery is to adjust muscle tension and balance muscle force. In order to adjust the muscle tension of the patient, neurosurgery is mainly performed on the patient such as selective posterior rhizotomy (SPR), which uses an electrophysiological equipment to monitor the electromyogram of multiple muscles of the limbs during the operation and choose continuous recording of somatosensory evoked potentials as an objective basis for the proportion of surgical resection (Turner, 2009). Thus, the muscle tension of the patients can be adjusted fully (Graham et al., 2016; Qijia et al., 2019). In recent years, functional selective posterior rhizotomy (FSPR) has been developed on the basis of SPR. The treatment technologies have risen from the anatomical level to the functional level, and it can regulate muscle tension more effectively. Orthopedic surgery is generally used to balance muscle force. Kapti (2014) utilized the posterior tibial muscle transfer method to treat foot drop, and Fox et al. (2009) solved knee stiffness by rectus femoris transfer surgery. Some studies showed that tibial anterior muscle transfer can treat clubfoot (El-Fadl and Mahmoud, 2013; El Batti et al., 2016; Agarwal et al., 2020a). In general, surgeons perform compound surgeries on patients for some specific malfunctions to adjust muscle tension and balance muscle force. With the increasing number of treatment options, the evaluation of surgical effect has become a very important work.

The surface electromyography (sEMG) signal has been proven to be a reliable reflection of the muscles in the gait of patients with CP (Granata et al., 2005; Patikas et al., 2005; Nardo et al., 2019; Parent et al., 2019). sEMG signal is important in clinical evaluation and rehabilitation medicine with specific focus on neurorehabilitation (Campanini et al., 2020; Cappellini et al., 2020). In recent years, there have been more and more researches

focused on the change of sEMG signals for patients with CP after surgical treatments. Some studies have demonstrated that surgery can affect sEMG signals of patients with CP (Patikas et al., 2007). It was proven that the semitendinosus activation timing was delayed and the burst duration of the vastus lateralis was decreased after surgery (Buurke et al., 2004). Lauer et al. (2007) have also proven time–frequency changes of the sEMG signal after hamstring lengthening in children with CP. Wang et al. (2011) reported that EMG signals have changed significantly after selective femoral neurotomy, which deduced that surgery could reduce the muscle tension of the quadriceps muscle. These studies suggested that muscle tension could be reflected by the root mean square (RMS) of sEMG signal. At the same time, studies have shown that the RMS of the sEMG signal is a reliable parameter (Farina et al., 2004) and displayed a positive correlation with muscle force and muscle tension under positive and passive conditions (Onishi et al., 2000). In a complete gait cycle, the activation states of sEMG signals in different subphases are varied (Perc, 2005). However, there are few studies on the muscle force and muscle tension of patients with CP during walking.

In this study, we analyzed the treatment of patients undergoing both FSPR and tibial anterior muscle transfer surgeries. The overall aim of this article was to evaluate the neuromuscular function of CP during walking by the muscle activation state and the RMS of the sEMG signal. By analyzing the changes of the RMS in each subphase, the outcome showed that the patient's muscle force increased and muscle tension decreased after multilevel surgeries. It implies that the neuromuscular function has been improved greatly.

## METHODS

### Subjects

Sixteen patients with CP who underwent orthopedic surgery from July 2019 to May 2020 were enrolled in this study. These subjects consisted of 13 cases of diplegia and three cases of hemiplegia in 10 male patients and six female patients, aged 4–17 years (mean age,  $9.8 \pm 5.0$  years). The clinical data of examined patients are shown in **Table 1**. The muscle tension of the knee and ankle joints on the sagittal plane was tested separately by the Modified Ashworth Scale (MAS). The higher the grade, the higher the abnormal muscle tension in children with CP, and grade 0 represents normal muscle tension. In the clinic, doctors use the Manual Muscle Testing (MMT) to detect the muscle force level of patients. Level 5 is the highest level and represents normal muscle force. As the level decreases, the muscle force decreases. The main manifestations of patients were crouching gait and jumping gait. These two symptoms are specifically manifested as abnormal knee flexion, limited ankle dorsiflexion, and foot varus during walking. No subject had received any treatment (surgery, orthopedics, or Botox injection) before the test, and all were able to walk independently without assistance.

### Procedure and Instruments

All patients were carried out to collect kinetic parameters and sEMG signals during a gait cycle. The Motion Analysis

**TABLE 1** | Demographic and clinical data of the patients.

ID	Involved side	Age (years)	Modified Ashworth Scale (MAS)				Manual Muscle Testing (MMT)			
			KE	KF	AD	AP	Qua	Ham	Tib	Gas
1	Right	6–18	3	2	3	2	3	3	2	2
2	Right	3–6	2	2	3	2	3	3	3	3
3	Right	6–18	2	2	3	2	3	3	2	2
4	Both	6–18	3	2	3	2	3	3	2	2
5	Both	6–18	2	2	3	2	3	3	3	3
6	Both	6–18	2	2	3	2	4	4	4	4
7	Both	6–18	2	2	3	2	4	3	3	3
8	Both	3–6	1	1	3	1	4	3	3	3
9	Both	3–6	2	2	3	2	4	4	3	3
10	Both	3–6	2	2	3	2	4	3	3	3
11	Both	6–18	2	2	3	2	3	3	2	2
12	Both	3–6	2	2	3	2	4	3	3	3
13	Both	6–18	2	2	1	2	4	3	3	3
14	Both	6–18	1	1	3	1	4	3	4	4
15	Both	3–6	2	2	3	2	4	3	3	3
16	Both	6–18	2	2	3	2	4	4	4	4

KE, knee extension; KF, knee flexion; AD, ankle dorsiflexion; AP, ankle plantar flexion; Qua, quadriceps femoris; Ham, hamstring; Tib, tibialis anterior; Gas, gastrocnemius.

(NORAXON Inc., Scottsdale, AZ, USA) including Myomotion and Myomuscle module was used to synchronously collect dynamic joint angle and sEMG signals, respectively. The sample frequency of the Myomuscle module is 1,500 Hz. All sensors are wireless, which are simple and light to wear and reduce the impact on the original gait of patients. The electrode pads have been applied over the respective muscles with an interelectrode distance of 2 cm. The direction of these two test electrodes was parallel to the direction of the long axis of the test muscle fiber, and then the corresponding sensors were fixed (**Figure 1**). After all subjects have put on the equipment, they first perform short exercises to adapt to their own walking rhythm. When the test started officially, the subjects were asked to walk barefoot at a self-selected speed on a 15-m-long lane.

Kinematic parameters were recorded in the sagittal, coronal, and transverse planes for the hip, knee, and ankle to document the preoperative and postoperative status of the patients. For reasons of simplicity, the presentations of the kinematic parameters were focused on the hip and knee joint on the sagittal plane and the ankle joint on the sagittal plane and the coronal plane. The sEMG signals of some muscles were simultaneously recorded. Six muscles were selected as representatives for the knee and ankle. The measured muscles included thigh muscles: rectus femoris, biceps femoris, semitendinosus; and calf muscles: tibialis anterior, lateral gastrocnemius, and medial gastrocnemius.

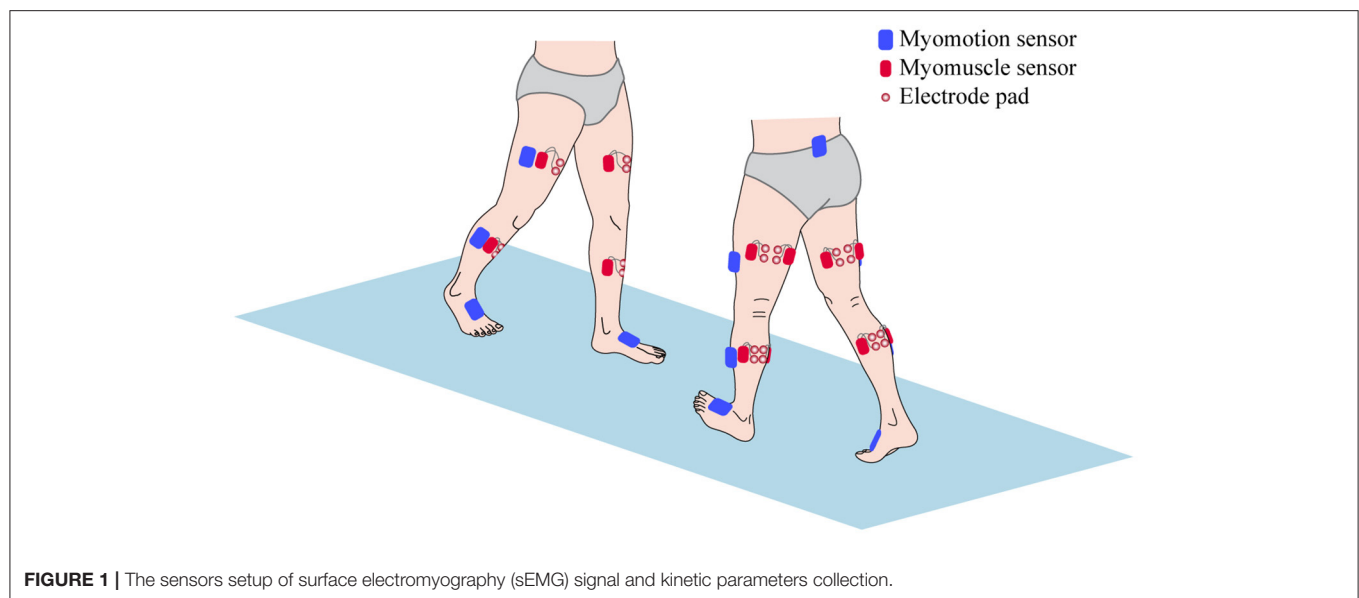
## Signal Analysis

For each of the following subphases of a gait cycle: loading response, mid-stance, terminal stance, pre-swing, initial swing, mid-swing, and terminal swing, the averaging of all strides for each side, the sEMG signal, and joint angles were calculated separately. In order to reduce the measurement error, six gait

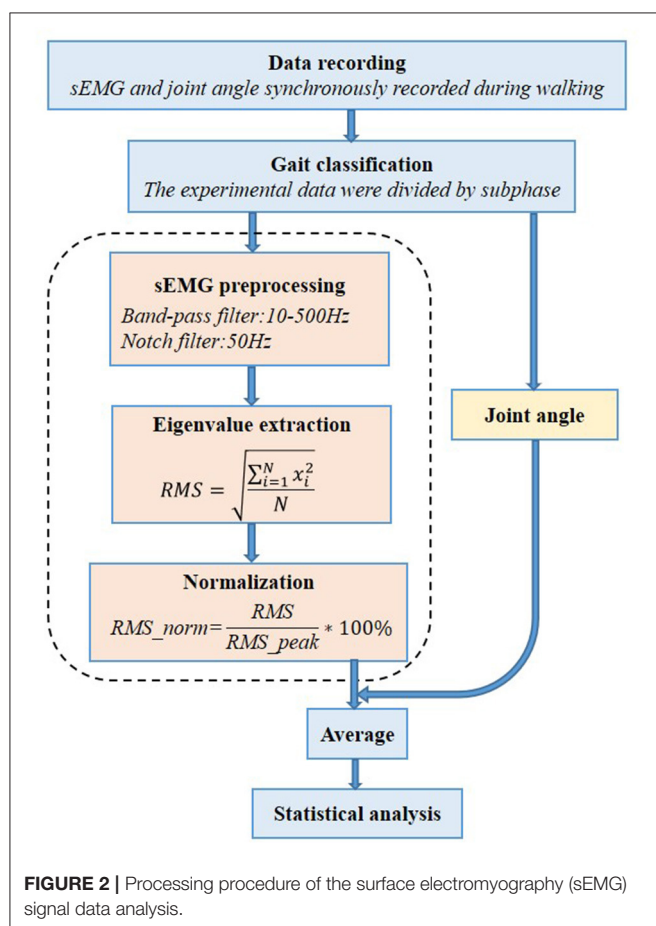
cycles for each dependent variable and condition were calculated. The definition of these subphases was made according to the foot strike and foot off of both feet (Perry and Davids, 1992). The kinematics data of the knee and ankle joints were analyzed mainly in order to analyze the surgical effects of the crouching gait and clubfoot. The crouching gait of the knee joint and the clubfoot were reflected mainly in the knee angle of the sagittal plane and the ankle angle of the sagittal plane and coronal plane, respectively.

The raw sEMG signal data were band-pass filtered using a Butterworth filter between 10 and 500 Hz to remove non-EMG artifacts. We also applied a 50-Hz notch filter to remove the power line interference (Daly et al., 2019). The sEMG signal amplitude is affected by several other factors; to adjust for this variability and allow comparison between participants, the sEMG signal is usually normalized to a standard value, usually the peak value of the sEMG signal obtained during the maximum voluntary isometric contraction (MVIC). But for the children with CP, it may be difficult to perform MVIC because it is a challenge to automatically generate the MVIC. In this case, it is considered a feasible and appropriate method to normalize the sEMG signal obtained in a specific task (such as walking) to the peak value. For each percentage of all sEMG signal channels and gait periods, the RMS of the sEMG signal was calculated with a 10-ms running window. For each sEMG signal channel, the highest RMS value (peak RMS) was obtained and used for normalization (Gagnat et al., 2020). The procedure of sEMG signal data processing is shown in **Figure 2**.

Normal sEMG signal patterns for the major muscles in the lower extremities were plotted as a function of the gait cycle (Perc, 2005), which are shown in **Figure 3**. In this study, the patient's gait cycle was divided into seven subphases, and the state of the muscle was defined according to **Figure 3**. As shown by the



**FIGURE 1** | The sensors setup of surface electromyography (sEMG) signal and kinetic parameters collection.



**FIGURE 2** | Processing procedure of the surface electromyography (sEMG) signal data analysis.

red horizontal bars, the muscles contract and produce muscle force to maintain a normal gait. Muscles are thought to contract because they are activated by nervous system stimulation. So

the red horizontal bars in **Figure 3** indicate that the selected muscles are active during the gait cycle. In other parts during a gait cycle, the stretched muscles are passive and produce muscle tension. The RMS is used to describe the average change characteristics of sEMG signals over a period of time and refers to the RMS value of all amplitudes in this period of time. The RMS of the sEMG signals can respond to the neuromuscular function, which displays a positive correlation with muscle force and muscle tension under positive and passive conditions, respectively (Wang et al., 2011). As shown by the red horizontal bars, the RMS of the sEMG signal is proportional to muscle force. In other parts, the RMS of the sEMG signal is proportional to muscle tension.

## Statistical Analysis

The joint angle and the RMS of the sEMG signals were analyzed in this study, and paired *t*-test was used to analyze the data before and after the surgeries. All data are expressed as mean value and standard deviation of the mean (SD). The level of significance was set at  $p < 0.05$ , and the 95% confidence intervals (95% CIs) were calculated. The statistical analysis was performed using the SPSS Version 24 software (The Apache Software Foundation, IL, USA).

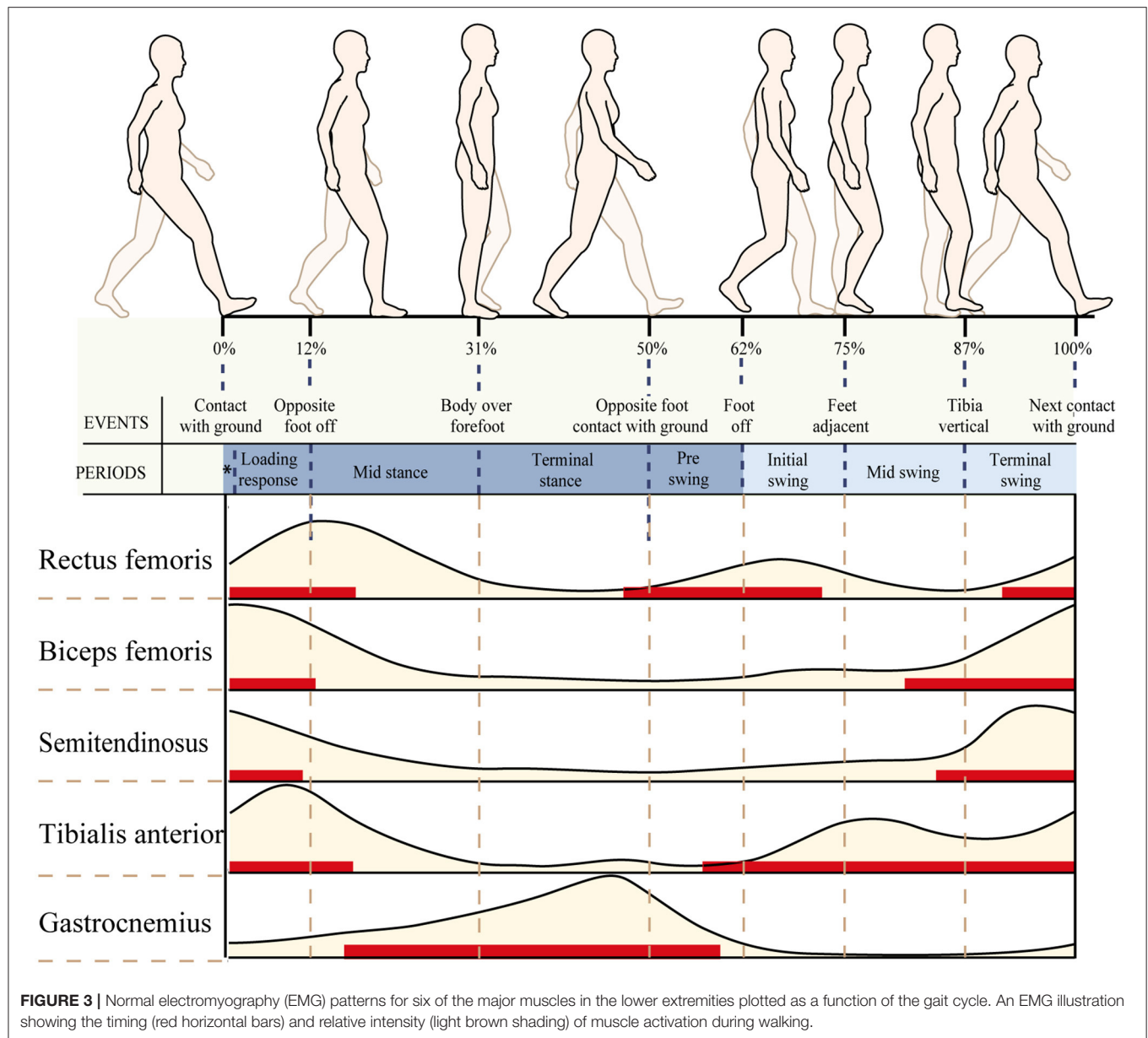
## RESULTS

### Kinematics

The ranges of motion (ROMs) on the sagittal plane before and after the multilevel surgeries were displayed and compared in **Table 2**. The results indicated that the ankle ROM increased significantly after the multilevel surgeries. The ankle joint angle was more plantar flexed during the whole gait cycle.

The kinematic parameters showed an overall improvement after surgery for the joint angles of the knee and ankle, as shown in **Figure 4**. Compared with those of pre-surgery, the knee flexion angle decreased significantly during the loading





**TABLE 2 |** The range of motion (ROM) on the sagittal plane before and after the multilevel surgeries.

ROM	Pre-operation (Deg.)	Post-operation (Deg.)
Hip	45.33 ± 4.5	50.79 ± 7.0
Knee	48.32 ± 8.8	47.66 ± 12.3
Ankle*	23.32 ± 4.2	29.21 ± 6.8

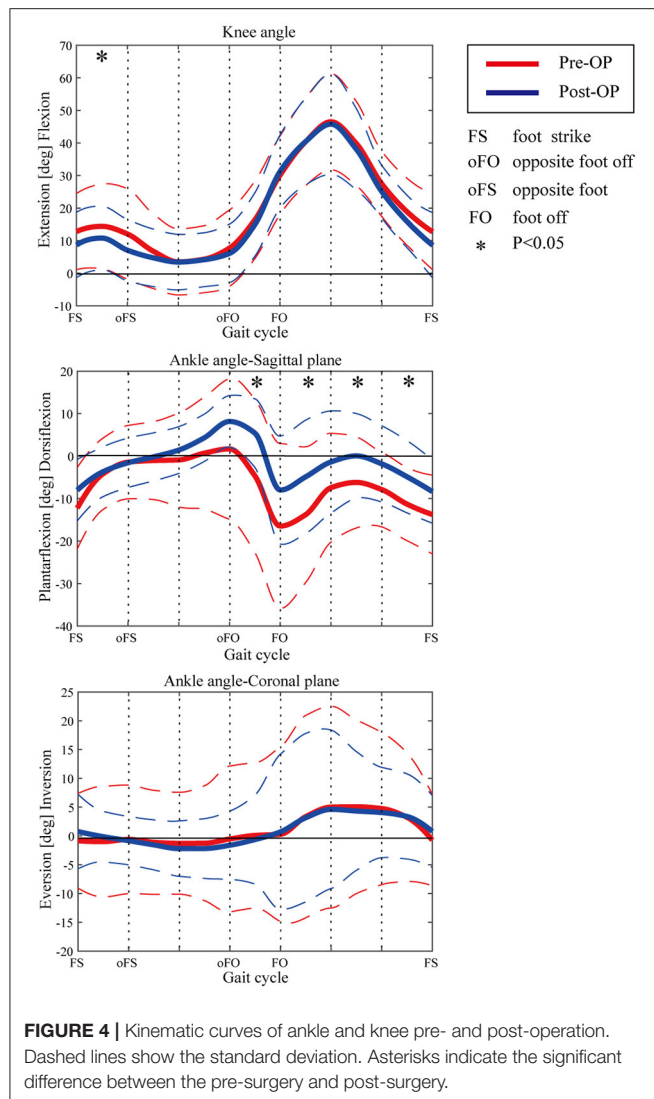
\*Significant difference between the pre-surgery and post-surgery.

response ( $p < 0.05$ ). The average knee flexion angle decreased from  $20.1^\circ$  to  $18.3^\circ$  in the whole gait cycle, and the overall knee flexion angle decreased. In the sagittal plane, the angle of ankle dorsiflexion increased significantly during the swing phase ( $p <$

0.05). In terms of the ankle, the maximum dorsiflexion angle changed from  $4.9^\circ$  to  $8.2^\circ$ , and the maximum plantar flexion angle decreased from  $16.5^\circ$  to  $8.3^\circ$  in the whole gait cycle. On the coronal plane, the joint changed from the original valgus to varus during the loading response. The valgus angle became larger at the terminal stance, and the varus angle decreased significantly during the mid-swing phase.

## Electromyogram

The sEMG-RMS values of the main thigh muscles before and after the surgery are presented in **Figure 5A**. The RMS of the rectus femoris muscle decreased significantly at the initial swing phase ( $p = 0.005$ ). The RMS of the biceps femoris muscle decreased significantly during the terminal stance ( $p = 0.011$ ),



pre-swing ( $p = 0.01$ ), and the initial swing phase ( $p < 0.001$ ). We also observed a statistically significant decrease during the terminal swing ( $p = 0.02$ ). The difference between several subphases was that the biceps femoris should be active during the terminal swing. The RMS of the semitendinosus muscle decreased significantly during the terminal stance ( $p = 0.016$ ) and pre-swing ( $p = 0.002$ ).

The sEMG-RMS values of the tibialis anterior, lateral gastrocnemius, and medial gastrocnemius muscles in the gait cycle before and after the surgeries are compared and illustrated in **Figure 5B**. Results revealed that the RMS of the tibial anterior muscle was significantly higher after the surgery than before during terminal swing ( $p = 0.003$ ). In addition, the RMS of the lateral gastrocnemius muscle was significantly higher pre-surgery during mid-stance ( $p = 0.001$ ) and terminal stance ( $p = 0.034$ ); in contrast, it became significantly lower compared to before surgery during the initial swing ( $p = 0.028$ ) and terminal swing ( $p < 0.001$ ). The medial gastrocnemius muscle showed significant

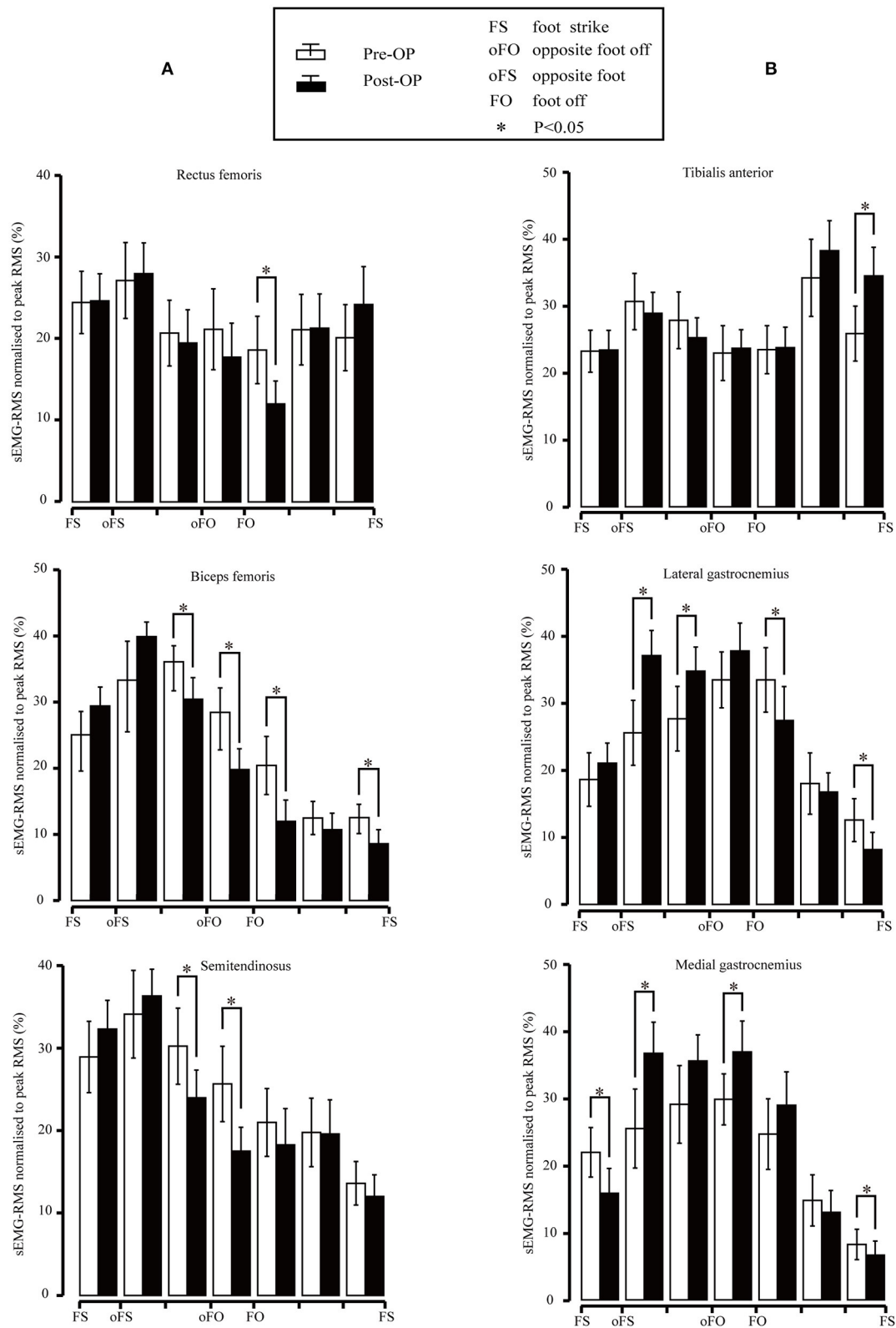
improvement compared to that of pre-surgery during mid-stance ( $p = 0.005$ ) and pre-swing ( $p = 0.019$ ); nevertheless, the RMS significantly decreased during the loading response ( $p = 0.009$ ) and terminal swing ( $p = 0.021$ ).

Based on **Figure 3**, the sEMG-RMS changes of muscle activities were transferred to the adjustments of muscle tension and force before and after the surgery during the gait cycle, displayed on **Table 3**. For the thigh muscles, the changes in the flexors were greater than the extensors. For the calf muscles, the changes in the plantar flexors were greater than those in the dorsiflexors. These showed that the changes in the muscles of the posterior side of the lower limbs are greater than those of the anterior side. It can be seen that muscle tension decreased, and some muscle forces increased after the surgery for most muscles. The muscle tension of the biceps femoris and semitendinosus muscles was reduced at the terminal stance, pre-swing, and initial swing. The medial gastrocnemius muscle tension during the loading response and terminal swing was significantly reduced. The lateral gastrocnemius muscle tension during the initial and terminal swing was significantly reduced. But the eccentric contraction muscle force of the gastrocnemius muscles increased in the stance phase. At the terminal swing, the force of the tibial anterior muscle improved. On the contrary, the muscle force of the rectus femoris and biceps femoris was reduced during the initial swing and terminal swing, respectively.

## DISCUSSION

The realization of every movement depends on the nervous system to regulate the coordinated activities of related muscle groups so as to complete a normal gait when walking (Lieber, 2002). Patients with neurological diseases also have obstacles in their muscle co-contraction function (Banks et al., 2017; Zhixian et al., 2018). Patikas et al. (2007) proved that the sEMG signal changed after multilevel surgeries during walking, but they did not explain the changes in neuromuscular function. The RMS of the sEMG signal in the passive state proved that the muscle tension decreased after selective femoral neurotomy, but we could not know the change of neuromuscular function during walking (Wang et al., 2011). Taking into consideration normal sEMG signal patterns for the major muscle, the muscles can be divided into passive and active movements (Perc, 2005). By studying the change of the RMS of the sEMG signal, we found that muscle force increased and muscle tension decreased. This study proves that sEMG signals can be used to evaluate neuromuscular function during walking.

The changes of muscle force and tension after multilevel surgeries had a good effect in children with CP. During the loading response, the gastrocnemius muscle tension at initial contact may result in a stretch reflex response. The tensed gastrocnemius muscle does not allow the knee to fully extend during the initial contact (Hullin et al., 1996). The gastrocnemius muscle tension during the loading response was significantly reduced from **Table 3**, which helped the knee joint to get the maximum extension when the heel is on the ground. In the



**FIGURE 5 | (A)** Root mean square (RMS) values for the rectus femoris, biceps femoris, and semitendinosus surface electromyography (sEMG) signal pre- and post-surgery. Vertical lines represent 1 SD of the mean, and asterisks indicate the significant difference between the pre-surgery and post-surgery. **(B)** RMS values for the subjects of the tibialis anterior, lateral gastrocnemius, and medial gastrocnemius sEMG signal pre- and post-surgery. Vertical lines represent 1 SD of the mean, and asterisks indicate the significant difference between pre-surgery and post-surgery.

**TABLE 3 |** The change of muscle function before and after the multilevel surgeries.

Muscles	Loading response	Mid-stance	Terminal stance	Pre-swing	Initial swing	Mid-swing	Terminal swing
Rectus femoris	/	/	/	/	MFD	/	/
Biceps femoris	/	/	MTD	MTD	MTD	/	MFD
Semitendinosus	/	/	MTD	MTD	/	/	/
Tibialis anterior	/	/	/	/	/	/	MFI
Lateral gastrocnemius	/	MFI	MFI	/	MTD	/	MTD
Medial gastrocnemius	MTD	MFI	/	MFI	/	/	MTD

MFI, muscle force increase; MFD, muscle force decrease; MTD, muscle tension decrease.

stance phase, the eccentric contraction muscle force of the gastrocnemius muscles increased, which could control the calf leaning forward, and generated the driving force for the human body to move forward. Coupled with the increase in ankle dorsiflexion, it helped to increase the power of the plantar flexors, which was very important for the body to move forward (Winter, 1983). The muscle tension of the biceps femoris and semitendinosus muscles is reduced. At this time, the knee joint was passively flexed and the lowered knee flexor muscle tension can relieve the burden of the patient's knee flexion on the knee joint (Nardo et al., 2017). In the swing phase, the muscle tension of the gastrocnemius muscles was reduced, which was conducive to the ankle joint from plantar flexion to dorsiflexion, so the patient's ankle dorsiflexion was improved. The reduced gastrocnemius muscle tension could also make the leg swing from fast to slow to make the heel land smoothly. At the terminal swing, the increase of tibial anterior muscle force could improve the ankle dorsiflexion ability, prevent foot drop, and push forward (Agarwal et al., 2020a). Unfortunately, the muscle force of the rectus femoris and biceps femoris was reduced during the initial swing and terminal swing, respectively. Biceps femoris muscle force can help to coordinate with the coordinated contraction of the rectus femoris to slow down the forward swinging calf and prepare for the heel landing, but the eccentric contraction muscle force decreased, which was not conducive to the recovery of normal gait posture for children with CP.

Children with CP mainly manifested as crouching gait and clubfoot. The crouching gait is specifically manifested that the knee flexion angle is too large, and the patient cannot walk upright. Long-term crouching posture could lead to knee cartilage degradation and joint pain (O'Sullivan et al., 2020). The outcomes of this study demonstrated that the knee flexion deformity of the patient had improved after surgery. Clubfoot is clinically manifested as restricted ankle dorsiflexion ability and foot varus. Flaccidity of foot and foot varus could cause the sole of the foot not to effectively touch the ground, and the body center is unable to move forward effectively, which resulted in walking dysfunction (Agarwal et al., 2020b). Through surgery, the patient's ankle dorsiflexion had been greatly improved. On the coronal plane, the condition of the foot varus was also relieved. It was worth mentioning that during the loading response,

the foot changed from varus to valgus, which was exactly in line with the law of normal gait. The normal subtalar joint movement of the human body during the stance phase is: a slight supination in the early and middle stages, then pronation rapidly, and supination again in the middle and late stages (Neumann, 2010).

## CONCLUSION

This article presented the assessments of multilevel surgical treatment effects in children with SCP by investigating the changes in sEMG signal patterns pre- and post-surgeries. By extracting the RMS of the sEMG signal and muscle activation state, the change of the RMS is transformed into the change of muscle force and muscle tension. After multilevel surgeries, for calf muscles, the muscle force increased and muscle tension decreased. Both the muscle force and muscle tension of thigh muscle decreased. This reduced muscle force could be compensated for by rehabilitation training. In conclusion, this is consistent with the operation principle that FSPR can reduce the muscle tension of the lower limb muscles, and the tibial anterior muscle transfer surgery is thought to balance the muscle force of the calf muscles. Therefore, the findings of the present study support that the RMS of the sEMG signal can describe neuromuscular function of the patients during walking, and the multilevel surgeries are feasible and effective to treat SCP.

In this study, we employed the muscle activation state during the walking cycle to establish the relationship between the RMS of the sEMG signal and muscle force and tension. Because the muscle activation states of CP are different from those of normal people, our subsequent work will focus on the muscle activation state of children with CP during walking. By dividing the muscle activation state of children with CP, the expected findings of future studies would be more meaningful and quantitative to the surgical treatments for CP.

## DATA AVAILABILITY STATEMENT

The raw data supporting the conclusions of this article will be made available by the authors, without undue reservation.



## ETHICS STATEMENT

The studies involving human participants were reviewed and approved by Ethical code from Shanghai University of Medicine and Health Sciences: 2019-ZYXM1-04–420300197109053525. Written informed consent to participate in this study was provided by the participants' legal guardian/next of kin.

## AUTHOR CONTRIBUTIONS

SL, XL, and SZ conceived and designed the experiments, analyzed and interpreted the data, and wrote the manuscript. SZ, YT, JS, and QM performed the experiments and wrote the manuscript. HY and CS designed, interpreted the data, and revised the

manuscript. All authors contributed to the article and approved the submitted version.

## FUNDING

The work was funded by the National Natural Science Foundation of China (62073224) and the Key R&D Program of the Ministry of Science and Technology (2020YFC2007902).

## ACKNOWLEDGMENTS

All authors would like to sincerely thank the parents, children, and therapists for their participation and thank the collaborators of our research center for their help.

## REFERENCES

- Agarwal, A., Gourav, J., and Neeraj, G. (2020a). Comparison of three different methods of anterior tibial tendon transfer for relapsed clubfoot: a pilot study. *J. Clin. Orthopaed. Trauma*. 11, 240–244. doi: 10.1016/j.jcot.2018.09.001
- Agarwal, A., Gupta, S., Sud, A., and Agarwal, S. (2020b). Results of modified ponseti technique in difficult clubfoot and a review of literature. *J. Clin. Orthopaed. Trauma* 11, 222–231. doi: 10.1016/j.jcot.2019.05.003
- Banks, C. L., Huang, H. J., Little, V. L., and Patten, C. (2017). Electromyography exposes heterogeneity in muscle co-contraction following stroke. *Front. Neurol.* 8:699. doi: 10.3389/fneur.2017.00699
- Bell, K. J., Öunpuu, S., DeLuca, P. A., and Romness, M. J. (2002). Natural progression of gait in children with cerebral palsy. *J. Pediatr. Orthop.* 22, 677–682. doi: 10.1097/01241398-200209000-00020
- Buddhdev, P., Fry, N. R., Lepage, R., Wiley, M., Gough, M., and Shortland, A. P. (2017). Abnormality of standing posture improves in patients with bilateral spastic cerebral palsy following lower limb surgery. *Gait Post.* 54:255. doi: 10.1016/j.gaitpost.2017.03.014
- Buurke, J. H., Hermens, H. J., Roetenberg, D., Harlaar, J., Rosenbaum, D., and Kleissen, R. F. M. (2004). Influence of hamstring lengthening on muscle activation timing. *Gait Post.* 20, 48–53. doi: 10.1016/S0966-6362(03)00092-4
- Campanini, I., Disselhorst-Klug, C., Rymer, W. Z., and Merletti, R. (2020). Surface EMG in clinical assessment and neurorehabilitation: barriers limiting its use. *Front. Neurol.* 11:934. doi: 10.3389/fneur.2020.00934
- Cappellini, G., Sylos-Labini, F., Assenza, C., Libernini, L., and Ivanenko, Y. (2020). Clinical relevance of state-of-the-art analysis of surface electromyography in cerebral palsy. *Front. Neurol.* 11:583296. doi: 10.3389/fneur.2020.583296
- Chin, E. M., Gwynn, H. E., Robinson, S., and Hoon, A. H. (2020). Principles of medical and surgical treatment of cerebral palsy. *Neurol. Clin.* 38, 397–416. doi: 10.1016/j.ncl.2020.01.009
- Crenna, P. (1998). Spasticity and spastic gait in children with cerebral palsy. *Neurosci. Biobehav. Rev.* 22:571. doi: 10.1016/S0149-7634(97)00046-8
- Daly, C., Lafferty, E., Joyce, M., and Malone, A. (2019). Determining the most effective exercise for gluteal muscle activation in children with cerebral palsy using surface electromyography. *Gait Post.* 70:270. doi: 10.1016/j.gaitpost.2019.03.013
- Domagalska-Szopa, M., and Szopa, A. (2019). Gait pattern differences among children with bilateral cerebral palsy. *Front. Neurol.* 10:183. doi: 10.3389/fneur.2019.00183
- El Batti, S., Solla, F., Clément, J. L., Rosello, O., Oborocianu, I., Chau, E., and Rampal, V. (2016). Initial treatment of congenital idiopathic clubfoot: prognostic factors. *Orthopaed. Traumatol. Surg. Res.* 102, 1081–1085. doi: 10.1016/j.otsr.2016.07.012
- El-Fadl, A., and Mahmoud, S. (2013). An unusual aberrant muscle in congenital clubfoot: an intraoperative finding. *J. Foot Ankle Surg.* 52, 380–382. doi: 10.1053/j.jfas.2012.12.012
- Farina, D., Merletti, R., and Enoka, R. M. (2004). The extraction of neural strategies from the surface EMG. *J. Appl. Physiol.* 96, 1486–1495. doi: 10.1152/japplphysiol.01070.2003
- Fox, M. D., Reinbolt, J. A., ÖUnpuu, S., and Delp, S. L. (2009). Mechanisms of improved knee flexion after rectus femoris transfer surgery. *J. Biomech.* 42, 614–619. doi: 10.1016/j.jbiomech.2008.12.007
- Gage, J. R., and Novacheck, T. F. (2001). An update on the treatment of gait problems in cerebral palsy. *J. Pediatr. Orthop.* 10, 265–274. doi: 10.1097/00009957-200110000-00001
- Gagnat, Y., Brndvik, S. M., and Roeleveld, K. (2020). Surface electromyography normalization affects the interpretation of muscle activity and coactivation in children with cerebral palsy during walking. *Front. Neurol.* 11:202. doi: 10.3389/fneur.2020.00202
- Graham, D., Aquilina, K., Cawker, S., Paget, S., and Wimalasundera, N. (2016). Single-level selective dorsal rhizotomy for spastic cerebral palsy. *J. Spine Surg.* 2:195. doi: 10.21037/jss.2016.08.08
- Granata, K. P., Darin, A. P., and Mark, F. A. (2005). Repeatability of surface EMG during gait in children. *Gait Post.* 22, 346–350. doi: 10.1016/j.gaitpost.2004.11.014
- Hullin, M. G., Robb, J. E., and Loudon, I. R. (1996). Gait patterns in children with hemiplegic spastic cerebral palsy. *J. Pediatr. Orthopaed.* 5, 247–251. doi: 10.1097/01202412-199605040-00006
- Kapti, A. O. (2014). Dynamic simulation of tibialis posterior tendon transfer in the treatment of drop-foot. *Biocybernet. Biomed. Eng.* 34, 132–138. doi: 10.1016/j.bbe.2014.01.001
- Lauer, R. T., Smith, B. T., Shewokis, P. A., McCarthy, J. J., and Tucker, C. A. (2007). Time–frequency changes in electromyographic signals after hamstring lengthening surgery in children with cerebral palsy. *J. Biomech.* 40, 2738–2743. doi: 10.1016/j.jbiomech.2007.01.001
- Lieber, R. L. (2002). *Skeletal Muscle Structure, Function, and Plasticity*. Baltimore: Lippincott Williams & Wilkins.
- Nardo, F. D., Strazza, A., Mengarelli, A., Cardarelli, S., Tigrini, A., and Verdini, F., et al. (2019). Emg-based characterization of walking asymmetry in children with mild hemiplegic cerebral palsy. *Biosensors* 9:82. doi: 10.3390/bios9030082
- Nardo, F. D., Strazza, A., Mengarelli, A., Ercolani, S., and Fioretti, S. (2017). Surface EMG patterns for quantification of thigh muscle co-contraction in school-age children: normative data during walking. *Gait Post.* 61, 25–33. doi: 10.1016/j.gaitpost.2017.12.025
- Neumann, D. A. (2010). *Kinesiology of the Musculoskeletal System; Foundation for Rehabilitation*. St. Louis: Mosby & Elsevier.
- Onishi, H., Yagi, R., Akasaka, K., Momose, K., Ihashi, K., and Handa, Y. (2000). Relationship between EMG signals and force in human vastus lateralis muscle using multiple bipolar wire electrodes. *J. Electromyogr. Kinesiol.* 10, 59–67. doi: 10.1016/S1050-6411(99)00020-6

- O'Sullivan, R. A., Marron, A., and Brady, K. (2020). Crouch gait or Flexed-knee gait in cerebral palsy; is there a difference? A systematic review. *Gait Post.* 81:233. doi: 10.1016/j.gaitpost.2020.09.001
- Parent, A., Pouliot-Laforte, A., Maso, F. D., Cherni, Y., and Ballaz, L. (2019). Muscle fatigue during a short walking exercise in children with cerebral palsy who walk in a crouch gait. *Gait Post.* 72:22–7. doi: 10.1016/j.gaitpost.2019.05.021
- Patikas, D., Wolf, S., and Döderlein, L. (2005). Electromyographic evaluation of the sound and involved side during gait of spastic hemiplegic children with cerebral palsy. *Eur. J. Neurol.* 12, 691–699. doi: 10.1111/j.1468-1331.2005.01047.x
- Patikas, D., Wolf, S. I., Schuster, W., Armbrust, P., Dreher, T., and Döderlein, L. (2007). Electromyographic patterns in children with cerebral palsy: do they change after surgery? *Gait Post.* 26, 362–371. doi: 10.1016/j.gaitpost.2006.10.012
- Perc, M. (2005). The dynamics of human gait. *Eur. J. Phys.* 26:525. doi: 10.1088/0143-0807/26/3/017
- Perry, J., and Davids, J. R. (1992). Gait analysis: normal and pathological function. *J. Pediatr. Orthop.* 12:815. doi: 10.1097/01241398-199211000-00023
- Qijia, Z., Liang, T., Yanyan, W., Bo, X., and Min, S. (2019). Feasibility and effectiveness of a newly modified protocol-guided selective dorsal rhizotomy via single-level approach to treat spastic hemiplegia in pediatric cases with cerebral palsy. *Child's Nerv. Syst.* 35, 2171–2178. doi: 10.1007/s00381-019-04194-0
- Turner, R. P. (2009). Neurophysiologic intraoperative monitoring during selective dorsal rhizotomy. *J. Clin. Neurophysiol.* 26:82. doi: 10.1097/WNP.0b013e31819f9077
- Wang, S., Miao, S., Zhuang, P., Chen, Y., Liu, H., and Zuo, H. (2011). Assessment of surface electromyographic clinical analysis of selective femoral neurotomy on cerebral palsy with stiff knee. *J. Neurosci. Methods* 199, 98–102. doi: 10.1016/j.jneumeth.2011.04.031
- Winter, D. A. (1983). Energy generation and absorption at the ankle and knee during fast, natural, and slow cadences. *Clin. Orthopaed. Relat. Res.* 175, 147–154. doi: 10.1097/00003086-198305000-00021
- Winters, T. F., Gage, J. R., and Hicks, R. R. (1987). Gait patterns in spastic hemiplegia in children and adults. *J. Bone Joint Surg.* 69, 437–441. doi: 10.2106/00004623-198769030-00016
- Zhixian, G., Lin, C., Qiliang, X., Nong, X., and Wei, J. (2018). Degraded synergistic recruitment of semg oscillations for cerebral palsy infants crawling. *Front. Neurol.* 9:760. doi: 10.3389/fneur.2018.00760

**Conflict of Interest:** The authors declare that the research was conducted in the absence of any commercial or financial relationships that could be construed as a potential conflict of interest.

Copyright © 2021 Li, Luo, Zhang, Tang, Sun, Meng, Yu and Sun. This is an open-access article distributed under the terms of the Creative Commons Attribution License (CC BY). The use, distribution or reproduction in other forums is permitted, provided the original author(s) and the copyright owner(s) are credited and that the original publication in this journal is cited, in accordance with accepted academic practice. No use, distribution or reproduction is permitted which does not comply with these terms.



# A Novel Two-Stage Refine Filtering Method for EEG-Based Motor Imagery Classification

Yuxin Yan<sup>1</sup>, Haifeng Zhou<sup>2</sup>, Lixin Huang<sup>1\*</sup>, Xiao Cheng<sup>3\*</sup> and Shaolong Kuang<sup>2</sup>

<sup>1</sup> The First Affiliated Hospital of Soochow University, Soochow University, Suzhou, China, <sup>2</sup> College of Mechanical and Electrical Engineering, Soochow University, Suzhou, China, <sup>3</sup> Applied Technology College of Soochow University, Suzhou, China

## OPEN ACCESS

### Edited by:

Mitsuhiro Hayashibe,  
Tohoku University, Japan

### Reviewed by:

Yu Zhang,  
Lehigh University, United States  
Xin Liu,  
University of California, San Diego,  
United States  
Saugat Bhattacharyya,  
Ulster University, United Kingdom

### \*Correspondence:

Lixin Huang  
szhuanglx@yeah.net  
Xiao Cheng  
cheng18251162064@163.com

### Specialty section:

This article was submitted to  
Neural Technology,  
a section of the journal  
Frontiers in Neuroscience

**Received:** 23 January 2021

**Accepted:** 27 July 2021

**Published:** 01 September 2021

### Citation:

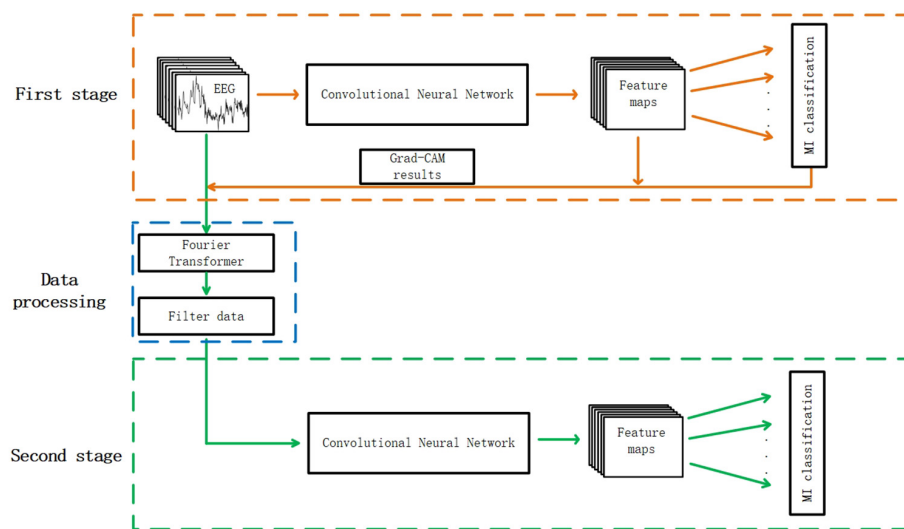
Yan Y, Zhou H, Huang L, Cheng X  
and Kuang S (2021) A Novel  
Two-Stage Refine Filtering Method  
for EEG-Based Motor Imagery  
Classification.  
Front. Neurosci. 15:657540.  
doi: 10.3389/fnins.2021.657540

Cerebral stroke is a common disease across the world, and it is a promising method to recognize the intention of stroke patients with the help of brain-computer interface (BCI). In the field of motor imagery (MI) classification, appropriate filtering is vital for feature extracting of electroencephalogram (EEG) signals and consequently influences the accuracy of MI classification. In this case, a novel two-stage refine filtering method was proposed, inspired by Gradient-weighted Class Activation Mapping (Grad-CAM), which uses the gradients of any target concept flowing into the final convolutional layer to highlight the important part of training data for predicting the concept. In the first stage, MI classification was carried out and then the frequency band to be filtered was calculated according to the Grad-CAM of the MI classification results. In the second stage, EEG was filtered and classified for a higher classification accuracy. To evaluate the filtering effect, this method was applied to the multi-branch neural network proposed in our previous work. Experiment results revealed that the proposed method reached state-of-the-art classification kappa value levels and acquired at least 3% higher kappa values than other methods. This study also proposed some promising application scenarios with this filtering method.

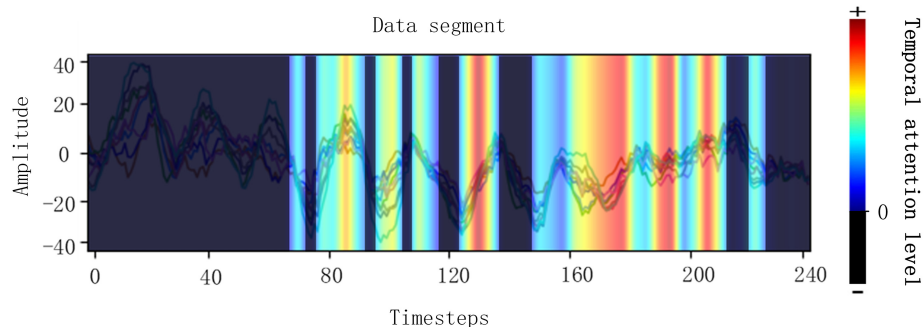
**Keywords:** electroencephalogram, motor imagery, 3D representation, multi-branch structure, two-stage refine filtering

## INTRODUCTION

Cerebral stroke (Albers and Olivot, 2007; Menon and Demchuk, 2011) is one of the most common diseases, and disorder in functions related to language and motor makes it hard for stroke patients to live a normal life. It is possible to recognize the intention of stroke patients with the development of brain-computer interface (BCI), which is based on the phenomenon of event-related synchronization (ERS) or event-related desynchronization (ERD) (Neuper et al., 2006; Wilson et al., 2019) in electroencephalogram (EEG) (Tanaka et al., 2005). In this case, the task of motor imagery (MI) classification (Qin et al., 2004; Herman et al., 2008; Taran and Bajaj, 2019; Kato et al., 2020) is carried out and a lot of achievements had been achieved. However, it is still a great



**FIGURE 1 |** The whole architecture of the two stage refine filtering method. The convolutional neural network of the first stage was the same as the one of the second stage.



**FIGURE 2 |** Visualizations of Grad-CAM for EEG signals. The bright regions mean EEG in this region contributes to correct classification results. The dark regions mean EEG in this region contributes a negative weight to correct classification results.

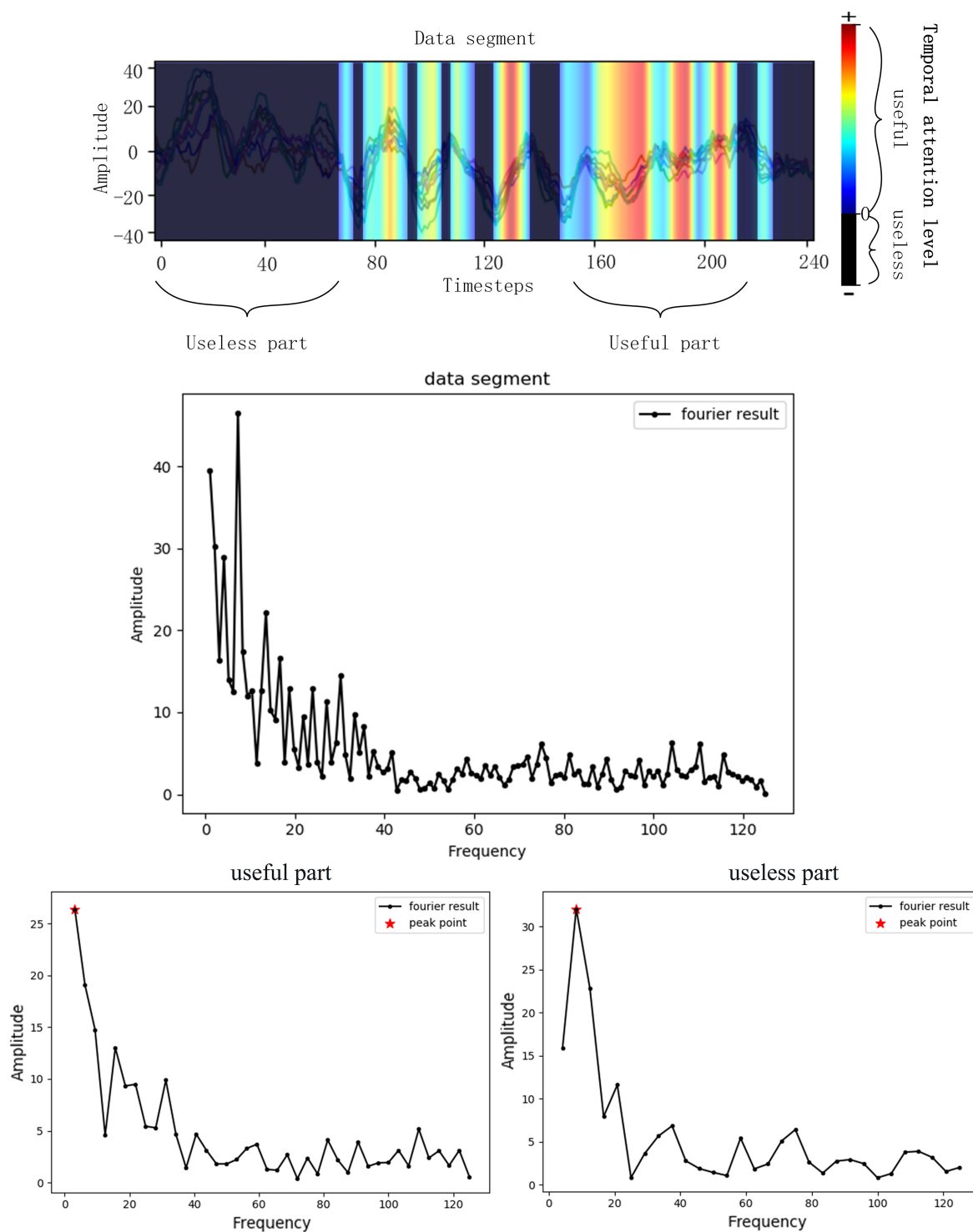
challenge to classify the EEG signals accurately. To enhance the accuracy of MI classification and consequently improve the performance of BCI (Schalk et al., 2004; Ge et al., 2019), a large amount of the methods had been proposed by researchers. All the MI classification methods can be generally divided into two categories: Common Spatial Pattern (CSP) (Kang et al., 2009; Lu et al., 2010)-based methods, such as Filter Bank Common Spatial Pattern (FBCSP) (Ang et al., 2012) and Common Spatio-Spectral Pattern (CSSP) (Lemm et al., 2005); and Deep learning based methods (Suwicha et al., 2014; Schirrmeister et al., 2017), such as C2CM (Sakhavi et al., 2018), Compact convolutional neural network (Lawhern et al., 2016), and shallow ConvNet (Schirrmeister et al., 2017).

No matter with which method to carry out MI classification, however, appropriate filtering, which suppresses high-amplitude noise and channel saturation, is also needed (Benigno et al., 2021). In FBCSP (Ang et al., 2012), nine band-pass filters covering the range of 4–40 Hz were used and a spatial filtering using the CSP method followed by each band-pass filter. Various

configurations proved to be as effective because these frequency ranges yielded a stable frequency response. Based on FBCSP, C2CM (Sakhavi et al., 2018) is a successful example that combines conventional method and deep learning. This method convolutes time features and spatial features separately, which achieved good performance but increased more parameters. Similarly, in shallow ConvNet (Schirrmeister et al., 2017), FBCSP was also adopted for data processing. A bandpass filtering and the CSP spatial filter are used in the network's first two layers. The classification results are then computed with the following convolution layers and pooling layers. It is more reasonable than FBCSP because the shallow ConvNet embedded all the computation process in one network and the parameters can be optimized together to acquire a better result. These methods have acquired a high accuracy of MI classification but no further study for the influence of filtering was carried out.

There are also several special filtering methods. In Schrödinger filtering (Benigno et al., 2021), gradient artifact spikes were removed and EEG signals were preserved and templates or





**FIGURE 3 |** Frequency selecting process. The Fourier transformer results of a data segment, a useless part of the segment and a useful part of the segment was presented. The frequency of peak point was the selected useful frequency or useless frequency.

references of the artifact or signal were used in this algorithm. Meanwhile, evoked activity was not affected in the filtering process, which proved the robustness of this method. However,

this method was based on the semi-classical signal analysis (SCSA), which is young and needs to be studied actively to acquire better performance. Bayesian filtering (Miran et al., 2018)

was a different filtering method that decoded real-time auditory attention from EEG and alleviated the need for large training datasets compared with other existing methods. This method is complicated in application to some extent. In clustering-based feature (Yu et al., 2020), the underlying structure of EEG data was explored and the data feature was optimized with a cluster-based multi-task learning algorithm that enhances the accuracy of classification. For the purpose of boosting the classification accuracy, a multi-scale optimization (MSO) of spatial patterns (Zhang et al., 2019; Jiao et al., 2020) was proposed, which optimizes filter bands via multi-view learning within CSP. This method also acquired good results in MI-related EEG datasets with the filtering method.

All the methods mentioned above tried to filter the EEG signals before MI classification, and these methods usually divided the filtering process into several steps, which seems to be complicated. In this study, a novel two-stage refine filtering method was proposed, inspired by the discussion of Gradient-weighted Class Activation Mapping (Grad-CAM) (Selvaraju et al., 2020) in our previous work (Xinqiao et al., 2019; Zhou et al., 2019), which proposed a 3D representation of EEG and constructed a multi-branch convolutional neural network for MI classification. Gradient-weighted Class Activation Mapping makes a good visual explanation by highlighting the important regions of predicted images according to the last convolutional layer of the network. In this case, we considered whether it is possible to improve the performance of our network by preserving the useful frequency (which means these frequencies contribute a lot to correct classification results) and suppress useless frequency (which means these frequencies contribute nothing to correct results).

The two-stage refine filtering method can be divided into two stages: In the first stage, raw EEG data were trained in the network and the frequency bands to be filtered were selected according to the Grad-CAM results of the last convolutional layers. In the second stage, the EEG data were filtered with the selected frequencies and put into the network again. This method was applied to the dataset of BCI competition IV-2a (Ang et al., 2012). The MI classification results of two stages were recorded and the result of the second stage was better than that of the first stage.

The remainder of this article is organized as follows. *Methods* gives a description of the MI classification strategy. The experiment and results are presented in *Experiment and Results*. The discussion is shown in *Discussion*. *Conclusion* concludes the article.

## MATERIALS AND METHODS

In this section, detailed configurations of the filtering method including the two-stage filtering process and the frequency selecting principles in this process are illustrated.

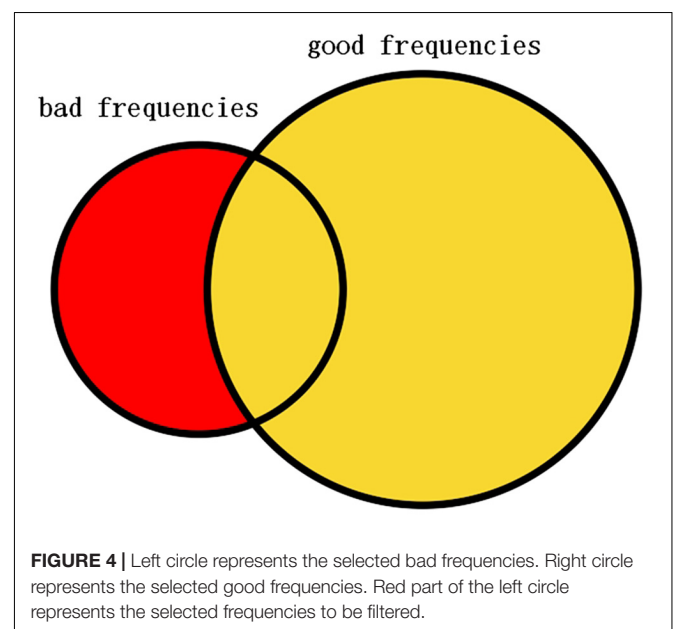
### Two-Stage Refine Filtering Process

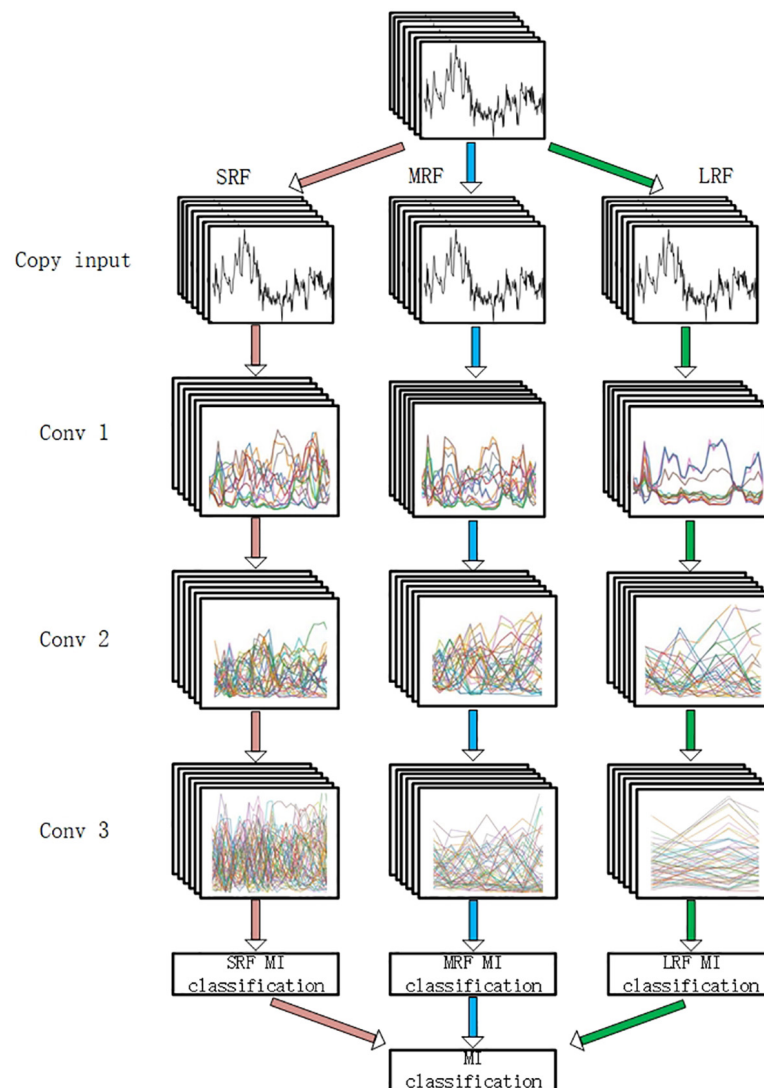
The whole process of this method is shown in **Figure 1**. The classification system was divided into two stages. In the first stage,

the EEG data without filtering were fed into a convolutional neural network to complete the first training and the weights were saved. The Grad-CAM results were acquired according to the feature maps and the MI classification results. Then, it can be figured out whether training data contribute a positive or negative weight to correct classification results. In the data processing process, the frequencies to be filtered were determined according to the Grad-CAM results and detailed frequency selecting principles are illustrated in the next section. In the second stage, the raw data were filtered with the frequencies selected according to the results of first stage. The filtered data were used as input in the second training process.

### Frequency Selecting Principles

After the first training process with the backbone network, the Grad-CAM, which is shown in **Figure 2**, is carried out to judge which part of a cropped data segment is beneficial to the correct results. The Grad-CAM was determined according to the classification results of the first stage and **Figure 2** shows that the signals with a bright color contribute to correct results and the signals with a dark color contribute nothing to correct results. The signals with a bright color were called useful data, which contribute a positive weight to correct classification results, and the dark one was called useless data, which contribute negative weights to correct results. Then, the data were transformed with Fourier transformation to extract frequency information. The frequency of useful data that contribute to correct results is named good frequency, and the frequency of useless data that contribute nothing to correct results is named bad frequency. It is obvious that different data samples have different random “useful” or “useless” time intervals and there are many intervals in each segment to be calculated. Considering the huge amount of training data, a tenth of the data were sampled for Grad-CAM.





**FIGURE 5 |** The backbone network. “SRF,” “MRF,” and “LRF” means three different branch networks with different receptive field. The input was copied as “copy input.” “Conv1,” “Conv2,” and “Conv3” mean three convolutional process. “SRF MI classification,” “MRF MI classification,” and “LRF MI classification” represents three classification results of three branches. The MI classification was computed according to three results.

### Details of the Selecting Process

As is introduced before, the EEG signals are assessed with Grad-CAM and then the bad and good frequencies of the signals are recorded, respectively, which is illustrated in **Figure 3**. A useless part of the data segment was Fourier transformed and the frequency with highest amplitude was recorded as the useless frequency considering that the frequency with the highest amplitude may be most representative. The useful part was processed the same as the useless part. The bad frequency data cannot just be filtered because many frequencies belong to both good and bad frequency due to the huge amount of EEG and the inaccuracy of the data acquisition process. The low frequencies will always be chosen due to the  $1/f$  characteristic of the power spectrum, and in this case, many low frequencies repeated in both good and bad frequencies. To get a better performance of the

network by filtering bad frequency, the bad frequency needs to be selected further according to its amount.

In this study, the selected frequencies were collected and the frequencies that belong to bad frequencies but do not belong to good frequencies are selected as the filtering frequency that is illustrated in **Figure 4**. The bad and good frequencies are sorted, respectively, in descending order according to their amount. To avoid filtering out useful signals, a small amount of the bad frequencies ranking ahead were selected and a large amount of the good frequencies ranking ahead were selected. Having tried several configurations, in this study, the top 20 bad frequencies are selected and the top 100 good frequencies are selected. Among the 20 bad frequencies, frequencies that do not belong to good frequencies are selected as the filtering frequency.

## EXPERIMENT AND RESULTS

### Experiment Setup

The methods proposed above are evaluated on BCI competition IV dataset 2a (Ang et al., 2012). The EEG dataset was recorded with 22 Ag/AgCl electrodes that are distributed according to the international 10–20 system. The data acquisition experiment prompts nine subjects to perform four different tasks named imagery movement of left hand, right hand, both feet, and tongue. For each subject, two sessions on different days were recorded and each session consists of 288 trials. Each trial belongs to one of the four classes and each trial consists of a fixation process of 2 s, a cue time of 1.25 s, and a MI time of 4 s; a short break followed after the MI process. A band-pass filter between 0.5 and 100 Hz was applied to the signals, and a notch filter of 50 Hz was taken to suppress line noise.

In this study, the 1.25-s period of EEG data after the visual cue was taken as experiment data. The EEG was then represented with the 3D representation method mentioned above and the label corresponding to the cropped EEG was presented with a one-hot-vector format.

To evaluate the experiment results, the 10-fold cross-validation method was used. All training data and testing data of BCI IV dataset 2a are combined and then divided into 10 subsets randomly. In each run, nine subsets were used to train and the other one was used as validation data. The final results were obtained by averaging 10 validation results. After the data was filtered, the filtered data were also evaluated with the above method. The *p*-values presented in the experiment were calculated from a two-tailed paired *t*-test.

### Backbone Network

To evaluate the filtering method, a MI classification structure is needed. In this study, a multi-branch convolutional neural network proposed in our former work (Xinqiao et al., 2019) was adopted. As is shown in **Figure 5**, our backbone network was made up of three CNNs with different receptive fields and the branches are, respectively, named small receptive field network (SRF), medium receptive field network (MRF), and large receptive field network (LRF). The input of the network was a concatenation of 22 electrode signals that contain both temporal and spatial information.

Three branches were fed, respectively, with 3D EEG proposed in our previous work and small convolutional filters are adopted in the light of VGG's architecture. Forward and back propagation is carried in different branches simultaneously and a soft-max (Liu and Liu, 2017) activation is set in the end of each branch. The final classification result is acquired by summing the branch networks' respective results and putting the summing result into an additional soft-max activation.

### Modification of Previous Network

In our previous study, it was discussed that different branches focus on different temporal information. For the purpose of recording each Grad-CAM result of all electrodes' signals in each branch and filtering them in each branch, the input needs

to be copied into three copies. In this circumstance, the first shared convolution layer of the previous network was replaced with three single convolution layers. To reduce the computation cost enhanced by this modification, the number of the dense layer's nodes was reduced. The convolution layer's parameters are presented in **Table 1**.

### Two-Stage Refine Training Evaluation MI Classification Experiments

The 10-fold validation results of the multi-branch network in the first stage and the second stage are presented in **Table 2**. In this table, MB-I represents the first classification stage and MB-II represents the second classification stage. MB-I and MB-II are two stages of one system whose former stage was fed with raw training data and the latter stage was fed with filtered training data. The results of the two stages were compared to determine whether the method can improve the classification results.

Comparing the results of nine subjects between MB-I and MB-II, it is obvious that all subjects with MB-II perform better

**TABLE 1** | Three convolution layers' parameters of three branches.

Conv layer	SRF	MRF	MRF
Conv1	Size: $3 \times 3 \times 5$ Strides: 2, 2, 4 Filters: 16	Size: $3 \times 3 \times 5$ Strides: 2, 2, 4 Filters: 16	Size: $3 \times 3 \times 5$ Strides: 2, 2, 4 Filters: 16
Conv2	Size: $2 \times 2 \times 1$ Strides: 2, 2, 1 Filters: 32	Size: $2 \times 2 \times 3$ Strides: 2, 2, 2 Filters: 32	Size: $2 \times 2 \times 5$ Strides: 2, 2, 4 Filters: 32
Conv3	Size: $2 \times 2 \times 1$ Strides: 2, 2, 1 Filters: 64	Size: $2 \times 2 \times 3$ Strides: 2, 2, 2 Filters: 64	Size: $2 \times 2 \times 5$ Strides: 2, 2, 4 Filters: 64

"Size" means the height, width, and depth of the 3D convolution window. "Strides" means the strides of the convolution window along each dimension. "Filters" means the number of output filters in each convolution layer.

**TABLE 2** | Comparison of 10-fold cross-validation results training with raw data and filtered data.

Subject	MB-I	MB-II
1	74.8125	75.3158
2	58.923	60.429
3	78.297	79.221
4	69.901	70.601
5	67.083	67.989
6	67.699	68.461
7	74.142	75.382
8	76.705	77.047
9	82.859	83.461
Mean	72.269	73.101
Standard deviation	7.156	6.937
<i>p</i> -value	1.3E-04	–

*p*-value means the significant difference of the cross-validation results carried by the same network training with raw data and filtered data.



than with MB-I on testing accuracy and the mean value of MB-II is nearly 1% higher than MB-I with  $p$ -value < 0.01. The standard deviation value of MB-I is 0.2% higher than MB-II, which means the filtered data are more stable than raw data in classification tasks.

### Learning Process Visualization

To explore the difference of learning process between raw data and filtered data, the data were trained for 30 epochs and the testing losses (the Negative log-likelihood cost) and accuracies of all subjects are monitored and recorded in **Figure 6**. The testing data were random one-fold data of each subject. MB-I represents the first classification stage and MB-II represents the second classification stage. The green line represents the loss in training process and the orange line represents the accuracy in training process. The left axis of each subplot represents the loss value of each subject and the right axis represents the accuracy value.

It is obvious that the accuracy of MB-II is higher than MB-I except for most subjects. For subject 4, the performances of the network evaluated with filtered data are outstanding with an accuracy of 4% higher than with raw data. Actually, the results of subject 4 ranges widely in the 10-fold validation

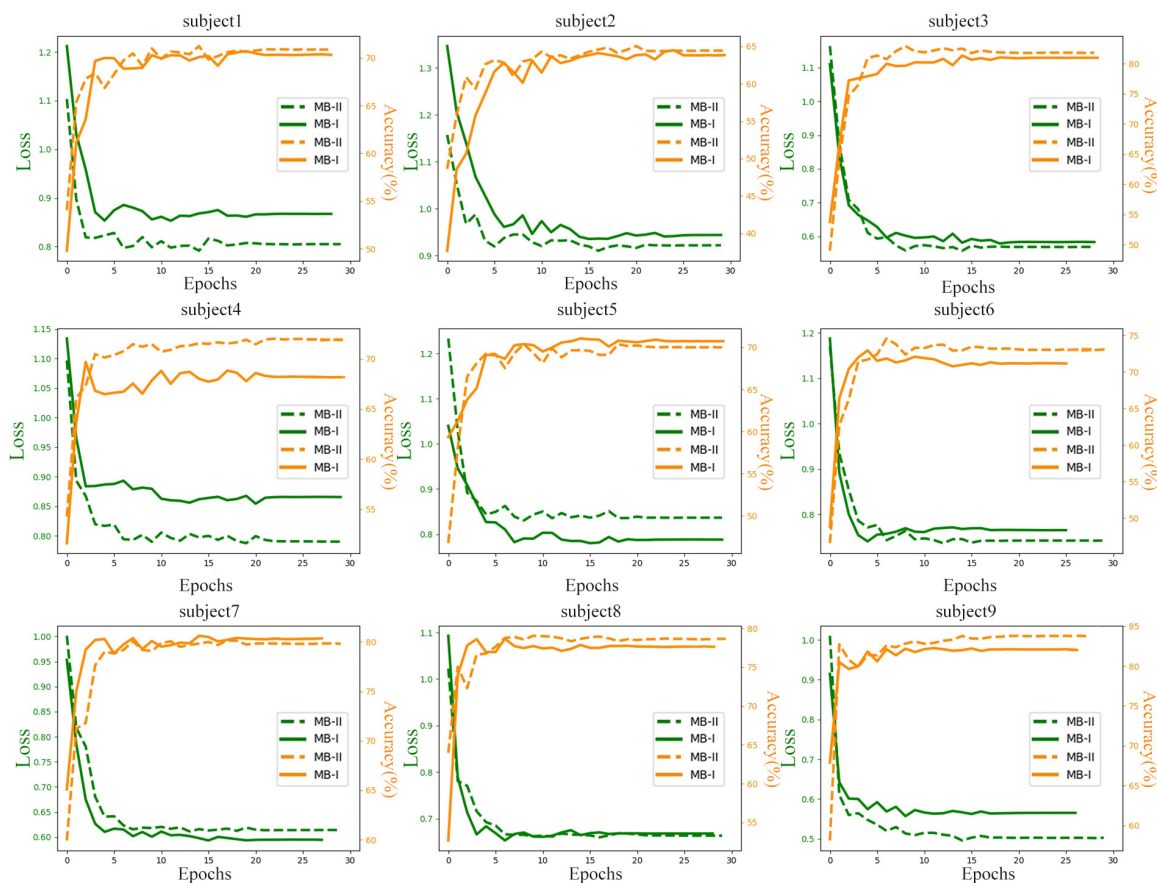
process, which means that the MB-II did not always perform much better in 10-fold validation results; however, the mean accuracy of MB-II was higher than MB-I as is illustrated in **Table 2**.

For subject 1, subject 6, and subject 8, the MB-II acquired a lower testing accuracy and a higher testing loss than MB-I in early epochs. However, in the end of the training process, the MB-II performed better than MB-I, which means the filtering method is useful for enhancing classification accuracy.

For subject 2 and subject 3, the accuracy of MB-I and MB-II is nearly the same but the network evaluated with filtered data acquired lower testing loss, which may benefit from filtering several bad frequencies.

### Comparison With the State-of-the-Art

Three state-of-the-art MI classification methods and our formal classification method are compared with the method proposed in this study. We firstly give a brief description of other methods having been introduced in the *Introduction* section and then analyze the kappa value (Lai et al., 2016; Wang et al., 2019) of different methods, which is defined to evaluate classification accuracy. Results of all methods are recorded in **Table 3**. “MB-M” represents the modified multi-branch network used in



**FIGURE 6 |** Test loss and accuracy of nine subjects in thirty epochs.

**TABLE 3** | Comparison of the kappa value with the state-of-the-art methods.

Subject	MB-M	MB	FBCSP	Shallow ConvNet	C2CM
1	0.698	0.699	0.68	0.820	0.833
2	0.523	0.459	0.42	0.432	0.537
3	0.787	0.788	0.75	0.835	0.87
4	0.629	0.594	0.48	0.621	0.556
5	0.669	0.647	0.40	0.490	0.5
6	0.622	0.538	0.27	0.380	0.273
7	0.642	0.653	0.77	0.898	0.861
8	0.746	0.702	0.76	0.758	0.778
9	0.825	0.713	0.61	0.657	0.727
Mean	0.682	0.644	0.571	0.655	0.659
Standard deviation	0.093	0.100	0.184	0.188	0.204

this study and “MB” represents the multi-branch network in our previous study.

**Filter Bank Common Spatial Pattern: FBCSP** was proposed in Ang et al. (2012) and is capable of autonomously selecting the proper subject-specific frequency range for bandpass filtering. The method performed best on the BCI Competition IV 2a dataset in competition.

**Shallow ConvNet** (Schirmer et al., 2017): Inspired by FBCSP, the network adopts bandpass and CSP spatial filters in the first two layers so as to optimize all parameters jointly.

**C2CM** (Sakhavi et al., 2018): C2CM adopts the strategy of breaking up 2D convolutions into two 1D convolutions and filtering data with FBCSP. This method makes the network more flexible for separating the information of time and space but increases the computation parameters for an additional layer.

As is shown in **Table 3**, the kappa value of MB-M is higher than MB for most subjects. For subject 6 and subject 9, the kappa value of MB-M is nearly 1% higher than MB, which reveals the advantage of the two-stage refine training method. The MB-M also outperforms other state-of-the-art methods with a higher mean value and a lower standard deviation value. For subject 9, the kappa value of MB-M was much higher than other methods, which means several vital bad frequencies were filtered in the second stage.

## DISCUSSION

The proposed two-stage refine filtering method, which is inspired by Grad-CAM, was novel and proved to improve the performance of the multi-branch network proposed in our previous study. In the field of MI classification, correct filtering suppresses the influence of noise and makes the feature extracting process easier. Consequently, the MI classification results are improved. According to the experiment results, it can be inferred that the filtered training data are more stable than the raw training data and the method is robust in different subjects.

It is special for this method to improve the performance of a network according to its mechanism. In other words, the method improves the classification results according to the characteristics

of training data with little artificial intervention. In this case, the filtering method could be commonly used in the majority of deep learning-related tasks. To further evaluate the method, the filtering method can be applied to different EEG-related networks proposed by others. Moreover, the method should not only be effective on MI classification since the filtering range is selected according to the performance of the network. Similarly, applying the method to other fields such as voice processing is an advisable attempt.

It is also worth mentioning that this method is actually an iterable process, which means we can filter the data after the last training process according to the Grad-CAM of the last classification results. However, multiple iterations may lead to overfitting in the training process and thus influence the correct MI classification. In this case, an appropriate amount of frequencies to be filtered is needed and higher accuracy of MI classification may be acquired in this way.

## CONCLUSION

In this study, a two-stage refine filtering method was proposed for MI classification inspired by Grad-CAM. The method was applied to the multi-branch network and proved to improve the performance of the network. This method is considered as a universal method and promising in many other fields.

## DATA AVAILABILITY STATEMENT

The original contributions presented in the study are included in the article/**Supplementary Material**, further inquiries can be directed to the corresponding author/s.

## AUTHOR CONTRIBUTIONS

All authors listed have made a substantial, direct and intellectual contribution to the work, and approved it for publication.

## FUNDING

This research was funded by the National Natural Science Foundation of China (grant numbers U1713218 and U1613224).

## ACKNOWLEDGMENTS

Our deepest gratitude goes to the reviewers and guest editor for their careful work and thoughtful suggestions that have helped to improve this article substantially.

## SUPPLEMENTARY MATERIAL

The Supplementary Material for this article can be found online at: <https://www.frontiersin.org/articles/10.3389/fnins.2021.657540/full#supplementary-material>

## REFERENCES

- Albers, G. W., and Olivot, J. M. (2007). Intravenous alteplase for ischemic stroke. *Lancet* 369, 249–250.
- Ang, K. K., Chin, Z. Y., Wang, C., Guan, C., and Zhang, H. (2012). Filter bank common spatial pattern algorithm on BCI competition IV datasets 2a and 2b. *Front. Neurosci.* 6:39. doi: 10.3389/fnins.2012.00039
- Benigno, G. B., Menon, R. S., and Serrai, H. (2021). Schrödinger filtering: a precise EEG despiking technique for EEG-fMRI gradient artifact. *NeuroImage* 226:117525. doi: 10.1016/j.neuroimage.2020.117525
- Ge, S., Jiang, Y., Wang, P., Wanga, H.-X., and Zheng, W.-M. (2019). Training-free steady-state visual evoked potential brain-computer interface based on filter bank canonical correlation analysis and spatiotemporal beamforming decoding. *Neural Syst. Rehabil. Eng IEEE Trans* 99:1.
- Herman, P., Prasad, G., McGinnity, T. M., and Coyle, D. (2008). Comparative analysis of spectral approaches to feature extraction for EEG-based motor imagery classification. *IEEE Trans. Neural Syst. Rehabil. Eng.* 16, 317–326. doi: 10.1109/tnsre.2008.926694
- Jiao, Y., Zhou, T., Yao, L., et al. (2020). Multi-view multi-scale optimization of feature representation for EEG classification improvement. *IEEE Trans. Neural Syst. Rehabil. Eng.* 28, 2589–2597. doi: 10.1109/tnsre.2020.3040984
- Kang, H., Nam, Y., and Choi, S. (2009). Composite common spatial pattern for subject-to-subject transfer. *IEEE Signal Process. Lett.* 16, 683–686. doi: 10.1109/lsp.2009.2022557
- Kato, M., Kanoga, S., Hoshino, T., and Fukami, T. (2020). “Motor imagery classification of finger motions using multiclass CSP” in *Proceedings of the 2020 42nd Annual International Conference of the IEEE Engineering in Medicine and Biology Society (EMBC) in conjunction with the 43rd Annual Conference of the Canadian Medical and Biological Engineering Society IEEE, 2020*, (Montreal, QC).
- Lai, T.-S., Mittal, H., Chao, W.-A., and Wu, Y. M. (2016). Study on Kappa value in Taiwan using borehole and surface seismic array *Bull. Seismol. Soc. Am.* 106, 1509–1517.
- Lawhern, V. J., Solon, A. J., Waytowich, N. R., Gordon, S. M., Hung, C. P., and Lance, B. J. (2016). EEGNet: a compact convolutional network for EEG-based brain-computer interfaces. *J. Neural Eng.* 15, 056013.1–056013.17.
- Lemm, S., Blankertz, B., Curio, G., and Müller, K.-R. (2005). Spatio-spectral filters for robust classification of single trial EEG. *IEEE Trans. Biomed. Eng.* 52, 1541–1548. doi: 10.1109/tbme.2005.851521
- Liu, Y., and Liu, Q. (2017). “Convolutional neural networks with large-margin softmax loss function for cognitive load recognition,” in *Proceedings of the 2017 36th Chinese Control Conference (CCC) 2017*, Dalian.
- Lu, H., Eng, H.-L., Guan, C., Plataniotis, K. N., and Veentsanopoulos, A. N. (2010). Regularized common spatial pattern with aggregation for EEG classification in small-sample setting. *IEEE Trans. Bio-Med. Eng.* 57, 2936–2946. doi: 10.1109/tbme.2010.2082540
- Menon, B. K., and Demchuk, A. M. (2011). Computed tomography angiography in the assessment of patients with stroke/TIA. *Neurohospitalist* 1, 187–199. doi: 10.1177/1941874411418523
- Miran, S., Akram, S., Sheikhattar, A., Simon, J. Z., Zhang, T., and Babadi, B. (2018). Real-time decoding of auditory attention from eeg via bayesian filtering. *Annu. Int. Conf. IEEE Eng. Med. Biol. Soc.* 2018, 25–28.
- Neuper, C., Wrtz, M., and Pfurtscheller, G. (2006). ERD/ERS patterns reflecting sensorimotor activation and deactivation. *Prog. Brain Res.* 159, 211–222. doi: 10.1016/s0079-6123(06)59014-4
- Qin, L., Ding, L., and He, B. (2004). Motor imagery classification by means of source analysis methods. *J. Neural Eng.* 1, 135–141. doi: 10.1088/1741-2560/1/3/002
- Sakhavi, S., Guan, C., and Yan, S. (2018). Learning temporal information for brain-computer interface using convolutional neural networks. *IEEE Trans. Neural Netw. Learn. Syst.* 29, 5619–5629. doi: 10.1109/tnnls.2018.2789927
- Schalk, G., McFarland, D. J., Hinterberger, T., Birbaumer, N., and Wolpaw, J. R. (2004). BCI2000: a general-purpose brain-computer interface (BCI) system. *IEEE Trans. Biomed. Eng.* 51, 1034–1043. doi: 10.1109/tbme.2004.827072
- Schirmer, R. T., Gemein, L., Eggensperger, K., Hutter, F., and Ball, T. (2017). Deep learning with convolutional neural networks for decoding and visualization of EEG pathology. *Hum. Brain Mapp.* 38, 5391–5420. doi: 10.1002/hbm.23730
- Selvaraju, R. R., Cogswell, M., Das, A., Vedantam, R., Parikh, D., Batra, D., et al. (2020). Grad-CAM: visual explanations from deep networks via gradient-based localization. *Int. J. Comp. Vis.* 128, 336–359. doi: 10.1007/s11263-019-01228-7
- Suwicha, J., Setha, P. N., and Pasin, I. (2014). EEG-based emotion recognition using deep learning network with principal component based covariate shift adaptation. *Sci. World J.* 2014:627892.
- Tanaka, K., Matsunaga, K., and Wang, H. O. (2005). Electroencephalogram-based control of an electric wheelchair. *IEEE Trans. Robot.* 21, 762–766. doi: 10.1109/tro.2004.842350
- Taran, S., and Bajaj, V. (2019). Motor imagery tasks-based EEG signals classification using tunable-Q wavelet transform. *Neural Comput. Appl.* 31, 6925–6932. doi: 10.1007/s00521-018-3531-0
- Wang, J., Yang, Y., and Xia, B. (2019). A simplified Cohen’s Kappa for use in binary classification data annotation tasks. *IEEE Access* 99:1.
- Wilson, R., Mullinger, K. J., Francis, S. T., and Mayhew, S. D. (2019). The relationship between negative BOLD responses and ERS and ERD of alpha/beta oscillations in visual and motor cortex. *NeuroImage* 199, 635–650. doi: 10.1016/j.neuroimage.2019.06.009
- Xinqiao, Z., Hongmiao, Z., Guilin, Z., Fengxiang, Y., and Shaolong, K. (2019). A multi-branch 3D convolutional neural network for EEG-based motor imagery classification. *IEEE Trans.* 27, 2164–2177.
- Yu, Z., Zhou, T., Wu, W., Xie, H., Zhu, H., Zhou, G., et al. (2020). Improving EEG decoding via clustering-based multi-task feature learning. *arXiv*.
- Zhang, X., Yao, L., Wang, X., Monaghan, J., McAlpine, D., Zhang, et al. (2019). A survey on deep learning based brain computer interface: recent advances and new frontiers. *J. Neural Eng.* 18:031002.
- Zhou, H., Zhao, X., Zhang, H., and Kuang, S. (2019). “The mechanism of a multi-branch structure for EEG-based motor imagery classification,” in *Proceedings of the 2019 IEEE International Conference on Robotics and Biomimetics (ROBIO)*, Piscataway, NJ: IEEE.

**Conflict of Interest:** The authors declare that the research was conducted in the absence of any commercial or financial relationships that could be construed as a potential conflict of interest.

**Publisher’s Note:** All claims expressed in this article are solely those of the authors and do not necessarily represent those of their affiliated organizations, or those of the publisher, the editors and the reviewers. Any product that may be evaluated in this article, or claim that may be made by its manufacturer, is not guaranteed or endorsed by the publisher.

Copyright © 2021 Yan, Zhou, Huang, Cheng and Kuang. This is an open-access article distributed under the terms of the Creative Commons Attribution License (CC BY). The use, distribution or reproduction in other forums is permitted, provided the original author(s) and the copyright owner(s) are credited and that the original publication in this journal is cited, in accordance with accepted academic practice. No use, distribution or reproduction is permitted which does not comply with these terms.



# An Improvement of Robot Stiffness-Adaptive Skill Primitive Generalization Using the Surface Electromyography in Human–Robot Collaboration

Yuan Guan, Ning Wang and Chenguang Yang\*

*Bristol Robotics Laboratory, University of the West of England, Bristol, United Kingdom*

## OPEN ACCESS

### Edited by:

Hong Cheng,  
University of Electronic Science and  
Technology of China, China

### Reviewed by:

Mingchuan Zhou,  
Technical University of Munich,  
Germany  
Shuai Li,  
Swansea University, United Kingdom

### \*Correspondence:

Chenguang Yang  
cyang@ieee.org

### Specialty section:

This article was submitted to  
Neural Technology,  
a section of the journal  
Frontiers in Neuroscience

**Received:** 14 April 2021

**Accepted:** 06 August 2021

**Published:** 14 September 2021

### Citation:

Guan Y, Wang N and Yang C (2021)  
An Improvement of Robot  
Stiffness-Adaptive Skill Primitive  
Generalization Using the Surface  
Electromyography in Human–Robot  
Collaboration.  
*Front. Neurosci.* 15:694914.  
doi: 10.3389/fnins.2021.694914

Learning from Demonstration in robotics has proved its efficiency in robot skill learning. The generalization goals of most skill expression models in real scenarios are specified by humans or associated with other perceptual data. Our proposed framework using the Probabilistic Movement Primitives (ProMPs) modeling to resolve the shortcomings of the previous research works; the coupling between stiffness and motion is inherently established in a single model. Such a framework can request a small amount of incomplete observation data to infer the entire skill primitive. It can be used as an intuitive generalization command sending tool to achieve collaboration between humans and robots with human-like stiffness modulation strategies on either side. Experiments (human–robot hand-over, object matching, pick-and-place) were conducted to prove the effectiveness of the work. Myo armband and Leap motion camera are used as surface electromyography (sEMG) signal and motion capture sensors respective in the experiments. Also, the experiments show that the proposed framework strengthened the ability to distinguish actions with similar movements under observation noise by introducing the sEMG signal into the ProMP model. The usage of the mixture model brings possibilities in achieving automation of multiple collaborative tasks.

**Keywords:** learning from demonstration, human-robot collaboration, Imitation learning, surface electromyography signal, human-like stiffness adaptation, action recognition, robot skill generalization, decision-making

## 1. INTRODUCTION

According to current trends, robots are more applicable in factories, medical, social service, and other domains and will become more extensive. More and more industries consider or have established complete autonomous robot systems or human–robot collaboration platforms to replace human labor entirely with machines or assist people in their work. This benefited from the development of robotics, communication, and artificial intelligence technologies, which indicates that robots will considerably liberate part of the labor in high-repetition, high-fatigue works. It provides services autonomously in more complex work scenarios and may require collaborating with multiple agents, such as the assembly of 3C products, robot-assisted surgery, and physical and social assistance. Typically, collaborative scenes that involve multiple agents tend to have relatively complex environmental conditions and great diversity of tasks (Villani et al., 2018). Only



by improving the accuracy of robot decision making and proffering it good adaptability and safety can it meet the ever-increasing demand in the future. Robot Imitation Learning [i.e., Learning from Demonstration (LfD)] dramatically improved robot pre-programming efficiency (Argall et al., 2009). People are transferring knowledge to the robot by endowing robots the ability to imitate via human demonstrations. This is a more intuitive and convenient way of teaching/programming. Because LfD modularizes skills, it simplifies the re-programming process when switching between work content and scenes. It does not require people with expertise in robots and computing to design task-dedicated programs.

In the previous literature, the demonstration-based robot skill learning framework usually comprises the following three processes: (1) human skill demonstrations; (2) skill mathematical expression and modeling; (3) skill reproduction and generalization. While demonstrating, the demonstrator selects the appropriate demonstration interface. Under typical circumstances, the interfaces are divided into three principal categories: kinesthetic teaching, teleoperation, and passive observation. Different interfaces have their advantages and limitations (Billard et al., 2016). The experiments conducted in this article employ the teleoperation method. Demonstrator using this method usually only pays attention to the movement of the robot end-effector and ignores the preceding joints. Nevertheless, because the movement of the demonstrator is less physically restricted, which makes it more flexible. This article presents a novel framework that improves the skill generalization efficiency and accuracy, and we exploit the benefits from bioelectrical signals like electromyography to better infer human intents and transfer human stiffness regulation strategy to the robot, which highly relates to processes 2 and 3 mentioned above.

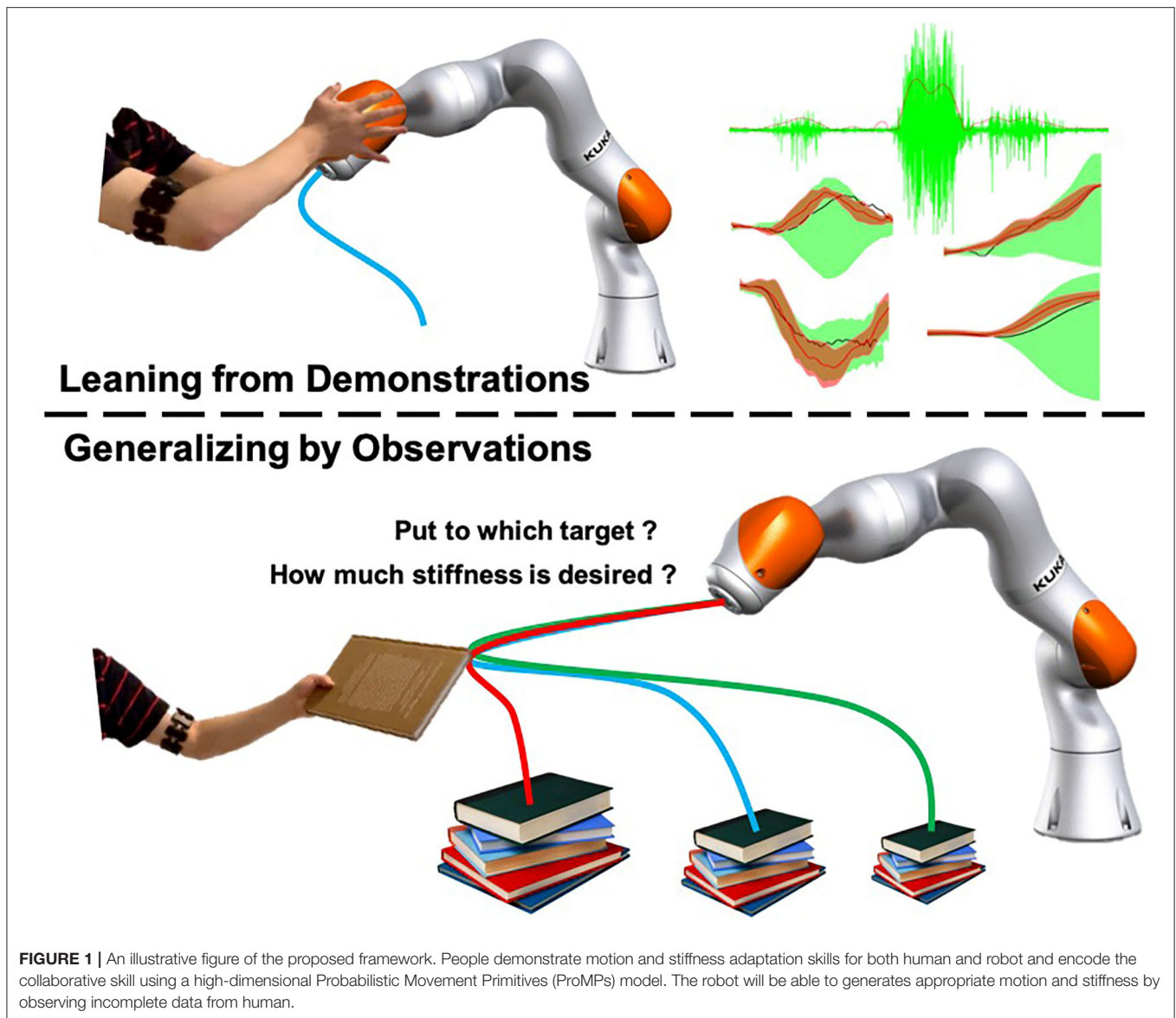
Stiffness is critical in robot dynamics that studies the relationship between force and motion. Hogan first proposed the theory of impedance control in 1985 (Hogan, 1985). It has been used until now. Impedance control and admittance control are now the most important controller types that realize the simultaneous control of the robot end-effector (or joint) position and contact force. It makes the robot's flexible operation possible and ensures the safety of human co-workers to the greatest extent. In addition to safety factors, the stiffness control also relates to the robot's success rate in performing tasks, especially when it is in direct physical contact with people, objects, or the external environment, and the force is as important as the position target (Migliore et al., 2005). **Figure 1** shows an interesting example problem that will arise in human-robot collaboration. Suppose we use the existing LfD framework to teach the robot a bunch of modularized and synthesized primitives. How will the robot select the appropriate skills from the skill library based on the current environment and the human co-worker's behavioral intentions and then generalize it to the correct goal? For example, after the robot acquires the ability to distribute books, can it accurately determine which stack of books to place the book on and plan a stable motion trajectory and a human-like stiffness regulation strategy? Most of the previous works divide human-robot collaboration problems into two independent parts: human action recognition and robot motion generation. This article

proposes a framework based on the Probabilistic Movement Primitives (ProMPs) (Paraschos et al., 2013), which adopt a unified motion-stiffness skill expression that combines human action recognition and motion generation "organically."

It is challenging that the robot cognition development meets our expectations, which can handle scenarios with a complexity level that a human found straightforward. A collaboration-enabled robot system will understand human behavior intent and then respond accordingly, where the human intention is partially embedded in the motion information itself. To not affect human movement, passive observation methods are commonly used to capture human movement information, such as a marker-based tracking system (Moeslund et al., 2006). However, phenomena such as occlusion, corrupted body tracking data due to the extremely unstructured environment, or computing power insufficiency may cause temporary observation loss or instability problems (Rabbi and Ullah, 2013). When two different motions quantified under the same sensor resolution scale are similar, the skill primitive similarity level increases. Moreover, the inevitable observation noise further aggravates the uncertainty of robots in identifying human action intents. These facts may eventually cause robots to generate unreliable reactions, which significantly reduces work efficiency; if such skill transfer technology is applied to robot-assisted surgery, it may even cause catastrophic danger. Hence, we aim to promote the collaboration capability in complex scenarios by seeking compliant physical interaction solutions with better decision making to further improve the existing LfD frameworks.

Using (surface) electromyography (i.e., sEMG) signals to predict human intentions and control robots is not a novel idea (Li et al., 2017; Chen et al., 2020a). Extracting the sEMG signal during natural human actions as an additional feature for skill expression, especially when interacting with robots or the environment, helps improve the resolution of human intention prediction results. We will use appropriate methods to extract useful information from a relatively high noise level and exploit it. Gomi and Osu (1998) examined the limb joint stiffness coefficients between shoulder and elbow; it shows that the stiffness is linear to the joint torque of the preceding joint. Burdet et al. (2000) developed a method to visualize the impedance change with respect to motion by introducing small positional displacement to human and measure the restoring elastic force. Yang et al. (2011) studied the human stiffness adaptation strategy using a well-designed experiment and revealed the possibility of transferring human stiffness adaptation skills to robots. Yang et al. (2018) later propose to use the stiffness trajectory estimated by sEMG signal to model dynamical movement primitives (DMPs). It successfully transfers the human-like stiffness regulation strategy from humans to a Baxter robot, and the framework was validated by designing cucumber-cutting and button-pushing experiments. Yu et al. (2019) then design a human-robot collaborative sawing system based on the sEMG-stiffness mapping to increase the efficiency and produce a smoother wood cutting section area.

In the previous work (Yang et al., 2018), the stiffness trajectory's generalization target was defined manually, which is empirical and biased. The reason behind this limitation is



that the DMPs skill modeling technique does not reflect the coupling between motion and stiffness. Users have to manually tune the parameters for each separated DMPs or modify the DMPs expression by adding additional coupling terms, making DMPs representation not compact anymore. Very recently, Zeng et al. (2020) propose to use hidden semi-Markov models (HSMMs) and Gaussian mixture regression (GMR) to offer the capability of capturing the correlation between position, speed, and stiffness. This article proposes an entirely different approach, which is easier to understand and implement, and also suitable for human-robot collaboration. Our proposed framework has the following advantages and contributions:

- Compared to Yang et al. (2018), our framework naturally extracts the coupling between position and stiffness, which is not artificially defined with bias.
- It triggers accurately generalized robot action by observing (incomplete) human data, which is more intuitive and natural, and considers human-in-the-loop.
- We exploit sEMG-stiffness mapping for collaboration tasks so that variable stiffness regulation is achieved. The action generalization becomes more robust to the observation noise from the motion tracking system.
- Using a mixture model to learn multiple non-linear correlated skill primitives, which not only increases the diversity of the skill library but also reduces the human effort in the skill demonstration phase since similar actions are automatically sorted out.

The remaining sections of this article are structured as follows. In section 2, we introduce the basic foreknowledge about ProMP and the other methods like sEMG-stiffness mapping,

ProMP modulation, and mixture model, which help to build the proposed framework. Section 3 introduce the setup of three experiments to verify the performance. And the results and discussions can be found in section 4. We list the future works in section 5 and make a final conclusion in section 6.

## 2. MATERIALS AND METHODS

There are plenty of ways to express skills. Modeling a skill means synthesizing the pattern of variation for each degree of freedom of various modalities involved at the trajectory level and representing them in a more compact and utilizable way. When using different mathematical tools to promote skills modeling, each expression model naturally incorporates the tool's capabilities. Thus, the corresponding tool limitations would also apply, which provide each skill modeling technique its own usage, functionalities, and possibilities. Generally, methods of skill modeling usually fall into one of two categories, dynamical system based or probabilistic approach based.

DMPs as the most well-known dynamical system-based modeling approach first officially proposed in 2003 (Schaal et al., 2003), and the procedure was then modified and improved by numerous researchers (Ijspeert et al., 2013; Wang et al., 2016; Ugur and Girgin, 2020). DMPs earn benefits from the robust and converge-definite characteristics of the second-order spring-damper system, and the flexibility of modification by using additional forcing terms in the dynamical equation as the system's variable virtual external force to encode a motion trajectory. The patterns of the trajectories are commonly encoded using Locally weighted regression (LWR) (Atkeson et al., 1997), which is a technique that well trade off the training time and non-linearity feature comparing to other conventional regression techniques.

Unlike DMPs, which is suitable for single demonstration modeling (i.e., one-shot learning) and learning control directly, another broad category probabilistic approach is to build a statistical model of the training information obtained through multiple demonstrations (or single demonstration). Typically, the utilization of probability theory allows the system to be more flexible in generalization, hence produces more interesting results that facilitate task planning in a higher abstraction level. Gaussian mixture model (GMM) (Hersch et al., 2008) turns both temporal information and other higher dimensional spatial information into a multi-variant Gaussian distribution containing multiple models. GMR (Khansari-Zadeh and Billard, 2011) practices the basic probability distribution operations in probability theory. The conditional probability of the Gaussian distribution and the superposition of the distribution are performed in turn to reproduce or generalize the skill from a trained GMM.

The uniqueness of DMP is not using LWR to learn weights for a bunch of radial basis functions but is the stability induced by the second-order dynamical equation. The learning speed of LWR becomes slower when the data becomes more and larger in size. Hence, to retain the advantages of using dynamical equations and speed-up, GMM-GMR can replace LWR (Calinon et al., 2012). Instead, it learns the joint distribution of the forcing term and time (i.e., the phase variable,  $s$ ) of each degree of

freedom, and expresses it in a GMM. Compared with GMM, the time series expressed by the Markov chain. The Markov chain encapsulates GMM or single multivariate-Gaussian in each state node and considers the transition probability between each state node. The hidden Markov model (HMM) and HSMM attach hidden variables and observation probabilities to the Markov chain (Zeeustraten et al., 2016). The duration of each state of HMM is implicitly encoded in the self-transition probability, while HSMM uses a duration probability to explicitly represent. Nevertheless, these kinds of implementations based on the Expectation-Maximization (EM) algorithm (Chernova and Veloso, 2007) may encounter local optima problems, especially when the data dimension is very high, or when the demonstration data are non-linearly correlated. But that would not be a severe problem since skill training can always be done offline.

Gaussian process regression (GPR) (Forte et al., 2012) is a very generic, powerful yet brute-force probabilistic modeling method, which utilizes mean plus noises to represent a high-dimensional function. Although this method captures the coupling relationship between each degree of freedom by a very large covariance Gram matrix and generalizes the skill base on the conditional probability of the given observation value, it is prone to the temporal/spatial variability during demonstrations. Hence, it requires more demonstrations to obtain a smooth trajectory. ProMPs was formally proposed by Paraschos et al. (2013) in 2013. It is a model that combines the ideas of DMPs-LWR and the probabilistic approaches. It interprets the high-dimensional trajectory using weighted basis functions and computes the Gaussian process regression model in the weight space. This idea of using probabilistic methods in a more abstracted space of the trajectory makes the production of generalized trajectories more flexible, and the expression structure is more compact.

Most of the existing human-robot skill transfer frameworks still relying on humans to choose appropriate skill primitive among the learned primitive library, and pre-defined a generalization target. Calinon et al. (2007) propose to couple the robot with the environment (e.g., using robot-object relative position) directly and train the skill model, thereby avoiding the problem of manual selection of generalization targets. Mülling et al. (2013) put forward the concept of query for generalization and propose a Mixture of Motor Primitive (MoMP). For tasks like robot table tennis or other difficult tasks, a robot may need to switch between/combine different motion styles to complete. MoMP establishes a gating network, which adapts the styles according to queries and performs superposition among each style to generalize tasks and adapt to new scenarios. Many researchers treat action recognition and skill generalization as two separated sequential procedures and use two different models; however, our work that is inspired by "query" treats two procedures as a whole and realizes generalization using ProMPs and other techniques introduced in later sections.

### 2.1. Probabilistic Movement Primitives

ProMPs encode the pattern of a high dimensional trajectory. The value of each degree of freedom (DoF) on the trajectory at time  $t$  is defined as  $p_t$ . For a trajectory with a temporal length of  $T$  (i.e., the trajectory was sampled at number  $T$  of points), the whole

trajectory is then the data points assembly  $\mathbf{p}_{1:T} = \{p_t\}_{t=1:T}$ . The ProMP model is a probability density function that indicates the value and changing rate distribution along the single high-dimensional trajectory. The trajectory value and the changing rate at time  $t$  were defined in the following generic form:

$$\zeta_t = \begin{bmatrix} p_t \\ \dot{p}_t \end{bmatrix} = \Phi_t \omega + \epsilon_{\zeta_t}, \quad (1)$$

where  $\Phi_t = [\psi_t \ \dot{\psi}_t]^T$ , which is the Gaussian basis value matrix at time  $t$ . It concatenates the value and changing rate of all basis function at time  $t$ .  $\omega$  is the weighting matrix, indicating the weight of each basis function.  $\Phi_t$  and  $\omega$  are of the dimensionality of  $\mathbb{R}^{2 \times K}$  and  $\mathbb{R}^{K \times 1}$ , respectively, where  $K$  is the number of basis functions pre-determined by the user.  $\epsilon_{\zeta_t} \sim \mathcal{N}(\mathbf{0}, \Sigma_{\zeta_t})$  represents the Gaussian noise at time  $t$  that embraces all the possibilities of executing this trajectory in the form of a covariance,  $\Sigma_{\zeta_t} \in \mathbb{R}^{2 \times 2}$ . This paper assuming the most common basis type—Gaussian basis—was used to model non-periodic skills as shown in **Figure 2**; other basis like Fourier basis and Bezier curve basis are also applicable.

$$p(\zeta_{1:T} | \omega) = \prod_t \mathcal{N}(\zeta_t; \Phi_t \omega, \Sigma_{\zeta_t}) \quad (2)$$

Equation (2) describes the probability of a trajectory  $\mathbf{p}_{1:T}$  conditioned on certain weighting matrix  $\omega$ , which is the product of  $p(\zeta_t | \omega)$  from time 1 to  $T$ . Similar to DMPs that utilizes a temporal scaling factor and a phase variable to control the skill execution rate and represent skill completion status (Ijspeert et al., 2013), the vanilla ProMP model also uses an arbitrary monotonically increasing function  $s(t)$  as a phase variable, which interprets movement completion status and decouples movement from time (Paraschos et al., 2018). The focus of this article is not on the changes in skill execution speed or temporal modulation, hence a linear time-phase mapping [i.e.,  $s(t) = t/T$ ] was adopted. To simplify it, we use  $(\cdot)_t$  to represent a variable at phase  $s(t)$ .

The term “Probability” in the ProMP model originated from the fact that it relies on statistics of multiple demonstrations to improve other movement primitives like DMPs that do not model the correlation between values, rates, and time. It condenses useful information from the raw data and shrinks the data structure to output a more compact form as a single skill primitive representation. The full training set of  $N$  demonstrations is defined as  $\zeta_{1:T}^{1:N} = [\zeta_{1:T}^1 \dots \zeta_{1:T}^N]^T$ , where  $\zeta_{1:T}^{(n)}$  indicates the whole trajectory of the  $n$ -th demonstration. Hence, we are expected to learn a series of weights  $\omega^{1:N} = [\omega^1 \dots \omega^N]^T$  for all demonstrations, where  $\omega^{(n)}$  would be the weights learned using the  $n$ th demonstration.

The essence of the original ProMP is to create a distribution over all the possible weights, so that  $\omega \sim \mathcal{N}(\omega; \mu, \Sigma)$ , where  $\mu = E(\omega^{1:N}) \in \mathbb{R}^{K \times 1}$  and  $\Sigma = \text{Cov}(\omega^{1:N}) \in \mathbb{R}^{K \times K}$ . The

probability of seeing the whole trajectory is computed by

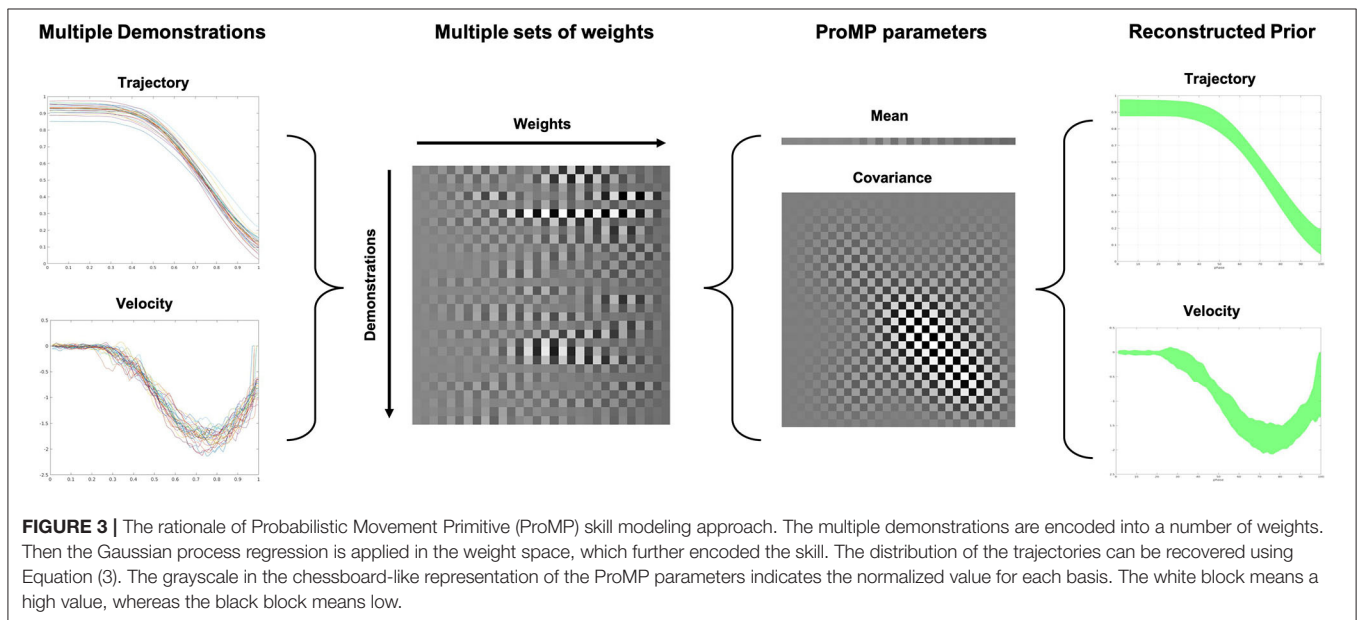
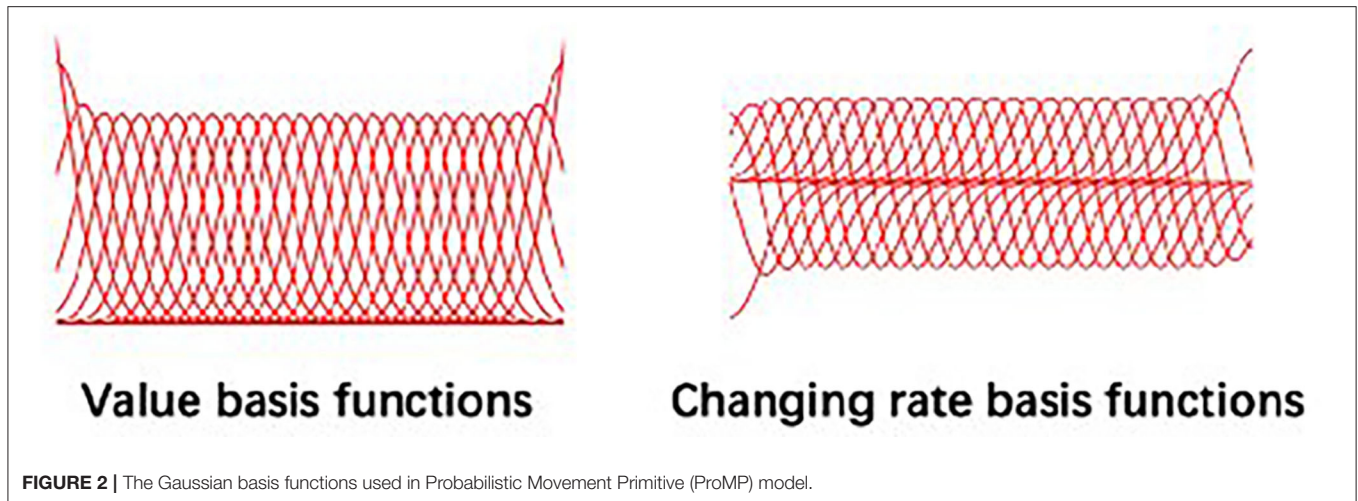
$$\begin{aligned} p(\zeta_{1:T}; \mu_{\zeta}^{1:T}, \Sigma_{\zeta}^{1:T}) &= \int \mathcal{N}(\zeta_{1:T} | \Phi_{1:T} \omega, \Sigma_{\zeta}) \mathcal{N}(\omega; \mu, \Sigma) d\omega \\ &= \mathcal{N}(\zeta_{1:T}; \Phi_{1:T} \mu, \Phi_{1:T} \Sigma \Phi_{1:T}^T + \Sigma_{\zeta}), \end{aligned} \quad (3)$$

where  $\mu_{\zeta}^{1:T} \in \mathbb{R}^{T \times 2}$  and  $\Sigma_{\zeta}^{1:T} \in \mathbb{R}^{T \times T}$  are the mean and covariance over the whole trajectory, representing in the trajectory space.  $\Phi_{1:T} \in \mathbb{R}^{(T \times 2) \times K}$  is the concatenation of basis function values for all the basis and at all the time points. The reason that a number 2 exist is that it contains both trajectories of position and velocity. In summary, the ProMP model encodes the trajectory into the weighting space and the trajectories can be reconstructed based on (3). The learning of the weights is actually a least-square problem, which could be solved using Moore-Penrose inverse that projects the trajectory from the original space to a weighting space (Calinon, 2020). **Figure 3** clearly demonstrates the rational of ProMP skill modeling approach.

## 2.2. Extraction of the Stiffness Adaptation Strategy Using sEMG

Here, we try to explain the necessity of sEMG signals to take part in our proposed framework from two perspectives. Then the signal handling processes are introduced in this section. First, the sEMG signal is used to estimate the human arm endpoint stiffness. As our previous work demonstrates, transferring human-like stiffness adaptation strategies from human to the robot end-effector or each joint will considerably prompt the success rate of tasks requiring both force control and position control (Huang et al., 2018; Chen et al., 2020b). Second, sEMG, as the additional signal being used to produce human side stiffness indication, increases the Shannon capacity of the “communication channel” between two different agents, assuming the proposed framework has good data encoding and decoding techniques (i.e., skill modeling as encoding and action recognition as decoding). To put it simply, the positive effect of the increased number of features for skill encoding is that the robot can recognize and produce more types of actions. The sEMG signal pre-processing would be straightforward, aiming to get a fitly smooth sEMG envelope for each channel. The signal is detrended to prevent any unwanted effects like sensor drift. Then, the global mean is subtracted to remove any possible offset. After then, a certain low-pass filter could be applied based on the choice of users. Filters can be chosen from linear/root-mean-square (RMS) moving average, Butterworth filter, and any other filters with a low-pass profile. To clarify, the choice of filtering techniques with their parameter settings will certainly influence the results. The users will have to choose their own filter types depending on the choice of sEMG signal collecting device. All of the sEMG envelope results generated in this paper were based on a low-pass Butterworth filter with a cut-off frequency at 5 Hz. **Algorithm 1** demonstrates the procedure of finding the envelope  $a$  for a single channel. **Figure 4** demonstrates the typical results of a weight raising





motion. The left and right images show the results of raw sEMG signals and computed envelopes while raising a weight to the posterior and anterior of body, respectively. It was easy to visualize that the muscles worked with co-activation, and the antagonistic muscles act in a opposite way to produce opposite functionalities.

Because of the effect of muscle synergies, a number of muscles can contribute to the end-point stiffness of each arm (Ison and Artemiadis, 2014). If a number of  $I$  muscles are considered, the calculation of the muscle activation indicator  $e$  is given by

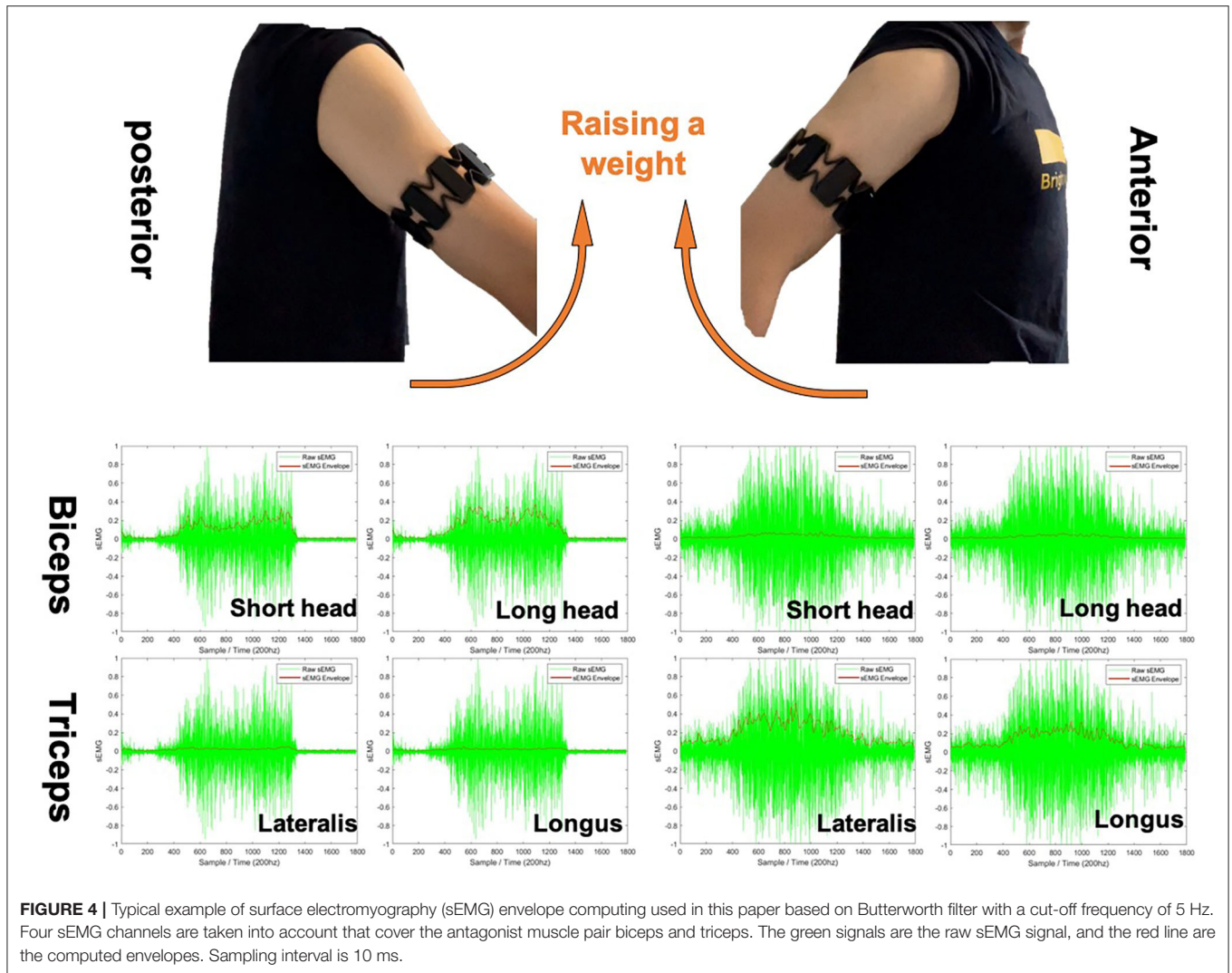
$$e(t) = \frac{1}{W} \sum_{i=1}^I \sum_{t=\frac{W-1}{2}}^{t+\frac{W-1}{2}} a_{(i)}(t), \quad (4)$$

where  $W$  is the window length defined by users and  $a_{(i)}(t)$  is the envelope value of the  $i$ th channel at time  $t$ . As indicated

in Yang et al. (2017), the stiffness model can be simplified by using an antagonistic pair (i.e., biceps and triceps). In this paper, four sEMG channels that cover the Biceps (i.e., brachii short head and long head) and the triceps (i.e., triceps lateralis and longus) were used to estimated the stiffness. Equation (5) defines the system mechanical impedance model (e.g., of a human arm/robot manipulator) that interacts with the external environment.

$$\mathcal{F}_{ext} = \Lambda(\ddot{\mathbf{x}} - \ddot{\mathbf{x}}_d) + \mathbf{D}(\dot{\mathbf{x}} - \dot{\mathbf{x}}_d) + \mathbf{K}_{cart}(\mathbf{x} - \mathbf{x}_d), \quad (5)$$

where  $\mathcal{F}_{ext}$  is the external force;  $\Lambda$ ,  $\mathbf{D}$  and  $\mathbf{K}_{cart}$  are the inertia, damping, and stiffness matrices in the task space;  $\mathbf{x}$  and  $\mathbf{x}_d$  are the real position and desired position in the task space, respectively. This equation implies that the interaction force can be controlled by adapting the stiffness matrix online. The Cartesian space stiffness is then estimated by a transformation



**FIGURE 4 |** Typical example of surface electromyography (sEMG) envelope computing used in this paper based on Butterworth filter with a cut-off frequency of 5 Hz. Four sEMG channels are taken into account that cover the antagonist muscle pair biceps and triceps. The green signals are the raw sEMG signal, and the red line are the computed envelopes. Sampling interval is 10 ms.

from the joint space (Ajoudani et al., 2015), as shown in (6) and (7).

$$\mathbf{K}_{cart}(e, \mathbf{q}_a) = ((\mathbf{J}_a(\mathbf{q}_a))^+)^T [\mathbf{K}_{joint}(e, \mathbf{q}_a) - \mathbf{G}(\mathbf{q}_a)] (\mathbf{J}_a(\mathbf{q}_a))^+ \quad (6)$$

$$\mathbf{K}_{joint}(e, \mathbf{q}_a) = c \bar{\mathbf{K}}_{joint} \quad (7)$$

$$c = 1 + \frac{\lambda_1 [1 - \exp(-\lambda_2 e)]}{1 + \exp(-\lambda_2 e)} \quad (8)$$

$\mathbf{K}_{joint}$  is the stiffness in the joint space;  $\mathbf{q}_a$  is the human arm joint angles, and  $\mathbf{J}_a(\mathbf{q}_a)^+$  is the pseudo-inverse of Jacobian matrix of the human arm; The human arm Jacobian is calculated based on the arm configuration estimated based on the IMU of the Myo armband.  $\mathbf{G}(\mathbf{q}_a)$  is a term that covers the effect of the external load and gravity on stiffness in the task space. The external load effect has been ignored since we could have no

prior knowledge about the external interaction; however, the gravitational effect can be estimated for each arm configuration based on the estimated arm Jacobian.  $c$  is the muscle co-contraction index.  $\lambda_1$  and  $\lambda_2$  are the constants identified by the user that affect the shape of the results, and  $\bar{\mathbf{K}}_{joint}$  is the joint stiffness matrix under the minimum muscle activation. Since this paper does not focus on designing of impedance controller, so it is worth simplifying the framework to easily verify our algorithms. Here, we only consider the linear force components and ignore the rotation and torques. The identification of  $\lambda_1$ ,  $\lambda_2$ , and  $\bar{\mathbf{K}}_{joint}$  should follow a rigorous procedures, which are different between different peoples and sEMG sensor setups (e.g., different sensors and different measuring positions on the arm). The readers could refer to the work of Ajoudani et al. (2015) and Clauser et al. (1969) for details and more information about  $\mathbf{G}$ , human arm Jacobian  $\mathbf{J}_a$  and the arm joint configuration. In this work, getting a reasonable variation profile of stiffness is already sufficient to conduct the experiments. Getting a very accurate absolute stiffness only from sEMG in real-time can be

**Algorithm 1:** sEMG Enveloping

**Require:**  $EMG_{raw}$ ; Sampling frequency  $f_s$ ; Cut-off frequency  $f_{co}$ ;  
Filter order  $O$ ; Window length  $T_w$ ; Number of points within  
window  $N_w$   
**Procedure :**  
 $EMG_{detrend} \leftarrow \text{detrend}(EMG_{raw})$   
 $EMG_{rectified} \leftarrow EMG_{detrend} - \text{mean}(EMG_{detrend})$   
**if** Linear Moving Average **then**  
 $a(t) = \frac{1}{N_w} \sum_{t-\frac{T_w}{2}}^{t+\frac{T_w}{2}} (|EMG_{rectified}(t)|)$   
**else if** RMS Moving Average **then**  
 $a(t) = \sqrt{\frac{1}{N_w} \sum_{t-\frac{T_w}{2}}^{t+\frac{T_w}{2}} (EMG_{rectified}(t))^2}$   
**else if** Butterworth Filter **then**  
 $a = \text{Butterworth}(f_s, f_{co}, O, |EMG_{rectified}|)$   
**end if**  
**return**  $a$   
**End Procedure**

extremely difficult, for readers who are interested in estimating stiffness more accurately can refer to Fang et al. (2017) and other resources.

### 2.3. Coupling Between Motion and Stiffness in Human–Robot Collaboration

ProMP has numerous fruitful properties that capable of manipulating the model to extend the possibilities. The most important properties that we adopt in the proposed human–robot collaboration framework design are coupling and modulation. **Coupling** is a property that allows to encode the correlation between each DoFs of a high-dimensional trajectory, which is formalized as

$$p(\zeta_{t,1:D} | \omega_{1:D}) = \mathcal{N}(\zeta_{t,1:D}; \Phi_{t,1:D} \omega_{1:D}, \Sigma_{\zeta,1:D}) = \mathcal{N}\left(\begin{bmatrix} \zeta_{t,1} \\ \vdots \\ \zeta_{t,D} \end{bmatrix}; \begin{bmatrix} \Phi_{t,1} & \dots & \mathbf{0} \\ \vdots & \ddots & \vdots \\ \mathbf{0} & \dots & \Phi_{t,D} \end{bmatrix} \begin{bmatrix} \omega_1^T \\ \vdots \\ \omega_D^T \end{bmatrix}, \Sigma_{\zeta,1:D}\right) \quad (9)$$

where  $D$  is the total number of DoFs.  $\zeta_{t,(d)}$ ,  $\Phi_{t,(d)}$ , and  $\omega_d$  are the trajectory values and trajectory value changing rates, basis value matrix, and weight matrix of the  $d$ th DoF at time  $t$ . To find the distribution for the whole trajectory over all the time from 1 to  $T$ , (9) is substituted into (2) and (3) to integrate out  $\omega_{1:D}$ , which yields  $\mu_{\zeta,1:D}^{1:T}$  and  $\Sigma_{\zeta,1:D}^{1:T}$  (i.e., mean and covariance of the  $D$ -dimensional trajectory from time 1 to  $T$ ). The off-diagonal blocks of  $\Sigma_{\zeta,1:D}^{1:T}$  clearly show the coupling between each DoF. From the above, multiple features can be encoded into a single skill primitives, hence multiple agents can be coupled together (e.g., human and robot). Our proposed framework encodes the Cartesian positions (3 DoFs) and estimated endpoint stiffness (3 DoFs, see section 2.2) for human arm and robot manipulator simultaneously. Recall that  $K_{cart} = \text{diag}([K_{cart,x}, K_{cart,y}, K_{cart,z}])$  is the Cartesian space stiffness matrix, where the diagonal terms are the stiffness constants on each axis. Therefore, six dimensions are encoded into the ProMP model for each agent (we ignored

the terms in the stiffness matrix that relate to the torque and rotation, hence the full framework should involve nine DoFs for each agent). For encoding human–robot coupling, the data types are defined as

$$\zeta_{t,1:D} \leftarrow [\zeta_{t,A}^T \zeta_{t,R}^T]^T, \quad (10)$$

$$\omega_{1:D} \leftarrow [\omega_A \ \omega_R]^T, \quad (11)$$

$$\Phi_{t,1:D} \leftarrow \begin{bmatrix} \Phi_{t,A} & \mathbf{0} \\ \mathbf{0} & \Phi_{t,R} \end{bmatrix}, \quad (12)$$

where the lower scripts  $(\cdot)_A$  and  $(\cdot)_R$  are used to indicate the DoFs for the human arm and the robot, respectively.

**Modulation** is the another property we used for skill generalization and adaptation (Maeda et al., 2017). Thanks to the fact that ProMP was build in a stochastic way, all the probability theories could still be applied. To implement the modulation, conditioning techniques are used. Suppose an observation  $[\tilde{\zeta}_{t,a}, \tilde{\Sigma}_{\zeta,1:D}]$  of the human arm is performed at time  $t$ , where  $\tilde{\Sigma}_{\zeta,1:D}$  denotes the measurement noise. Then, the conditional distribution  $p(\omega_{1:D} | [\tilde{\zeta}_{t,a}, \tilde{\Sigma}_{\zeta,1:D}])$  will update the model by “slicing” on  $p(\omega_{1:D})$ . The observation can be performed at a single time or multiple times, and can be performed for either a single DoF or any subset of all the DoFs. For each time that the observation happens, the conditional distribution of the weight will be updated recursively according to

$$\Phi_{t,1:D}^{obs} \leftarrow O_t \Phi_{t,1:D} \quad (13)$$

$$\hat{\mu}_{1:D} = \mu_{1:D} + \frac{\Sigma_{1:D}(\Phi_{t,1:D}^{obs})^T(\tilde{\zeta}_{t,a} - (\Phi_{t,1:D}^{obs})\mu_{1:D})}{\tilde{\Sigma}_{\zeta,1:D} + (\Phi_{t,1:D}^{obs})\Sigma_{1:D}(\Phi_{t,1:D}^{obs})^T} \quad (14)$$

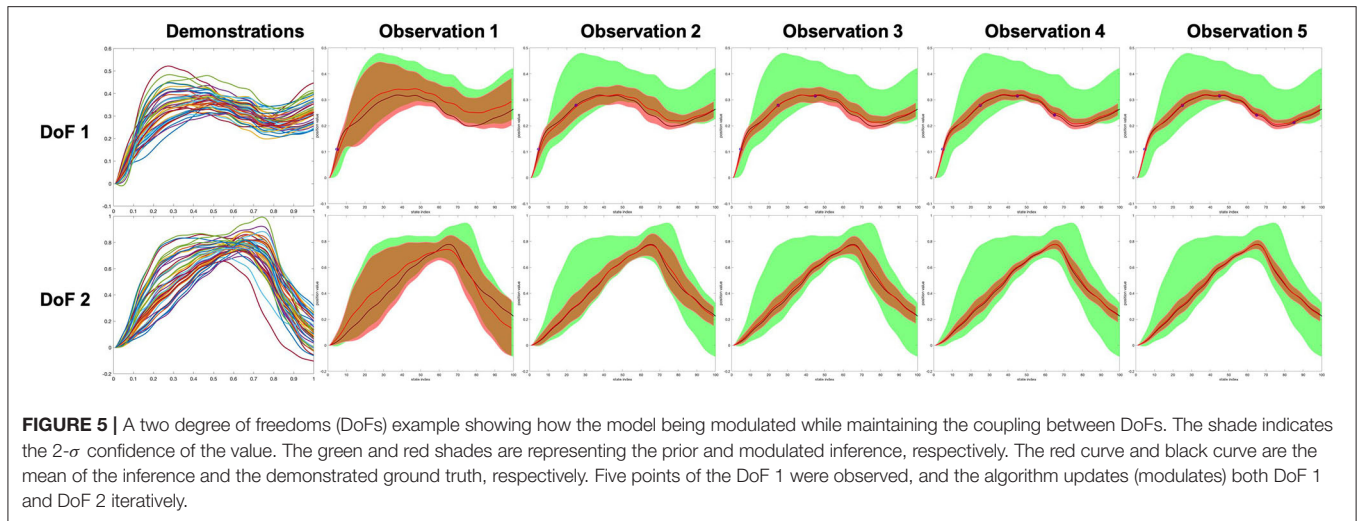
$$\hat{\Sigma}_{1:D} = \Sigma_{1:D} - \frac{\Sigma_{1:D}(\Phi_{t,1:D}^{obs})^T(\Phi_{t,1:D}^{obs})\Sigma_{1:D}}{\tilde{\Sigma}_{\zeta,1:D} + (\Phi_{t,1:D}^{obs})\Sigma_{1:D}(\Phi_{t,1:D}^{obs})^T}, \quad (15)$$

where  $\hat{\mu}_{1:D}$  and  $\hat{\Sigma}_{1:D}$  are the updated weight space mean and covariance of the modulated model, and  $O_t$  is an observation matrix that comprises identity matrices  $I \in \mathbb{R}^{2 \times 2}$  and zero matrices  $\mathbf{0} \in \mathbb{R}^{2 \times 2}$ , indicating which DoF(s) is(are) observed at time  $t$  (when only observing the position, the value one at the second diagonal entry of  $I$  is replaced with zero).  $O_t$  is then officially defined as

$$O_t \leftarrow [ [I \text{ or } \mathbf{0}]_1 \ \dots \ [I \text{ or } \mathbf{0}]_D ]^T \quad (16)$$

Using the updated weight space mean and covariance in (14) and (15), the task space mean  $\mu_{\zeta,1:D}^{1:T}$  and covariance  $\Sigma_{\zeta,1:D}^{1:T}$  are then reconstructed using (9), (2), and (3). Consequently, all the human/robot DoFs can be inferred/modulated by conditioning on observation; hence, a natural robot action generalization process is achieved. **Figure 5** shows a two DoFs example that clearly shows how model being modulated when considering the coupling between two DoFs.





**FIGURE 5 |** A two degree of freedoms (DoFs) example showing how the model being modulated while maintaining the coupling between DoFs. The shade indicates the 2- $\sigma$  confidence of the value. The green and red shades are representing the prior and modulated inference, respectively. The red curve and black curve are the mean of the inference and the demonstrated ground truth, respectively. Five points of the DoF 1 were observed, and the algorithm updates (modulates) both DoF 1 and DoF 2 iteratively.

## 2.4. Learning and Inference of Multiple Skill Primitives

The above sections consider only learning a single skill (assuming that the demonstrations for that skill are linearly correlated). In a real human-robot collaboration scenario, we need to consider making the robot possess many general skills and infer human intentions by observing a small amount of information and selecting the appropriate primitive in the skill library for generalization. The modeling of a single ProMP actually assumes that the weights of the Gaussian basis functions in a unified skill conform to a single modal multi-variant Gaussian distribution. As shown in **Figure 6**, we have obtained a set of pick-and-place demonstration data. In that figure, red represents the reach action, blue represents the pick action, and the green represents the place action. We use t-distributed stochastic neighbor embedding (t-SNE) (Van der Maaten and Hinton, 2008) to visualize all the sets of learned weights. It is clearly shown that the three behaviors are filed into three categories. This encourages us to model non-linear correlated skills using a GMM.

Assuming that the robot is expected to learn  $Q$  types of collaborative skills, our learning objective is a GMM distribution with  $Q$  local modals  $p(\omega_{1:D}; \pi^{(q)}, \mu_{1:D}^{(q)}, \Sigma_{1:D}^{(q)})$ , where  $q \in [1, Q]$ .  $\pi^{(q)}$  is the prior of the modal choice  $q$ .  $\mu_{1:D}^{(q)}$  and  $\Sigma_{1:D}^{(q)}$  are the mean and covariance of weights of the  $q$ -th local Gaussian modal. Hence, the GMM of weights is defined as

$$p(\omega_{1:D}) = \sum_q p(q)p(\omega_{1:D}|q) = \sum_q \pi^{(q)} p(\omega_{1:D}|\mu_{1:D}^{(q)}, \Sigma_{1:D}^{(q)}) \quad (17)$$

There are two approaches to learn the GMM parameters. The learning under human supervision would be straightforward. While in the demonstration process, human knows exactly about the category of the skill. Hence, for each demonstration, the label  $q$  is given. Hence, the rest of the work would be just training each local Gaussian modal individually, and the prior  $\pi^{(q)}$  can be calculated based on the number of demonstrations in each category  $q$ . To reduce human effort, unsupervised learning

methods like the EM algorithm can also be implemented. However, each set of weights of a ProMP is a very high-dimensional vector, typically more than a hundred dimensions; clustering algorithms can still result in local optima. Therefore, a validation procedure would be vital. Moreover, it is worth reminding that the log probability is always adopted to reduce the chance of encountering underflow issues since computing likelihood that involves very high-dimensional vectors often leads to an extremely small number. Using results of a K-mean algorithm as initialization of the EM algorithm would also reduce the chance of getting an error result.

After the GMM of weights is obtained, Bayes inference can be applied to recognize human action and get the best choice of label  $q = q_{est}$  based on the observation  $[\tilde{\xi}_{t,a}, \tilde{\Sigma}_{\xi,1:D}]$ , where  $q_{est}$  is the estimated action label.

$$q_{est} = \arg \max_q p(q|\tilde{\xi}_{t,a}) = \arg \max_q p(\tilde{\xi}_{t,a}|q)p(q) \quad (18)$$

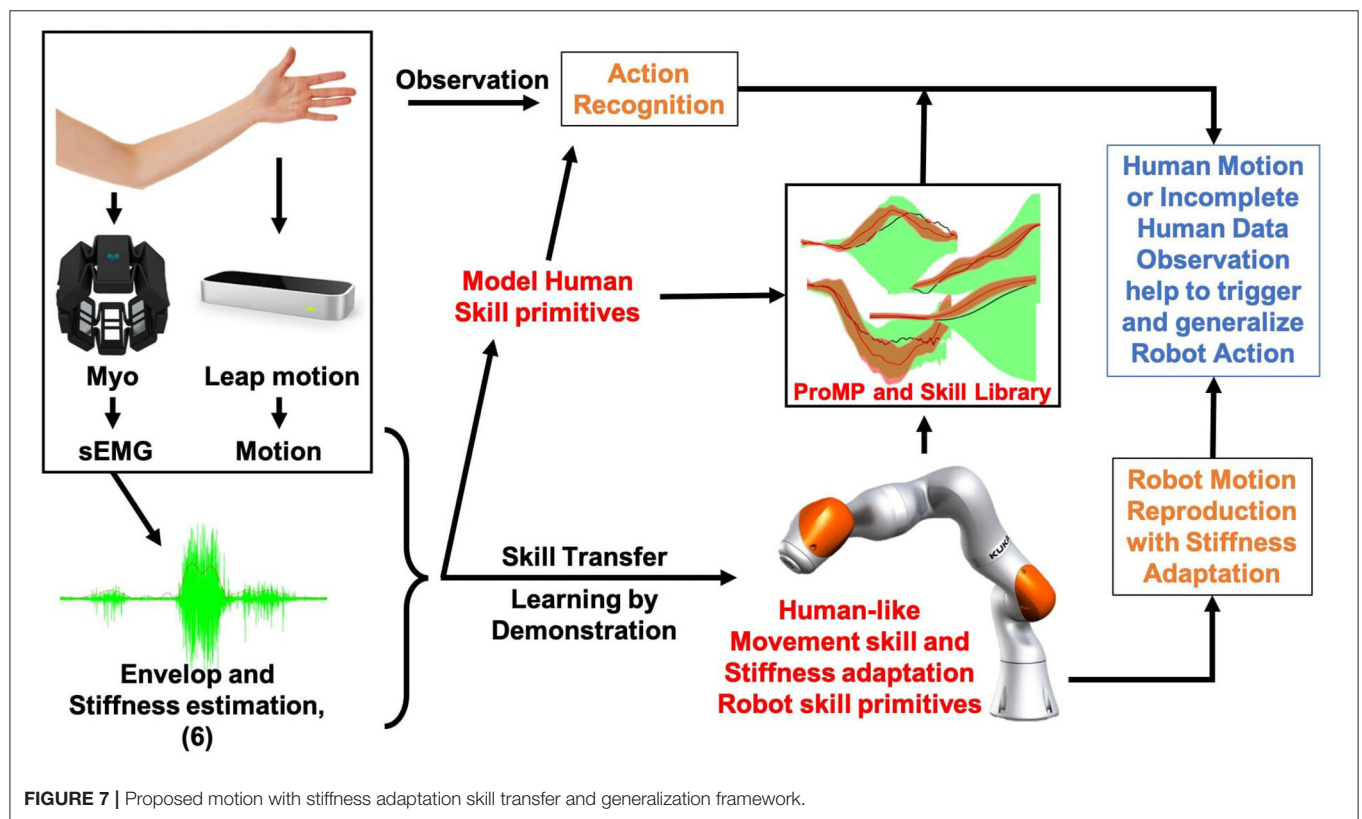
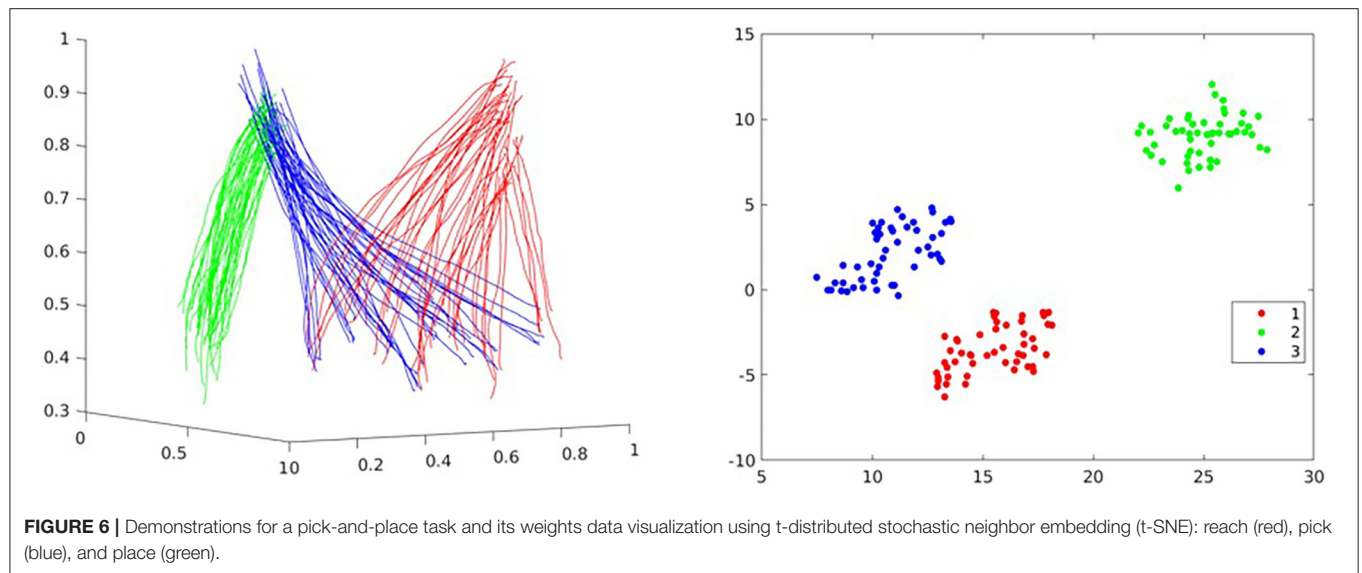
$$\begin{aligned} p(\tilde{\xi}_{t,a}|q) &= \int p(\tilde{\xi}_{t,a}|\Phi_{t,1:D}^{obs}\omega, \tilde{\Sigma}_{\xi,1:D})p(\omega|\mu_{1:D}^{(q)}, \Sigma_{1:D}^{(q)})d\omega \\ &= \mathcal{N}(\tilde{\xi}_{t,a}; \Phi_{t,1:D}^{obs}\mu_{1:D}^{(q)}, \Phi_{t,1:D}^{obs}\Sigma_{1:D}^{(q)}(\Phi_{t,1:D}^{obs})^T + \tilde{\Sigma}_{\xi,1:D}), \end{aligned} \quad (19)$$

The inference of  $q_{est}$  considers a series of observations at arbitrary times. Typically, more the observations used, the more confident about the inference results. Finally, the model was modulated using all the observations and the parameters of the local Gaussian modal  $\mu_{1:D}^{(q_{est})}$  and  $\Sigma_{1:D}^{(q_{est})}$  based on Equations (14) and (15).

## 3. EXPERIMENTS

We design a series of experiments to verify the practicability of the proposed framework. The hardware used in the experiments includes Myo Armband, Leap motion, and PC. Myo armband is a wireless sEMG signal monitoring device, which has a maximum sampling rate  $f_s$  of 200 Hz. Myo has eight sEMG channels that

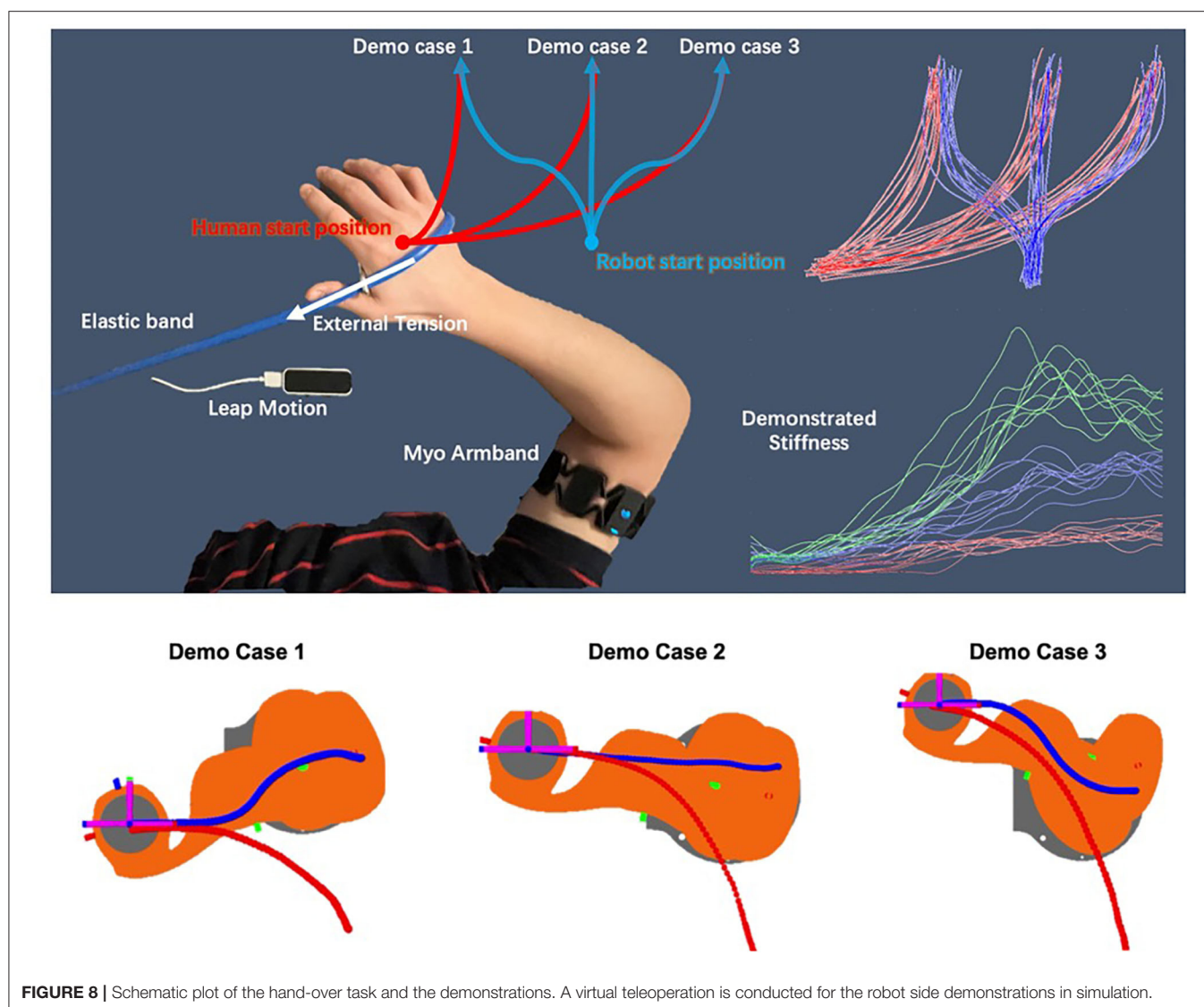




designed to be fixed on the human arm. Leap motion is a hand and finger tracking device, which utilizes monochromatic IR cameras and infrared LEDs to operate. As shown in **Figure 8**, in the experiment, the armband was worn on the right upper arm to measure the sEMG data of the antagonistic muscles (i.e., biceps and triceps) of the human demonstrator and estimate the stiffness of the arm endpoint according to the method introduced in section 2.2. Hence, in the Equation (4),  $I = 4$ . We adopted

a Butterworth filter for sEMG signal processing since the cut-off frequency can be controlled, where  $O = 3$  and  $f_{co} = 5\text{Hz}$ . Leap motion was placed on a flat surface, and the hand was required to move in the cone shape workspace above the Leap motion camera.

The rationale and basic workflow of the proposed framework is shown in **Figure 7** intuitively. In order to transfer the human-like stiffness adaptation skills, the human arm endpoint stiffness



**FIGURE 8 |** Schematic plot of the hand-over task and the demonstrations. A virtual teleoperation is conducted for the robot side demonstrations in simulation.

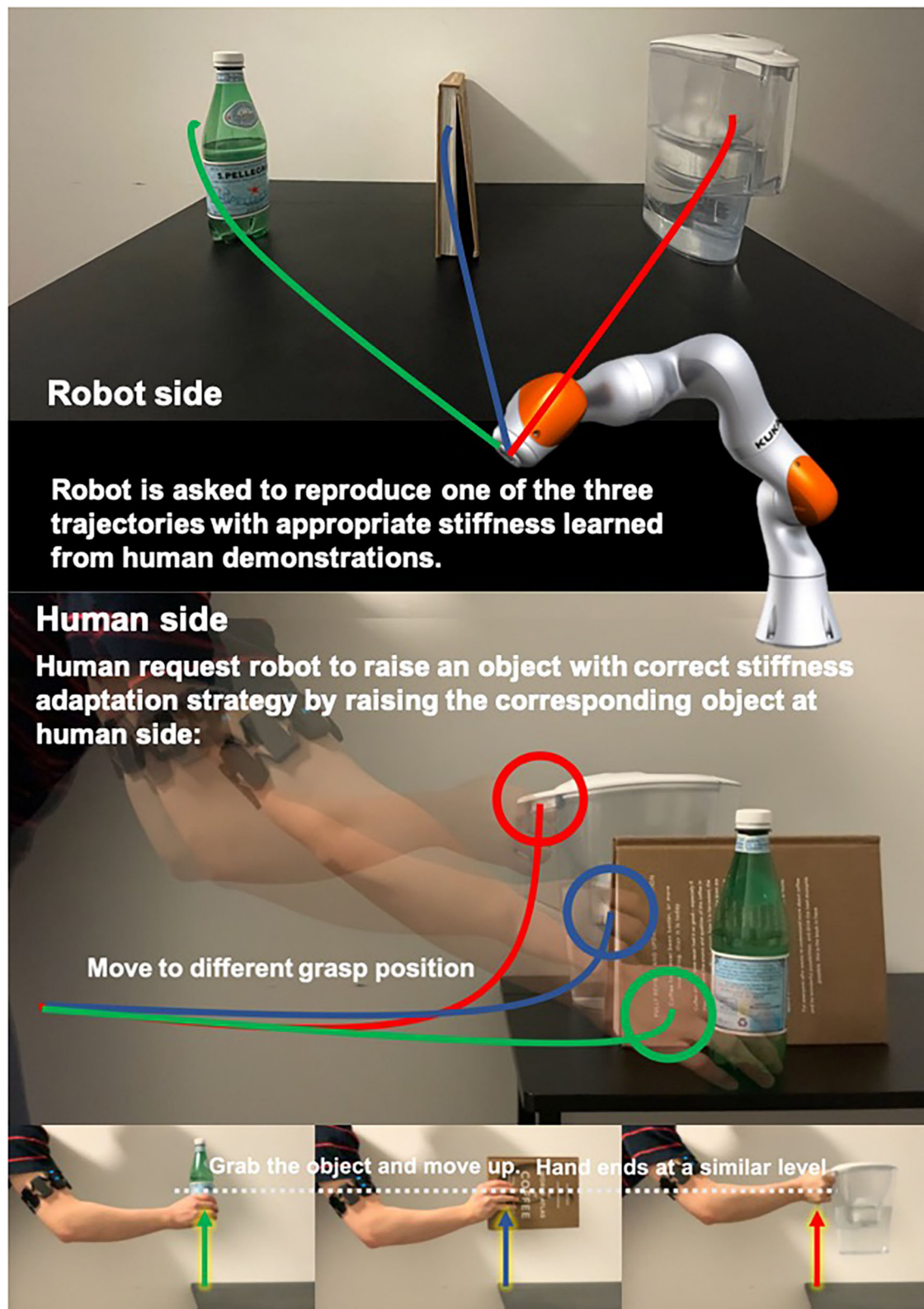
adaptation trajectories estimated using sEMG signal are added as additional features to the skill model. In order to make the robot autonomously find the generalization target of the desired stiffness based on different generalized motions, we model the stiffness feature through ProMP innovatively. Humans can then naturally impart the coupling between stiffness and motion to robots during demonstrations. Further, to achieve better collaboration between humans and robots, we suggest combining our previous research outcomes on stiffness adaptation skill with the benefits of ProMP in modulation. We model the human skills and robot skills simultaneously to establish coupling so that robots can generalize appropriate actions and collaborate with humans even when they have incomplete observations of human signals.

### 3.1. Hand-Over Experiment

To verify that our framework can naturally encode the coupling of stiffness and motion, a hand-over experiment scenario (see

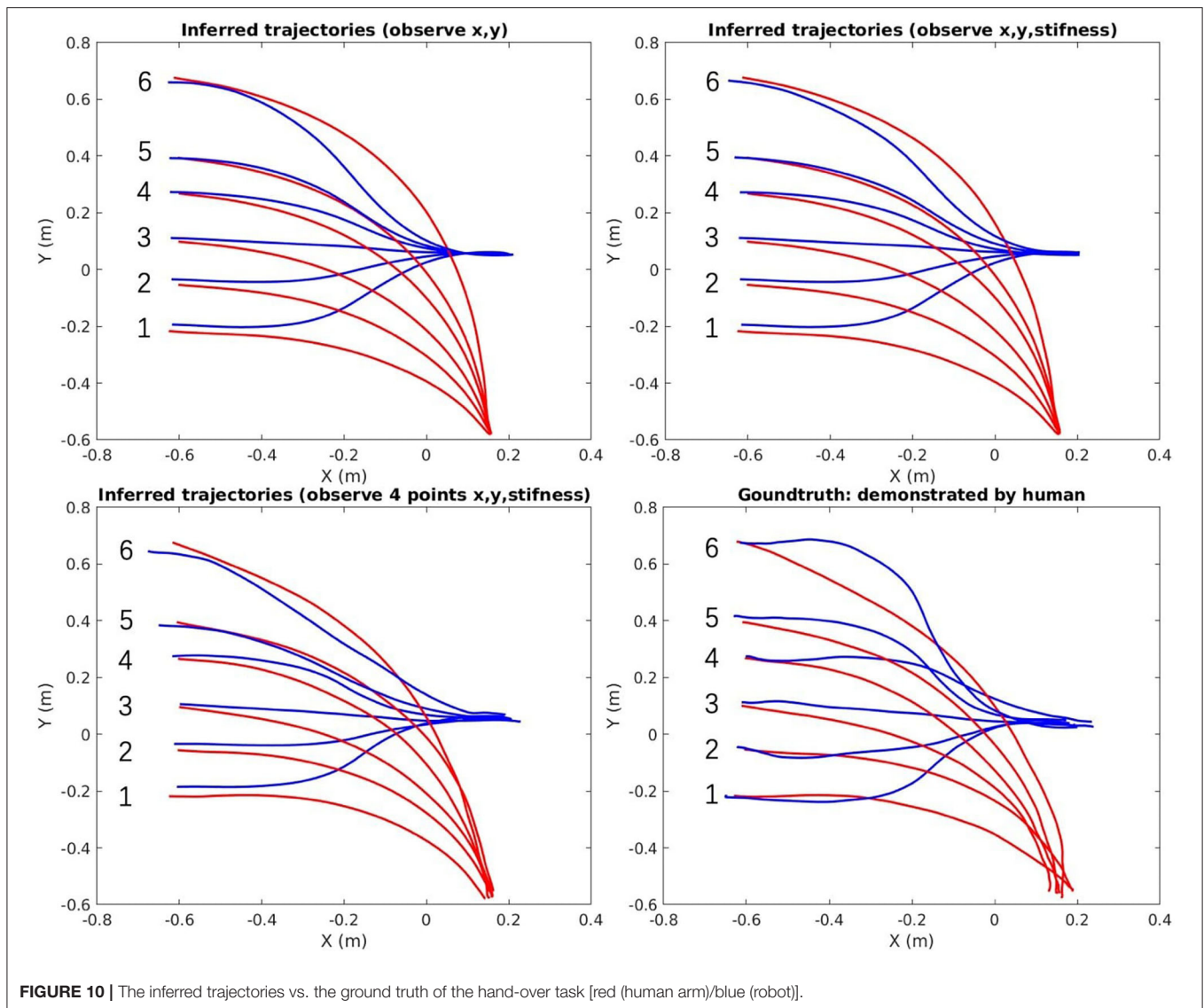
**Figure 8**) was designed. In the experiment, people pull one end of the elastic band and quickly, stably and naturally move along the given red trajectories on the x-y plane in 2 s, the captured hand motion and estimated stiffness are recorded to learn motion primitives for the human side. The other end of the elastic band is fixed on a pile. During the movement, the demonstrator's arm experiences three stages: no external tension, external tension occurs, and increasing external tension. To maintain a high trajectory tracking accuracy in the presence of external forces within 2 s, the demonstrator will perform with an adaptive stiffness strategy.

To demonstrate the robot skills, a virtual teleoperation scene in Matlab simulation was built, which use the same demonstration interface to control the robot end-effector to move along each desired blue trajectory in a simulation within 2 s. The simulated robot was controlled using a simple Cartesian positional PID controller and inverse kinematics solver with the captured human hand position as the desired position.



**FIGURE 9 |** Illustration of the object matching experiment.





While teleoperating the blue trajectories, the red trajectories are also replayed. For each demo case, the demonstrator is asked to perform 10 demonstrations, hence  $N = 30$  in total. All the recorded data are then used to train a 12-dimensional ProMP model, where 3 DoFs for human arm position, 3 DoFs for the human arm translational stiffness, and the same DoFs apply to the robot. The number of weights in this experiment is set to be  $K=30$ . Using the conditioning method introduced in section 2.3, the demonstrator then shows 6 new motions to verify the framework's generalization ability and accuracy. Ideally, by only observing the last time point of the arm position trajectory, it can still infer an appropriate stiffness trajectory and an appropriate robot motion.

### 3.2. Object Matching Experiment

As shown in **Figure 9**, we design an object matching task to test our framework. We test our framework that has the

ability to distinguish between human intents by adding stiffness information to the model when motions are similar. Using too large or small stiffness to pick up heavy object would result in motion fluctuations or pick-up failures, respectively. Hence, in this task, the demonstrator is first asked to demonstrate the pick-up skill with stiffness adaptation strategies for encoding robot side skill primitive. For each robot side trajectory, demonstrator also demonstrate the human side pick-up motion. Each object will have 10 demonstrations. The red, blue, and green lines at human side in **Figure 9** illustrate the human motions. For each object, the motion trajectory will only be differed at the grasping positions since we grasp at different levels. Although the human side motions are similar, the stiffness trajectories can be significantly differed. Finally, the demonstrator pickups different objects at human side as observation to trigger modulated robot actions and see if that system performs as expected (e.g., generate motion and stiffness trajectories correctly).



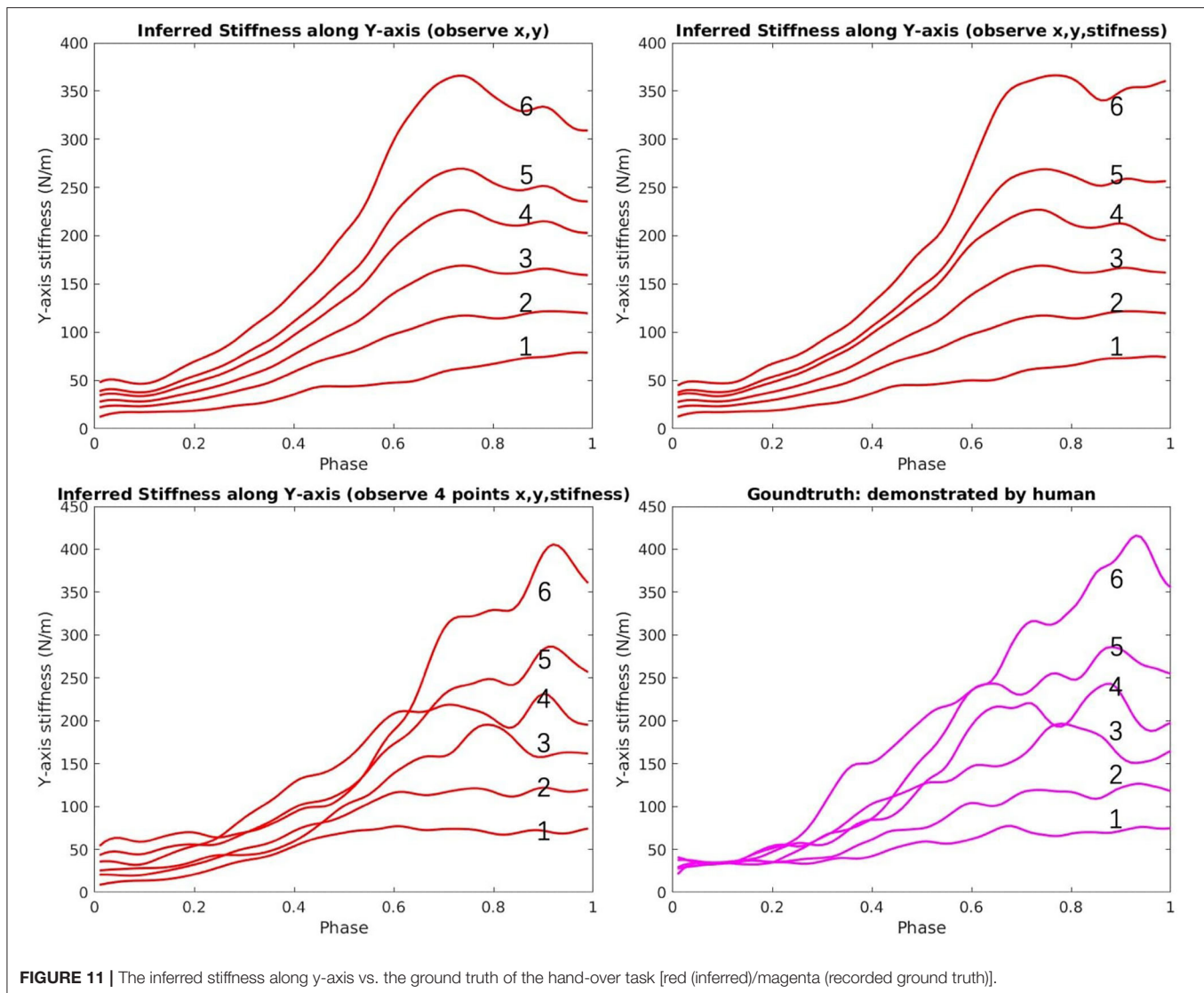


FIGURE 11 | The inferred stiffness along y-axis vs. the ground truth of the hand-over task [red (inferred)/magenta (recorded ground truth)].

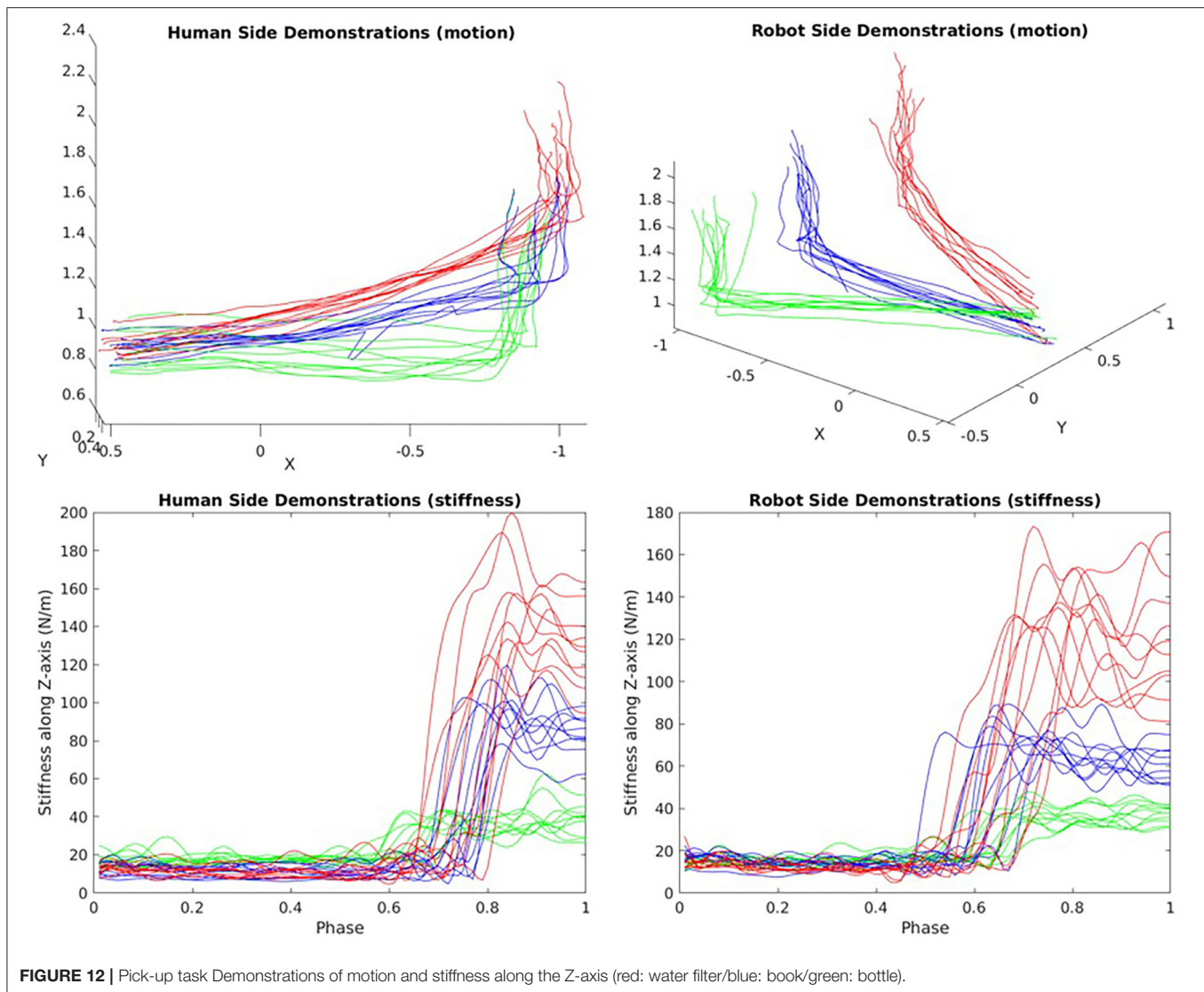
### 3.3. Pick-and-Place Experiment

We use the recorded pick-and-place demonstrations, as shown in Figure 6, to verify the framework's ability to recognize human action; hence, we choose correct action label to generalize the ProMP according to observations. Three actions are considered as primitives, which are reach, pick, and place, respectively. We were assuming the object is initially located at a random position inside a circular area. Therefore, all the demonstrations of reach start at a similar position but end in different places, while the pick demonstrations start at different positions but end in a similar position. The place demonstrations should always travel along a similar trajectory. Each primitive has 50 demonstrations, thus 150 in total. All the parameter settings are the same as before, and all 150 demonstration are then used as test data to verify the framework performance in action recognition. For each demonstration, 10 equally spaced data point were chosen as the observations.

## 4. RESULTS AND DISCUSSION

### 4.1. Hand-Over Experiment

The top-right area in Figure 8 shows all the demonstrated trajectories for both motion and estimated stiffness  $K_{cart,y}$  along the y-axis. As shown in Figures 10, 11, the reproduced action with index 1, 3, and 5 corresponds to the demo case 1, 2, and 3 in Figure 8, respectively. The rest three reproduced actions with index 2, 4, and 6 are the novel cases to test the generalization accuracy. Three trajectory inference results are shown in Figure 8. The upper-left one shows the result that only observing human arm x-y positions at time 2 s. The upper-right one shows the result that observes human arm x-y positions and estimated stiffness at time 2 s. The lower-left one shows the result that observes human arm x-y positions and estimated stiffness at time 1.4, 1.6, 1.8, and 2 s. Comparing with the recorded ground truth at the lower-right, we can see that all cases can generalize reasonably well trajectories and complete the hand-over task. It



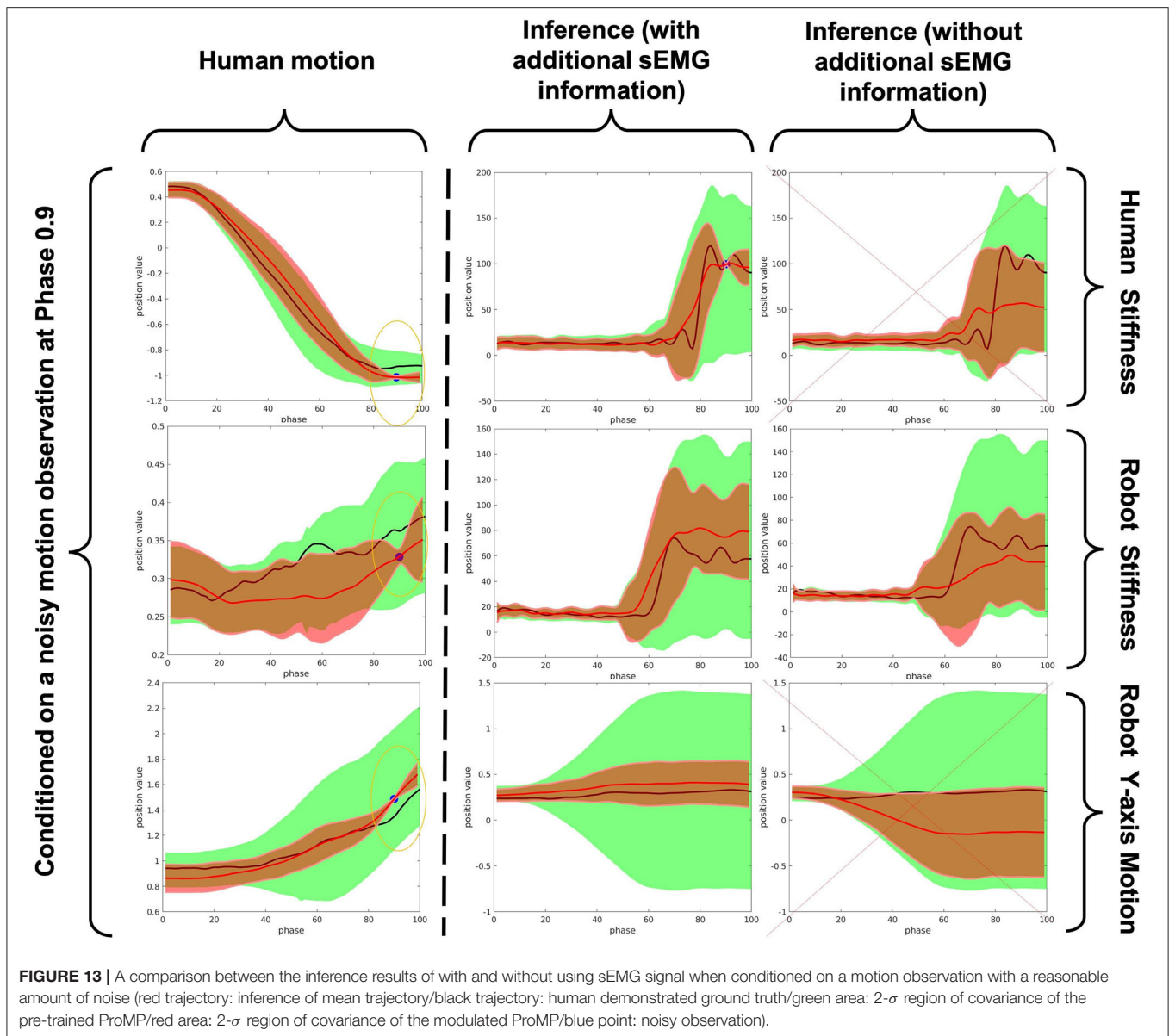
can be seen that the ground truth trajectories are not ideally smooth in shape even though we call it the “Ground Truth.” That is because single demonstration always having large bias, using a larger number of demonstrations to synthesize the data will make the trajectory smooth and reliable. And that is further proved by comparing two upper results with the lower results. When robot inferring actions by conditioning on biased information, the model “believes” more about “bias,” while the upper two cases “believe” more about the synthesized skill trajectories mean, which makes them look more reliable.

In **Figure 11**, the upper-left graph shows the results of inferred stiffness along the y-axis when only observing the x-y position of the arm at time 2 s. It proves that our proposed ProMP-based framework can encode coupling between motion and stiffness. The larger travel-distance along the y-axis, the larger stiffness along the y-axis is required, which is the tendency we expect. The upper-right graph shows that the stiffness trajectories were updated by observing stiffness at 2 s. The lower-left graph shows

the same problems of “believing in bias”; however, that can also be utilized to generate different action styles when there are various distinct styles among demonstrations. Overall, the framework works more ideally when (1) human DoFs are fully observable; (2) model trained by a sufficiently large number of demonstrations; (3) inferring robot actions by observing (conditioning) at a single time point (to reduce bias).

## 4.2. Object Matching Experiment

The human demonstrations are all shown in **Figure 12**. The upper-left shows that although the 3 kind of motions are distinguishable by human’s inspection, it may also be vague to tell when noise exists. The lower two graphs are the demonstrated stiffness along Z-axis since that is the most interested axis when picking up objects. It can be seen that the bottle requires the least amount of stiffness to raise while the water filter requires the largest stiffness. From the graph, we see that a human use a very good stiffness control strategy. When grasping object, because the



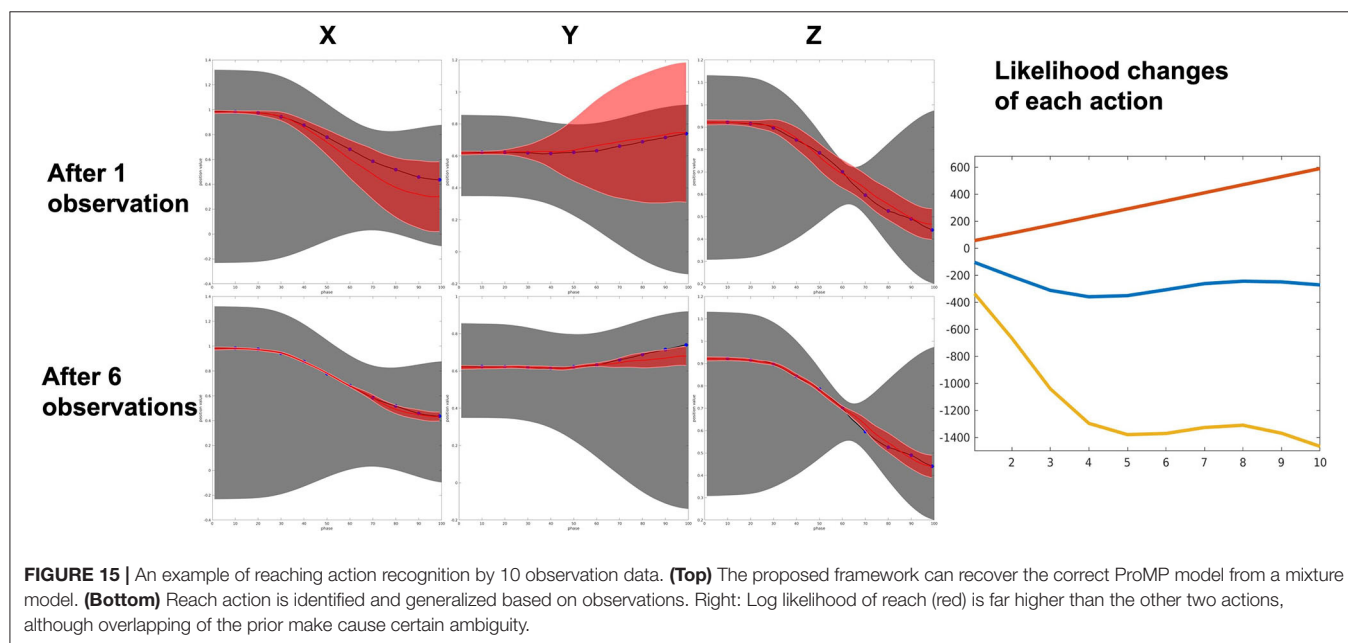
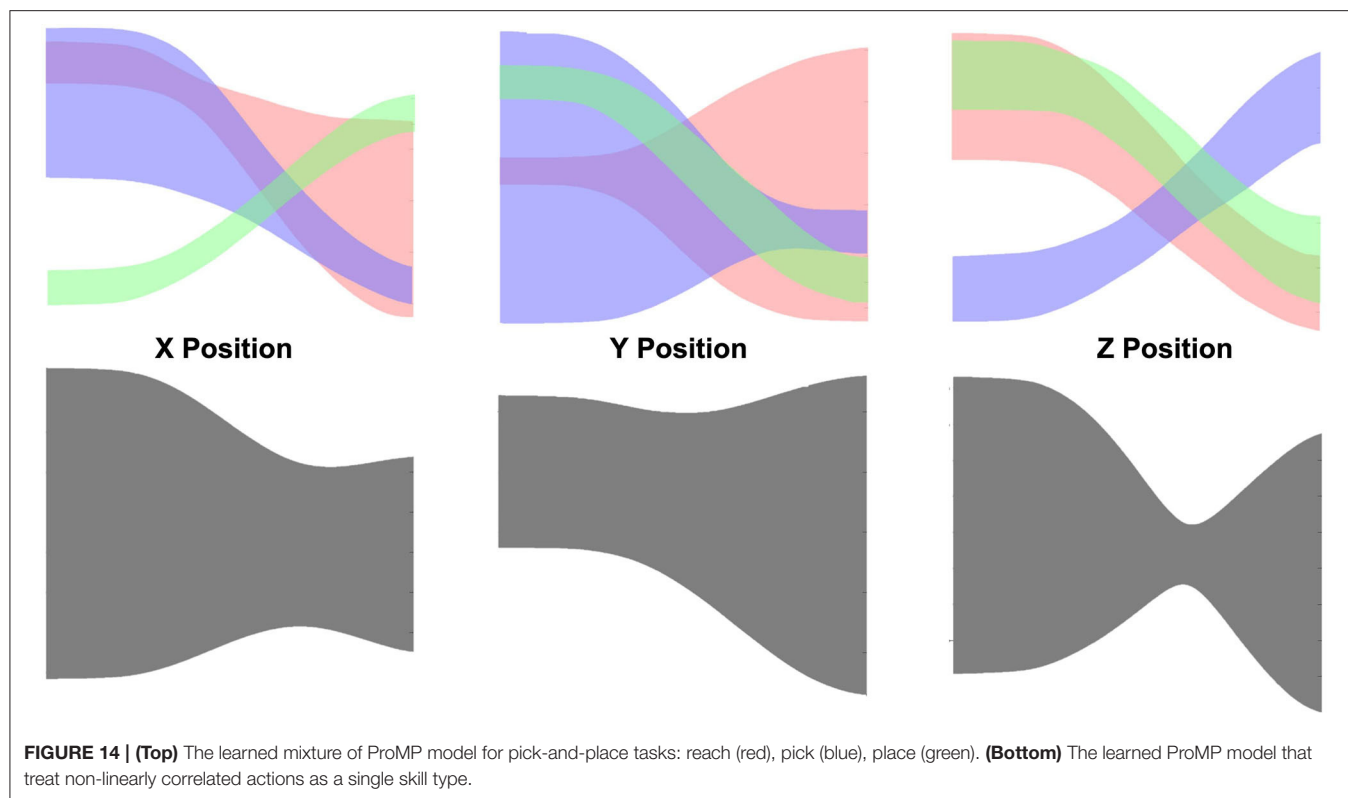
exacted weight of that object is not known, humans create an over shoot of stiffness to ensure that the task space motion is not off-track. After that, the arm will swiftly reduce the stiffness to an appropriate value so that the energy consumption is minimized.

**Figure 13** clearly demonstrates the effectiveness of our proposed framework in distinguishing human action and generate accurate robot motion with correct amount of stiffness activation when the actions are similar and observation noise exists. The blue points is the observation; in this experiment, we adopt a random generated noise of a very reasonable amount; such amount of noise may also be the bias of human motion in each run-time (i.e., people do not always have a 100% correct motion). We clearly see that our framework works very well under the help of sEMG signal (see the middle column). This is compared to the results with no help of sEMG, where

the inference process provides a absolutely incorrect human stiffness and robot motion and the robot stiffness inference is not what we expect (low stiffness activation when raising the object, this may leads to a distortion of motion trajectory during execution in the real application). Hence, we could say that the proposed framework can be used as an effective command sending interface to trigger appropriate robot actions in a very intuitive and convenient manner, which greatly reduce the effort of reprogramming.

### 4.3. Pick-and-Place Experiment

The top side of **Figure 14** shows the learned prior of reach (red), pick (blue), and place (green) individually. Obviously, the ProMP model learned by non-linearly correlated demonstrations (i.e., gray shade in **Figure 14**) cannot be used to generalize



or recognize motions. All 150 tested demonstrations result in a 100% success rate. An inference of a test demonstration is considered to be succeeded if the action label is correctly inferred. An example of recognition and generalization of a reach action is shown in **Figure 15**. Once the action label is correctly labeled, the sum of the squared difference between

the ground truth and inferred trajectory can be very low, as can be seen in **Figure 15**. As more and more observations coming, the log-likelihood of reach action keeps increasing with very high confidence. The overlapping of the prior (mostly occurs in the middle) does increase the likelihood of the other two actions; however, our algorithm considers the



whole observation sequence from the beginning to the current time. Hence, there would be no significant ambiguity caused by overlapping.

Reducing the number of observations or increasing the number of Gaussian models (i.e., skills) stored in the Gaussian mixture ProMP will introduce more inference ambiguity. However, since the proposed framework considers using stiffness profile as additional features, the inference accuracy may still keep at a satisfying level. In our framework, the action recognition functionality is associated with the ProMP model itself since it requires the prior knowledge stored in the ProMP (i.e.,  $\mu_{1:D}^{(q)}$ ,  $\Sigma_{1:D}^{(q)}$ ). Then, the prior knowledge is modulated based on the recognized action label and all the observed information, which makes the robot be able to adapt actions to accommodate different situations.

## 5. FUTURE WORK

The action recognition functionality allows identifying the most similar actions in the learned skill library. This implies that we could find skill substitution for any coming novel action without learning and storing them into the skill library. The idea of blending in ProMP could transform one type of action to another, which means the learned skills could still be disassembled and then regrouped as a substitute for novel action. To investigate the possibility of fully automated robot operations, we can combine the ProMP-based framework proposed in this article with concepts such as skill execution sequence, environmental awareness, and affordance. Time series such as HMM can be used to model and train the robot's task-level planning ability. This article largely focuses on the theoretical study. When considering real robot control, we will encounter many foreseeable and new challenges, such as motor acceleration not reaching the desired speed, difficulties in implementing human-robot real-time collaboration, etc.

## REFERENCES

- Ajoudani, A., Fang, C., Tsagarakis, N. G., and Bicchi, A. (2015). "A reduced-complexity description of arm endpoint stiffness with applications to teleimpedance control," in *2015 IEEE/RSJ International Conference on Intelligent Robots and Systems (IROS)* (Hamburg), 1017–1023. doi: 10.1109/IROS.2015.7353495
- Argall, B. D., Chernova, S., Veloso, M., and Browning, B. (2009). A survey of robot learning from demonstration. *Robot. Auton. Syst.* 57, 469–483. doi: 10.1016/j.robot.2008.10.024
- Atkeson, C. G., Moore, A. W., and Schaal, S. (1997). "Locally weighted learning for control," in *Lazy Learning*, eds D. W. Aha (Dordrecht: Springer), 75–113.
- Billard, A. G., Calinon, S., and Dillmann, R. (2016). "Learning from humans," in *Springer Handbook of Robotics*, eds B. Siciliano and O. Khatib (Cham: Springer), 1995–2014.
- Burdet, E., Osu, R., Franklin, D., Yoshioka, T., Milner, T., and Kawato, M. (2000). A method for measuring endpoint stiffness during multi-joint arm movements. *J. Biomech.* 33, 1705–1709. doi: 10.1016/S0021-9290(00)00142-1

## 6. CONCLUSION

This paper demonstrates an adaptive stiffness human-robot skill transfer framework based on ProMP for collaborative tasks, which is very easy to understand and is effective. We discuss the importance of stiffness property in real applications and propose to use sEMG signal to estimate human arm endpoint stiffness, which can then be transferred to the robot. Moreover, the use of sEMG increases the generalization accuracy and decision-making success rate. We also illustrate why the ProMP model has benefits in building such a skill model. To prove our idea, we design experiments using the Myo armband and Leap motion, which gives results that positively support our work. We find the coupling between the adaptive stiffness strategy and motion can be encoded and transferred from humans to robots in a very intuitive manner comparing to other works. The proposed framework can be used as an intuitive interface to trigger robot action generalization via observing human action, ideal for a human-robot collaboration scenario. In the future, we will exploit the other properties of ProMP and other techniques, like skill combining and blending, mixture models to improve the flexibility of our framework further, and verify it using real robots.

## AUTHOR CONTRIBUTIONS

YG conceptualized the framework, developed the software, designed and conducted the experiments, and wrote the paper. NW and CY supervised, reviewed, and approved the work. All authors contributed to the article and approved the submitted version.

## FUNDING

This work was partially supported by Engineering and Physical Sciences Research Council (EPSRC) under Grant EP/S001913.

- Calinon, S. (2020). "Mixture models for the analysis, edition, and synthesis of continuous time series," in *Mixture Models and Applications*, eds N. Bouguila and W. Fan (Cham: Springer), 39–57.
- Calinon, S., Guenter, F., and Billard, A. (2007). On learning, representing, and generalizing a task in a humanoid robot. *IEEE Trans. Syst. Man Cybernet. Part B* 37, 286–298. doi: 10.1109/TSMCB.2006.886952
- Calinon, S., Li, Z., Alizadeh, T., Tsagarakis, N. G., and Caldwell, D. G. (2012). "Statistical dynamical systems for skills acquisition in humanoids," in *2012 12th IEEE-RAS International Conference on Humanoid Robots (Humanoids 2012)* (Osaka), 323–329. doi: 10.1109/HUMANOIDS.2012.6651539
- Chen, X., Jiang, Y., and Yang, C. (2020a). "Stiffness estimation and intention detection for human-robot collaboration," in *2020 15th IEEE Conference on Industrial Electronics and Applications (ICIEA)* (Kristiansand), 1802–1807. doi: 10.1109/ICIEA48937.2020.9248186
- Chen, X., Wang, N., Cheng, H., and Yang, C. (2020b). Neural learning enhanced variable admittance control for human-robot collaboration. *IEEE Access* 8, 25727–25737. doi: 10.1109/ACCESS.2020.2969085

- Chernova, S., and Veloso, M. (2007). "Confidence-based policy learning from demonstration using Gaussian mixture models," in *Proceedings of the 6th International Joint Conference on Autonomous Agents and Multiagent Systems* (Honolulu, HI), 1–8. doi: 10.1145/1329125.1329407
- Clauser, C. E., McConville, J. T., and Young, J. W. (1969). *Weight, Volume, and Center of Mass of Segments of the Human Body*. Technical report, Antioch College, Yellow Springs, OH. doi: 10.21236/AD0710622
- Fang, C., Ajoudani, A., Bicchi, A., and Tsagarakis, N. G. (2017). Online model based estimation of complete joint stiffness of human arm. *IEEE Robot. Autom. Lett.* 3, 84–91. doi: 10.1109/LRA.2017.2731524
- Forte, D., Gams, A., Morimoto, J., and Ude, A. (2012). On-line motion synthesis and adaptation using a trajectory database. *Robot. Auton. Syst.* 60, 1327–1339. doi: 10.1016/j.robot.2012.05.004
- Gomi, H., and Osu, R. (1998). Task-dependent viscoelasticity of human multijoint arm and its spatial characteristics for interaction with environments. *J. Neurosci.* 18, 8965–8978. doi: 10.1523/JNEUROSCI.18-21-08965.1998
- Hersch, M., Guenter, F., Calinon, S., and Billard, A. (2008). Dynamical system modulation for robot learning via kinesthetic demonstrations. *IEEE Trans. Robot.* 24, 1463–1467. doi: 10.1109/TRO.2008.2006703
- Hogan, N. (1985). "Impedance control: an approach to manipulation: Part I-theory," in *IEEE 1984 American Control Conference* (San Diego, CA). doi: 10.23919/ACC.1984.4788393
- Huang, R., Cheng, H., Guo, H., Lin, X., and Zhang, J. (2018). Hierarchical learning control with physical human-exoskeleton interaction. *Inform. Sci.* 432, 584–595. doi: 10.1016/j.ins.2017.09.068
- Ijspeert, A. J., Nakanishi, J., Hoffmann, H., Pastor, P., and Schaal, S. (2013). Dynamical movement primitives: learning attractor models for motor behaviors. *Neural Comput.* 25, 328–373. doi: 10.1162/NECO\_a\_00393
- Ison, M., and Artemiadis, P. (2014). The role of muscle synergies in myoelectric control: trends and challenges for simultaneous multifunction control. *J. Neural Eng.* 11:051001. doi: 10.1088/1741-2560/11/5/051001
- Khansari-Zadeh, S. M., and Billard, A. (2011). Learning stable nonlinear dynamical systems with gaussian mixture models. *IEEE Trans. Robot.* 27, 943–957. doi: 10.1109/TRO.2011.2159412
- Li, Z., Cheng, H., Guo, H., and Sun, X. (2017). Compliant training control of ankle joint by exoskeleton with human emg-torque interface. *Assembly Autom.* 37, 349–355. doi: 10.1108/AA-12-2016-161
- Maeda, G. J., Neumann, G., Ewerton, M., Lioutikov, R., Kroemer, O., and Peters, J. (2017). Probabilistic movement primitives for coordination of multiple human-robot collaborative tasks. *Auton. Robots* 41, 593–612. doi: 10.1007/s10514-016-9556-2
- Migliore, S. A., Brown, E. A., and DeWeerth, S. P. (2005). "Biologically inspired joint stiffness control," in *Proceedings of the 2005 IEEE International Conference on Robotics and Automation* (Barcelona), 4508–4513. doi: 10.1109/ROBOT.2005.1570814
- Moeslund, T. B., Hilton, A., and Krüger, V. (2006). A survey of advances in vision-based human motion capture and analysis. *Comput. Vis. Image Understand.* 104, 90–126. doi: 10.1016/j.cviu.2006.08.002
- Mülling, K., Kober, J., Kroemer, O., and Peters, J. (2013). Learning to select and generalize striking movements in robot table tennis. *Int. J. Robot. Res.* 32, 263–279. doi: 10.1177/0278364912472380
- Paraschos, A., Daniel, C., Peters, J., and Neumann, G. (2013). "Probabilistic movement primitives," in *27th Annual Conference on Neural Information Processing Systems 2013* (Lake Tahoe, NV).
- Paraschos, A., Daniel, C., Peters, J., and Neumann, G. (2018). Using probabilistic movement primitives in robotics. *Auton. Robots* 42, 529–551. doi: 10.1007/s10514-017-9648-7
- Rabbi, I., and Ullah, S. (2013). A survey on augmented reality challenges and tracking. *Acta Graph.* 24, 29–46. doi: 10.9790/0661-0222329
- Schaal, S., Peters, J., Nakanishi, J., and Ijspeert, A. (2003). "Control, planning, learning, and imitation with dynamic movement primitives," in *Workshop on Bilateral Paradigms on Humans and Humanoids: IEEE International Conference on Intelligent Robots and Systems (IROS 2003)* (Las Vegas, NV), 1–21.
- Ugur, E., and Girgin, H. (2020). Compliant parametric dynamic movement primitives. *Robotica* 38, 457–474. doi: 10.1017/S026357471900078X
- van der Maaten, L., and Hinton, G. (2008). Visualizing data using t-SNE. *J. Mach. Learn. Res.* 9, 2579–2605. Available online at: [https://www.bibsonomy.org/bibtex/28b9aebb404ad4a4c6a436ea413550b30/lopusz\\_kdd](https://www.bibsonomy.org/bibtex/28b9aebb404ad4a4c6a436ea413550b30/lopusz_kdd)
- Villani, V., Pini, F., Leali, F., and Secchi, C. (2018). Survey on human-robot collaboration in industrial settings: safety, intuitive interfaces and applications. *Mechatronics* 55, 248–266. doi: 10.1016/j.mechatronics.2018.02.009
- Wang, R., Wu, Y., Chan, W. L., and Tee, K. P. (2016). "Dynamic movement primitives plus: for enhanced reproduction quality and efficient trajectory modification using truncated kernels and local biases," in *2016 IEEE/RSJ International Conference on Intelligent Robots and Systems (IROS)* (Daejeon), 3765–3771. doi: 10.1109/IROS.2016.7759554
- Yang, C., Ganesh, G., Haddadin, S., Parusel, S., Albu-Schaeffer, A., and Burdet, E. (2011). Human-like adaptation of force and impedance in stable and unstable interactions. *IEEE Trans. Robot.* 27, 918–930. doi: 10.1109/TRO.2011.2158251
- Yang, C., Zeng, C., Fang, C., He, W., and Li, Z. (2018). A DMPS-based framework for robot learning and generalization of humanlike variable impedance skills. *IEEE/ASME Trans. Mechatron.* 23, 1193–1203. doi: 10.1109/TMECH.2018.2817589
- Yang, C., Zeng, C., Liang, P., Li, Z., Li, R., and Su, C.-Y. (2017). Interface design of a physical human-robot interaction system for human impedance adaptive skill transfer. *IEEE Trans. Autom. Sci. Eng.* 15, 329–340. doi: 10.1109/TASE.2017.2743000
- Yu, X., He, W., Li, Y., Xue, C., Li, J., Zou, J., et al. (2019). Bayesian estimation of human impedance and motion intention for human-robot collaboration. *IEEE Trans. Cybern.* 51, 1822–1834. doi: 10.1109/TCYB.2019.2940276
- Zeestraten, M. J., Calinon, S., and Caldwell, D. G. (2016). "Variable duration movement encoding with minimal intervention control," in *2016 IEEE International Conference on Robotics and Automation (ICRA)* (Stockholm), 497–503. doi: 10.1109/ICRA.2016.7487171
- Zeng, C., Yang, C., Cheng, H., Li, Y., and Dai, S.-L. (2020). Simultaneously encoding movement and sEMG-based stiffness for robotic skill learning. *IEEE Trans. Indus. Inform.* 17, 1244–1252. doi: 10.1109/TII.2020.2984482

**Conflict of Interest:** The authors declare that the research was conducted in the absence of any commercial or financial relationships that could be construed as a potential conflict of interest.

**Publisher's Note:** All claims expressed in this article are solely those of the authors and do not necessarily represent those of their affiliated organizations, or those of the publisher, the editors and the reviewers. Any product that may be evaluated in this article, or claim that may be made by its manufacturer, is not guaranteed or endorsed by the publisher.

Copyright © 2021 Guan, Wang and Yang. This is an open-access article distributed under the terms of the Creative Commons Attribution License (CC BY). The use, distribution or reproduction in other forums is permitted, provided the original author(s) and the copyright owner(s) are credited and that the original publication in this journal is cited, in accordance with accepted academic practice. No use, distribution or reproduction is permitted which does not comply with these terms.



# Bayesian Estimation of Potential Performance Improvement Elicited by Robot-Guided Training

Asuka Takai<sup>1,2\*</sup>, Giuseppe Lisi<sup>1</sup>, Tomoyuki Noda<sup>1</sup>, Tatsuya Teramae<sup>1</sup>, Hiroshi Imamizu<sup>3,4</sup> and Jun Morimoto<sup>1,5\*</sup>

<sup>1</sup> Department of Brain Robot Interface, Computational Neuroscience Laboratories, Advanced Telecommunications Research Institute International (ATR), Kyoto, Japan, <sup>2</sup> Mechanical and Physical Engineering Course, Graduate School of Engineering, Osaka City University, Osaka, Japan, <sup>3</sup> Department of Psychology, The University of Tokyo, Tokyo, Japan, <sup>4</sup> Department of Cognitive Neuroscience, Brain Information Communication Research Laboratory Group, ATR, Kyoto, Japan, <sup>5</sup> Graduate School of Informatics, Kyoto University, Kyoto, Japan

## OPEN ACCESS

### Edited by:

Mitsuhiko Hayashibe,  
Tohoku University, Japan

### Reviewed by:

Atsushi Takagi,  
NTT Communication Science  
Laboratories, Japan  
Guillermo Peris Fajarnes,  
Universitat Politècnica de València,  
Spain

### \*Correspondence:

Asuka Takai  
ataikai@atr.jp  
Jun Morimoto  
xmorimo@atr.jp

### Specialty section:

This article was submitted to  
Neural Technology,  
a section of the journal  
Frontiers in Neuroscience

**Received:** 02 May 2021

**Accepted:** 23 September 2021

**Published:** 21 October 2021

### Citation:

Takai A, Lisi G, Noda T,  
Teramae T, Imamizu H and  
Morimoto J (2021) Bayesian  
Estimation of Potential Performance  
Improvement Elicited by  
Robot-Guided Training.  
Front. Neurosci. 15:704402.  
doi: 10.3389/fnins.2021.704402

Improving human motor performance via physical guidance by an assist robot device is a major field of interest of the society in many different contexts, such as rehabilitation and sports training. In this study, we propose a Bayesian estimation method to predict whether motor performance of a user can be improved or not by the robot guidance from the user's initial skill level. We designed a robot-guided motor training procedure in which subjects were asked to generate a desired circular hand movement. We then evaluated the tracking error between the desired and actual subject's hand movement. Results showed that we were able to predict whether a novel user can reduce the tracking error after the robot-guided training from the user's initial movement performance by checking whether the initial error was larger than a certain threshold, where the threshold was derived by using the proposed Bayesian estimation method. Our proposed approach can potentially help users to decide if they should try a robot-guided training or not without conducting the time-consuming robot-guided movement training.

**Keywords:** haptic guidance, skill level, motor training, robotic teaching, human-robot interaction

## INTRODUCTION

Collaboration between robots and humans can expand human capabilities and has been investigated on the applicability in fields ranging from rehabilitation to collaborative manufacturing. Many different approaches have been developed to train human movements with robots by providing motor instructions and feedback. For this kind of application, it is essential to predict whether an individual responds to a specific robotic training (Sigrist et al., 2013) before actual training to avoid wasted time and effort, but such estimation methods have not been established.

Furthermore, the efficacy of robotic instruction through haptic sense has not been sufficiently investigated while the haptic interface that provides motor instructions to human users has been long-term explored (Mussa-Ivaldi et al., 1985; Sigrist et al., 2013). The effect of somatosensory feedback has been compared to that of visual guidance. For example, Feygin et al. examined haptic guidance in short-term training to learn novel three-dimensional (3D) circular trajectories. They found that haptic training alone was less effective than lone visual training for positional

reproduction performance (Feygin et al., 2002). Liu et al. also studied the short-term performance of tracking novel 3D circular trajectories. They found that haptic input in addition to visual demonstration did not improve the tracing error compared to the visual-alone condition (Liu et al., 2006). Wong et al. examined skill learning in 3-day consecutive haptic interface training of drawing two-dimensional (2D) trajectories. They rather found that additional haptic demonstration showed greater improvements than visual-alone conditions (Wong et al., 2012).

On the other hand, previous studies suggested that haptic instructions seem to be beneficial to initially less-skilled participants (Sigrist et al., 2013). Marchal-Crespo et al. (2010) found that initially less-skilled participants significantly improved their steering skills after training using the haptic guided driving task. However, the previous studies did not provide a systematic approach either to verifying the grouping depending on individual initial skill level or selecting a specific boundary to estimate potential motor improvement. They rather found a linear correlation between the initial skill level and its change after robotic haptic interaction (Marchal-Crespo et al., 2010, 2017; Duarte and Reinkensmeyer, 2015). Although only Duarte and Reinkensmeyer used information criteria and identified the relevance of initial skills to the change, they have not tried to define the boundary value.

Identifying the boundary promises positive training effects for target users of each task or the type of robotic training. This study proposes an identification method to evaluate the dependence of the training effect on the initial skill level by modeling the skill level change between before and after receiving the haptic guidance training. We verify the grouping's validity based on model fitness and propose a systematic method to set a theoretically sound boundary value.

## MATERIALS AND METHODS

### Bayesian Modeling of the Skill Level Change

To provide the boundary for estimating whether motor performance of a user can be improved or not, we first verify the skill level change model differs between individuals depending on their initial skill level. For this, we referred to Sigrist's summary. Sigrist et al. (2013) suggested that position haptic guidance may be useful for novices or less skilled. This can be interpreted as the skill level change model that allows to vary both the intercept and slope by the initial participant's skill. We prepared four different hypothetical models, as shown in **Table 1**. To model changes in skill level for an evaluation metric, we employed the Bayesian statistical modeling based on Markov Chain Monte Carlo (MCMC) with a No-U-turn sampler and variational inference (Salvatier et al., 2016). Specifically, the linear models in **Table 1** have both the intercept ( $\alpha$ ) and slope ( $\beta$ ), which were allowed to vary between models. The analysis used

the following basic formula:

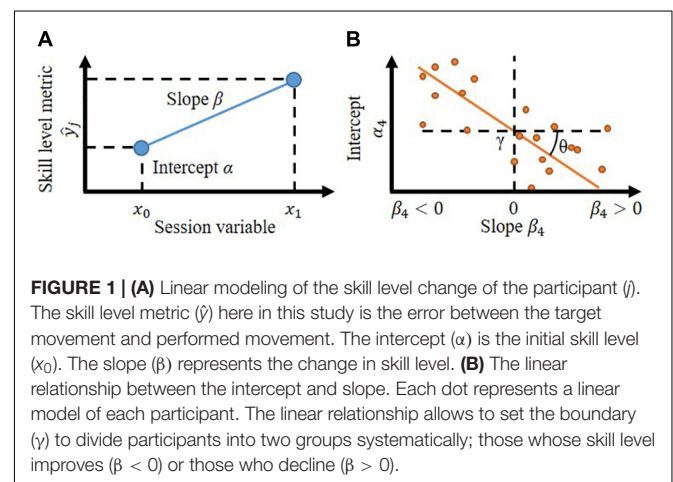
$$\hat{y}_{ij} = \alpha_{ij}[k] + \beta_{ij}[k]x_k + \epsilon_k \quad (1)$$

where  $i$  is the number of the model,  $j$  is the index of each participant,  $k$  is the index of each trial,  $\hat{y}$  is the variable of interest, and  $x$  is the session variable (that is, 0: first, 1: second session). The formula for a participant ( $j$ ) is illustrated in **Figure 1A**.

Model 1 (in **Table 1**) has the participant independent intercept and slope, which means the change in metric is independent of the participants and their initial skill level. If this is the case, all participants can attain the benefit of robotic instruction. This means all participants have the same skill level change model and highly likely the lowest model fitness among the four. Model 2 has a participant-dependent slope, which means the change in skill varies among participants but cannot be predicted by their initial skill level. Model 3 has the participant-dependent intercept, which means that the robotic instruction can equally affect their skill change regardless of their initial skill level. Although Model 3 is ideal as an instruction, it is highly unlikely to have a high fitness to the haptic instruction. Model 4 has varying intercepts and slopes. Thus, the skill level change can be predicted by their initial skill level. If the metric's fitness to Model 4 is greater than the others, it signifies that the haptic instruction is beneficial to initially less skilled participants. This supports the initial skill-based grouping statistically. Spontaneously, it also suggests that the initial performance can result in motor improvements after receiving instructions from the existing dataset.

**TABLE 1** | Models of the skill level change.

Model number (i)	Formula	Description
1. Pooled	$\hat{y}_{1j} = \alpha_1 + \beta_1 x_j$	<ul style="list-style-type: none"> <li>Independent to initial skill</li> <li>Effective equally to everybody</li> </ul>
2. Varying slope	$\hat{y}_{2j} = \alpha_2 + \beta_{2j} x_j$	<ul style="list-style-type: none"> <li>Independent to initial skill</li> <li>Effective differently for individual</li> </ul>
3. Varying intercept	$\hat{y}_{3j} = \alpha_{3j} + \beta_3 x_j$	<ul style="list-style-type: none"> <li>Dependent on the initial skill</li> <li>Effective equally to everybody</li> </ul>
4. Varying intercept and slope	$\hat{y}_{4j} = \alpha_{4j} + \beta_{4j} x_j$	<ul style="list-style-type: none"> <li>Dependent on the initial skill</li> <li>Effective differently for individual</li> </ul>





## Linear Relationship Between the Intercept and Slope to Define the Boundary

If the skill level change model differs between individuals, we can derive the boundary using the relationship between the initial metric (that is, the intercept) and the change in the metric (that is, the slope). Hence, we included the following linear equation in model 4:

$$\alpha_j = \theta\beta_j + \gamma \quad (2)$$

The formula is illustrated in **Figure 1B**. A non-zero  $\theta$  would highlight a significant relationship between  $\alpha$  and  $\beta$ , while a non-zero  $\gamma$  would signify that for some participants, performance improved ( $\beta < 0$ ), while for other participants, performance declined ( $\beta > 0$ ). Thus,  $\gamma$  is the boundary of the initial skill level.  $\gamma$  was estimated simultaneously while estimating  $\alpha$  and  $\beta$  by MCMC, so posthoc analysis was not needed.

The complete probabilistic model is defined as follows:

$$Y \sim \mathcal{N}(\mu_i, \sigma^2) \quad \mu_i \sim \alpha_{ij} + \beta_{ij} \cdot X \quad \sigma \sim |\mathcal{C}(5)| \quad (3)$$

$$\alpha_{ij} \sim \begin{cases} \mathcal{N}(0, 10^{-5}) & i = 1, 2 \\ \mathcal{N}(\mu_{ai}, \sigma_a^2) & i = 3, 4 \end{cases} \quad \mu_{ai} \sim \begin{cases} \mathcal{N}(0, 10^{-5}) & i = 3 \\ \theta \cdot \beta_{ij} + \gamma & i = 4 \end{cases} \quad \sigma_a \sim |\mathcal{C}(5)| \quad (4)$$

$$\sigma_\theta \sim \mathcal{F} \quad \sigma_\gamma \sim \mathcal{F} \quad (5)$$

$$\beta_{ij} \sim \begin{cases} \mathcal{N}(0, 10^{-5}) & i = 1, 3 \\ \mathcal{N}(\mu_\beta, \sigma_\beta^2) & i = 2, 4 \end{cases} \quad \mu_\beta \sim \mathcal{N}(0, 10^{-5}) \quad \sigma_\beta \sim |\mathcal{C}(5)| \quad (6)$$

where all the quantities defined in the previous paragraph still hold,  $Y$  represents the outcomes (skill level metric),  $X$  represents the predictors (that is, 0: first, 1: second session),  $\mathcal{N}$  is the Gaussian distribution,  $|\mathcal{C}(5)|$  is a Half-Cauchy distribution with parameter 5, and  $\mathcal{F}$  is an uninformative (flat) prior. All the parameters of the prior distributions were based on the default settings of the probabilistic modeling software (Salvatier et al., 2016).

## Sample Dataset: Experiment With a Haptic Interface

The above model was applied to the experimental data of participants who interacted with a robot-assisted motor training system from our laboratory, which guided the participant's hand to show the procedure to process an actual motor task of interest.

### Participants

Participants included 20 healthy right-handed adults (17 men, 3 women; age range: 21–34 years; mean  $\pm$  standard deviation [SD] = 24.017  $\pm$  2.596). The handedness was determined by a verbal inquiry based on the Edinburgh inventory. All participants provided written informed consent before participation. The ATR Review Board Ethics Committee approved the study protocol.

### Task and Apparatus

The target task involved drawing a true circle of 10 cm radius on a horizontal plane using one's left hand. We selected our task referencing existing studies with healthy subjects introduced in section "Introduction," especially Wong et al. (2012). Feygin et al. (2002) identified an interference between the visual and haptic modal, so we decided not to provide visual feedback to our participants during haptic feedback. The subject's hand is hidden under a white table, on top of which additional information can be visualized using a projector. Participants were asked to complete the drawing within approximately 2 s. They started drawing the circle from the 12 o'clock position and moved in a counter-clockwise direction. All the task details were consistent with those in our previous experiment (Takai et al., 2018). A robotic manipulandum located under a white table guided the target movement (**Figure 2A**). The table prevented the participant from viewing their hand as it moved. The robot was programmed to provide negligible resistance to movement while the participants were drawing. For safety, the robot stopped moving when the force applied at the end effector exceeded the prescribed range or when the handle left a specified safe area.

### Haptic Feedback

The manipulandum moved the participant's left hand along the targeted movement trajectory. Participants received proprioceptive afferent information during the entire movement. The robot handle moved at a constant velocity outside the acceleration/deceleration (A/D) period, set to 0.2 s after it starts and before it finishes the movement. The target circle was visible during movement guidance. As with our previous study (Takai et al., 2018), the participants could not see their hand's current position or the robot's end-effector at any moment. During the robotic guidance, the participants were instructed not to move their arms with or against the robot's movement. However, the participants were not completely passive to the guidance, as they maintained the posture of their arms to avoid coming in contact with the table.

### Score Feedback

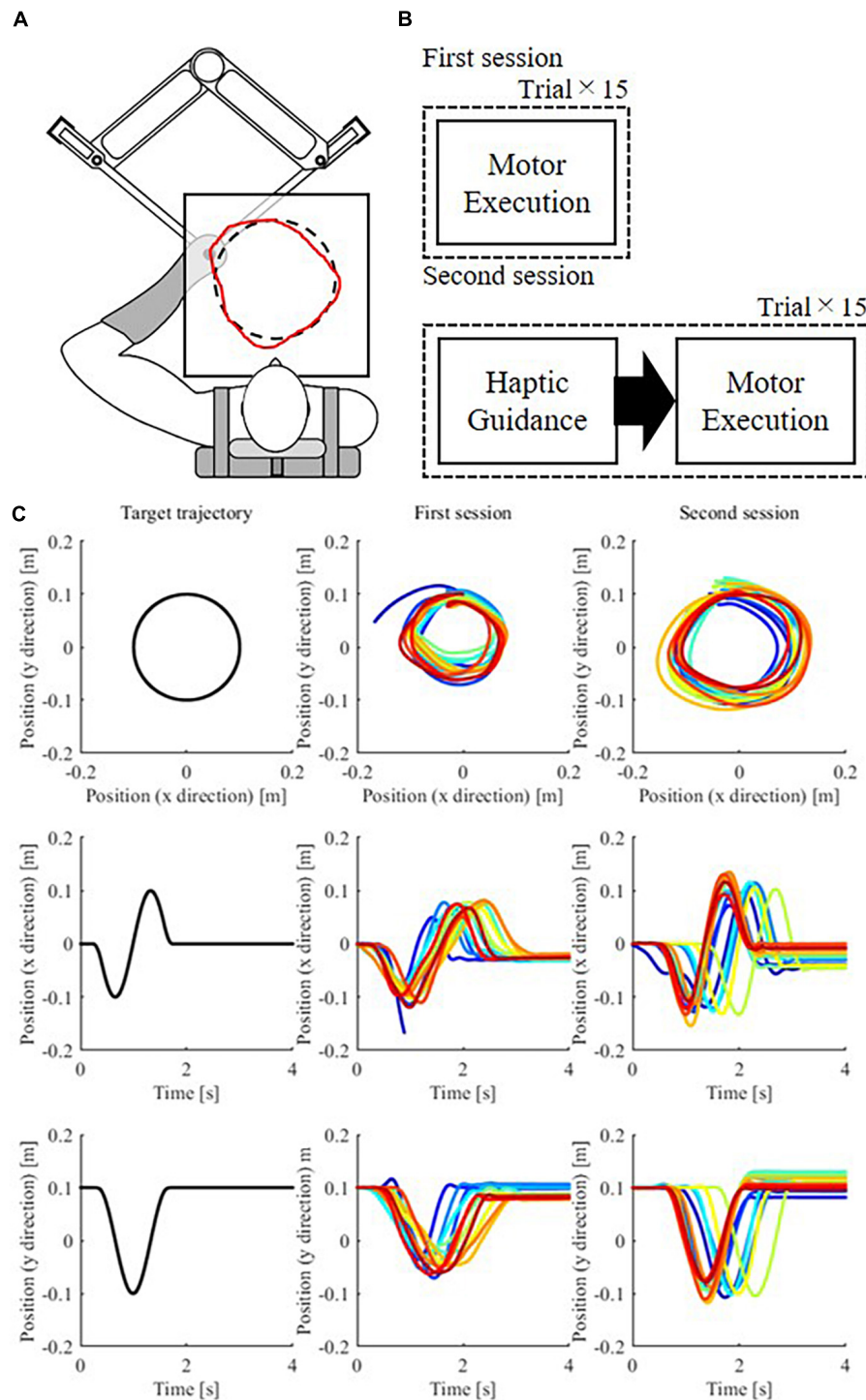
We evaluated the drawn circles by the participants and fed back the score to the participants soon after each trial. The equations used to calculate the score are as follows:

$$\text{ERR}(t) = \sqrt{(x_{\text{hand}}(t) - x_{\text{target}}(t))^2 + (y_{\text{hand}}(t) - y_{\text{target}}(t))^2} \quad (7)$$

$$\text{Score}(t) = 100 \frac{E_{\text{max.}} - \text{ERR}(t)}{E_{\text{max.}}} \quad (8)$$

$$\text{Trial Score} = \frac{1}{t_e - t_s} \sum_{t=t_s}^{t_e} \text{Score}(t) \quad (9)$$

where  $\text{ERR}(t)$  is the error between the hand and target position at time  $t$ ,  $x_{\text{hand}}(t)$  and  $y_{\text{hand}}(t)$  are the coordinates of the hand position at time  $t$ , and  $x_{\text{target}}(t)$ ,  $y_{\text{target}}(t)$  are the coordinates of the target position at time  $t$ ,  $t_s$  is the starting time, and  $t_e$  is the ending time.  $E_{\text{max.}}$  is the maximum allowed error and is set to be the same as the target circle radius.



**FIGURE 2 | (A)** Motor task and apparatus. Participants were asked to draw a true circle (dashed line) using their left hand within 2 s. A manipulator located under the table provided haptic guidance. The participants could hold a handle on the manipulator, and it moved to guide their hand in the desired direction. The red line shows a representative example of a handwritten trajectory. Both the target circle and drawn figures were hidden from the participants during motor execution, such that the participants never saw the actual hand position. **(B)** Procedure. The participants completed 15 trials in which they drew a circle with score feedback at the end of each trial. Next, the participants completed 15 trials in which they first received haptic guidance from the robot, that is, allowed the robot to move their hand in the desired trajectory, and then executed the drawing movement by themselves without being assisted by the robot. Finally, they received their score at the end of each trial. **(C)** Target movement and executed movements by a participant at both sessions in the x–y plane and its time trajectory in the x and y directions. Early trials are plotted as blue traces, and subsequent trials are denoted by “warmer” colors.

## Experimental Design

At the beginning of the experiment, participants were familiarized with the task by observing a human instructor performing the task. Participants have been told the diameter of the target circle is 10 cm. Although we did not explicitly show ideal velocity profiles to a subject, we asked the subject to generate the hand movement with a constant speed and also informed that the task duration was 2 s.

Subsequently, they underwent the experimental procedure as shown in **Figure 2B**. During the first session, the participants were instructed to reproduce the target movements in terms of both position and velocity as accurately as possible without any assistance from the manipulandum. The participants' active movements were measured for 15 trials (**Figure 2B**, top). Before starting a trial, the target circle is projected on the table for approximately 3 s. Subsequently, the circle is removed, and no visual information about the circle size, speed, or the current hand position is provided. We evaluated the circles drawn by the participants in each trial. The average error between the target and the performed movement was normalized such that the values ranged from 0 to 100 (as shown in Eq. (8)). After each trial, the score was projected on the table for approximately 3 s using a projector. Subjects are asked to improve their score. While the target circle and the current hand position are also visualized with the score, the performed trajectory was not shown to the participants.

In the second session, participants received haptic guidance from the manipulandum. Subjects are instructed to memorize the position and velocity of the guided motion as accurately as possible in preparation for the following motor execution. **Figure 2B** bottom shows that each trial consisted of one haptic guided presentation by the robot and one participant's motor execution. There were 5 s intervals before and after the haptic guidance. The score was shown to the participant at the end of each trial, similar to the first session. This session continued until the participants completed 15 trials (**Figure 2B**, bottom).

Both session trials in which the movement exceeded the specified safe area were not evaluated. However, they were counted to reach a predetermined number of 15 trials. The average number of trials for evaluation was 14.8 (SD 0.44) in the first session and 14.1 (SD 1.47) in the second session.

## Skill Level of Each Trial

Skill level was evaluated as the positional distance from the target circle as well as the difference between the performed velocity and the actual target velocity. Previous studies (Feygin et al., 2002; Liu et al., 2006; Lüttgen and Heuer, 2012; Wong et al., 2012) suggested that tracking performances of different physical variables such as position and velocity in a trajectory learning task could be sensitive to different types of modalities such as vision and haptics, respectively. These studies identified that the shape accuracy improved more in visual training, while haptic training was better for training the temporal aspects. Since our robot-guided training provides haptic feedback to a user, tracking performances of velocity profiles would be improved more than that of position trajectories. Thus, we separately evaluated

position and velocity tracking performances to investigate the effectiveness of the robot-guided haptic feedback. For each trial, the position and velocity errors were evaluated for 1.46 s, starting at the moment when the participants' hand left the start zone, within a circle with a diameter of 3 cm centered at 12 o'clock position. The position and velocity errors defined in Eqs (10, 11) were only used for analysis. Note that executed movements only by participants among all trials in the second session were evaluated.

$$E_p = \frac{1}{t_e - t_s} \sum_{t=t_s}^{t_e} |r_h(t) - r| \quad (10)$$

$$E_v = \frac{1}{t_e - t_s} \sum_{t=t_s}^{t_e} \|\mathbf{v}_h(t) - \mathbf{v}(t)\| \quad (11)$$

where  $E_p$  is the positional error from the target,  $t_s$  is the starting time,  $t_e$  is the ending time,  $r_h(t)$  is the current hand radius with respect to the workspace center at time  $t$ , and  $r = 10$  cm is the constant target radius.  $E_v$  is the velocity error from the target velocity  $\|\mathbf{v}\| = 37.62$  cm/s.  $\mathbf{v}_h(t)$  is the current hand velocity with respect to the workspace center at time  $t$ .

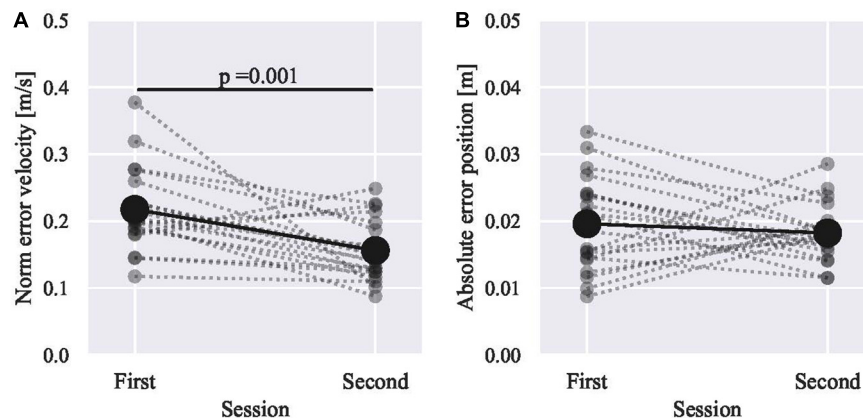
## RESULTS

### Evaluation of Models' Fitness to the Sample Dataset

The experimental result of a representative participant is shown in **Figure 2C**. The participant drew the circle smaller than the target in the first session, but the size increased after receiving the haptic guidance in the second session. The participants ( $n = 20$ ) mean errors as a function of the trial numbers decreases within each session, except the position error in the first session (**Supplementary Figure 1**). After the first session, still 4.3 mm error remained as the lowest position error. Therefore, the lowest position-error participant could further improve the tracking performance. In other words, the remained error indicated that the obtained results were not due to a ceiling effect on the performance. Meanwhile, there were marginally positive relationships between the mean of 15 trials among each participant's position and velocity errors in both sessions (**Supplementary Figure 2**).

The position and velocity errors are shown in **Figure 3**. Looking into the change in skill level for each participant (gray lines in **Figure 3**), the slope ranges from strong positive to strong negative. The lack of significant improvement in positional accuracy could have been due to the use of average data for all participants instead of classifying participants into groups. We fitted the models in **Table 1** to the metric to determine whether such grouping is reasonable. The results are shown in **Table 2** for velocity and **Table 3** for position.

The models' fitnesses were evaluated using the widely applicable information criterion (WAIC; Watanabe, 2010). The smaller the WAIC, the better the fit. By the leave-one-subject-out (LOSO) analysis, both criteria were tested 20 times, and the mean and SD are as shown in **Tables 2, 3**. Model 4 with



**FIGURE 3 |** The skill level change between sessions. The average of all participants metric is shown in black, and that of each participant is superimposed in gray. The metric is **(A)** the norm of error velocity and **(B)** the absolute error in position. The target peripheral speed is 0.376 m/s, and the radius of the target circle is 10 cm. The paired two-sample tests are Student's *t* for the velocity and Wilcoxon signed-rank test for the position.

**TABLE 2 |** Models' fitness of norm of error velocity.

Models	WAIC (Mean $\pm$ SD)
1. Pooled	$-1,129 \pm 16$
2. Varying slope	$-1,175 \pm 17$
3. Varying intercept	$-1,217 \pm 18$
4. Varying intercept and slope	$-1,311 \pm 12$

**TABLE 3 |** Models' fitness of absolute positional error.

Models	WAIC (Mean $\pm$ SD)
1. Pooled	$-3,733 \pm 22$
2. Varying slope	$-3,774 \pm 22$
3. Varying intercept	$-3,856 \pm 17$
4. Varying intercept and slope	$-4,035 \pm 16$

varying intercepts and slopes had the best fit for both velocity and position metrics. Therefore, it was fair to divide participants based on their initial skill level.

## Deriving the Boundary

Subsequently, we inspected the linear model between the intercept ( $\alpha$ ) and slope ( $\beta$ ) to derive the boundary ( $\gamma$ ). The LOSO analysis was conducted, and the sample result excluding subject 1 is as shown in **Figures 4, 5** (**Figure 4** for the position and **Figure 5** for the velocity). After fitting the linear model, the distributions of  $\theta$  and  $\gamma$  do not include zero. Thus, a significant relationship between  $\alpha$  and  $\beta$  was identified, and it signified that for some participants, performance improved ( $\beta < 0$ ), while for other participants, performance declined ( $\beta > 0$ ). As shown in **Figure 4B**, the slope ( $\beta$ ) of subjects who have an initial error above the boundary  $\gamma$  are negative; however, those with an initial error below are positive. Based on the confusion matrix, the accuracy of classification was 0.9 for the position and 0.7 for the velocity models. The F measure was 0.91 for the position model and 0.82 for the velocity model. The excluded subject's

performance in the second session was predicted by the initial skill level. As shown in **Figure 6**, the subjects are well classified into two groups based on the boundary.

## Group-Based Haptic Guidance Effect

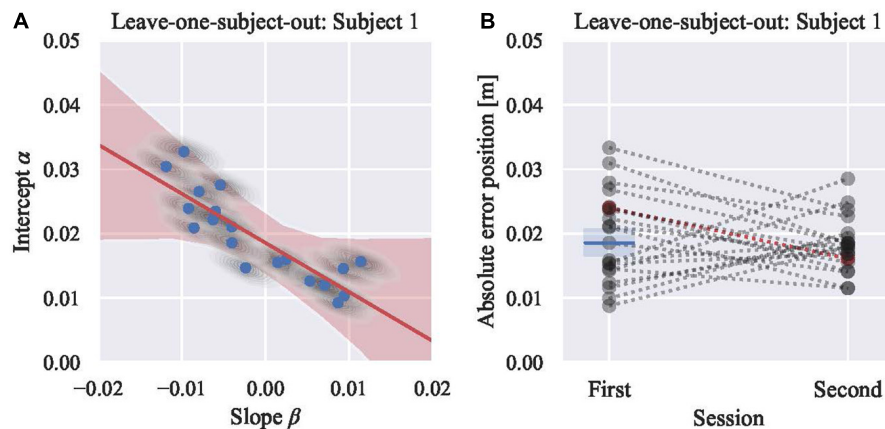
The 20 participants were allocated into three groups based on position and velocity boundary. The numbers of participants in each group are shown in **Table 4**. **Figure 7** shows the skill level change between sessions of all the three groups. The participants in the red group were initially low-skilled in terms of both position and velocity, while the participants in the green group were initially high-skilled. The blue group was initially low-skilled in terms of velocity but was highly skilled in terms of position. The initially low-skilled participants in terms of position but highly skilled in terms of velocity were not found in the dataset.

Without grouping, the efficacy of haptic guidance was not significant, especially in positional accuracy, as shown in **Figure 3B**. However, by grouping, the red group showed significant improvements in both metrics (the velocity and position). On the contrary, the green group shows a minor deterioration in terms of position, while a minor improvement in terms of velocity was also observed. These results suggest that the initially low-skilled participants significantly improved their skill level. Regarding the blue group, the initially low-skilled aspect (velocity) improved; however, the initially high-skilled aspect (position) did not improve, while both did not significantly change. Those of who increased the velocity error also increased the positional error (2 out of 3 subjects).

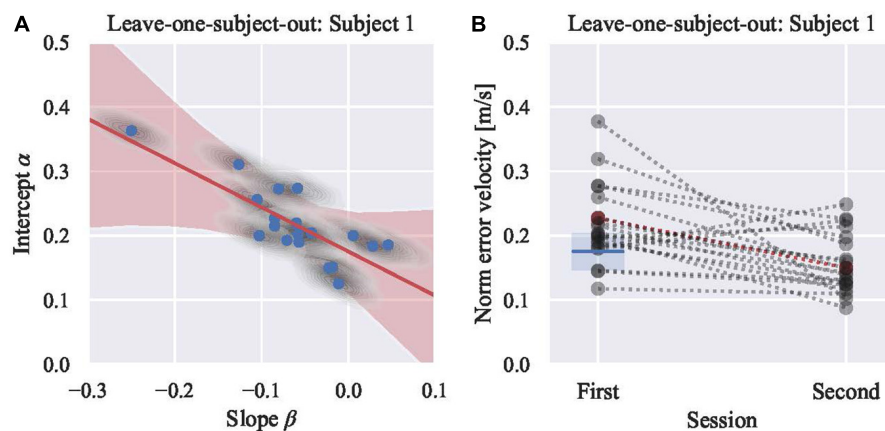
## DISCUSSION

Due to the increasing demand to improve motor performance via human-robot collaboration, numerous different approaches have emerged; however, not all of them guarantee motor performance improvements (Williams and Carnahan, 2014). It would be useful





**FIGURE 4 | (A)** Posterior predictive plot of model 4 using 19 participants' absolute position errors (leaving subject 1). Each gray shaded area represents multiple samples from the posterior [the intercepts ( $\alpha$ ) and the slopes ( $\beta$ )] of each subject, and each blue circle shows the average of each area. Red shaded area represents regression lines for all samples, and red line shows their average. The boundary ( $\gamma$ , the intercept of the red line) is 0.019 m with the credible interval (94%) from 0.017 to 0.021 m. **(B)** Visualization of classifying results. Subject 1, showing in red marker, is tested. Rest of 19 participants are showing in gray markers. Blue line shows the boundary derived from model 4 in **(A)**. Blue shaded area shows the 94% credible interval. Mean absolute position error of Subject 1 in the first session was above the boundary. Thus, subject 1 is classified into a group that is expected to improve the performance in the second session. Actual mean absolute position error in the second session is less than that of the first session.



**FIGURE 5 | (A)** Posterior predictive plot of model 4 using 19 participants' norm of error velocity (leaving subject 1). Each gray shaded area represents multiple samples from the posterior [the intercepts ( $\alpha$ ) and the slopes ( $\beta$ )] of each subject, and each blue circle shows the average of each area. Red shaded area represents regression lines for all samples, and red line shows their average. The boundary ( $\gamma$ , the intercept of the red line) is 0.175 m/s with the credible interval (94%) from 0.147 to 0.204 m/s. **(B)** Visualization of classifying results. Subject 1, showing in red marker, is tested. Rest of 19 participants are showing in gray markers. Blue line shows the boundary derived from model 4 in **(A)**. Blue shaded area shows the 94% credible interval. Mean norm of error velocity of Subject 1 in the first session was above the boundary. Thus, subject 1 is classified into a group that is expected to improve the performance in the second session. Actual mean norm of error velocity in the second session is less than that of the first session.

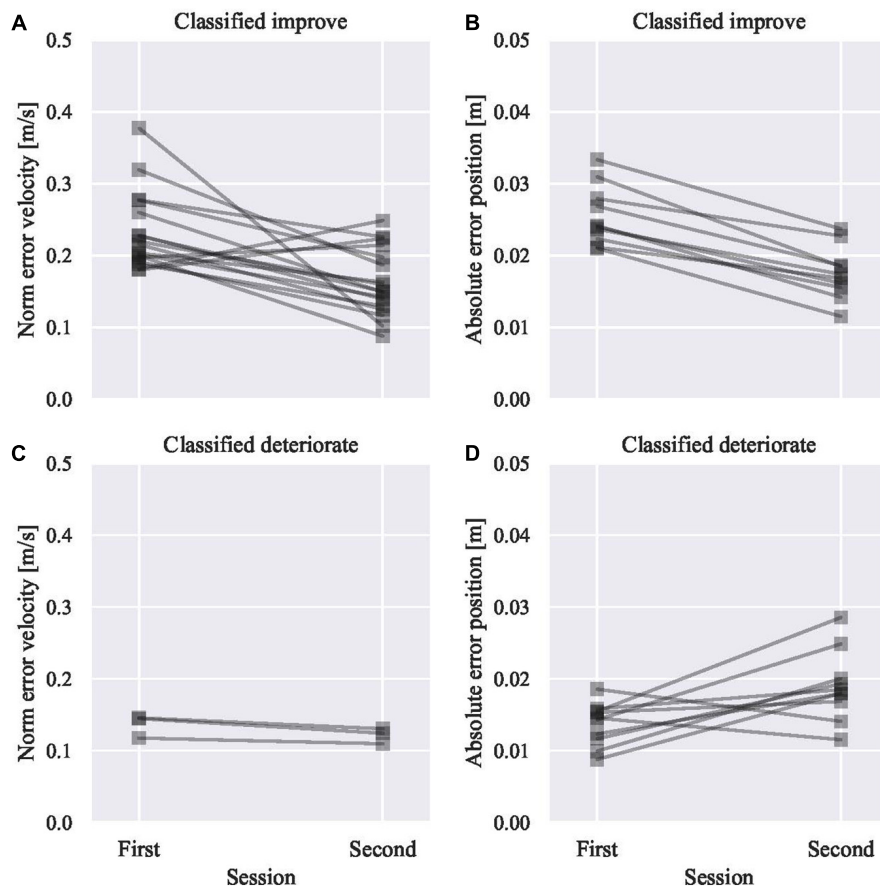
and efficient if the chance of success for a user could be estimated prior to training. Our study proposes a versatile method that can statistically elaborate on the relationship between performance improvements and the person's initial skill level.

## Identifying Target People Through the Statistical Grouping Method

In this study, we have proposed a Bayesian estimation method for examining different linear models that explain the relationship between the initial skill level and its change. By comparing

these models, the most appropriate model to explain this relationship can be identified. This provides a non-heuristic but hypothesis-based approach to analyze the benefit of interest. Moreover, hypothetical models, that is, the relationship between motor performance and the initial skill level, can be explicitly implemented and even compared to identify which model the data with maximum likelihood.

Four different models have been examined in this study (Table 1). These are fully against (Model 1), partially against (Models 2 and 3), or in agreement with Sigrist's summary (Model 4). If the metric's fitness to Model 4 is greater than the others,



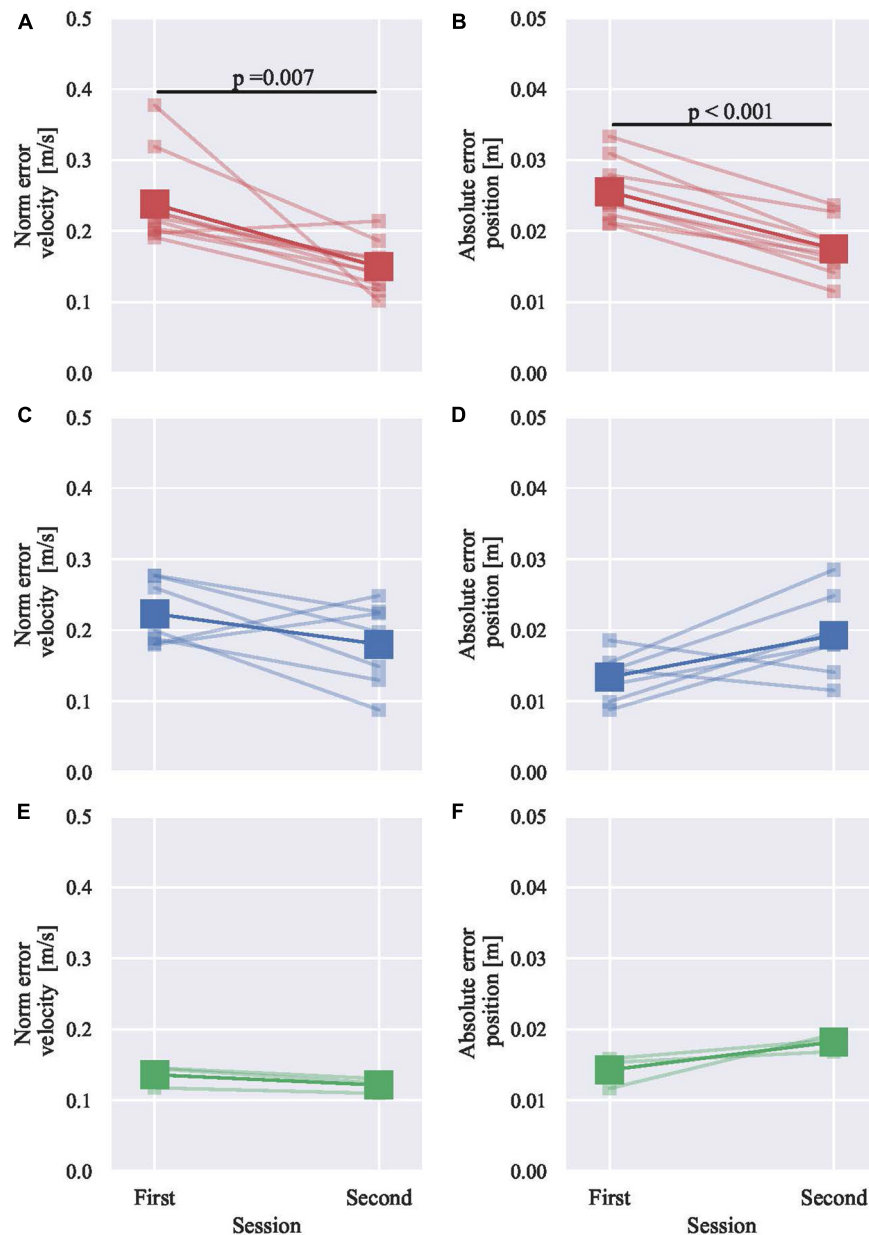
**FIGURE 6 | (A)** The classified subject for improving velocity error based on LOSO method. Subjects were above the boundary in the first session, so they are predicted to improve their performance in the second session. Most of them scored fewer errors in the second session. **(B)** Subject predicted as to improve positional error. **(C)** Subject predicted as to deteriorate velocity error. **(D)** Subject predicted as to deteriorate positional error.

**TABLE 4 |** Classification in groups.

	Below position threshold	Above position threshold
Above velocity threshold	Number of subjects = 7 (Color in <b>Figure 7</b> : Blue)	Number of subjects = 10 (Color in <b>Figure 7</b> : Red)
Below velocity threshold	Number of subjects = 0	Number of subjects = 3 (Color in <b>Figure 7</b> : Green)

it can signify that the skill level change model differs between individuals. Hence, the performance improvement is a function of the initial skill level and statistically supports the initial skill-based grouping. We used WAIC for model evaluation, which aims to select a model that makes good predictions, rather than the likelihood ratio test, which aims for the safe rejection of the null hypothesis and cannot show that the alternative hypothesis is good (Posada and Buckley, 2004). As a result, WAIC is the lowest in Model 4 with varying intercepts and slopes than the other models for both velocity and position metrics. Therefore, it statistically supports dividing participants based on their initial skill level. The skill level metric ( $\hat{y}$ ) used in this study is the error between the target and performed movement. Thus, the method is neither parameter- nor task-dependent and is expected to work in a wide range of applications.

Grouping of participants either qualitatively or quantitatively has been explored in previous studies. For example, to define participants' experiences, authors generally used classification terms, such as Novice and Expert (Beilock et al., 2002). While in another study, the motor skill level is sometimes referred to as participants' symptoms, for example in autism, where the patients have motor difficulties to some extent, or typically developed (Staples and Reid, 2010). In other studies, participants who scored on a motor test under a specified threshold (Marchal-Crespo et al., 2010) or the median among the participants (Etnier and Landers, 1998) are grouped as less-skilled. Participants are also sometimes grouped based on quantiles (Malina et al., 2007). Grouping into an equal number of participants (Yamamoto et al., 2019) has also been introduced insofar. However, the reason why grouping is reasonable is not well explained. Metric-based



**FIGURE 7 |** The skill level change between sessions with participants grouping based on the derived boundaries. **(A)** Red group velocity. **(B)** Red group position. **(C,D)** Blue group and **(E,F)** Green group. The paired two-sample tests are Wilcoxon signed-rank test in **(A)** and Student's *t*-test in **(B)**.

approaches have also been introduced (Hook et al., 2004; Gruber et al., 2006; Dose et al., 2007). These studies identified unique and best metrics among many options to identify handwriting. They developed feature-based classification algorithms. However, the method to verify clustering relies on subjective labeling. Aharonson and Krebs (2012) used the no-labeling method but still had to run an exhaustive search. Thus, heuristic-based approaches could not be avoided in previous studies. Limitations regarding our approach are discussed in section “Challenges and Prospects on Model Interpretation Regarding Potential Motor Improvements.”

## Defining the Skill Level Boundary Through Linear Modeling of Its Change

We included a linear relationship between the coefficients of the linear model (Figure 1B) to derive the boundary. By inferring the parameters using the Bayesian inference, non-zero coefficients provided evidence of a linear relationship. This shows an effective boundary to identify those that can benefit from haptic guidance. The parameters are inferred in consideration of the uncertainty under the limited data assuming the existence of a certain true value for each parameter because the Bayesian approach

takes into account the uncertainties of parameter values while providing exact inference. In contrast, most maximum likelihood (or least squares) estimation fixes the parameter values though there is considerable uncertainty (Punt and Hilborn, 2001). The boundary that is suitable for practical use needs to be estimated from a small number of data samples -as is the case in exploratory experiments with human subjects (Sabatini and Mannini, 2016; Kim et al., 2017)- and to be robust for new data, and it is better not to vary with each re-estimation. Bayesian estimates obtained from MCMC procedures are appropriate in small samples (Dunson, 2001; Gray et al., 2015). Since Bayesian models accommodate unobserved variables (in our case, gamma) with associated uncertainty (Dunson, 2001), we can confidently build a threshold.

The linear relationship between the intercept ( $\alpha$ ) and the slope ( $\beta$ ) fits the skill-level metric change of absolute error in position as well as the norm of error velocity. As a result, the boundary ( $\gamma$ ) is derived with sufficiently low WAIC. Non-zero  $\theta$  clearly shows that for some participants' performance improved, while for others, performance declined. The difference in metric change trends between the first and second session is also visible between the participants who are above and below the boundary (Figures 4B, 5B). Such Bayesian estimation using a complex model cannot be done with simple linear regression (Dunson, 2001; Punt and Hilborn, 2001). Although the metrics relationship may fit more with a non-linear model or may need more data (Figures 4A, 5A), these results prove the concept of model-based interpretation of the motor training effects and potential. In future studies, an extended (for example, mixed effect, order effect) model-based inference could be applied.

In the scenario of using the estimated parameters in this study, an examiner of the haptic guided training can classify subjects with confidence because the boundary is provided with the credible interval as the most likely value from the computed posterior distribution. When a subject's initial skill is at the vicinity of the boundary, the posterior probability distribution (the certainty of the boundary) can support the examiner's judgment. The estimated boundary value fixed with considerable uncertainty (Punt and Hilborn, 2001) has little merit in the above interpretation. Hespanhol et al. (2019) demonstrated that the credible interval is more natural and easy-to-interpret than the frequentist intervals. Even in a small sample size, the percent of the credible interval that contained the true population mean is higher than that of the confidence interval (Gray et al., 2015).

Previous studies have already identified the linear correlation of initial skill level to its change following robotic haptic interaction (Marchal-Crespo et al., 2010, 2017; Duarte and Reinkensmeyer, 2015). Although only Duarte and Reinkensmeyer (Duarte and Reinkensmeyer, 2015) performed information criteria and identified the relevance of initial skills to changes other than fixed effects, the statistical test does not answer the use of the identified effect in real-world applications. Looking at rehabilitation studies, many studies have been made regression models for predicting trial-by-trial change in impairment (Casadio and Sanguineti, 2012) or long-term effect, including daily-life usage-dependent changes implicitly (Reinkensmeyer et al., 2016). Although the potential benefit

of making a prognosis based on the clinical scores and the brain images, these studies do not predict whether a patient responds to a specific intervention or a robotic treatment. Meanwhile, Schweighofer and colleagues not only statistically identified potential predictor of changes in clinical score after arm rehabilitation but also derived a functional threshold for who can benefit (Schweighofer et al., 2009). They successfully proved their concept, but the accuracy was not as high as in this study. This highlights the importance of verification using different hypothetical models rather than examining a single model.

A linear relationship between initial skill level and changes after robotic haptic interaction may be found in various tasks, ranging from driving a car (Marchal-Crespo et al., 2010), golf patting (Duarte and Reinkensmeyer, 2015), leg rehabilitation (Marchal-Crespo et al., 2017), and tasks related to upper arm motor functionality, as are, in this study. Therefore, the linear modeling method may be applicable and useful in other motor tasks and training approaches.

## Efficacy of Haptic Guidance in Motor Training

In previous studies, haptic training methods were evaluated based on the means of all participants' metrics (Feygin et al., 2002; Liu et al., 2006; Lüttgen and Heuer, 2012; Wong et al., 2012). Without grouping, as shown in Figure 3, the norm of error velocity decreased (improved) after haptic guidance training. However, the absolute error in position shows no change on average. Therefore, the training effect suggested from our dataset without grouping is questionable as is in line with previous studies. For example, haptic training improved the timing aspect (Feygin et al., 2002; Lüttgen and Heuer, 2012) with short-term training but not for positional error (Wong et al., 2012). These consistencies prove that the dataset is not peculiar or an artificial one prepared to explain the proposed method.

This study verified the fairness in dividing participants based on the initial skill level using a derived boundary. By grouping, initially low-skilled participants significantly improved their average skill level regarding both position and timing aspects. The training's effectiveness and identified target participants are consistent with a previous study that used the heuristics grouping method (Marchal-Crespo et al., 2010). Haptic guidance is a major approach in robotic rehabilitation to facilitate motor functional recovery (Marchal-Crespo and Reinkensmeyer, 2009; Sigrist et al., 2013). This may be an appropriate approach for patients who have lost motor skills.

For high-skilled participants, their performance did not change much. This is consistent with previous studies; for example, "Benefit of guidance-based training was not detected for the more skilled young/old participants" (Marchal-Crespo et al., 2010). Some previous studies explained this by referring to the challenge point theory (Guadagnoli and Lee, 2004). The theory states that task difficulty should be appropriately adjusted to meet the participant's skill level to maximize the training effect. However, this study explains this differently using the derived boundary and explains that performance deterioration may result from difficulty in recognizing the difference between a goal and



their movements. High-skilled participants make a very small error from the goal movement but need to identify the error only through somatosensory information. The error is in the same range of the correctly identifiable difference between the reference and test, as reported by Wilson et al. (2010). Since information is successfully processed only when uncertainty is reduced (Fitts, 1954), unreliable haptic guidance for them may not result in motor improvements. Meanwhile, high-skilled participants may improve their performance using score feedback that is specific to the feature to be enhanced or using alternative haptic interaction approaches, for example, error amplification (Milot et al., 2010; Duarte and Reinkensmeyer, 2015; Marchal-Crespo et al., 2017).

The motor performance of the participants in the blue group was partially improved by the haptic guidance. This is consistent with previous experiments that showed learning of timing (Marchal-Crespo et al., 2010), rather than spatial. Participants might be trapped with the speed-accuracy trade-off as the difference in speed to be a difference in the difficulty level of the task (Shmuelof et al., 2012). In other words, the positional accuracy deteriorated because of improved speed accuracy. In this study, the participants can obtain better scores if they attempt to reduce position error at the cost of velocity error or vice versa because the score accounts for both positional and velocity performance. One possible solution might be to feedback velocity and position score separately.

## Challenges and Prospects on Model Interpretation Regarding Potential Motor Improvements

In this study, we have applied the modeling method to sample data of 20 participants and interpreted the outcome to divide participants into discrete groups. Grouping analysis provided a detailed interpretation of the efficacy of haptic guidance for each participant at the specific initial skill level, as discussed in section “Efficacy of Haptic Guidance in Motor Training.” For other tasks, all subjects may improve skill level similarly (that is, no boundary exists). This would make the fit of Model 4 worse or equal to the others. Besides, this method may help to find other kinds of structures in larger data. When the fit of Model 4 is better than the others, there are two possible phenomena: the participant-dependent training effect and the regression toward the mean. Both can be expressed by Model 4; however, they are separable, as the former has a large mean slope in the absolute and the latter has a small one. Nonetheless, this approach would be valuable for exploring the data.

To fit the Bayesian linear model, it requires datasets *a priori*, similar to other data-driven methods. Also, the boundary is highly dependent and influenced by the task. These limitations are common to the studies presented previously; for example, Gruber et al. (2012) made a handedness classifier. Nevertheless, it is beneficial for trainees as they can perceive the possible outcome before continuing the ineffective and time-consuming training. There is, for example, a possible solution to alternate robot approaches to fit the individuals at any

level to guarantee the motor improvements (Brown et al., 2016), but our solution is to help identify responders who can benefit from existing approaches. The interpretation can also be useful in assigning suitable next motor skill training protocols, not only for neuro-rehabilitation (Aharonson and Krebs, 2012) but also for skill development manufacturing (Ma, 2014), for establishing personalized and comprehensive motor training programs.

## CONCLUSION

In this study, we proposed a Bayesian estimation method for examining models that describe the changes in the skill level of haptic guidance training and deriving a boundary for dividing participants into initial skill-level groups. Results showed that we were able to predict whether a novel user can improve the performance by checking that the user's initial skill level was larger than the boundary. We have also demonstrated that the general idea/heuristic suggested by previous studies can be systematically evaluated. Such methods may be essential to select an effective approach for individuals among other different approaches.

## DATA AVAILABILITY STATEMENT

The datasets generated for this study are available on request to the corresponding author.

## ETHICS STATEMENT

The studies involving human participants were reviewed and approved by The ATR Review Board Ethics Committee. The patients/participants provided their written informed consent to participate in this study.

## AUTHOR CONTRIBUTIONS

AT, TN, HI, and JM contributed to the study design and project supervision. AT, GL, TN, and JM participated in the experimental design. AT, TN, and TT performed data acquisition. AT and GL performed data analysis, interpretation of results, and prepared the manuscript. All authors have read and approved the final manuscript.

## FUNDING

This research has been supported by the Commissioned Research of National Institute of Information and Communications Technology (NICT), Japan, Impulsing Paradigm Change through Disruptive Technologies (ImPACT) Program of Council for Science, Technology and Innovation (Cabinet Office, Government of Japan), The Japan Society for the Promotion

of Science (JSPS) KAKENHI, Grant Numbers: JP19H05725, JP15J11807, JP20K20263, and JP21H04911, Japan Agency for Medical Research and Development (AMED), Grant Number: JP21he2202005, and Japan Science and Technology Agency (JST) Moonshot R&D, Grant Number: JPMJPS2034.

## REFERENCES

- Aharonson, V., and Krebs, H. I. (2012). Prediction of response to robot-aided motor neuro-rehabilitation of children with cerebral palsy. *Biomed. Signal Process. Control* 7, 180–184. doi: 10.1016/j.bspc.2011.03.003
- Beilock, S. L., Carr, T. H., MacMahon, C., and Starkes, J. L. (2002). When paying attention becomes counterproductive: impact of divided versus skill-focused attention on novice and experienced performance of sensorimotor skills. *J. Exp. Psychol. Appl.* 8, 6–16. doi: 10.1037/1076-898X.8.1.6
- Brown, D. A., Lee, T. D., Reinkensmeyer, D. J., and Duarte, J. E. (2016). “Designing robots that challenge to optimize motor learning,” in *Neurorehabilitation Technology*, eds D. J. Reinkensmeyer and V. Dietz (Cham: Springer International Publishing), 39–58. doi: 10.1007/978-3-319-28603-7\_3
- Casadio, M., and Sanguineti, V. (2012). Learning, retention, and slacking: a model of the dynamics of recovery in robot therapy. *IEEE Trans. Neural Syst. Rehabil. Eng.* 20, 286–296. doi: 10.1109/TNSRE.2012.2190827
- Dose, M., Gruber, C., Grunz, A., Hook, C., Kempf, J., Scharfenberg, G., et al. (2007). “Towards an automated analysis of neuroleptics’ impact on human hand motor skills,” in *Proceedings of the 2007 IEEE Symposium on Computational Intelligence and Bioinformatics and Computational Biology*, (Honolulu, HI: IEEE), 494–501. doi: 10.1109/CIBCB.2007.4221261
- Duarte, J. E., and Reinkensmeyer, D. J. (2015). Effects of robotically modulating kinematic variability on motor skill learning and motivation. *J. Neurophysiol.* 113, 2682–2691. doi: 10.1152/jn.00163.2014
- Dunson, D. B. (2001). Commentary: practical advantages of bayesian analysis of epidemiologic data. *Am. J. Epidemiol.* 153, 1222–1226. doi: 10.1093/aje/153.12.1222
- Etnier, J. L., and Landers, D. M. (1998). Motor performance and motor learning as a function of age and fitness. *Res. Q. Exerc. Sport* 69, 136–146. doi: 10.1080/02701367.1998.10607679
- Feygin, D., Keehner, M., and Tendick, R. (2002). “Haptic guidance: experimental evaluation of a haptic training method for a perceptual motor skill,” in *Proceedings 10th Symposium on Haptic Interfaces for Virtual Environment and Teleoperator Systems. HAPTICS 2002*, (Orlando, FL: IEEE), 40–47.
- Fitts, P. M. (1954). The information capacity of the human motor system in controlling the amplitude of movement. *J. Exp. Psychol.* 47, 381–391. doi: 10.1037/h0055392
- Gray, K., Hampton, B., Silveti-Falls, T., McConnell, A., and Bausell, C. (2015). Comparison of Bayesian credible intervals to frequentist confidence intervals. *J. Modern Appl. Stat. Methods* 14:8. doi: 10.22237/jmasm/1430453220
- Gruber, C., Hook, C., Kempf, J., Scharfenberg, G., and Sick, B. (2006). “A flexible architecture for online signature verification based on a novel biometric pen,” in *Proceedings of the 2006 IEEE Mountain Workshop on Adaptive and Learning Systems*, (Logan, UT: IEEE), 110–115. doi: 10.1109/SMCAL.2006.250700
- Gruber, T., Meixner, B., Prosser, J., and Sick, B. (2012). Handedness tests for preschool children: a novel approach based on graphics tablets and support vector machines. *Appl. Soft Comput.* 12, 1390–1398. doi: 10.1016/j.asoc.2011.11.022
- Guadagnoli, M. A., and Lee, T. D. (2004). Challenge point: a framework for conceptualizing the effects of various practice conditions in motor learning. *J. Mot. Behav.* 36, 212–224. doi: 10.3200/JMBR.36.2.212-224
- Hespanhol, L., Vallio, C. S., Costa, L. M., and Saragiotto, B. T. (2019). Understanding and interpreting confidence and credible intervals around effect estimates. *Braz. J. Phys. Ther.* 23, 290–301. doi: 10.1016/j.bjpt.2018.12.006
- Hook, C., Kempf, J., and Scharfenberg, G. (2004). “A novel digitizing pen for the analysis of pen pressure and inclination in handwriting biometrics,” in *Biometric Authentication. BioAW 2004*, Vol. 3087, eds D. Maltoni and A. K. Jain (Berlin: Springer), 283–294. doi: 10.1007/978-3-540-25976-3\_26
- Kim, M., Ding, Y., Malcolm, P., Speckaert, J., Sivi, C. J., Walsh, C. J., et al. (2017). Human-in-the-loop Bayesian optimization of wearable device parameters. *PLoS One* 12:e0184054. doi: 10.1371/journal.pone.0184054
- Liu, J., Cramer, S. C., and Reinkensmeyer, D. J. (2006). Learning to perform a new movement with robotic assistance: comparison of haptic guidance and visual demonstration. *J. Neuroeng. Rehabil.* 3:20. doi: 10.1186/1743-0003-3-20
- Lüttgen, J., and Heuer, H. (2012). Robotic guidance benefits the learning of dynamic, but not of spatial movement characteristics. *Exp. Brain Res.* 222, 1–9. doi: 10.1007/s00221-012-3190-9
- Ma, W. (2014). An Application of Quantitative Methods for Motor Ability Level Classification, Performance Prediction and Training Protocol Selection. Doctoral dissertation at North Carolina State University. Available online at: <https://repository.lib.ncsu.edu/handle/1840.16/9546>
- Malina, R. M., Ribeiro, B., Aroso, J., and Cumming, S. P. (2007). Characteristics of youth soccer players aged 13–15 years classified by skill level. *Br. J. Sports Med.* 41, 290–295. discussion 295. doi: 10.1136/bjsm.2006.031294
- Marchal-Crespo, L., McHughen, S., Cramer, S. C., and Reinkensmeyer, D. J. (2010). The effect of haptic guidance, aging, and initial skill level on motor learning of a steering task. *Exp. Brain Res.* 201, 209–220. doi: 10.1007/s00221-009-2026-8
- Marchal-Crespo, L., Michels, L., Jaeger, L., López-Olóriz, J., and Riener, R. (2017). Effect of error augmentation on brain activation and motor learning of a complex locomotor task. *Front. Neurosci.* 11:526. doi: 10.3389/fnins.2017.00526
- Marchal-Crespo, L., and Reinkensmeyer, D. J. (2009). Review of control strategies for robotic movement training after neurologic injury. *J. Neuroeng. Rehabil.* 6:20. doi: 10.1186/1743-0003-6-20
- Milot, M. H., Marchal-Crespo, L., Green, C. S., Cramer, S. C., and Reinkensmeyer, D. J. (2010). Comparison of error-amplification and haptic-guidance training techniques for learning of a timing-based motor task by healthy individuals. *Exp. Brain Res.* 201, 119–131. doi: 10.1007/s00221-009-2014-z
- Mussa-Ivaldi, F. A., Hogan, N., and Bizzi, E. (1985). Neural, mechanical, and geometric factors subserving arm posture in humans. *J. Neurosci.* 5, 2732–2743. doi: 10.1523/JNEUROSCI.05-10-02732.1985
- Posada, D., and Buckley, T. R. (2004). Model selection and model averaging in phylogenetics: advantages of akaike information criterion and bayesian approaches over likelihood ratio tests. *Syst. Biol.* 53, 793–808. doi: 10.1080/10635150490522304
- Punt, A. E., and Hilborn, R. (2001). *BAYES-SA Bayesian Stock Assessment Methods in Fisheries: User’s Manual*. Rome: Food and Agriculture Organization of the United Nations.
- Reinkensmeyer, D. J., Burdet, E., Casadio, M., Krakauer, J. W., Kwakkel, G., Lang, C. E., et al. (2016). Computational neurorehabilitation: modeling plasticity and learning to predict recovery. *J. Neuroeng. Rehabil.* 13:42. doi: 10.1186/s12984-016-0148-3
- Sabatini, A. M., and Mannini, A. (2016). Ambulatory assessment of instantaneous velocity during walking using inertial sensor measurements. *Sensors* 16:2206. doi: 10.3390/s16122206
- Salvatier, J., Wiecki, T. V., and Fonnesbeck, C. (2016). Probabilistic programming in Python using PyMC3. *PeerJ Comput. Sci.* 2:e55. doi: 10.7717/peerj-cs.55
- Schweighofer, N., Han, C. E., Wolf, S. L., Arbib, M. A., and Winstein, C. J. (2009). A functional threshold for long-term use of hand and arm function can be determined: predictions from a computational model and supporting data from the extremity constraint-induced therapy evaluation (EXCITE) trial. *Phys. Ther.* 89, 1327–1336. doi: 10.2522/ptj.20080402
- Shmuelof, L., Krakauer, J. W., and Mazzoni, P. (2012). How is a motor skill learned? Change and invariance at the levels of task success and trajectory control. *J. Neurophysiol.* 108, 578–594. doi: 10.1152/jn.00856.2011

## SUPPLEMENTARY MATERIAL

The Supplementary Material for this article can be found online at: <https://www.frontiersin.org/articles/10.3389/fnins.2021.704402/full#supplementary-material>

- Sigrist, R., Rauter, G., Riener, R., and Wolf, P. (2013). Augmented visual, auditory, haptic, and multimodal feedback in motor learning: a review. *Psychon. Bull. Rev.* 20, 21–53. doi: 10.3758/s13423-012-0333-8
- Staples, K. L., and Reid, G. (2010). Fundamental movement skills and autism spectrum disorders. *J. Autism. Dev. Disord.* 40, 209–217. doi: 10.1007/s10803-009-0854-9
- Takai, A., Rivela, D., Lisi, G., Noda, T., Teramae, T., Imamizu, H., et al. (2018). “Investigation on the neural correlates of haptic training,” in *Proceedings of the 2018 IEEE International Conference on Systems, Man, and Cybernetics (SMC)*, (Miyazaki: IEEE), 519–523. doi: 10.1109/SMC.2018.00098
- Watanabe, S. (2010). Asymptotic equivalence of bayes cross validation and widely applicable information criterion in singular learning theory. *J. Mach. Learn. Res.* 11, 3571–3594.
- Williams, C. K., and Carnahan, H. (2014). Motor learning perspectives on haptic training for the upper extremities. *IEEE Trans. Haptics* 7, 240–250. doi: 10.1109/TOH.2013.2297102
- Wilson, E. T., Wong, J., and Gribble, P. L. (2010). Mapping proprioception across a 2D horizontal workspace. *PLoS One* 5:e11851. doi: 10.1371/journal.pone.0011851
- Wong, J. D., Kistemaker, D. A., Chin, A., and Gribble, P. L. (2012). Can proprioceptive training improve motor learning? *J. Neurophysiol.* 108, 3313–3321. doi: 10.1152/jn.00122.2012
- Yamamoto, R., Akizuki, K., Kanai, Y., Nakano, W., Kobayashi, Y., and Ohashi, Y. (2019). Differences in skill level influence the effects of visual feedback on motor learning. *J. Phys. Ther. Sci.* 31, 939–945. doi: 10.1589/jpts.31.939

**Conflict of Interest:** The authors declare that the research was conducted in the absence of any commercial or financial relationships that could be construed as a potential conflict of interest.

**Publisher’s Note:** All claims expressed in this article are solely those of the authors and do not necessarily represent those of their affiliated organizations, or those of the publisher, the editors and the reviewers. Any product that may be evaluated in this article, or claim that may be made by its manufacturer, is not guaranteed or endorsed by the publisher.

Copyright © 2021 Takai, Lisi, Noda, Teramae, Imamizu and Morimoto. This is an open-access article distributed under the terms of the Creative Commons Attribution License (CC BY). The use, distribution or reproduction in other forums is permitted, provided the original author(s) and the copyright owner(s) are credited and that the original publication in this journal is cited, in accordance with accepted academic practice. No use, distribution or reproduction is permitted which does not comply with these terms.



# MCSNet: Channel Synergy-Based Human-Exoskeleton Interface With Surface Electromyogram

Kecheng Shi<sup>1,2,3</sup>, Rui Huang<sup>1,2,3\*</sup>, Zhinan Peng<sup>1,2,3</sup>, Fengjun Mu<sup>2,3</sup> and Xiao Yang<sup>4\*</sup>

<sup>1</sup> School of Automation Engineering, University of Electronic Science and Technology of China, Chengdu, China, <sup>2</sup> Center for Robotics, University of Electronic Science and Technology of China, Chengdu, China, <sup>3</sup> Engineering Research Center of Human Robot Hybrid Intelligent Technologies and Systems, Ministry of Education, University of Electronic Science and Technology of China, Chengdu, China, <sup>4</sup> Department of Orthopedics, Sichuan Provincial People's Hospital, University of Electronic Science and Technology of China, Chengdu, China

## OPEN ACCESS

### Edited by:

Xiaodong Guo,  
Huazhong University of Science and  
Technology, China

### Reviewed by:

Bin Fang,  
Tsinghua University, China  
Yue Ma,  
Shenzhen Institutes of Advanced  
Technology, Chinese Academy of  
Sciences (CAS), China

### \*Correspondence:

Rui Huang  
ruihuang@uestc.edu.cn  
Xiao Yang  
yangxiaomed@hotmail.com

### Specialty section:

This article was submitted to  
Neuroprosthetics,  
a section of the journal  
Frontiers in Neuroscience

**Received:** 03 May 2021

**Accepted:** 08 October 2021

**Published:** 17 November 2021

### Citation:

Shi K, Huang R, Peng Z, Mu F and  
Yang X (2021) MCSNet: Channel  
Synergy-Based Human-Exoskeleton  
Interface With Surface  
Electromyogram.  
Front. Neurosci. 15:704603.  
doi: 10.3389/fnins.2021.704603

The human-robot interface (HRI) based on biological signals can realize the natural interaction between human and robot. It has been widely used in exoskeleton robots recently to help predict the wearer's movement. Surface electromyography (sEMG)-based HRI has mature applications on the exoskeleton. However, the sEMG signals of paraplegic patients' lower limbs are weak, which means that most HRI based on lower limb sEMG signals cannot be applied to the exoskeleton. Few studies have explored the possibility of using upper limb sEMG signals to predict lower limb movement. In addition, most HRIs do not consider the contribution and synergy of sEMG signal channels. This paper proposes a human-exoskeleton interface based on upper limb sEMG signals to predict lower limb movements of paraplegic patients. The interface constructs an channel synergy-based network (MCSNet) to extract the contribution and synergy of different feature channels. An sEMG data acquisition experiment is designed to verify the effectiveness of MCSNet. The experimental results show that our method has a good movement prediction performance in both within-subject and cross-subject situations, reaching an accuracy of 94.51 and 80.75%, respectively. Furthermore, feature visualization and model ablation analysis show that the features extracted by MCSNet are physiologically interpretable.

**Keywords:** human-robot interface, lower limb movement prediction, channel synergy-based network, exoskeleton, paraplegic patients, surface electromyography

## 1. INTRODUCTION

The development of artificial intelligence technology and wearable sensors has promoted the rise of human-robot interaction. As the core of human-robot interaction, an human-robot interface (HRI) enables direct communication with a robot via physical or biological signals, which has received widespread attention in the past decade (Simao et al., 2019; Fang et al., 2020). Exoskeleton is a typical application scenario of HRI, and some HRI based on physical signals, such as inertial measurement units or pressure signals, have been used in the walking-assistant exoskeleton to realize the movement prediction of patients with hemiplegia/paraplegia (Beil et al., 2018; Ding et al., 2020; Zhu et al., 2020a). In recent years, with the decoding of biological signals, HRI based on biological signals (such as electroencephalogram and electromyography) have been designed,



opening up the possibility of realizing more natural and efficient movement predictions between human and exoskeleton (Suplino et al., 2019; Ortiz et al., 2020; Zhuang et al., 2021). For paraplegic patients, the loss of lower limb motor and sensory function makes the exoskeleton difficult to predict the patients' movement, and the previous work has not yet proposed a high-efficiency HRI specifically for paraplegic patients. Therefore, it is urgent to propose an HRI with high movement prediction accuracy for paraplegic patients.

Brain-computer interface (BCI) is an HRI based on electroencephalogram (EEG). It can directly obtain patients' motion intention from the EEG signal and without actual limb movement, so the BCI has been used to predict the movement of paraplegic patients (Tariq et al., 2018; Wang et al., 2018; Gu et al., 2020). The BCI consists of three main processing stages (Lotte et al., 2018): data collection and processing stage, where EEG data is recorded and preprocessed; feature extraction stage, where meaningful information is extracted from the EEG data; and classification stage, where a motion intention is interpreted from the data. The EEG signal's signal-to-noise ratio is low. It is susceptible to interference from the environment and the patient's own limb movement and mood, and the signal between different people is quite different (Rashid et al., 2020). The movement prediction accuracy of BCI is usually unstable, which is unacceptable for the exoskeleton movement assistance tasks of paraplegic patients.

Compared with the EEG signal, the sEMG signal has a higher signal-to-noise ratio and is less interfered with by external factors. Therefore, the sEMG-based human-robot interface (MHRI) has been earlier and more widely used in the walking-assistant exoskeleton (Kawamoto et al., 2003; Wang et al., 2021). The previous MHRI mostly used the sEMG signal of the lower limb muscles to predict movements. However, the sEMG signal of the lower limbs of paraplegic patients is weak or even no signal. So recent studies have attempted to use the sEMG signal of the upper body muscles to predict the lower limb movement (Villa-Parra et al., 2018). Similarly, MHRI also includes three stages of data collection and processing, feature extraction, and classification. Each stage relies on manual specifications. Many outstanding studies have shown that feature extraction is crucial for MHRI movement prediction, and it determines the upper limit of the prediction accuracy (Phinyomark et al., 2012; Samuel et al., 2018). Feature extraction often requires significant subject-matter expertise and a priori knowledge about the expected sEMG signal (Xiong et al., 2021). It is tough and time consuming to obtain an optimal feature set manually for different subjects.

Deep learning has largely alleviated the need for manual feature extraction, achieving state-of-the-art performance in fields such as computer vision and natural language processing (Hinton et al., 2012). In fact, deep convolutional neural networks (CNNs) can automatically extract appropriate features from the data. It has succeeded in many challenging image classification tasks (Huang et al., 2017; Jeyaraj and Nadar, 2019), surpassing methods that rely on handcrafted features (Hinton et al., 2012; Huang et al., 2017). Although most research still relies on handcrafted features, many recent works have explored the

application of deep learning in MHRI (Allard et al., 2016; Cote-Allard et al., 2019; Jabbari et al., 2020). This kind of MHRI mostly combines long short-term memory networks (LSTM) and CNNs simply, ignoring the difference in contribution and synergy of sEMG feature channels of different subjects under the same movement. Moreover, most researchers do not pay much attention to whether the features extracted by CNNs have physiological significance.

In this paper, a channel synergy-based MHRI is proposed for lower limb movement prediction in paraplegic patients. It uses the sEMG signals of 12 upper limb muscles to predict the lower limb movements. The proposed movement prediction model uses LSTM, depthwise and separable convolutions to extract the spatiotemporal features of multi-channel sEMG signals, and introduces an attention module to extract the synergy of different sEMG feature channels. An sEMG data acquisition experiment is designed to verify the proposed channel synergy-based network (MCSNet). The experimental results verify that MCSNet's prediction accuracy is better than the traditional machine learning-based MHRI and two mainstream deep learning-based MHRI in both within-subject and cross-subject situations. Furthermore, we visualize the features extracted through MCSNet model and perform model ablation analysis. The analysis results show that the features proposed by MCSNet are physiologically interpretable.

In summary, the main contributions of this paper are shown as follows:

- A channel synergy-based MHRI is proposed for lower limb movement prediction of paraplegics. It uses the sEMG signals of upper limb to predict lower limb movements, and extracts the contribution, spatiotemporal, and synergy features among different sEMG channels, which improves the accuracy of lower limb movement prediction.
- This paper visualizes the features proposed by the MCSNet model and performs the model ablation analysis, and the results show that the features proposed by MCSNet are physiologically interpretable.

## 2. RELATED WORKS

Human-robot interfaces used to predict the movement of patients with damaged limb are mainly divided into BCI and MHRI.

### 2.1. BCI-Based Movement Prediction Related Work

The research of neuroengineering promotes the development of BCI, and it is mainly used in the field of medical rehabilitation to realize the perception of user intent. An entire BCI includes three main processing stages of data collection and processing, feature extraction, and classification (Lotte et al., 2018). Traditional BCI mainly extracts some manual normative time-domain, frequency-domain, and spatial domain features (Lee et al., 2019), and then uses machine learning methods to construct the mapping between features and different movements (Kaper et al., 2004; Wang et al., 2017). Wang et al. proposed a BCI based

on support vector machine (SVM). It uses the common space pattern (CSP) model to extract the spatial features of the subject's motor imagery (MI) EEG signals, and uses the SVM model to realize the classification of lower limb movements (Wang et al., 2017).

Recent research has explored the application of deep learning in BCI (Tayeb et al., 2019; Tortora et al., 2020). Tayeb et al. used a CNN architecture to predict the movement of the raw MI EEG signals, achieving an accuracy of 84% (Tayeb et al., 2019). Tortora et al. proposed a gait pattern prediction method based on an LSTM architecture. This method uses the LSTM model to automatically extract and classify the timing features of the EEG signal (Tortora et al., 2020), which can achieve an accuracy of 92.8%. Considering the low signal-to-noise ratio of EEG signals, some research have tried to combine EEG with other signals to improve the movement prediction accuracy. Zhu et al. used the combination of EEG and electrooculogram (EOG) signals to realize the grasping and moving tasks of the robotic arm (Zhu et al., 2020b), with an average accuracy of 92.09%. BCI is unacceptable for the exoskeleton movement assistance tasks of paraplegic patients, because EEG signal is susceptible to interference from the environment and the patient's own limb movement and mood (Rashid et al., 2020).

## 2.2. MHRI-Based Movement Prediction Related Work

As the biological signal most relevant to exercise, sEMG has been applied to human-robot interaction for a long time, and the research on MHRI is particularly rich. According to the granularity of movement prediction, traditional MHRI can be divided into two categories, one is MHRI based on motion curve prediction, and the other is MHRI based on motion mode(movement) prediction. The former uses machine learning methods or Hill's musculoskeletal model to build a mapping between handcrafted features and joint angles/torques, which can achieve finer-grained movement prediction. Literature (Suplino et al., 2020) proposed an elbow joint angle estimation model based on a non-linear autoregressive with exogenous inputs neural network. This model can accurately predict the elbow joint's torque and angle during flexion and extension movement, with a mean square error within  $7^\circ$ . This kind of MHRI can only be predicted in one movement. The model involves many parameters and requires high quality of the sEMG signal, which is not suitable for the movement prediction of paraplegic patients.

The MHRI in the back is similar to BCI, which also includes three processing stages. Its main principle is using machine learning methods to map handcrafted features and movements (Afzal et al., 2017; Li et al., 2017; Cai et al., 2019; Kyeong et al., 2019; Tao et al., 2019). Cai et al. proposed an SVM-based upper limb movement prediction method (Cai et al., 2019), which uses the sEMG signal of the uninhibited upper limb muscle of the hemiplegic patient to predict the movement of the patient's shoulder and elbow joints, with an accuracy of 93.56%. Tao et al. proposed a multi-channel lower limb movement prediction method based on back propagation neural network, which can achieve a prediction accuracy of 93.6% in six lower limb

movements such as the flexion movement of hip joint (Tao et al., 2019).

Deep learning can automatically extract the best feature set from sEMG signals. Many researchers have explored the application of deep learning in MHRI-based movement prediction methods (Allard et al., 2016; Cote-Allard et al., 2019; Jabbari et al., 2020). Allard et al. proposed a multi-layer CNN gesture prediction model based on sEMG for robot guidance tasks (Allard et al., 2016). The model automatically extracts the frequency domain features of different gesture movements through the CNN architecture, and the average accuracy of gesture prediction for 18 subjects is 93.14%. Considering the effectiveness of the LSTM architecture for timing feature extraction, Jabbari et al. proposed an ankle joint movement prediction model based on the CNN-LSTM architecture. The CNN and LSTM architectures were used to extract the spatial and temporal features of the sEMG signals, respectively, under different ankle joint movements (Jabbari et al., 2020), and the prediction accuracy of five ankle joint movements is 97.55%. Most deep learning-based MHRI combine LSTM and CNNs simply to extract the timing or time-frequency features of the sEMG signal, but ignore the contribution and synergy differences of the sEMG feature channels of different subjects under the same movement. These are important features for different limb movements (d'Avella et al., 2003).

## 2.3. Application of HRI on Exoskeleton

As a tightly human-machine coupled system, the exoskeleton is a typical application scenario of HRI. The application of HRI on exoskeleton can be divided into movement prediction (Kyeong et al., 2019; Read et al., 2020) and state monitoring (Bae et al., 2019). Movement prediction is to help the exoskeleton recognize the wearer's motion intention and realize natural human-exoskeleton interaction. An HRI based on the wearer's upper limb inertial measurement unit signal and crutches pressure signal was applied to the Ekso exoskeleton (Read et al., 2020). It helps the exoskeleton realize the prediction of standing and walking movements. Kyeong et al. proposed a hybrid HRI based on the wearer's lower limb sEMG signals and the sole pressure signals (Kyeong et al., 2019), achieving the prediction of the gait cycle. HRI based on state monitoring is to help observe the changes in the wearer's physiological state when using the exoskeleton. Bae et al. designed an MHRI for their wrist-rehabilitation exoskeleton robot (Bae et al., 2019). It can monitor whether the wearer has spasticity during the exoskeleton assistance task.

Our work is mainly based on the lower limb movement prediction of the walking-assistant exoskeleton for paraplegia patients. It is most closely related to the MHRI based on deep learning, which uses CNN and LSTM architecture to extract the sEMG signal features of different lower limb movements. In contrast to deep learning-based MHRI, this paper propose a channel synergy-based MHRI, which extracts the contribution and synergy of the sEMG feature channel. Its performance is better than traditional machine learning-based MHRI and two mainstream deep learning-based MHRI.

### 3. METHODS

This section presents the methodology details of the proposed movement prediction model. Section 3.1 describes the overall architecture of the MCSNet model. In section 3.2, we introduce seven traditional MHRIs and two mainstream deep learning-based MHRIs, which are used to compare to the MCSNet model.

#### 3.1. Description of the MCSNet Model

**Figure 1** visualizes the proposed MCSNet model. The entire model architecture consists of three parts. The first part is data input, input the processed sEMG data; the second part is feature extraction, which mainly contains four blocks, each block establishes the connection between the feature channels of the sEMG signal in different dimensions; the third part is movement classification/prediction, which classifies the extracted features. This section mainly describes the feature extraction part, because it is the core of the entire model. For sEMG trials, it was collected at a 1,500 Hz sampling rate, having  $C$  channels and  $T$  time samples.

- sEMG is a kind of non-stationary time series data. For movement prediction, extracting more timing features is the basic requirement to improve accuracy. In block 1, for each input sEMG sample segment (size  $C \times 300$ , multiple shown in **Figure 1**), we performed a channel-by-channel LSTM step to extract the timing features of different signal channels. Since the deepening of the LSTM layers will cause over-fitting, we found this phenomenon is more serious for sEMG data during the experiment, so we choose to use a single-layer LSTM as the timing feature extraction block. In this process, we define the  $k$ th sEMG channel signal as

$$F_{sEMG}^k, (k = 1, \dots, C) \quad (1)$$

which  $k$  indicates the serial number of the channel. In order to better describe the relationship between the LSTM block and the sEMG feature channel, a more fine-grained channel-by-channel representation is used. The operation with LSTM block is defined as follows:

$$F_{temp}^k = N_{lstm}^k(F_{sEMG}^k), \quad (2)$$

In Equation (2), each of the sEMG signal channels is used to generate its timing feature independently, the timing feature from all the channels will be contacted into  $F_{temp}$ , which size is  $C * L$ ,  $L$  represents the length of input signal's sample. Since the input feature channel  $F_{sEMG}^k, (k = 1, \dots, C/2)$  and  $F_{sEMG}^{k+C/2}, (k = 1, \dots, C/2)$  in our data acquisition process is opposite the left and right symmetrical relationships on the muscle blocks in the acquisition, the muscles of the symmetry position have similar behavior patterns when the subjects are under various movements, so we use the LSTM units with shared weights used in the corresponding channel.

- In block 2, we perform two convolutional steps in sequence. First, we fit  $F_1$  2D convolution filters with a size of (1, 65) and output  $F_1$  feature maps containing different timing information. We then use a depthwise convolution of size

( $C, 1$ ) (Chollet, 2017) to extract spatial features for every channel. This operation provides a direct way to learn spatial filters for different timing information, which can effectively extract different timing and spatial features. The depth parameter  $D$  represents the number of spatial filters to be learned for each time series feature map ( $D = 1$  is shown in **Figure 1** for illustration purposes). In this block,  $F_{temp}$  is transformed with the first convolution layer as follows:

$$F_{conv} = N_{conv}(F_{temp}), \quad (3)$$

$$F_{d-conv} = N_{d-conv}(F_{conv}), \quad (4)$$

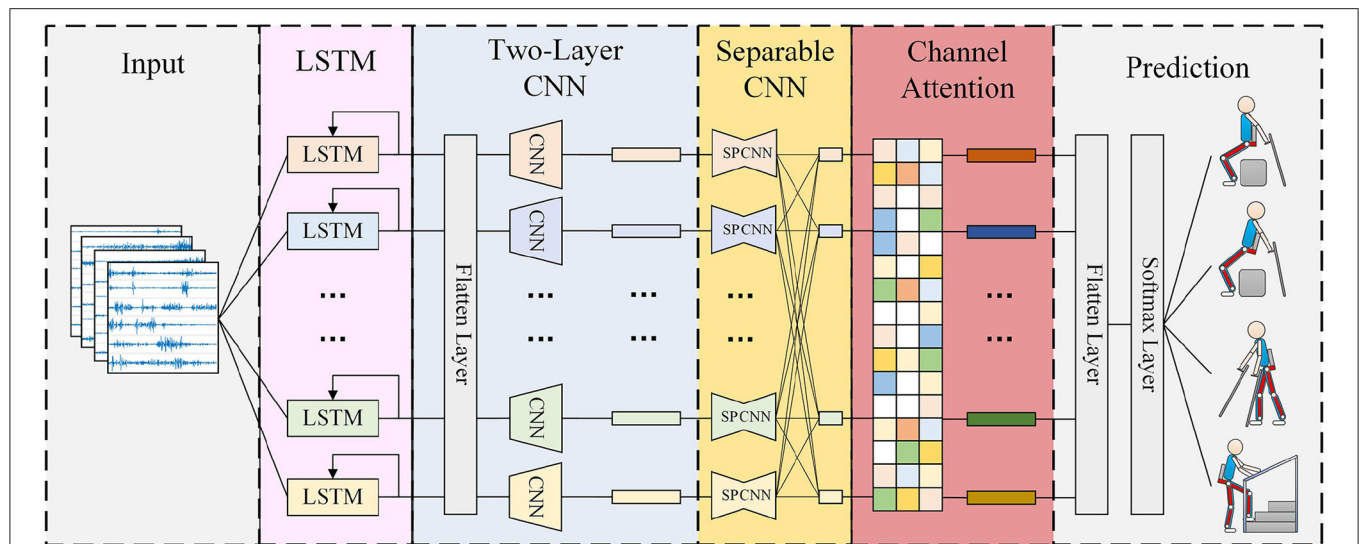
In Equations (3) and (4), the size of  $F_{conv}$  and  $F_{d-conv}$  is  $F_1 * C * L$  and  $(D * F_1) * 1 * L$ , respectively.

- In block 3, we use a separable convolution, a depthwise convolution of size (1, 15) followed by  $F_2$  pointwise convolutions of size (1, 1). The separable convolutions first learn the kernel of each spatiotemporal feature map individually, then optimally merge the outputs afterward, which can explicitly decouple the relationship within and across feature maps. This operation separates the learning of spatiotemporal features from the combination of optimal features, which is very effective for sEMG signals. Because sEMG signals have different synergy between channels when performing different movements (muscle synergy effect, d'Avella et al., 2003), this is similar to a synergy feature, which the separable convolutions can extract. Because the padding is used in the first stage of separable convolution, and the pixel-wised convolution will not change the size of the feature, the output  $F_{sep-conv}$  has the same size as  $F_{d-conv}$ .
- For block 4, we introduced a channel attention module. This operation learns the weights of different synergy features, which can effectively associate movements with the most relevant synergy features and improve the movement prediction accuracy. Moreover, there are differences in the feature contributions of sEMG channels in different subjects under the same movement (muscle compensatory behavior, d'Avella et al., 2006), which will amplify the differences in the synergy feature of different subjects under the same movement. The channel attention module can learn different weights for different subjects to deal with the differences in synergy features, thereby improving the robustness of the entire movement prediction model. The operation of this block can be described as:

$$W_{channel}(F_{sep-conv}) = \sigma(MLP(AvgPool(F_{sep-conv})) + MLP(MaxPool(F_{sep-conv}))), \quad (5)$$

$$F = W_{channel}(F_{sep-conv}) \otimes F_{sep-conv}, \quad (6)$$

We input the generated attention-based spatiotemporal features into the movement classification/prediction part. As shown in **Figure 1**, the extracted features first perform a Flatten layer step, and then pass directly to a softmax classification with  $N$  units, where  $N$  is the number of classes in the data. The



**FIGURE 1** | Overall architecture of the MCSNet model. Lines denote the convolutional kernel connectivity between inputs and outputs (called feature maps). The network starts with a channel-by-channel long short-term memory networks (LSTM) (second column) to learn the timing feature, then uses a two-layer convolution (third column) to learn different spatiotemporal features. The separable convolution (fourth column) is a combination of a depthwise convolution followed by a pointwise convolution, which can explicitly decouple the relationship within and across feature maps and learns the synergy feature of surface electromyography (sEMG).

entire model architecture uses the cross-entropy loss function to optimize the parameters, and input 10 sEMG samples with time-sequence everytime.

## 3.2. Comparison With Other MHRI Movement Prediction Approaches

### 3.2.1. Comparison With Traditional MHRI Movement Prediction Approaches

We compared the performance of MCSNet with seven traditional MHRI based on handcrafted features and machine learning models in lower limb movement prediction. In the selection of features, referring to the research conclusions of time domain and frequency domain features in the literature (Phinyomark et al., 2012) and four commonly used feature sets (Englehart and Hudgins, 2003) (Phinyomark et al., 2013), we finally select the feature of Mean Absolute Value (MAV), WaveLength (WL), Zero Crossings (ZC), 6-order AutoRegressive coefficient (6-AR), and average Power Spectral Density (PSD). Furthermore, we choose Linear Discriminant Analysis (LDA), Decision Tree (DT), Naive Bayes (BES), Linear Kernel-based Support Vector Machine (LSVM), Radial Basis Function-based Support Vector Machine (RBFSVM), K Nearest Neighbor (KNN), and Artificial Neural Network (ANN) as the classification/prediction model. We use MATLAB's Classification Learner Toolbox and Neural Net Pattern Recognition Toolbox to implement these models. The hyperparameter settings of each model are shown in Table 1.

### 3.2.2. Comparison With Deep Learning-Based MHRI Movement Prediction Approaches

In deep learning, we compared the performance of MCSNet with two-layers CNN (TCNN) and CNN-LSTM models. The TCNN architecture consists of two convolutional layers and

**TABLE 1** | Parameter list of traditional MHRI movement prediction approaches.

Method	Hyperparameter and model detail setting
LDA	Covariance structure: full rank (for within-subject), diagonal (for cross-subject)
DT	Maximum fission number: 100
BES	Kernel: Radial Basis Function,
LSVM	Kernel: linear, $C = 1$ , Multiple classification method: OVO
RBFSVM	Kernel: RBF, $C = 1.9$ , Multiple classification method: OVO
KNN	Number of neighboring points: 1, Metric function: mahalanobis distance function
ANN	Number of hidden unit: 28

a softmax layer which is for classification. The CNN-LSTM architecture includes two LSTM layers, three convolutional layers, and a softmax layer. We implemented these models in PyTorch. For specific details of the model, see <https://github.com/mufengjun260/MCSNet>.

In general, the most significant difference between MCSNet and traditional MHRI movement prediction approaches is the feature extraction method, and the most significant difference from other deep learning-based movement prediction methods is the network architecture. By comparing with other methods, we can prove the effectiveness of the feature extraction architecture we designed.

## 4. EXPERIMENTS AND RESULTS

In this part, an sEMG signal acquisition experiment based on upper limb muscles is designed to verify the effectiveness of



the method proposed in this paper. Section 4.1 describes the process of the acquisition experiment and the process of data preprocessing. Section 4.2 gives the implementation details of model training. In section 4.3, we show the MCSNet movement prediction model results and compare MCSNet with other movement prediction models in the case of within-subject and cross-subject. Section 4.4 explains the results of MCSNet model ablation analysis and feature visualization.

## 4.1. sEMG Data Acquisition Experiment

A total of 8 healthy subjects were invited to participate in the experiment. Each subject completed four lower limb movements of standing, sitting, walking, and going up stairs while wearing the AIDER exoskeleton. During this period, the sEMG signals of the subjects' upper limbs were collected.

1. **Participants:** The eight subjects (7 males, one female) had an average age of 26 years, a height between 165 and 185 cm, and a weight between 59 and 82 kg. All subjects can independently use the AIDER exoskeleton to complete the lower limb movements involved in the experiment, and are in good physical condition with no injuries to the arm. Before the experiment, each subject had been explained the contents of the experiment and signed an informed consent form. This experiment was approved by the Research Ethics Committee of the University of Electronic Science and Technology of China.
2. **Procedures:** Before the experiment, record the relevant physical parameters of the subject, inform the experimental procedure to the subject, and let the subject use crutches to freely practice the four lower limbs movements of standing, sitting, walking, and going upstairs while wearing the AIDER exoskeleton for 30 min. Then paste sEMG acquisition electrodes on the 12 muscles of the subject's left and right upper limbs, including the deltoid anterior, biceps, and superior trapezius muscles (as shown in **Figure 2**). Before pasting, wipe the corresponding muscles with alcohol cotton and remove the surface hair with a hair removal knife. The subject puts on the AIDER exoskeleton (Wang et al., 2019), supports the crutches with both hands, stands in the designated position, and completes the sitting, standing, and going upstairs movements 10 times after hearing the instructions, and then completes walking movement 20 times (a complete gait cycle is one time). Each movement is completed within 8 s, all subjects are required to perform the specified movements without using their legs as much as possible to ensure that the collected upper limb sEMG signals are close to the paraplegic patients. After the movement starts, the subject maintains the lower limb movement preparation posture for 2 s (see **Figure 3**) and then controls the AIDER exoskeleton to complete the corresponding lower limb movement. Throughout the experiment, the camera is turned on to record, and myoMUSCLE (an sEMG acquisition device, Scottsdale, American) is used to collect the sEMG signals of the upper limbs.
3. **Data Processing:** myoMUSCLE (1,500 Hz) collects the upper limb sEMG signal data of each lower limb movement of

the subject throughout the whole process. After obtaining the sEMG data, a 50 Hz notch filter is used to remove the power frequency interference of the current, and a 10–450 Hz bandpass filter is used to retain the effective information of the sEMG signal. Since our application is lower limb movement prediction, we only intercept the sEMG data during the movement preparation period (the period when keeping the preparation posture still). In addition, to achieve continuous movement prediction of lower limb, this paper uses 200 ms (including 300-time series data) as a time window to segment the sEMG signal, and the movement step of the time window is 100-time series data.

## 4.2. Implementation Details

After preprocessing the sEMG data, for the traditional MHRI movement prediction model, use the relevant formula to calculate the features mentioned in section 3.2.1, and then input the features into the Classification Learner Toolbox and Neural Net Pattern Recognition Toolbox to train the prediction model. For the problem of imbalance in the number of samples between movements, we apply a movement class-weight to the loss function. The class-weight we apply is the inverse of the proportion in the training data, with the majority movement class set to 1.

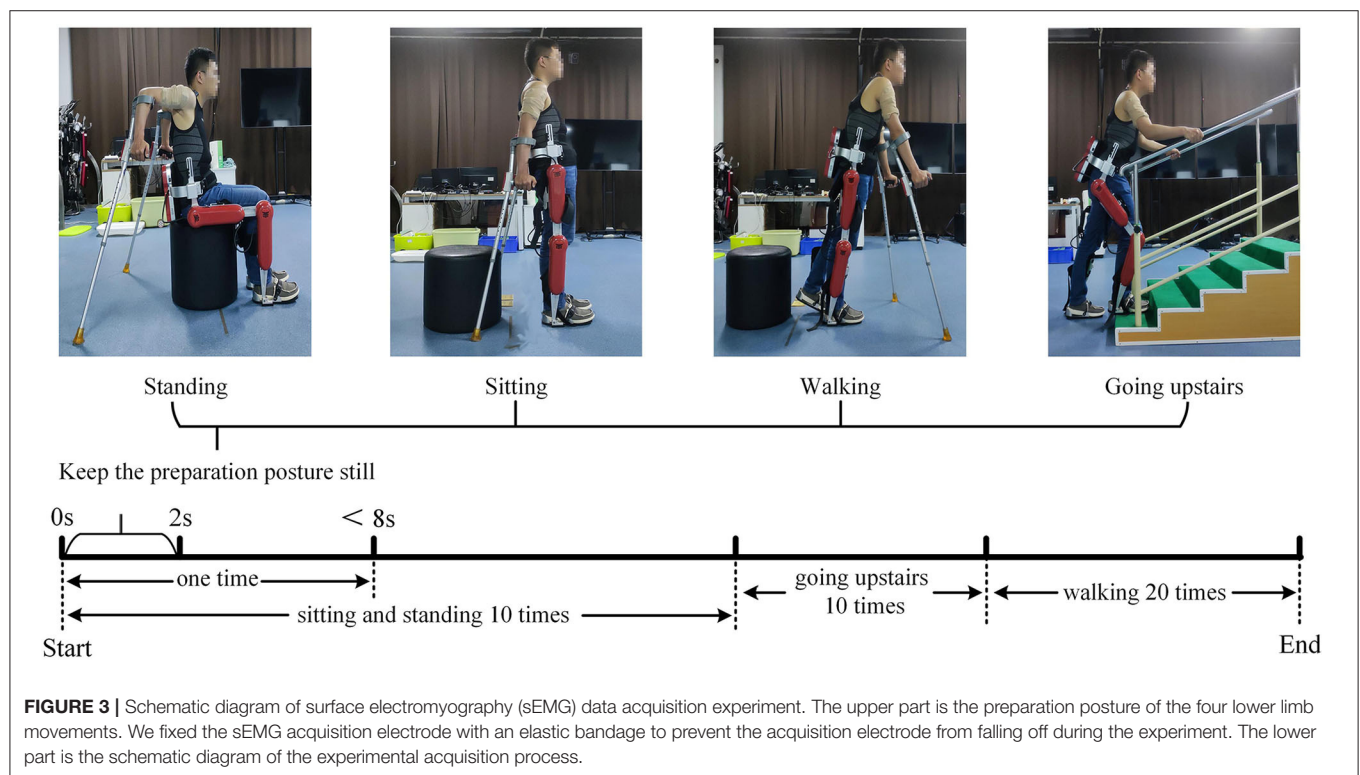
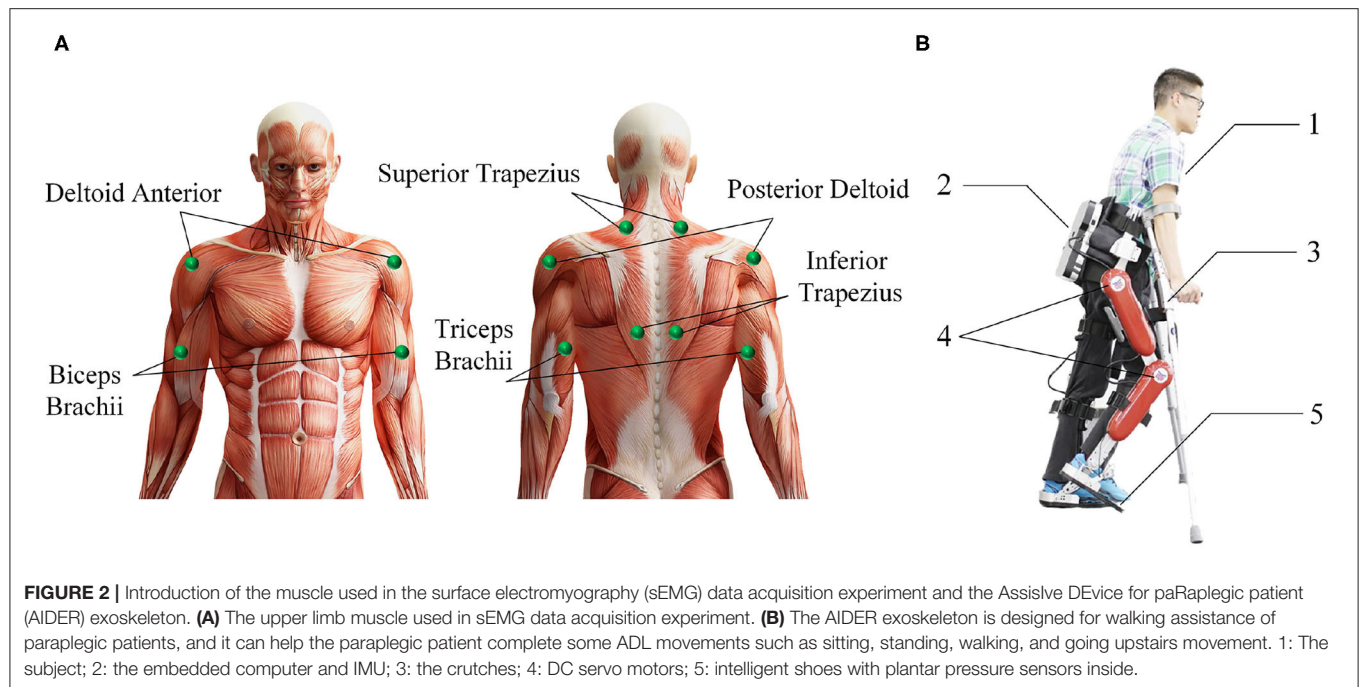
MCSNet and the deep learning-based MHRI movement prediction models are implemented using the PyTorch library (Paszke et al., 2017). In MCSNet, both LSTM's output and hidden unit are of dimension 300, and the network's hyperparameters ( $D, F1, L$ ) is set to (2, 12, 300). The model with TCNN uses the same dimension as the MCSNet's CNN layers, and the CNN-LSTM model enlarged the deepness of MCSNet's LSTM block, it uses a two-layer LSTM network architecture. Exponential linear units (ELU) (Clevert et al., 2015) are used to introduce the non-linearity of each convolutional layer. To train ours and other deep learning-based models, we use the Adam optimizer to optimize the model's parameters, with default setting described in (Kingma and Ba, 2014) to minimize the categorical cross-entropy loss function. We run 1,000 training iterations (epochs) and perform validation stopping, saving the model weights, which produce the lowest validation set loss. All models are trained on NVIDIA RTX2080Ti, with CUDA10.1 and cuDNN V7.6. Our code implementation can be found in <https://github.com/mufengjun260/MCSNet>.

## 4.3. Experiments Result

We compared the performance of the proposed MCSNet model with other MHRIs in movement classification/prediction in both the within-subject and cross-subject situations.

### 4.3.1. Within-Subject Classification

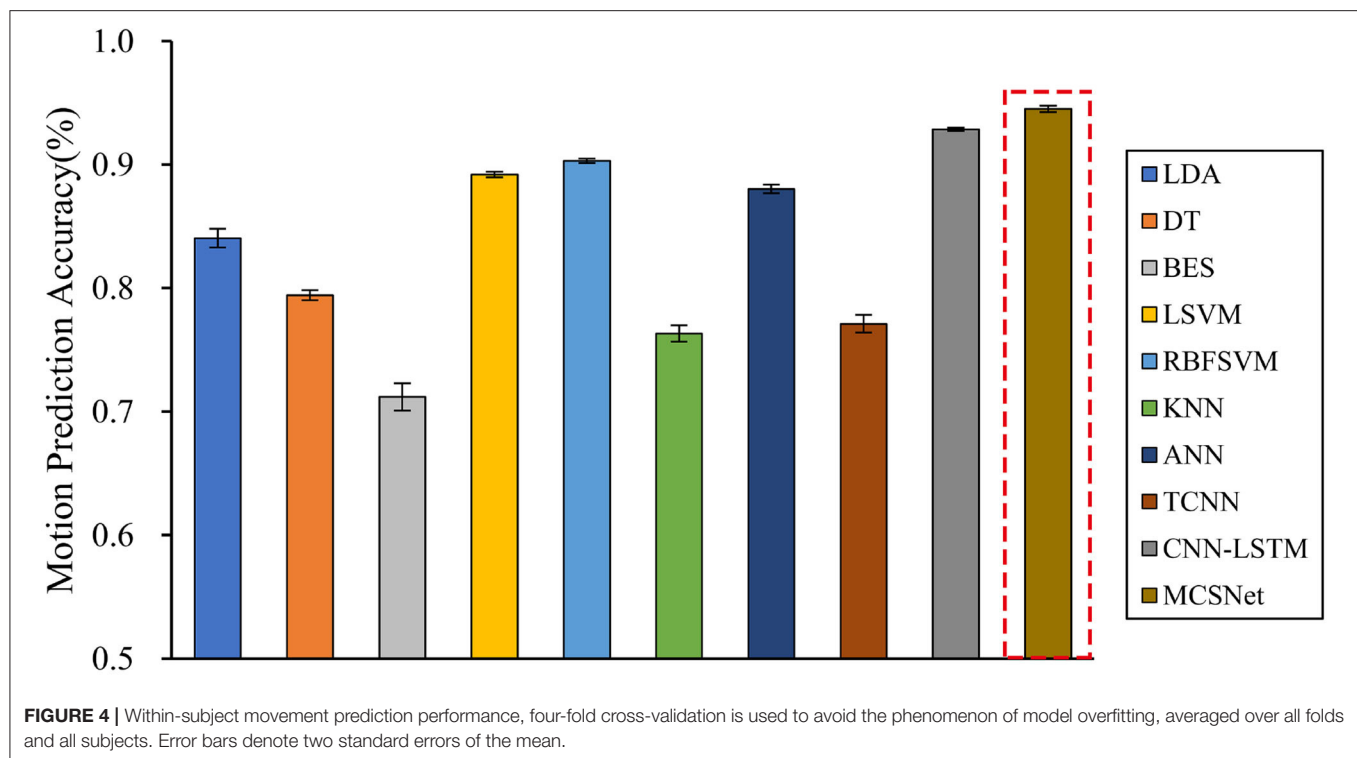
For within-subject, we divide the data of the same subject according to a ratio of 7:3 and then use 70% of the data to train the model for that subject. Four-fold cross-validation is used to avoid the phenomenon of model overfitting. Simultaneously, repeated-measures analysis of variance (ANOVA) is used to test the results statistically (using the number of subjects and the classification model as factors,



and the model classification/prediction result (accuracy) as the response variable).

We compare the performance of both traditional machine learning-based MHRI movement prediction models (LDA, DT, BES, LSVM, RBF SVM, KNN, and ANN) and deep learning-based

MHRI movement prediction models (TCNN and CNN-LSTM) with MCSNet. Within-subject results across all models are shown in **Figure 4**. It can be observed that, across the average lower limb movement prediction accuracy of 7 subjects, MCSNet outperforms traditional machine learning-based and



**TABLE 2 |** Within-subject movement prediction performance (test set ACC).

Subject	Traditional machine learning-based MHRI							Deep learning-based MHRI		
	LDA	DT	BES	LSVM	RBFSVM	KNN	ANN	TCNN	CNN-LSTM	MCSNet (ours)
1	0.9200	0.7520	0.8496	0.9451	0.9504	0.8387	0.9315	0.8377	0.9570	<b>0.9928</b>
2	0.8731	0.8097	0.7718	0.9026	0.9159	0.8000	0.9008	0.5849	0.9034	<b>0.9295</b>
3	0.7105	0.8724	0.7852	0.8146	0.8503	0.6018	0.7590	0.7722	0.9089	<b>0.9772</b>
4	0.7888	0.6630	0.6818	0.8594	0.8526	0.7294	0.8428	0.7543	0.9075	<b>0.9513</b>
5	0.7430	0.7962	0.4937	0.8675	0.8911	0.7091	0.8828	0.8525	<b>0.9434</b>	0.9212
6	0.8872	0.8188	0.6747	<b>0.8936</b>	0.8927	0.8358	0.8923	0.8373	0.8844	0.8437
7	0.9600	0.8467	0.7263	0.9602	0.9687	0.8261	0.9523	0.7576	0.9960	<b>1.0000</b>
Average ACC	0.8404	0.7941	0.7119	0.8918	0.9031	0.7630	0.8802	0.7709	0.9287	<b>0.9451</b>

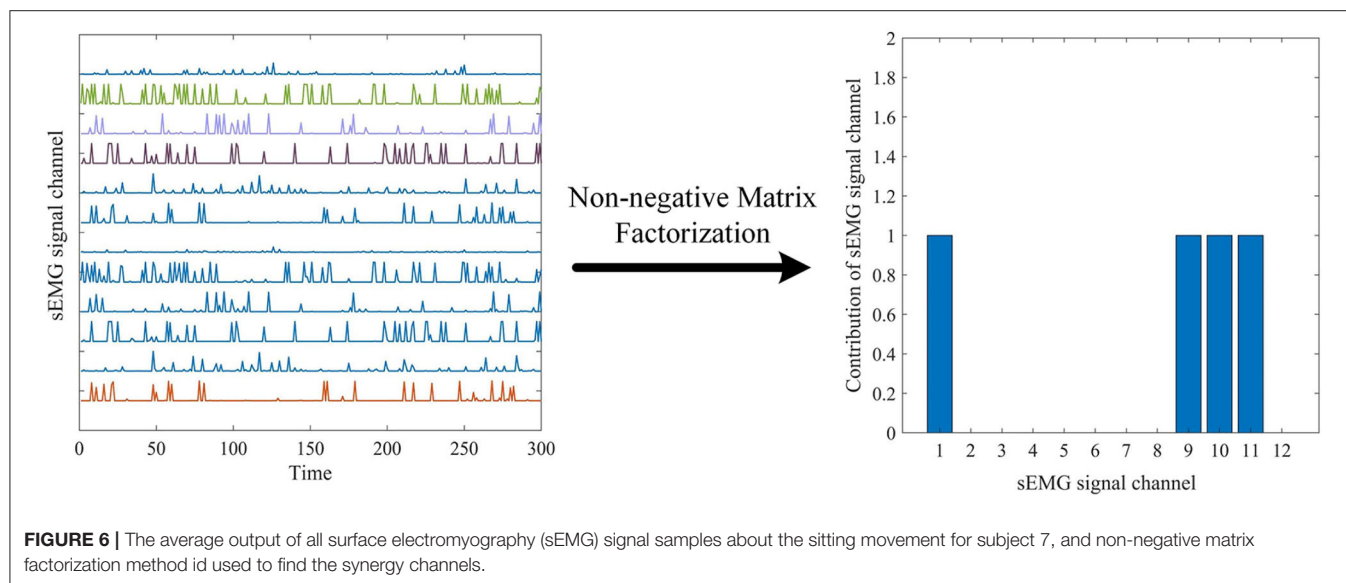
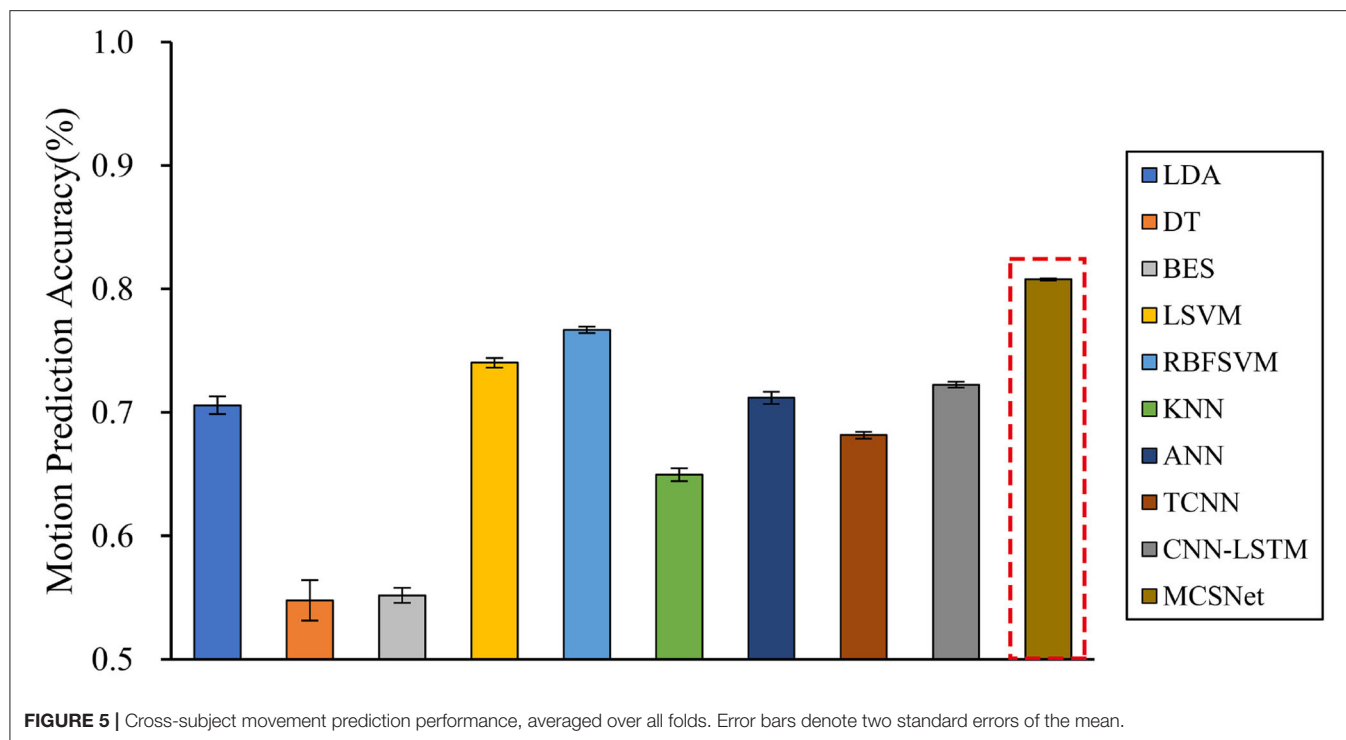
Bold means the highest prediction accuracy rate of the subject corresponding to the row.

deep learning-based MHRI models. But there is no significant statistical difference ( $P > 0.05$ ). Among the traditional MHRI movement prediction models, the RBFSVM model has the highest average accuracy of 7 subjects, reaching 90.31%. It is consistent with the conclusions obtained in previous work (Ceseracciu et al., 2010). **Table 2** shows the prediction accuracy of each subject under different MHRI movement prediction models. It can be found that the same movement prediction model has a large difference in the accuracy for different subjects (especially the traditional MHRI movement prediction model). In contrast, MCSNet has a high accuracy rate of lower limb movement prediction for all subjects, and the accuracy rate is evenly distributed. It means that MCSNet can effectively extract each subject's lower limb movement feature, thereby achieving good movement prediction.

#### 4.3.2. Cross-Subject Classification

In the case of cross-subject, we randomly selected the data of three subjects to train the model and selected the data of two subjects as the validation set. The whole process is repeated ten times, producing ten different folds.

Cross-subject prediction results across all models are shown in **Figure 5**. It can be seen that the traditional and deep learning-based MHRI movement prediction models have poor performance in the cross-subject situation, with an average accuracy rate of about 70%. However, the MCSNet model proposed in this paper can still achieve an accuracy of 80.25% in lower limb movement prediction, which has a significant statistical difference ( $P < 0.05$ ). This result shows that the MCSNet model proposed in this paper can extract the deep common features of different subjects



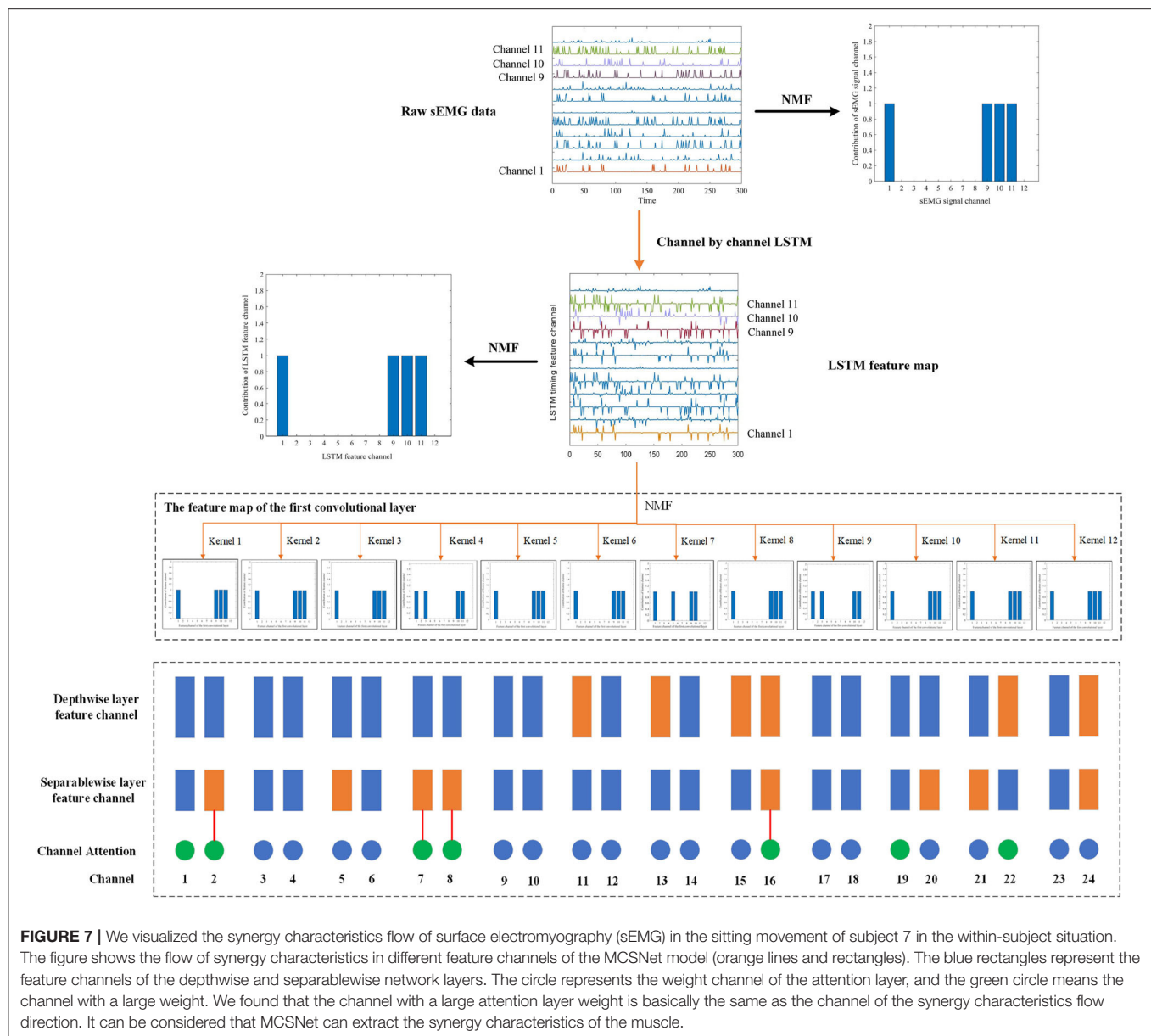
under the same lower limb movement. The model has good robustness.

#### 4.4. MCSNet Feature Explainability

The development of methods for enabling feature explainability from deep neural networks has gradually become the focus of attention over the past few years, and has been proposed as an essential component of a robust model validation procedure, to ensure that the classification performance is being driven by relevant features as opposed to noise in the data (Ancona et al.,

2017; Montavon et al., 2018). This paper uses data information flow tracking to understand the features proposed by the MCSNet model. **Figure 6** shows the average output of all sEMG signal samples about the sitting movement for subject 7. Using the non-negative matrix factorization method, we can intuitively see that the sEMG channel 1, 9, 10, 11 are the main contribution channels for subject 7 to complete the sitting movement (i.e., the muscles corresponding to the channel 1, 9, 10, and 11 assume the main synergistic effect in the sitting movement) (d'Avella et al., 2003). Muscle synergy is an important physiological





**FIGURE 7 |** We visualized the synergy characteristics flow of surface electromyography (sEMG) in the sitting movement of subject 7 in the within-subject situation. The figure shows the flow of synergy characteristics in different feature channels of the MCSNet model (orange lines and rectangles). The blue rectangles represent the feature channels of the depthwise and separablewise network layers. The circle represents the weight channel of the attention layer, and the green circle means the channel with a large weight. We found that the channel with a large attention layer weight is basically the same as the channel of the synergy characteristics flow direction. It can be considered that MCSNet can extract the synergy characteristics of the muscle.

characteristic for humans to complete different movements. In order to explore whether the MCSNet network can reflect muscle synergy, we extracted the feature output and channel weights of each layer of MCSNet, and realized the information flow tracking of sEMG data through non-negative matrix factorization and weight screening.

We performed non-negative matrix decomposition on the output of LSTM and the first convolutional layer, as shown in **Figure 7**. It can be observed that the main contribution channels of the features extracted by the LSTM and the first convolutional layer are still the channel 1, 9, 10, and 11, which means that the timing features currently extracted by MCSNet mainly come from the sEMG channel 1, 9, 10, and 11, and the synergy characteristics of these four channels are also included.

The depthwise convolutional layer's function is to combine different timing feature channels, and then extract different spatiotemporal features. We analyzed the channel weights of the depthwise convolutional layer and focused on the spatiotemporal feature channels, which have a large weight for channel 1, 9, 10, and 11. Because these spatiotemporal feature channels are the main flow direction of the synergy characteristics. The results showed that the synergy characteristics are mainly contained in the spatiotemporal feature channels 11, 13, 15, 16, 22, and 24. In the same way, we analyzed the channel weights of the separable convolutional layer and compared the channels, which the synergy characteristics mainly flow, with the important channels learned by the attention mechanism. The results show that the channels selected by the two are basically the same

**TABLE 3 |** The result of model ablation analysis.

Layer removed	Test set ACC
Depthwise layer	0.7258
Sparablewise layer	0.7241
Attention layer	0.7187
None	0.8075

(as shown in **Figure 7**). It means that the features extracted by MCSNet can reflect the synergy of muscles.

In addition, we performed a model ablation analysis on MCSNet under the cross-subject situation, removing depthwise, sparablewise, and attention network structure layers in turn and observing the changes in the prediction performance of the MCSNet model. According to the results in **Table 3**, removing any network structure layer will significantly reduce the prediction performance of the MCSNet model, which shows that each layer of the MCSNet model plays an essential role in the final prediction results.

## 5. CONCLUSIONS

In this paper, a channel synergy-based human-exoskeleton interface is proposed for lower limb movement prediction in paraplegic patients. It uses the sEMG signals of 12 upper limb muscles as input signals, which can avoid the problem of weak sEMG signals in the lower limbs of paraplegic patients. The interface constructs a channel synergy-based network (MCSNet), it uses LSTM, depthwise, and separable convolutions to extract the spatiotemporal features of multi-channel sEMG signals, and introduces an attention module to extract the synergy of different sEMG feature channels. An sEMG acquisition experiment is designed to verify the effectiveness of the MCSNet model. The results show that MCSNet has a good movement prediction performance in both within-subject and cross-subject situations. Furthermore, feature visualization and the model ablation analysis of MCSNet is performed, the result show that the features extracted by MCSNet are physiologically interpretable. In the future, we consider applying the proposed

human-exoskeleton interface to an actual exoskeleton platform. In addition, we will focus on multi-modal movement prediction based on sEMG and EEG.

## DATA AVAILABILITY STATEMENT

The datasets presented in this study can be found in online repositories. The names of the repository/repositories and accession number(s) can be found below: <https://github.com/mufengjun260/MCSNet>.

## ETHICS STATEMENT

The studies involving human participants were reviewed and approved by Ethics Committee of University of Electronic Science and Technology of China. The patients/participants provided their written informed consent to participate in this study. Written informed consent was obtained from the individual(s) for the publication of any potentially identifiable images or data included in this article.

## AUTHOR CONTRIBUTIONS

KS designed the movement prediction model, performed the experiments, and drafted the manuscript. RH and FM participated in the design of the movement prediction model and assisted in the manuscript writing. ZP and XY guided writing paper and doing experiments. All authors contributed to the article and approved the submitted version.

## FUNDING

This work was supported by the National Key Research and Development Program of China (No. 2018AAA0102504), the National Natural Science Foundation of China (NSFC) (No. 62003073), the Sichuan Science and Technology Program (Nos. 2021YFG0184, 2020YFSY0012, and 2018GZDZX0037), and the Research Foundation of Sichuan Provincial People's Hospital (No. 2021LY12).

## REFERENCES

- Afzal, T., Iqbal, K., White, G., and Wright, A. B. (2017). A method for locomotion mode identification using muscle synergies. *IEEE Trans. Neural Syst. Rehabil. Eng.* 25, 608–617. doi: 10.1109/TNSRE.2016.2585962
- Allard, U. C., Nougare, F., Fall, C. L., Giguere, P., Gosselin, C., Laviolette, F., et al. (2016). "A convolutional neural network for robotic arm guidance using sEMG based frequency-features," in *2016 IEEE/RSJ International Conference on Intelligent Robots and Systems (IROS 2016)* (Daejeon), 2464–2470.
- Ancona, M., Ceolini, E., Öztireli, C., and Gross, M. (2017). Towards better understanding of gradient-based attribution methods for deep neural networks. *arXiv preprint arXiv:1711.06104* (Vancouver, BC).
- Bae, J.-H., Hwang, S.-J., and Moon, I. (2019). "Evaluation and verification of a novel wrist rehabilitation robot employing safety-related mechanism," in *2019 IEEE 16th International Conference on Rehabilitation Robotics (ICORR)* (Toronto, ON: IEEE), 288–293. doi: 10.1109/ICORR.2019.8779511
- Beil, J., Ehrenberger, I., Scherer, C., Mandery, C., and Asfour, T. (2018). "Human motion classification based on multi-modal sensor data for lower limb exoskeletons," in *2018 IEEE/RSJ International Conference on Intelligent Robots and Systems (IROS)* (Madrid: IEEE), 5431–5436. doi: 10.1109/IROS.2018.8594110
- Cai, S., Chen, Y., Huang, S., Wu, Y., Zheng, H., Li, X., et al. (2019). SVM-based classification of sEMG signals for upper-limb self-rehabilitation training. *Front. Neurobot.* 13:31. doi: 10.3389/fnbot.2019.00031
- Ceseracciu, E., Reggiani, M., Sawacha, Z., Sartori, M., Spolaor, F., Cobelli, C., et al. (2010). "SVM classification of locomotion modes using surface electromyography for applications in rehabilitation robotics," in *19th International Symposium in Robot and Human Interactive Communication (Viareggio: IEEE)*, 165–170. doi: 10.1109/ROMAN.2010.5598664

- Chollet, F. (2017). "Xception: deep learning with depthwise separable convolutions," in *30th IEEE Conference on Computer vision and Pattern Recognition (CVPR 2017)* (Honolulu, HI), 1800–1807. doi: 10.1109/CVPR.2017.195
- Clevert, D.-A., Unterthiner, T., and Hochreiter, S. (2015). Fast and accurate deep network learning by exponential linear units (ELUs). *arXiv preprint arXiv:1511.07289* (San Juan).
- Cote-Allard, U., Fall, C. L., Drouin, A., Campeau-Lecours, A., Gosselin, C., Glette, K., et al. (2019). Deep learning for electromyographic hand gesture signal classification using transfer learning. *IEEE Trans. Neural Syst. Rehabil. Eng.* 27, 760–771. doi: 10.1109/TNSRE.2019.2896269
- d'Avella, A., Portone, A., Fernandez, L., and Lacquaniti, F. (2006). Control of fast-reaching movements by muscle synergy combinations. *J. Neurosci.* 26, 7791–7810. doi: 10.1523/JNEUROSCI.0830-06.2006
- d'Avella, A., Saltiel, P., and Bizzi, E. (2003). Combinations of muscle synergies in the construction of a natural motor behavior. *Nat. Neurosci.* 6, 300–308. doi: 10.1038/nn1010
- Ding, M., Nagashima, M., Cho, S.-G., Takamatsu, J., and Ogasawara, T. (2020). Control of walking assist exoskeleton with time-delay based on the prediction of plantar force. *IEEE Access* 8, 138642–138651. doi: 10.1109/ACCESS.2020.3010644
- Englehart, K., and Hudgins, B. (2003). A robust, real-time control scheme for multifunction myoelectric control. *IEEE Trans. Biomed. Eng.* 50, 848–854. doi: 10.1109/TBME.2003.813539
- Fang, B., Zhou, Q., Sun, F., Shan, J., Wang, M., Xiang, C., et al. (2020). Gait neural network for human-exoskeleton interaction. *Front. Neurobot.* 14:58. doi: 10.3389/fnbot.2020.00058
- Gu, L., Yu, Z., Ma, T., Wang, H., Li, Z., and Fan, H. (2020). EEG-based classification of lower limb motor imagery with brain network analysis. *Neuroscience* 436, 93–109. doi: 10.1016/j.neuroscience.2020.04.006
- Hinton, G., Deng, L., Yu, D., Dahl, G. E., Mohamed, A.-R., Jaitly, N., et al. (2012). Deep neural networks for acoustic modeling in speech recognition. *IEEE Signal Process. Mag.* 29, 82–97. doi: 10.1109/MSP.2012.2205597
- Huang, G., Liu, X., van der Maaten, L., and Weinberger, K. Q. (2017). "Densely connected convolutional networks," in *30th IEEE Conference on Computer Vision and Pattern Recognition (CVPR 2017)*, *IEEE Conference on Computer Vision and Pattern Recognition* (Honolulu, HI), 2261–2269. doi: 10.1109/CVPR.2017.243
- Jabbari, M., Khushaba, R. N., and Nazarpour, K. (2020). "EMG-based hand gesture classification with long short-term memory deep recurrent neural networks," in *2020 42nd Annual International Conference of the IEEE Engineering in Medicine Biology Society (EMBC)* (Montreal, QC), 3302–3305. doi: 10.1109/EMBC44109.2020.9175279
- Jeyaraj, P. R., and Nadar, E. R. S. (2019). Deep Boltzmann machine algorithm for accurate medical image analysis for classification of cancerous region. *Cogn. Comput. Syst.* 1, 85–90. doi: 10.1049/ccs.2019.0004
- Kaper, M., Meinicke, P., Grossekhoefer, U., Lingner, T., and Ritter, H. (2004). Bci competition 2003-data set IIB: support vector machines for the p300 speller paradigm. *IEEE Trans. Biomed. Eng.* 51, 1073–1076. doi: 10.1109/TBME.2004.826698
- Kawamoto, H., Lee, S., Kanbe, S., and Sankai, Y. (2003). "Power assist method for Hal-3 using EMG-based feedback controller," in *2003 IEEE International Conference on Systems, Man and Cybernetics* (Washington, DC), 1648–1653. doi: 10.1109/ICSMC.2003.1244649
- Kingma, D. P., and Ba, J. (2014). Adam: a method for stochastic optimization. *arXiv preprint arXiv:1412.6980* (San Diego, CA).
- Kyeong, S., Shin, W., Yang, M., Heo, U., Feng, J.-R., and Kim, J. (2019). Recognition of walking environments and gait period by surface electromyography. *Front. Inform. Technol. Electron. Eng.* 20, 342–352. doi: 10.1631/FITEE.1800601
- Lee, S.-B., Kim, H.-J., Kim, H., Jeong, J.-H., Lee, S.-W., and Kim, D.-J. (2019). Comparative analysis of features extracted from EEG spatial, spectral and temporal domains for binary and multiclass motor imagery classification. *Inform. Sci.* 502, 190–200. doi: 10.1016/j.ins.2019.06.008
- Li, X., Fang, P., Tian, L., and Li, G. (2017). "Increasing the robustness against force variation in EMG motion classification by common spatial patterns," in *2017 39th Annual International Conference of the IEEE Engineering in Medicine and Biology Society (EMBC)* (Jeju), 406–409. doi: 10.1109/EMBC.2017.8036848
- Lotte, F., Bougrain, L., Cichocki, A., Clerc, M., Congedo, M., Rakotomamonjy, A., et al. (2018). A review of classification algorithms for EEG-based brain computer interfaces: a 10 year update. *J. Neural Eng.* 15:031005. doi: 10.1088/1741-2552/aab2f2
- Montavon, G., Samek, W., and Müller, K.-R. (2018). Methods for interpreting and understanding deep neural networks. *Digit. Signal Process.* 73, 1–15. doi: 10.1016/j.dsp.2017.10.011
- Ortiz, M., Ianez, E., Contreras-Vidal, J. L., and Azorin, J. M. (2020). Analysis of the EEG rhythms based on the empirical mode decomposition during motor imagery when using a lower-limb exoskeleton. A case study. *Front. Neurobot.* 14:48. doi: 10.3389/fnbot.2020.00048
- Paszke, A., Gross, S., Chintala, S., Chanan, G., Yang, E., DeVito, Z., et al. (2017). "Automatic differentiation in pytorch," in *31st Conference on Neural Information Processing Systems (NIPS 2017)*.
- Phinyomark, A., Phukpattaranont, P., and Limsakul, C. (2012). Feature reduction and selection for EMG signal classification. *Expert Syst. Appl.* 39, 7420–7431. doi: 10.1016/j.eswa.2012.01.102
- Phinyomark, A., Quaine, F., Charbonnier, S., Serviere, C., Tarpin-Bernard, F., and Laurillau, Y. (2013). EMG feature evaluation for improving myoelectric pattern recognition robustness. *Expert Syst. Appl.* 40, 4832–4840. doi: 10.1016/j.eswa.2013.02.023
- Rashid, M., Sulaiman, N., Majeed, A. P. P. A., Musa, R. M., Ab Nasir, A. F., Bari, B. S., et al. (2020). Current status, challenges, and possible solutions of EEG-based brain-computer interface: a comprehensive review. *Front. Neurobot.* 14:25. doi: 10.3389/fnbot.2020.00025
- Read, E., Woolsey, C., McGibbon, C. A., and O'Connell, C. (2020). Physiotherapists experiences using the ekso bionic exoskeleton with patients in a neurological rehabilitation hospital: a qualitative study. *Rehabil. Res. Pract.* 2020:2939573. doi: 10.1155/2020/2939573
- Samuel, O. W., Zhou, H., Li, X., Wang, H., Zhang, H., Sangaiah, A. K., et al. (2018). Pattern recognition of electromyography signals based on novel time domain features for amputees' limb motion classification. *Comput. Electric. Eng.* 67, 646–655. doi: 10.1016/j.compeleceng.2017.04.003
- Simao, M., Mendes, N., Gibaru, O., and Neto, P. (2019). A review on electromyography decoding and pattern recognition for human-machine interaction. *IEEE Access* 7, 39564–39582. doi: 10.1109/ACCESS.2019.2906584
- Suplino, L., de Melo, G., Umemura, G., and Forner-Cordero, A. (2020). "Elbow movement estimation based on EMG with narx neural networks," in *2020 42nd Annual International Conference of the IEEE Engineering in Medicine Biology Society (EMBC)* (Montreal, QC: IEEE), 3767–3770. doi: 10.1109/EMBC44109.2020.9176129
- Suplino, L. O., Sommer, L. F., and Forner-Cordero, A. (2019). "EMG-based control in a test platform for exoskeleton with one degree of freedom," in *2019 41st Annual International Conference of the IEEE Engineering in Medicine and Biology Society (EMBC)* (Berlin: IEEE), 5366–5369. doi: 10.1109/EMBC.2019.8856836
- Tao, Y., Huang, Y., Zheng, J., Chen, J., Zhang, Z., Guo, Y., et al. (2019). "Multi-channel sEMG based human lower limb motion intention recognition method," in *2019 IEEE/ASME International Conference on Advanced Intelligent Mechatronics (AIM)* (Hong Kong), 1037–1042. doi: 10.1109/AIM.2019.8868529
- Tariq, M., Trivailo, P. M., and Simic, M. (2018). EEG-based BCI control schemes for lower-limb assistive-robots. *Front. Hum. Neurosci.* 12:312. doi: 10.3389/fnhum.2018.00312
- Tayeb, Z., Fedjaev, J., Ghaboosi, N., Richter, C., Everding, L., Qu, X., et al. (2019). Validating deep neural networks for online decoding of motor imagery movements from EEG signals. *Sensors* 19:210. doi: 10.3390/s19010210
- Tortora, S., Ghidoni, S., Chisari, C., Micera, S., and Artoni, F. (2020). Deep learning-based BCI for gait decoding from EEG with LSTM recurrent neural network. *J. Neural Eng.* 17:046011. doi: 10.1088/1741-2552/ab9842
- Villa-Parra, A. C., Delisle-Rodriguez, D., Botelho, T., Mayor, J. J. V., Delis, A. L., Carelli, R., et al. (2018). Control of a robotic knee exoskeleton for assistance and rehabilitation based on motion intention from sEMG. *Res. Biomed. Eng.* 34, 198–210. doi: 10.1590/2446-4740.07417
- Wang, C., Guo, Z., Duan, S., He, B., Yuan, Y., and Wu, X. (2021). A real-time stability control method through sEMG interface for lower extremity rehabilitation exoskeletons. *Front. Neurosci.* 15:280. doi: 10.3389/fnins.2021.645374

- Wang, C., Wu, X., Wang, Z., and Ma, Y. (2018). Implementation of a brain-computer interface on a lower-limb exoskeleton. *IEEE Access* 6, 38524–38534. doi: 10.1109/ACCESS.2018.2853628
- Wang, Y., Cheng, H., and Hou, L. (2019). c 2 aider: cognitive cloud exoskeleton system and its applications. *Cogn. Comput. Syst.* 1, 33–39. doi: 10.1049/ccs.2018.0012
- Wang, Z., Wang, C., Wu, G., Luo, Y., and Wu, X. (2017). “A control system of lower limb exoskeleton robots based on motor imagery,” in *2017 IEEE International Conference on Information and Automation (ICIA)* (Macao), 311–316. doi: 10.1109/ICInfA.2017.8078925
- Xiong, D., Zhang, D., Zhao, X., and Zhao, Y. (2021). Deep learning for EMG-based human-machine interaction: a review. *IEEE CAA J. Automat. Sigica* 8, 512–533. doi: 10.1109/JAS.2021.1003865
- Zhu, L., Wang, Z., Ning, Z., Zhang, Y., Liu, Y., Cao, W., et al. (2020a). A novel motion intention recognition approach for soft exoskeleton via IMU. *Electronics* 9:2176. doi: 10.3390/electronics9122176
- Zhu, Y., Li, Y., Lu, J., and Li, P. (2020b). A hybrid BCI based on SSVEP and EOG for robotic arm control. *Front. Neurobot.* 14:583641. doi: 10.3389/fnbot.2020.583641
- Zhuang, Y., Leng, Y., Zhou, J., Song, R., Li, L., and Su, S. W. (2021). Voluntary control of an ankle joint exoskeleton by able-bodied individuals and stroke survivors using EMG-based admittance control scheme. *IEEE Trans. Biomed. Eng.* 68, 695–705. doi: 10.1109/TBME.2020.3012296
- Conflict of Interest:** The authors declare that the research was conducted in the absence of any commercial or financial relationships that could be construed as a potential conflict of interest.
- Publisher’s Note:** All claims expressed in this article are solely those of the authors and do not necessarily represent those of their affiliated organizations, or those of the publisher, the editors and the reviewers. Any product that may be evaluated in this article, or claim that may be made by its manufacturer, is not guaranteed or endorsed by the publisher.

Copyright © 2021 Shi, Huang, Peng, Mu and Yang. This is an open-access article distributed under the terms of the Creative Commons Attribution License (CC BY). The use, distribution or reproduction in other forums is permitted, provided the original author(s) and the copyright owner(s) are credited and that the original publication in this journal is cited, in accordance with accepted academic practice. No use, distribution or reproduction is permitted which does not comply with these terms.



# Advantages of publishing in Frontiers



## OPEN ACCESS

Articles are free to read  
for greatest visibility  
and readership



## FAST PUBLICATION

Around 90 days  
from submission  
to decision



## HIGH QUALITY PEER-REVIEW

Rigorous, collaborative,  
and constructive  
peer-review



## TRANSPARENT PEER-REVIEW

Editors and reviewers  
acknowledged by name  
on published articles

## Frontiers

Avenue du Tribunal-Fédéral 34  
1005 Lausanne | Switzerland

**Visit us:** [www.frontiersin.org](http://www.frontiersin.org)

**Contact us:** [frontiersin.org/about/contact](http://frontiersin.org/about/contact)



## REPRODUCIBILITY OF RESEARCH

Support open data  
and methods to enhance  
research reproducibility



## DIGITAL PUBLISHING

Articles designed  
for optimal readership  
across devices



## FOLLOW US

@frontiersin



## IMPACT METRICS

Advanced article metrics  
track visibility across  
digital media



## EXTENSIVE PROMOTION

Marketing  
and promotion  
of impactful research



## LOOP RESEARCH NETWORK

Our network  
increases your  
article's readership